Dissertation zur Erlangung des Doktorgrades

der Fakultät für Chemie und Pharmazie

der Ludwig-Maximilians-Universität München

Design and Synthesis of Potential STING-Degrading PROTACs via a Modular Click Chemistry Approach

Giacomo Ganazzoli

aus

Correggio, Italy

2024

Erklärung

Diese Dissertation wurde im Sinne von §7 der Promotionsordnung von 28. November 2011 von Herrn Prof. Dr. Thomas Carell betreut.

Eidesstattliche Versicherung

Diese Dissertation wurde selbstständig, ohne unerlaubte Hilfe erarbeitet.

München, 07.02.2024 ……

Giacomo Ganazzoli

Dissertation eingereicht am: 07.02.2024

1. Gutachter: Prof. Dr. Thomas Carell

2. Gutachter: Dr. Pavel Kielkowski

Mündliche Prüfung am: 18.03.2024

“Fatti non foste a viver come bruti,

ma per seguir virtute e canoscenza”

Ulysses crossing the Pillars of Hercules
Dante Alighieri – *Divina Commedia*, Inferno, v. 119

Acknowledgments

First of all, I would like to thank my PhD supervisor *Prof. Dr. Thomas Carell*. I feel honoured to have had the opportunity to be a part of your amazing group, working on cutting-edge interdisciplinary research, with great scientific freedom and wonderful people. During this time, I have learned how to address challenges with enthusiasm, how to be self-sufficient and independent and I grew as a scientist as well as a person. These are lessons that I will always carry with me.

I would like to thank *Dr. Pavel Kielkowski* for kindly accepting to be my second evaluator, and the other members of my PhD committee for taking the time for reading my thesis.

My gratitude goes also to *Dr. Markus Müller* for correcting my dissertation and for his invaluable help in all the aspects of my PhD, from scientific advices to non-scientific and more philosophical discussions.

I would like to thank the permanent staff as well, without whom the group would not function. *Frau Slava Gärtner* and *Dr. Nädä Raddaoui* for the organization and management, *Kerstin Kurz* for her patience and help regarding ordering and providing lab equipment and *Claudia Scherübl* for taking care of instruments.

A special thank goes to the members, past and present, of the PROTAC and cGAMP subgroups, with whom I shared the challenge and the pleasure to work on such a wonderful topic. In particular, *Johann de Graaff*, *Dr. Dilara Özdemir* and *Yasmin Gärtner* for their scientific contribution to the work reported in this dissertation. Regarding my scientific research, I would also like to express my deep gratitude to *Dr. Samuele Stazzoni* for his guidance, help and patience, especially at the beginning of my journey.

A big thank goes also to *Dr. Lucia Natarelli* and *Dr. Zahra Abedi* from the LMU *Institute for Cardiovascular Prevention* (IPEK) for their kind help and advices in the development of biological methods.

In general, I would like to thank all the people that I had the pleasure to meet during my time in AK Carell for the great science done together, the great working environment and the parties in and outside the lab. Among you I had the fortune to find many true friends that I will carry in my heart for the rest of my life.

It's hard to express in few words how deeply grateful I am to my friends for the time of my PhD. To my "old" friends from home I would like to say thank you for supporting me from distance, during the good and particularly the long less-good times, for having never made me feel far away and for making me realize how lucky I am to have you, every time I came back. To the "new" friends I made along this way. I would have never expected to establish so deep and true connections with people I met at work. I shared with you difficult times through which we supported each other and this, in addition to the amazing moments spent together, made our friendship priceless. Despite life may separate us around the globe, I will remember you forever.
I owe you all a lot and I hope I will be able to express my gratitude better in person than by naming each one of you in these lines.

Thanks also to all my teachers and professors that I encountered during my studies. Each of you left me something and hence led me to this achievement.

Finally, to my family, to which I dedicate this achievement and to whom many others are owed. This following part will therefore be in Italian.

Vorrei ringraziare tutta la mia famiglia per il supporto che ho ricevuto durante questi cinque anni. I miei zii e cugini per l'affetto che mi avete dimostrato ogni volta che sono tornato a casa.

Ringrazio i miei nonni. Il vostro amore e fiducia incondizionati mi danno ogni giorno la forza di cercare di rendervi sempre orgogliosi di me.

Ringrazio mia sorella *Bianca*, alla quale ho forse troppo poco spesso espresso la mia gratitudine. Grazie per avermi sopportato e supportato quando ne ho avuto bisogno, senza chiedere nulla in cambio. Spero di saper fare altrettanto bene se mai ne dovessi aver bisogno tu.

Infine grazie ai miei genitori, a cui devo tutto. I vostri insegnamenti, il vostro supporto e il vostro amore mi hanno portato dove sono ora e a voi devo questo e tutti i prossimi traguardi che riuscirò a raggiungere nella vita. In particolare, ringrazio mia mamma *Fausta* per essere esempio di coraggio ed avermi insegnato ad affrontare le avversità. Il tuo supporto è stato semplicemente fondamentale. Ringrazio mio papà *Roberto* per aver acceso in me la fiamma della curiosità. La tua infinita conoscenza è sempre stata, sin da bambino, una fonte di ispirazione ed è ciò che mi ha portato ad amare la scienza. Vi ringrazio inoltre per tutto l'amore che avete messo nei piccoli gesti durante questi cinque anni, dai passaggi per tornare/partire, alle torte da portare via, agli abbracci, alle telefonate. Grazie di cuore.

Published Work

- Milda Nainytė, Felix Müller, **Giacomo Ganazzoli**, Chun-Yin Chan, Antony Crisp, Daniel Globisch, Thomas Carell, Amino Acid Modified RNA Bases as Building Blocks of an Early Earth RNA-Peptide World, *Chem. Eur. J.*, **26**, 1-6 (2020).

Conference and Meeting Attendances

- **Giacomo Ganazzoli**, Dilara Özdemir, Thomas Carell, "*Downregulation of STING via PROTAC approach: Synthesis and biological evaluation of cGAMP-CRBN derivatives*", Poster presentation at Scientific School and Conference on Bioinspired Complex Systems from Basic Science to Practical Applications, The Minerva Center for Bio-hybrid Complex Systems, **2022**, Jerusalem, Israel.

Table of Contents

Abstract

In recent years, the cGAS-STING pathway has gained great interest among the medicinal chemistry community, because of its critical role in various diseases and conditions. Its main cellular function, as part of the immune system, is to sense genetic material present in the cytosol and induce a pro-inflammatory response. Double-stranded DNA (dsDNA), when present in the cytosol, is often associated with detrimental conditions for the cell such as bacterial or viral infection, as well as chromosomal instability related to carcinogenesis. As a danger signal, it can be recognized by the DNA sensor cyclic GMP-AMP synthase (cGAS) which, upon binding, catalyses the formation of the cyclic dinucleotide 2',3'-cGAMP from ATP and GTP. Once released in the cytosol, cGAMP acts as a second messenger, binding the enzyme stimulator of interferon genes (STING) and inducing a conformational change that initiates the pro-inflammatory response to clear the threat.

An aberrant over-activation of STING has lately been proven to be linked to an increasing number of autoinflammatory and autoimmune diseases, along with aging, senescence and metastatic progression in cancer. Different studies have demonstrated how the downregulation of STING could be beneficial in reducing the harmful inflammatory state in these conditions. This fostered the study and development of new covalent and non-covalent STING inhibitors, whose number is constantly rising. Next to classical inhibition strategies, promising results for the treatment of different diseases can be accomplished by targeted protein degradation techniques and by proteolysis targeting chimeras (PROTACs) in particular. These heterobifunctional small molecules, consisting of one recruiter for the protein of interest (POI) and another for an E3 ligase enzyme, connected by a chemical linker, are able to bring the two proteins into close proximity in a ternary complex and to induce the ubiquitination of the target, ultimately being degraded by the 26S proteasome (Figure **a**).

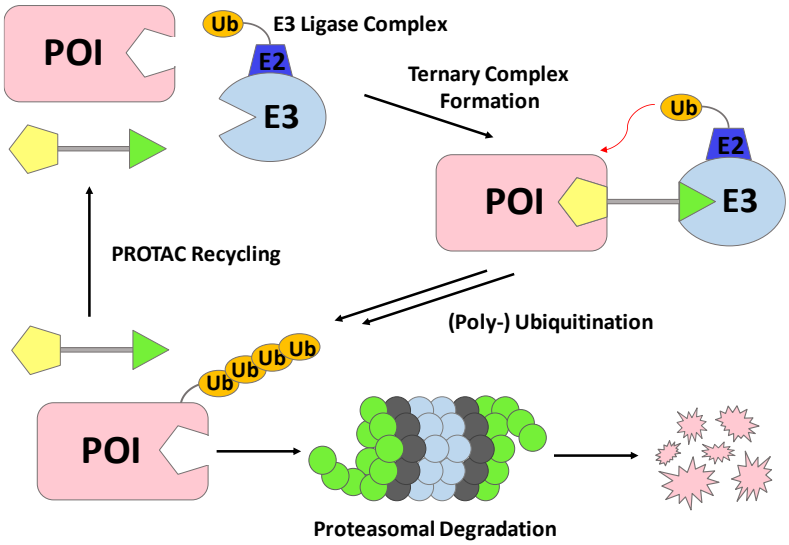

Figure a: PROTAC mechanism.

In this work the PROTAC technology is applied to the targeted degradation of STING for potential treatment of autoimmune and autoinflammatory diseases. A modular click chemistry approach was developed for the production of a library of various compounds through the efficient coupling of different POI and E3 ligase recruiters. cGAMP-based STING recruiters (**52** and **53**) were designed and synthesised via phosphoramidite chemistry with the introduction on adenosine's *N*6 position of a PEG linker bearing a terminal alkyne available for Cu(I)-catalysed azide-alkyne cycloaddition (CuAAC). To tackle possible drawbacks in terms of stability and cell membrane permeation ability due to the negative charges present on the CDN phosphates, a different POI recruiter (**64**) was designed and synthesised from a

novel small molecule STING inhibitor, functionalised with a clickable PEG linker. This could synergistically increase the efficacy of small-molecule-based STING inhibitors by promoting degradation of the target protein. On the other side of the PROTAC structure, various recruiters of the most commonly used E3 ligases, cereblon (CRBN) and Von Hippel-Lindau (VHL), were tested. The presence of a PEG linker of different lengths carrying an azide on one end, allowed the coupling with the complementary alkyne of the STING binding units. In order to expand the pool of E3 ligases engaged for the degradation, a novel potential recruiter was derived from the modification of a known agonist of RNF5. This E3 ligase is responsible for mediating the physiological proteasomal degradation of STING and its recruitment via PROTAC is purposely aiming at the formation of a naturally favoured ternary complex between the two protein surfaces, resulting in a more potent degradation. Compound **92** was hence obtained from the original activator structure by the insertion of a PEG linker with a terminal azide. The combination of the various components via click chemistry led to the efficient creation of a library of compounds that could be used as a valuable starting point for the optimization and development of new promising PROTACs to treat STING-dependent aberrant inflammatory conditions (Figure **b**).

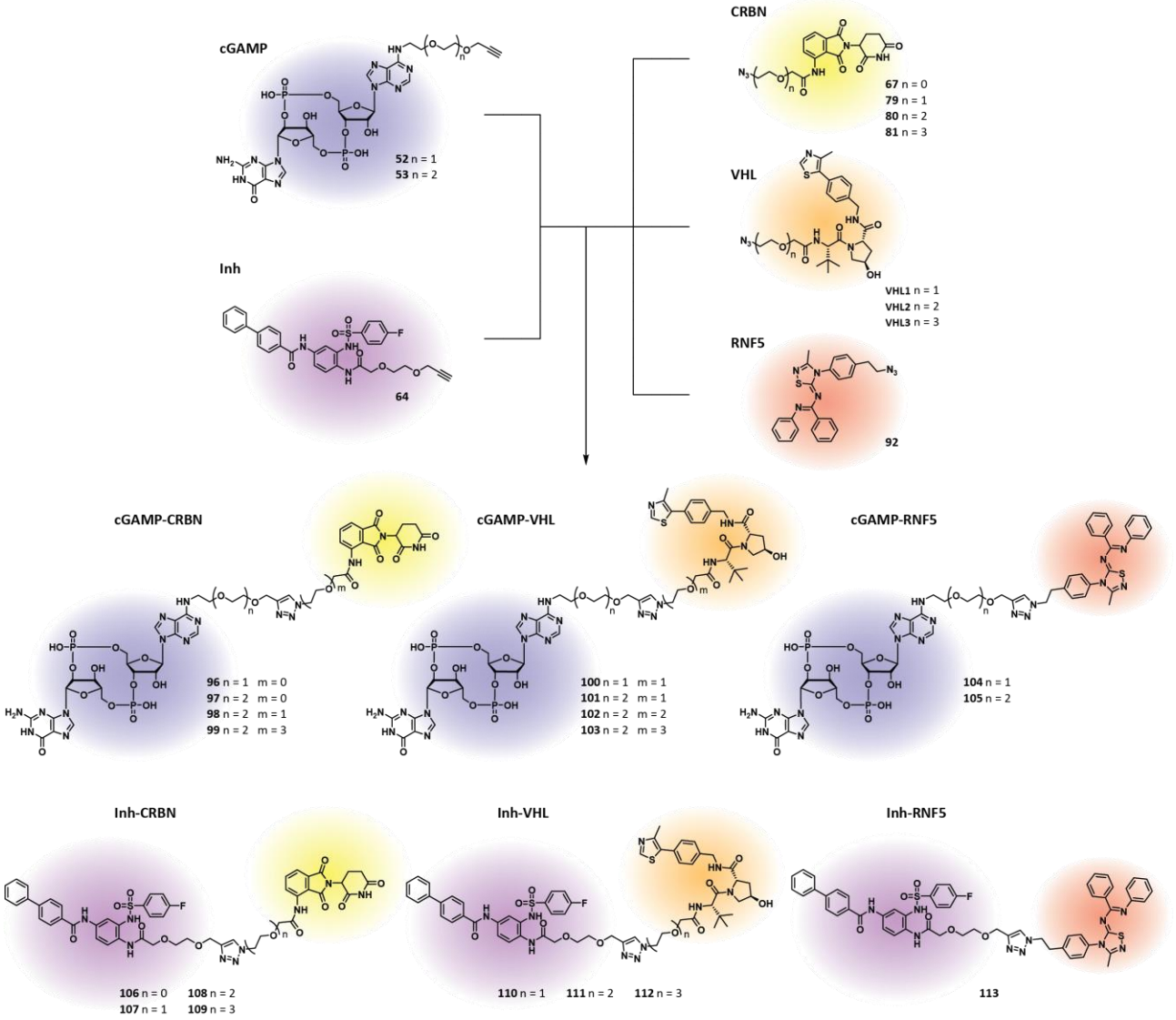

Figure b: Combination of different STING and E3 ligase recruiters via Cu(I)-catalysed click chemistry for the synthesis of a library of potential STING-degrading PROTACs.

1 Introduction

1.1 The Immune System

During evolution, every living organism faced the necessity to protect itself from external or internal factors that are a threat for its own existence. The whole set of different strategies developed by each of them to address this necessity is defined as immune system.

In many advanced forms of life, such as humans, this complex network of biological structures and processes responsible for the defence against pathogens, can be rationalized in two main categories: the innate and the adaptive immune systems. The innate immune system represents the first, fast, non-specific and preconfigured response after pathogen sensing and it is present, in different forms, in all multicellular organisms. The adaptive immune system on the other hand, generates a slower, however highly specific, tailored defence against the target threat, leading to a longer lasting protection through immunological memory. The adaptive system comprises humoral immunity, constituted by macromolecules like antibodies found in extracellular fluids, and cell-mediated immunity, via B and T lymphocytes, which can develop antigen-specific receptors, secrete antibodies specific towards pathogen-associated antigens and mature immunological memory. [1-3] These two components of the immune system, despite their independence and substantial difference in the mechanisms of action, have been proven to act synergistically in generating a fully effective immune response and maintenance of homeostasis (Figure **1.1**).

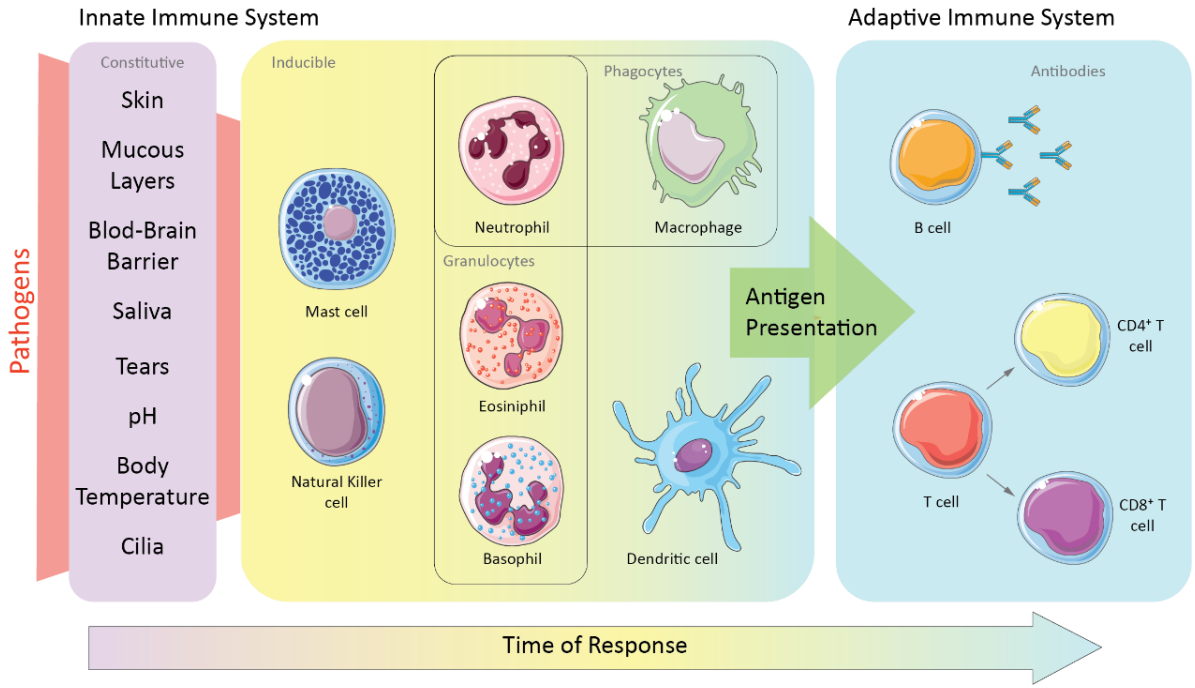

Figure 1.1: Schematic representation of the immune system.

1.1.1 Innate Immune System

The innate immune system includes an entire range of immune defence mechanisms that are encoded in the host's genome in their mature and fully operational form, present from birth and

ready to function.[4] Alongside physical and chemical barriers that block or destroy entering pathogens (constitutive immunity),[5, 6] inducible mechanisms are activated in response to the detection of pathogenic stimuli, mediated through pattern recognition receptors (PRRs), which trigger signal transduction and gene expression, to induce inflammation.

Inflammation is the complex result of the action of chemical mediators such as cytokines and chemokines, released consequently to the downstream of various immune signalling pathways. These inflammation effectors promote the recruitment of immune cells and antibodies to eliminate the pathogen and are also involved in the initiation and regulation of adaptive immunity by inducing the maturation of antigen-specific responses, as part of the numerous interplays between innate and adaptive immune systems.[7-9] Among cytokines, interferons are known for their ability of interfering with viral replication by impairing protein synthesis and for activating the transcription of interferon-stimulated genes (ISGs) which encode other pro-inflammatory small proteins.[10, 11] Interferons are also responsible for promoting apoptosis, inhibiting angiogenesis, suppressing proliferation of endothelial cells and to directly activate other immune cells, resulting in antitumor defence.[12]

The different cells constituting the immune system can rely on pattern recognition receptors (PRRs) to recognize structural and molecular motives expressed by or related to a wide variety of pathogens. Conserved motives, not found in the host, which therefore allow the discrimination of self from non-self, consist of diverse bacterial or viral molecules such as lipids, proteins, carbohydrates or nucleic acids, that are essential for the survival of the microbe. These factors are generally referred to as pathogen-associated molecular patterns (PAMPs).[13, 14] On the other hand, PRRs are also able to sense endogenous molecules and proteins leaking from damaged or dying cells such as cellular debris or secreted messengers. These by-products, often associated with infection, tumorigenesis and senescence, are also known as danger-associated molecular patterns (DAMPs).[15, 16] Upon recognition of the pathogenic patterns, PRRs initiate downstream signalling pathways (NF-κB, MAPK and TBK1-IRF-3 signalling) inducing the transport of transcription factors to the nucleus for the transcription of inflammatory genes.[17-19]

Among all the PAMPs and DAMPs sensed by PRRs, nucleic acids constitute an important class of triggers for the immune response.[20] Depending on the origin, either from bacterial or viral infection (PAMPs) or host's genetic material such as nuclear or mitochondrial DNA derived from tumorigenesis, oxidative stress or apoptosis (DAMPs), nucleic acids can be found as single-stranded RNA (ssRNA), double-stranded RNA (dsRNA), single-stranded DNA (ssDNA), double stranded DNA (dsDNA) or DNA:RNA hybrids, each of which is sensed by specific receptors.[21]

1.2 The cGAS – STING Pathway

The enzyme cyclic GMP-AMP synthase (cGAS) is a sensor for cytosolic DNA that belongs to the nucleotidyltransferase family. It is part of the cGAS-STING axis and responsible for initiating a downstream signalling pathway that leads to the triggering of interferon responses. Its main function is to sense double stranded cytosolic DNA of self or non-self origin and catalyse the production of the non-canonical cyclic dinucleotide 2',3'-cyclic guanosine adenosine monophosphate (2',3'-cGAMP, **1**) from ATP and GTP (Figure **1.2**).

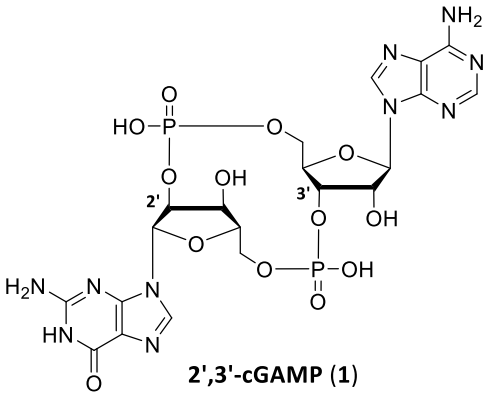

Figure 1.2: Structure of the non-canonical cyclic dinucleotide 2',3'-cGAMP (**1**).

Once produced, this second messenger can then diffuse through the cytosol and bind the adaptor protein stimulator of interferon genes (STING or MITA) on the endoplasmic reticulum (ER). Upon activation by cGAMP, STING undergoes a conformational change and translocates to the Golgi in the perinuclear region, activating a downstream signal that stimulates the transcription of inflammatory genes (Figure **1.3**).[27, 28]

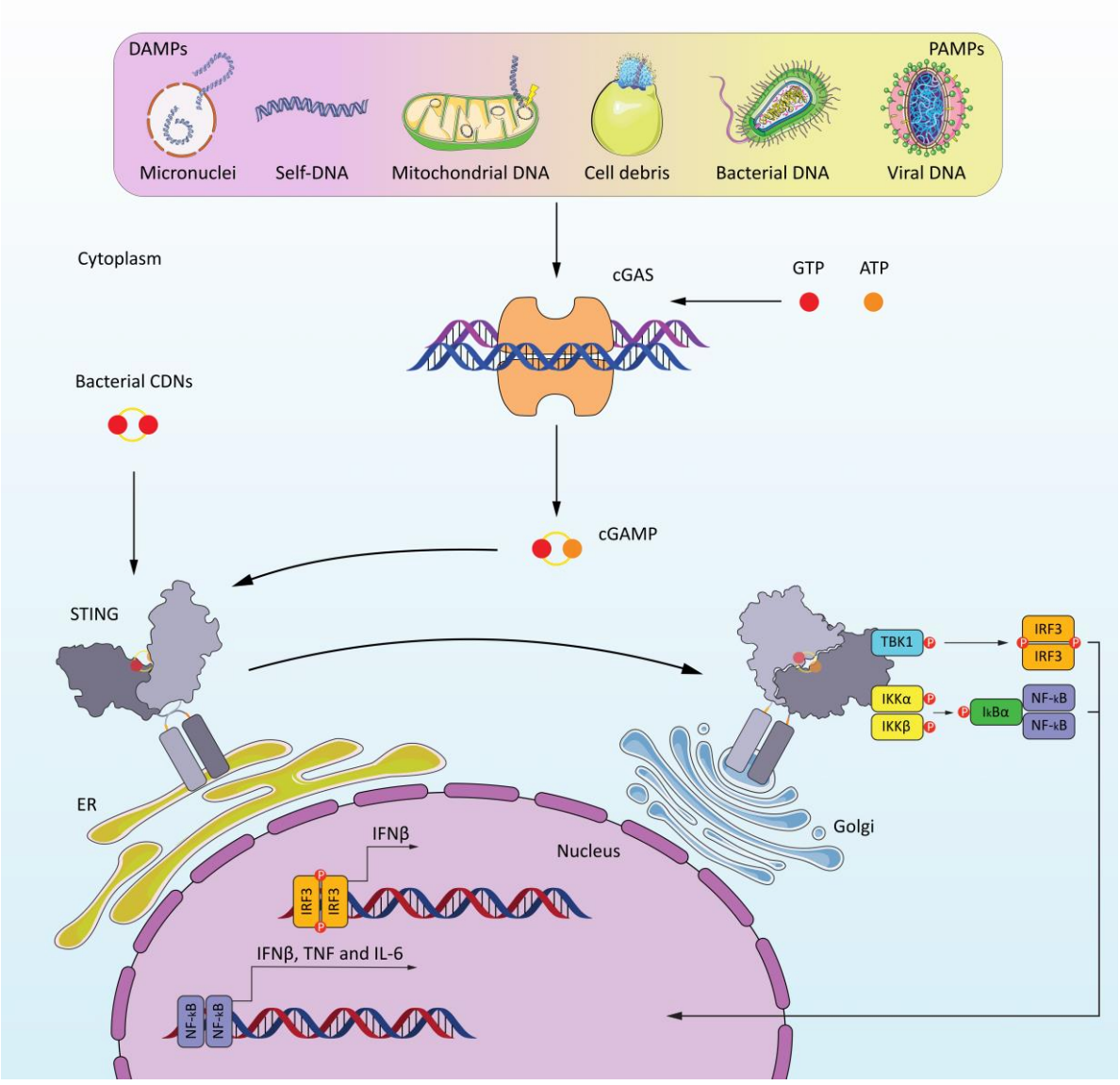

Figure 1.3: General scheme of the cGAS-STING signalling pathway.

1.2.1 cyclic GMP-AMP Synthase (cGAS)

Human cGAS is a small cytosolic protein of 522 amino acids and is composed of a globular C-terminal domain and an unstructured, high positively charged N-terminal domain, that anchors the enzyme to the plasma membrane far away from the nucleus to avoid erroneous self-activation.[22] The C-terminal domain contains the nucleotidyltransferase (NTase) domain, catalytic part of the enzyme, forming a bilobate architecture that interacts with the negatively charged sugar phosphate backbone of DNA, together with the positively charged N-terminal domain.[23-27] Upon binding of dsDNA, cGAS undergoes conformational changes, dimerizing and forming of an active 2:2 cGAS-DNA complex, with subsequent rearrangement of the NTase catalytic pocket at the interface of the two lobes of the enzyme, allowing an optimal interaction with the substrates ATP and GTP for the synthesis of cGAMP (Figure **1.4**).[29, 31-33] Multiple cGAS dimers can bind two separate stretches of dsDNA or on one long curved dsDNA helix, forming "ladder-like" networks that stabilize the overall complex, resulting in a stronger activation of the whole pathway by long dsDNAs.[28, 29]

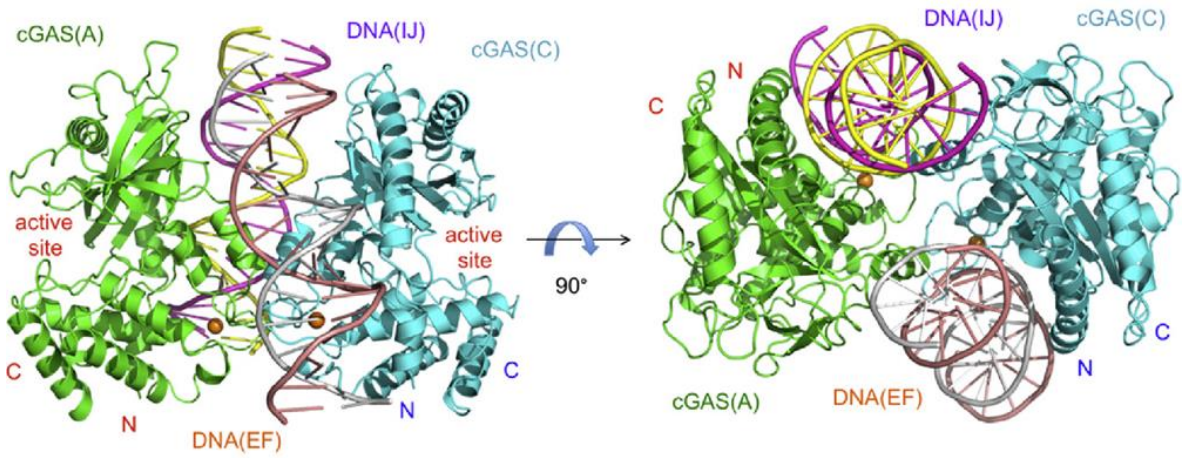

Figure 1.4: Crystal structure of dsDNA bound to cGAS in a 2:2 ratio. Figure adapted from Li *et al*.[25]

This allosteric process turns cGAS into the active state for the conversion of ATP and GTP to cGAMP in a two-step reaction through an intermediate linear dinucleotide. At the same catalytic pocket, on the first stage, the 2'-OH of GTP in the acceptor site reacts with the α-phosphate of ATP in the donor site with elimination of a pyrophosphate. At this point, because of steric constraints in the active site, the linear pppG(2'-5')pA intermediate is released and retaken flipped by 180°, inverting the donor and acceptor positions and promoting the final cyclization step with the formation of the canonical 3'-5' linkage, as shown in Figure **1.5**.[27, 28, 34] This process in human cGAS permits the formation of the unique non-symmetrical 2',3'-cGAMP bearing a canonical 3',5'-phosphodiester bond between the 3'-OH of AMP and the 5'-OH of GMP and a non-canonical 2',5'-phosphodiester connecting the 2'-OH of GMP with the 5'-OH of AMP. This unusual connection is responsible for its higher affinity towards h-STING in comparison to 3',3'-cGAMP or to symmetrical cyclic dinucleotides, as the bacterial cyclic diadenosine monophosphate (c-di-AMP) and cyclic diguanosine monophosphate (c-di-GMP). However, STING can also act as a direct sensor of bacterial infection through the direct interaction with the latter ones.[28, 30, 31]

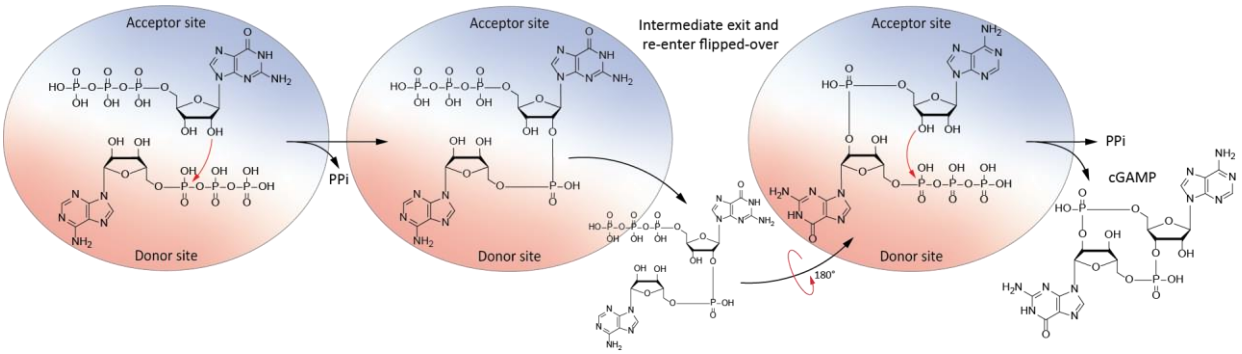

Figure 1.5: Schematic representation of the cGAMP synthesis mechanism in cGAS catalytic pocket.

1.2.2 Stimulator of Interferon Genes (STING)

Once released in the cytosol, the second messenger cGAMP diffuses until it reaches STING on the endoplasmic reticulum membrane, promoting its activation upon binding.[32, 33] This protein, composed of 378 amino acids, sits on the ER membrane in its inactive form. Structurally, it can be divided into a short cytosolic N-terminal segment, a four-span transmembrane domain, a connector region and a cytosolic ligand-binding domain (LBD) to which a C- terminal tail (CTT) is connected. In its apo-form (unbound to cGAMP), STING is found as an open homodimer, forming a deep V-shaped binding pocket at the interfaces of the two monomer's LBDs, which are in a swapped conformation compared to each other's transmembrane domains, resulting in a crossover of the two connector helices (Figure **1.6**).[34-36]

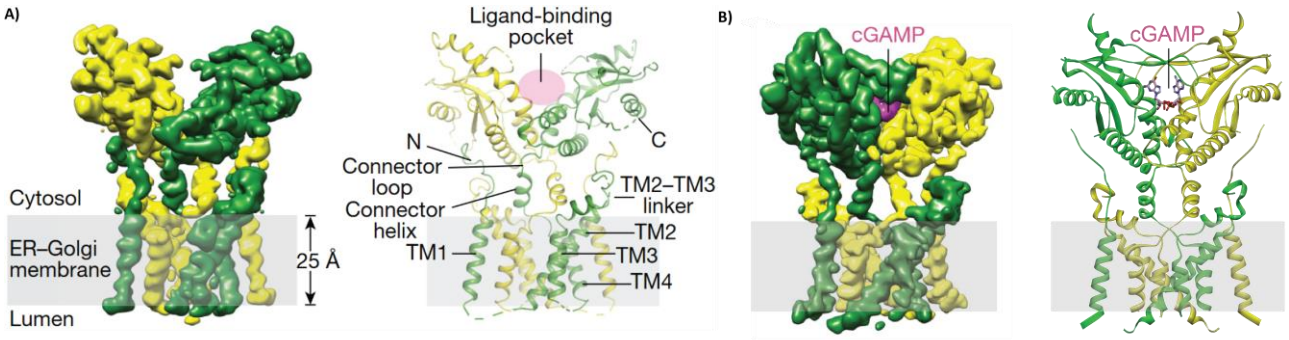

Figure 1.6: Cryo-EM 3D reconstruction of full length STING.[37] **A**) STING dimer in the unbound apo form and **B**) bound with cGAMP in the CDN binding site. Figure adapted from Shang *et al*.[37]

From crystallographic data, the 2',3'-cGAMP-hSTING binding conformation was identified as mainly stabilized by π-stacking interactions between the purines and the aromatic side chains of Tyr167 and Tyr240 residues and the ionic interactions between the negatively charged phosphates of cGAMP and the positive charge of arginine side chains in position 238 and 232. In addition to these, other hydrogen bond interactions between the guanine base and Glu260 and Thr263, as well as the main-chain carbonyl oxygen of Val239, are further contributing to the stabilization of the ligand-protein complex. Moreover, the free 3'-OH of GMP points to two Ser162 residues from the lower part of the pocket, explaining why 2',3'-cGAMP is a specific and high-affinity ligand for hSTING (Figure **1.7**).[37]

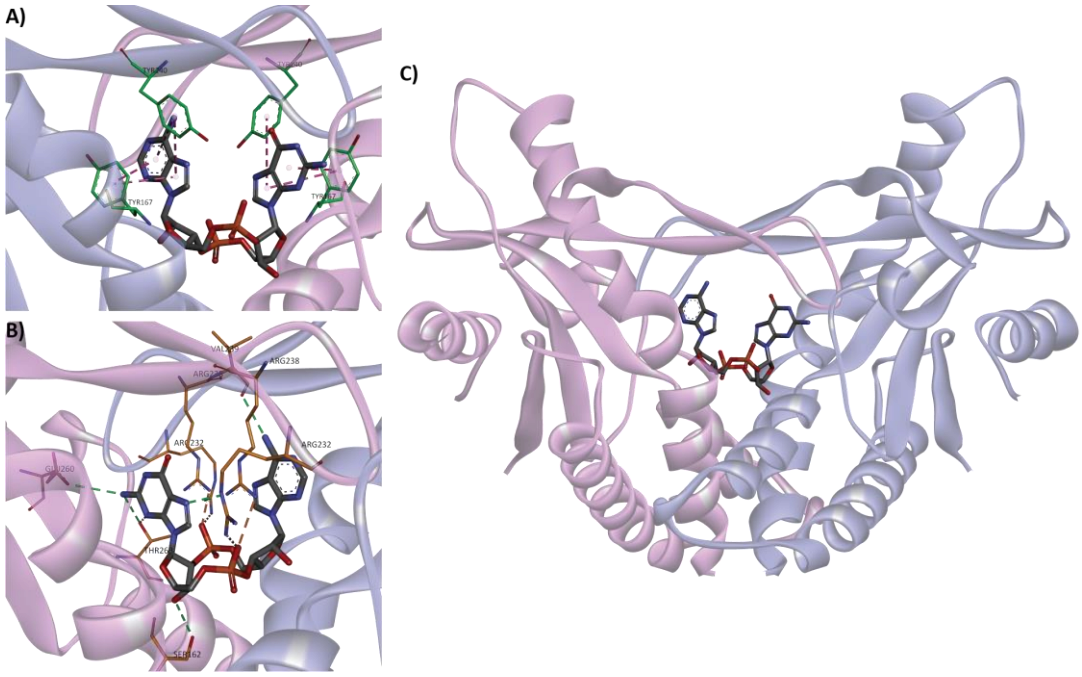

Figure 1.7: Interaction of STING with cGAMP in the crystal structure.[38] **A**) Non-polar π-stacking interactions between purines basis and aromatic amino acids (tyrosines). **B**) Polar ionic interactions between the positively charged arginine side chains and the negative charges of phosphates (orange) and hydrogen bonds between cGAMP and amino acid residues in the STING active site (green). **C**) Complete representation of the crystal structure of STING in the closed conformation, bound to cGAMP in the active site.

Consequent to cGAMP binding, the STING dimer undergoes a conformational rearrangement consisting of a 180° rotation of the LBD domains (untwisting in respect to their transmembrane portions) and concurrent inward rotation that, together with the formation of a lid (ordered β-sheet structure), results in the closure of the dimer on top of the cyclic dinucleotide. This conformational switch creates a surface geometry that promotes a lateral oligomerization of sequential STING dimers through the formation of disulphide bonds between the Cys148 residues in the connector helices (Figure **1.8A**).[37, 39] This process is fundamental for STING in gaining the signalling competence and it is believed to induce the translocation of the protein from the ER to the Golgi through the ER-Golgi intermediate compartment (ERGIC).[40] After trafficking to the Golgi, STING is also palmitoylated at Cys88 and Cys91, further promoting dimer oligomerization and subsequent activation of the downstream signalling process.[41] The oligomerization is also responsible for the rearrangement of the CTT domain which becomes more accessible for the recruitment of the kinase TANK-binding kinase 1 (TBK1) during the transfer to the Golgi, fostering *trans*-phosphorylation of the neighbouring recruited kinases.[42, 43] Now activated TBK1 phosphorylates the adjacent STING at Ser366, as part of a conserved pLxIS motif in the CTT, which allows the STING-TBK1 complex to recruit interferon regulatory factor 3 (IRF3). IRF3 is in turn phosphorylated and, after forming an active homodimer, translocates to the nucleus, initiating the transcription of type-I interferons as well as other interferon-stimulated genes (ISGs) (Figure **1.8B**). Once the downstream signalling is not needed anymore, STING is transported back from the Golgi to the ER by coat protein complex I (COPI) or alternatively undergoes lysosomal, as well as proteasomal, degradation.[44-46]

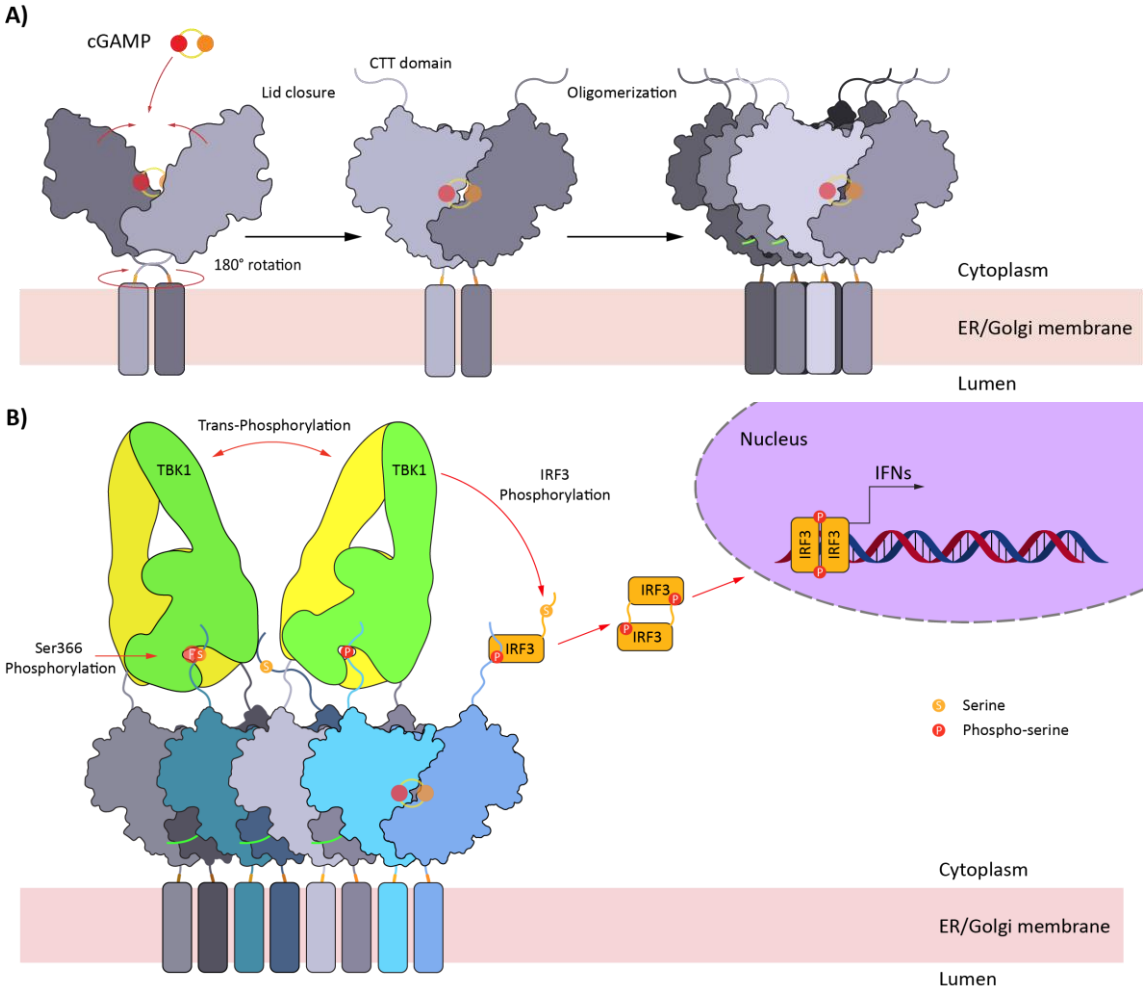

Figure 1.8: Mechanism of STING activation and downstream signalling for interferon expression. **A**) cGAMP binding to the open STING induces a conformational transition to the closed form and subsequent oligomerization via disulphide bonds in the loop connector area. The structural change also favours the protrusion of the CTT domains. **B**) TBK1 binding leads to self-phosphorylation and consecutive phosphorylation of the neighbouring unit's CTT domain. This allows the recruitment and phosphorylation of IRF3, dimerization and is translocation to the nucleus, leading to interferon expression.

Besides the stimulation of IRF3 transcription, the activation of the cGAS-STING axis is also responsible for binding and stimulating the IkB kinase to trigger the production of pro-inflammatory cytokines such as IL-6, IFN-α and INF-β expression, through the NF-κB signalling pathway via the nuclear factor κB, in a still not completely clear way.[47, 48] This signalling pathway regulates autophagy, probably a vestige of primordial defence function,[49] and promotes anti-proliferative cell states, including cellular senescence and cell death through the induction of cell-cycle inhibitors (such as p21) and pro-apoptotic proteins (e.g. tumour necrosis factor TNF).[50-53]

1.2.3 Intercellular cGAMP Trafficking

In addition to its cytosolic function, cGAMP has been proven to be involved in extra/intercellular signalling, alerting surrounding cells towards the danger and amplifying the overall immune response by direct STING activation. This phenomenon in adjacent cells is mediated by gap junctions, intercellular channels made of connexins, directly connecting the cytosols of two neighbouring cells.[54] cGAMP can also travel longer distances being transported via encapsulation in

viral capsids, vesicles or dying tumor cells, as well as after being released into the extracellular microenvironment upon cell damage or necrotic cell death.[55-57] Extracellular cyclic dinucleotides are most likely entering the cell via carrier proteins and channel-dependent mechanisms. Various non-specific transmembrane transporters have been described as capable of shuttling cGAMP across cellular membranes, expressed in different levels depending on the cell type. Hints from several studies suggest that the uptake of extracellular cGAMP may be mediated by two folate solute carriers, SLC19A1 and SLC46A2,[58, 59] as well by the purinergic receptor P2XR7,[60] the latter by the formation of an ATP-gated non-selective pore for hydrophilic substances. Volume-regulated anion channel LRRC8 can also act as a cGAMP transporter through the formation of an hexameric channel both in import and export under different conditions.[61, 62] Finally, the transmembrane transporter ABCC1 was shown to export cGAMP in an ATP dependent manner through a pore.[63]

Regarding the fate of extracellular cGAMP, Ectonucleotide Pyrophosphatase/ Phosphodiesterase 1 (ENPP1), a transmembrane protein usually involved in the hydrolysis of ATP to AMP and diphosphate, is the only human enzyme known so far responsible for the degradation of 2',3'-cGAMP by cleaving the 2'-5' phosphodiester bond.[64] Presenting its active site exclusively on the extracellular space, the question about the existence of a specific cooperation of this enzyme with transmembrane carriers in the regulation of cGAMP, remains open. In addition to the human enzyme ENPP1, some highly conserved viral proteins belonging to the family of poxivirus immune nucleases or poxins, are also able to hydrolyse cGAMP intracellularly by cleavage of the 3'-5' phosphodiester bond, to prevent the downstream signalling within the infected cell and the extracellular propagation through new viral capsids, thereby impairing the immune response of the host.[65]

1.2.4 Activation of the cGAS-STING Pathway Under Steady State Conditions

Under normal and healthy conditions, the cGAS-STING pathway can respond to a large variety of exogenous, endogenous, self or non-self stimuli, triggering the immune response that is supposed to help clearing the menace.

Among the extrinsic stimuli, cGAS is responsible for sensing dsDNA, released during microbial infection both directly, through the recognition of bacterial or viral genetic material (non-self DNA) in the cytosol or in the nucleus,[66-73] or indirectly, binding released self mitochondrial DNA (mtDNA) often induced by RNA viruses.[74-77]

Intrinsic stimuli that can activate the cGAS-STING signalling pathway and the consequent immune response via self-dsDNA are different. Exogenous sources of self DNA are associated with increased non-apoptotic cell death or perturbed phagocytic digestion and can be delivered to the cytosol via extracellular vesicles, such as exosomes, or more directly internalized via endocytosis from the extracellular space. Endogenous cytosolic self-DNA can have mitochondrial or nuclear origin, leaking from the respective membranes or from cytosolic micronuclei. Self-mitochondrial DNA (mtDNA) is a powerful cGAS agonist that can be related to external pathogen infection or by intrinsic apoptosis under mitochondrial stress conditions (e.g. reactive oxygen species, ROS), causing its release in the cytosol.[74]

The accumulation of intrinsic genomic DNA outside the nucleus is the prototypical danger-associated molecular pattern (DAMP) often associated with conditions such as tumorigenesis, senescence, aging and autoinflammatory diseases, causing activation of the cGAS-STING pathway. In particular, DNA damage, defective replication and impaired repair mechanisms induced by malfunction of the DNA-damage response (DDR) system, oncogenes, or external factors such as ionizing radiations, may lead to chromosomal missegregation resulting in the formation of micronuclei or release of cytosolic chromatin.[78, 79] Micronuclei consist of non-incorporated chromatin or chromosomal fragments enveloped in an unstable nuclear membrane as a result of mitotic errors or problems in DNA replication. Once the envelope collapses, the genetic material is released in the cytosol and is sensed by cGAS initiating the downstream signal.[78, 80, 81]

1.2.5 The cGAS-STING Pathway and Cancer

The host's anti-tumor responses include innate immune attack to cancer cells by specific innate cell populations like cytotoxic lymphocyte natural killer (NK) cells as well as dendritic cells (DC) and macrophages. Together and consequently to these, the adaptive immune action is mainly exerted by cytotoxic mature T-cells and B-cells. The cGAS-STING pathway, through the production of interferons, cytokines and chemokines, has a central role in the regulation of these processes.[82] In particular, the balance of these pro-inflammatory molecules is responsible for the activation and polarization of tumor associated macrophages (TAM) (antitumor cytotoxic M1 or immunosuppressive M2 phenotypes),[83-87] for promoting the recruitment, maturation, activation, and differentiation of T lymphocytes (antitumor cytotoxic $CD8^+$ T-cells and $CD4^+$ T-cells into T helper or immunosuppressive Treg phenotypes) and directing their subsequent adaptive immune responses.[88-93] Apart from inducing maturation of DCs and T-cells, type I INFs can promote the mobilization, migration and recruitment of other immune cells, such as DCs, TAM, T-cells and NK cells, on the site of the tumor to enhance the immune response.[94-96]

Despite its primary anti-tumor activity, the cGAS-STING pathway has been reported to have, in different cases, pro-tumorigenic effects, favouring accelerated tumor outgrowth and/or metastatic distribution. These outcomes are associated with chronic high levels of pro-inflammatory cytokines that can stimulate non-canonical NF-κB signalling responsible for inducing carcinogenesis and, particularly in cancer cells with high chromosomal instability (CIN), promoting invasion and metastasis through the epithelial-to-mesenchymal transition.[97] In these specific cases, an immunosuppressive tumor microenvironment (TME) is generated through different mechanisms, also reinforced by the induced STING-dependent apoptosis of T-cell via overstimulation by tumor-secreted cGAMP, fostering immune escape and tumor growth.[61, 98-106]

Therefore, the final pro- or anti- tumoral effect of the cGAS-STING pathway is highly context dependent, with timing and magnitude of STING stimulation and STING-responsive target cells playing critical, independent roles in dictating the outcome. Whereas acute and moderate STING engagement in early-stage cancers favours tumor-suppressive effects, persistent or excessive activation of STING on mature and highly CIN-defined cancers results in immunosuppression and metastatic development.[107, 108]

1.2.6 Senescence and Aging

Senescence is a biological state characterized by ceased cell division while maintaining metabolic activity. It occurs in response to DNA damage due to ageing-related dysfunctional repair mechanism or elevated reactive oxygen species (ROS), activation of oncogenes and cell-cell fusion.[109, 110] This cellular state is associated with an immunogenic phenotype, known as Senescence Associated Secretory Phenotype (SASP), consisting of upregulated secretion of pro-inflammatory cytokines, growth factors and proteases that can attract and activate innate (NK cells and macrophages) and adaptive (T-cells) immune responses to eliminate senescent and potential pre-cancerous cells.[111-113] These factors can act in a paracrine way by inducing inflammation and senescence in surrounding tissues. While this strategy may result protective and tumor-suppressive in young cells, an increased number of senescent cells in older organisms is linked to organ dysfunction, carcinogenesis and aging-related diseases often associated with a constant state of basal inflammation, known as "inflammaging".[110] Genetic ablation of senescent cells in mice resulted in prolonged lifespan and healthspan, ameliorating tissue inflammation and ageing-associated dysfunctions.[114]

In senescent cells, the cGAS-STING pathway is strictly related to the production of SASP components through continuous stimulation by cytosolic DNA fragments derived from ruptured micronuclei or chromatin herniation, caused by chronic DNA damage and disruption of the nuclear envelope, characteristic features of senescent cells, leading to IRF3 and NF-κB induction.[79-81, 115] Therefore, the fundamental role of cGAS and STING in senescence and aging represents a great opportunity for the modulation of these processes and associated diseases through inhibition of the inflammation pathway via potential senomorphic drugs.

1.2.7 The cGAS-STING Pathway and Inflammatory Diseases

Due to its critical role in the regulation of the immune system, errors in the balance of cytoplasmic self-DNA and aberrant cGAS-STING over-activation are often related to chronic inflammation and autoimmune diseases. Downregulation or inhibition of this axis, has been proven to have beneficial potential in the treatment of many syndromes.

1.2.7.1 STING-Associated Vasculopathy with Onset in Infancy

STING-associated vasculopathy with onset in infancy (SAVI) is an autoimmune disease derived from STING gain-of-function mutations which induce a constitutive cGAMP-independent activation and consequent uncontrolled IFN-I signalling.[116, 117] The syndrome is characterized by early-onset systemic inflammation, interstitial lung disease resulting in pulmonary fibrosis and severe skin vascular disease.[118, 119] Recent studies have investigated the effect of small molecule inhibitors on mutated STING able to reduce the aberrant inflammation, showing the potential of STING inhibitors in SAVI treatment.[120, 121]

1.2.7.2 Aicardi-Goutières Syndrome

Aicardi-Goutières syndrome (AGS) is a rare autosomal recessive genetic disorder causing systemic inflammatory disease with an early onset. Here, genetic mutations are responsible for deficiency of several nucleases such as TREX1, involved in the metabolism of ss and dsDNA,[122] SAMHD1, regulating the stalled DNA replication fork reset,[123] and RNase H2, normally degrading RNA-DNA

complexes.[124] These mutations cause abnormal accumulation of endogenous genetic material in the cytosol, constantly stimulating cGAS and inducing autoimmunity. A similar syndrome was identified to be caused by mutations in DNASE2 gene, associated with an elevated type I interferon signature and neonatal anaemia, kidney disease and arthropathy.[125] In both cases, co-depletion of cGAS or STING in mice has been shown to reverse the pathogenesis.[126-128]

1.2.7.3 COPA Syndrome

COPA syndrome is a rare early-onset monogenic autoinflammatory disease marked with arthritis and lung disease, caused by the mutation of the COPA gene encoding COPα, subunit of the COPI complex responsible for the retrieval of STING from the Golgi to ER and resulting in continuous STING polymerization and spontaneous activation at the Golgi.[129] The elevated type I interferon could be reduced by genetic or pharmacological interference with STING.[130, 131]

1.2.7.4 Systemic Lupus Erythematous

Systemic lupus erythematosus (SLE) is a chronic systemic autoimmune disease involving different organs characterized by an amplified type I interferon production via the cGAS-STING pathway. Despite the non-clear cause of SLE due to the high complexity of the disease and the considerable heterogeneity of SLE in humans, mutations in TREX1 and RNase H2, similarly to AGS, have been found in SLE patients.[132, 133] Upregulated levels of dsDNA, type I IFN and expression of type I IFN-stimulating genes (ISGs) in SLE patients, suggests an abnormal cGAS-STING regulation and leaves hope for potential treatment via inhibition of this pathway.

1.2.7.5 Rheumatoid Arthritis

Rheumatoid arthritis (RA), a specific autoimmune disease, is characterized by persistent inflammation and joint destruction by chronic inflammation, with tissue injury resulting from overproduction of cytokines, abnormal behaviour of adaptive immune cells and altered phenotype of fibroblast-like synoviocytes (FLS). The inflammation related to this disease was shown to be alleviated by the knockdown of cGAS or STING.[134, 135]

1.2.7.6 Neurological and Neurodegenerative Disorders

The cGAS-STING has been found to play a role in different neurological and neurodegenerative disorders, as well.[136] Amyotrophic lateral sclerosis (ALS), an incurable and fatal neurodegenerative disease, is associated with mitochondrial mislocalization of a DNA/RNA-binding protein (TDP43) causing mtDNA release into the cytosol and NF-κB -induced increased levels of pro-inflammatory factors and IFNs. Co-depletion of STING or its pharmacological inhibition via H-151, dampened neuroinflammation in ALS models and protected from early death.[137] Connections between the cGAS-STING pathway and Parkinson's diseases were identified. Mutations in PARKIN and PINK1 genes, encoding E3 ligase proteins that assist in the removal of dysfunctional mitochondria, result in mitochondrial stress, accumulation of cytosolic mtDNA and increased cytokine and interferon production. Depletion of STING rescued these inflammatory phenotypes, loss of dopaminergic neurons and motor deficit observed in Parkin-deficient mice models.[138] In a similar manner, Alzheimer disease is characterized by mitochondrial dysfunction due to accumulation of toxic proteins amyloid-β and hyperphosphorylated tau, causing oxidative damage in DNA and mtDNA and

release of mtDNA and dsDNA into the cytosol, promoting neuroinflammation.[139, 140] Again, genetic deletion of cGAS and pharmacological inhibition of STING using H-151, resulted in reduction of neuroinflammation and amelioration of general conditions by reducing toxic amyloid-β accumulation.[141] Together these results show how the development of STING inhibitors could positively impact on treatment of neurodegenerative diseases.

1.3 STING as a Therapeutic Target

Because of its central role in the regulation of the immune system and in the development of various disease, from cancer to auto-immune and inflammatory disorders, the interest in the modulation of the cGAS-STING pathway as therapeutic target is constantly increasing. In particular, a lot of effort has been made in the development of activators and inhibitors of STING to target different conditions, which will be discussed in the following section.

1.3.1 STING Agonists

STING activators represent a promising treatment option in cancer immunotherapy because of their ability to stimulate pro-inflammatory molecules such as type I IFNs and other cytokines, promoting an innate and adaptive immune response towards cancer. These agonists are often used in combination with existing anti-cancer therapies (e.g. radiotherapy, chemotherapy, checkpoint inhibitors, CAR-T) rather than alone. Some of the most significant representatives are discussed below and depicted in Figure **1.9**.

As one of the earliest example, the family of DMXAA (**2**) and derived analogues is a group of non-CDN small molecules xanthenone derivatives that has been developed in order to solve the poor metabolic stability and membrane permeability of natural CDNs. DMXAA initially showed promising results as anticancer agent by activation of the STING pathway and interferon expression in mouse models.[142] However, the compound was retracted from clinical trials due to no effect.[143] Structural binding studies unveiled the specificity towards mouse STING contrarily to human STING, due to minor differences in the LBS of the two enzymes.[144, 145] Similarly, CMA (**3**) showed specificity for murine but not human STING.[146] Another xanthenone derivative, α-mangostin (**4**), resulted in the ability to activate hSTING, inducing IFN production in human cells, however with a lower potency than natural cGAMP.[87] Recent discoveries showed how STING agonists like DMXAA and cGAMP, are able to boost the activity of genetically engineered T cells (CAR-T) by enhancing their trafficking and persistence in solid tumours, representing a promising advance in personalized anticancer therapies.[147]

Another family of non-CDN STING agonists based on amidobenzimidazole have shown strong binding and the ability to stimulate STING activity. Interestingly, crystal structures revealed that the interaction occurs with the open dimer conformation of STING, suggesting a non-canonical activation mechanism.[148, 149] Between these, diABZI (**5**), on top of a strong STING binding (K_D = 1.6 nM), resulted in being more potent than cGAMP (EC_{50} 130 nM vs 53.9 nM) due to the better membrane permeability.

Synthetic derivatives of the natural substrate CDNs have been widely explored as potential STING agonists in order to combine selectivity with higher metabolic stability and better drug delivery.[150]

Modifications on the negatively charged phosphate group may result in increased stability towards phosphodiesterases like ENPP1, for example by substitution of the phosphodiester with a more stable phosphorothioate, already widely studied for siRNA and antisense therapy.[64, 151-155] In order to facilitate drug delivery and membrane permeability, the substitution of the phosphodiester with urea and thiourea groups has been reported to retain the stimulation ability. An alternative approach consists in masking the negative charge via prodrug strategy by introducing a chemical group that would release the free CDN inside the cell after enzymatic cleavage.[156, 157] Modifications of the sugar, including the removal of the free hydroxyl groups or substitution by fluorine atom, are often used for stabilizing siRNA or mRNA -based therapeutics towards nucleases resulting in an increased cellular uptake and STING binding of the cGAMP analogues.[158-160] Remarkable examples are the phosphorothioate derivatives (R_p,R_p pure diastereoisomers) 2',3'-cG^{S}A^{S}MP (**6**) and 2',3'-cA^{S}A^{S}MP (ADU-S100, first STING agonist to enter clinical trials, **7**) that showed similar STING binding affinity but 10-fold increased interferon response in THP-1 monocytes compared to 2',3'-cGAMP.[153, 161] *Novartis* developed and patented (R_p,R_p) 2',3'-cA$_F$^{S}A$_F$^{S}MP (**8**), a modified version of 2',3'-c-di-AMP with thiophosphate bonds and fluorination of the sugar, increasing the activity in comparison to the former phosphorothioates. More recently, E7766 (S_p,R_p pure isomer) (**9**) was designed with macrocycle-bridged structure, rigidly pre-organised in the bioactive conformation of a CDN agonist, resulting in entropic benefits and strong anti-tumor activity.[162] Finally, modifications of the nucleobases (such as the introduction of inosine) were reported to improve binding and activation of STING.[163]

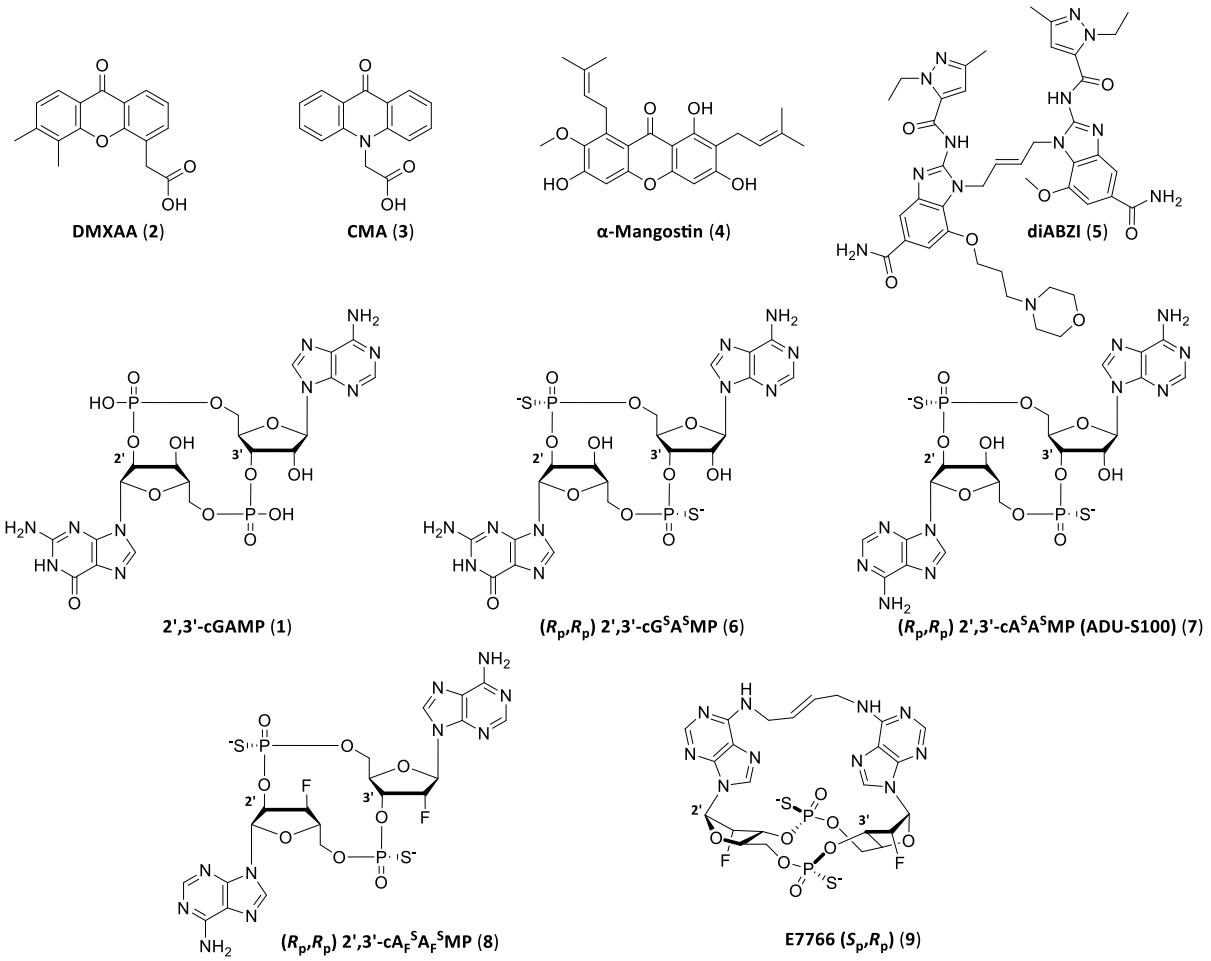

Figure 1.9: STING agonists.

1.3.2 STING Antagonists

Taking into account the strong involvement of STING in the pathogenesis of several autoimmune, autoinflammatory diseases as well as the development and metastatic expansion of certain types of cancer due to abnormal and chronic inflammation, strategies that could downregulate the interferon and cytokine release are constantly gaining interest. The different approaches consist of the covalent or non-covalent inhibition of STING or by inducing proteasomal degradation of the enzyme via PROTAC (see paragraph **1.4**).

Covalent inhibition of STING involves the formation of irreversible chemical bonds with cysteines 88 and 91 close to the transmembrane domain, usually involved in palmitoylation, which is essential for STING activation.[164] As shown in Figure **1.10**, nitrofuran derivatives C-176 (**10**) and C-178 (**11**), whose four-position of the furan ring can undergo a nucleophilic addition reaction with STING C91, were first identified as palmitoylation inhibitors selectively reducing STING-mediated type I interferon and IL-6 production in mice. After discovering their specificity towards mSTING, substitution on the benzene ring led to identification of C-170 (**12**) and C-171 (**13**), active against both m and hSTING.[165] 3-acrylamino indole derivative H-151 (**14**) was also identified via high throughput screening (HTS) inhibiting STING palmitoylation on STING C91 in mouse and human proteins and blocking TBK1 phosphorylation, thereby reducing type I interferon response.[165] Endogenous nitro fatty acids (NO_2-FAs, **15** to **17**), formed during viral infection by the addition of NO_2 to unsaturated fatty acids as oleic and linoleic acids, have been proven to covalently modify STING via nitro-alkylation (*Michael addition*) of C88, C91 and H16, reducing the release of type I IFN in SAVI patients fibroblasts.[166] *Vinogradova et al.* also identified acrylamides BPK-21 (**18**) and BPK-25 (**19**) to react with STING C91 and induce inhibition however with low specificity.[167] Alongside with the targeting of palmitoylation sites, STING inhibition was proven to be possible via covalent modification of the oligomerization site Cys 148, involved in disulphide bond formation between the enzyme units. BB-Cl-Amidine (**20**) was in fact identified as able to inhibit STING activity by reacting with this essential residue, impairing oligomers formation.[168] In general, limitations of covalent inhibition are related to the high reactivity of the chemical groups, leading to low specificity and possible off-target effects.

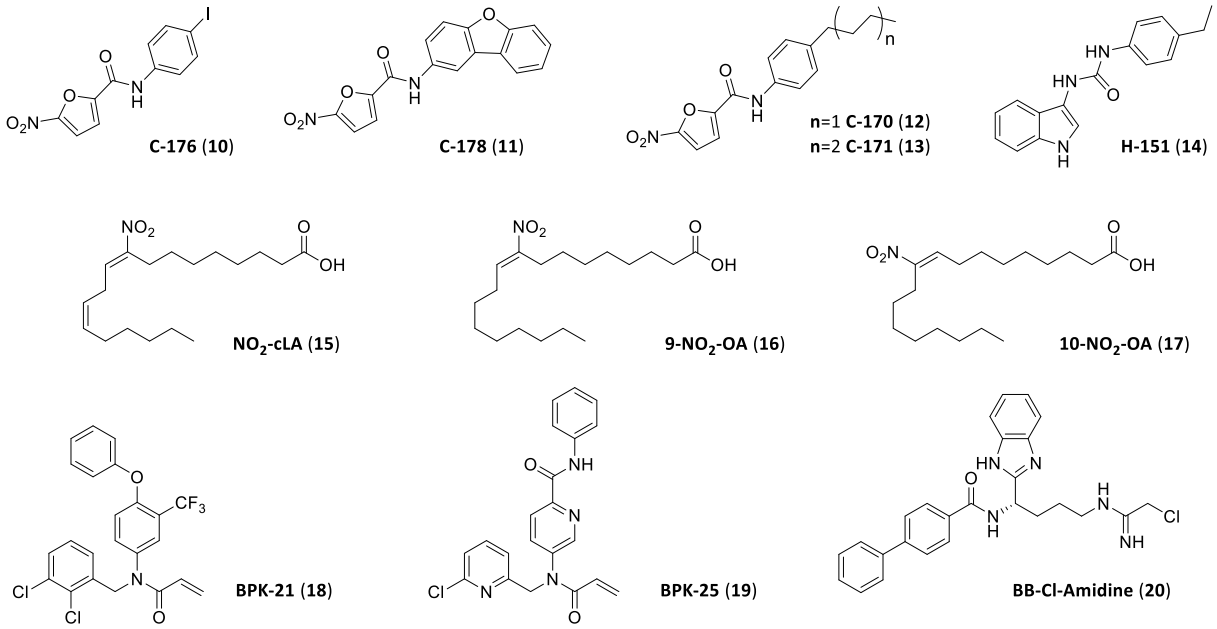

Figure 1.10: STING covalent inhibitors targeting palmitoylation sites Cys 88 and 91 and disulphide bonds oligomerization site Cys 148 (BB-Cl-Amidine, **20**).

Non-covalent inhibition comprises compounds that can competitively occupy the CDN binding pocket at the interface of the dimer without inducing the conformational change or blocking STING in an open inactive conformation as shown for c-di-GMP.[39, 169] Some examples are reported in Figure **1.11**. Initially, the cyclic peptide Astin C (**21**), isolated from the medicinal plant *Aster tataricus*, was identified as a STING inhibitor able to block the recruitment of IRF3 by competitively binding to the CDN binding site.[170] After discovering that the tetrahydroisoquinoline family had some inhibition activity towards STING, SAR studies identified compound 18 (**22**) as competitive inhibitor binding the active site with a 2:1 ratio in the open inactive conformation, however with relatively low efficiency towards hSTING.[171] In 2021 *Hong et al.* reported compound SN-011 (**23**) as a STING inhibitor, competing with cGAMP for CDN binding site in a 2:1 ratio and inducing an inactive conformation, able to effectively suppress systemic inflammation in mice with lower cytotoxicity and higher specificity than H-151.[121] Palbociclib (**24**), a cyclin-dependent kinase (CDK) inhibitor was found to block STING homodimerization by interacting with STING Y167 and was able to alleviate auto-immune disease features.[172] Different derivatives of fusidic acid, as compound 30 (**25**), showed STING inhibition properties by directly interaction with residues in the STING CTD.[173] More recently in 2023, *Ong et al.* reported a novel quinoline containing STING inhibitor HSD1077 (**26**) that could compete with cGAMP in binding STING and exert anti-inflammatory activity *in vitro*, although with relevant toxicity.[174] Interestingly, from crystal structure analysis of mSTING agonist DMXAA and derivatives, *Chang et al.* were able to design two derivatives, compound 11 (**27**) and 27 (**28**), by *in silico* docking studies that showed hSTING inhibitory ability, competing with cGAMP for binding the CDN pocket and holding STING in an inactive open conformation. These compounds proved to be able to inhibit the induction of interferon and inflammatory cytokines *in vitro* without cytotoxicity.[175] Later this same year, Gelsevirine (**29**), a natural alkaloid, was identified to inhibit STING activity by competitively occupying the CDN, impairing its dimerization and was proposed as a potential treatment for sepsis-induced multiple-organ dysfunction, characterized by high levels of pro-inflammatory cytokines.[176]

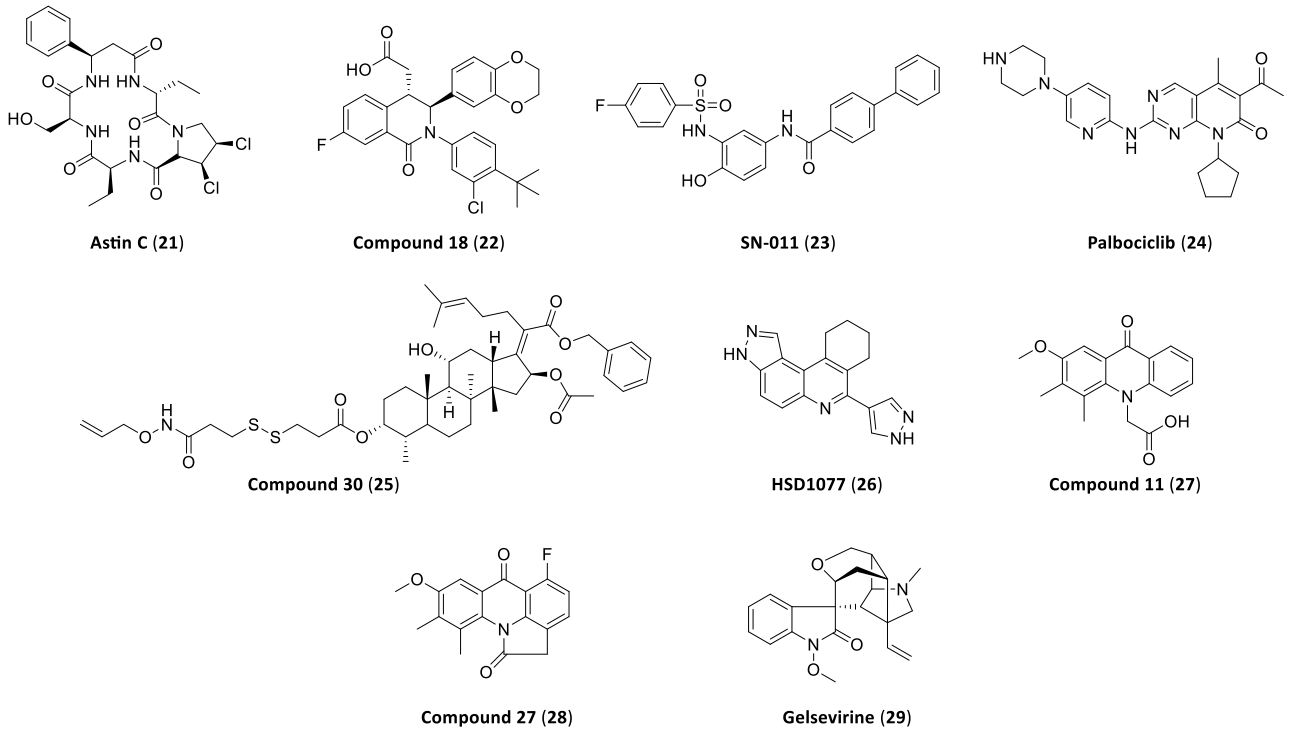

Figure 1.11: STING non-covalent inhibitors targeting CDN binding site.

A novel alternative to classical inhibition is represented by the proteolysis-targeting chimera (PROTAC) technology able to induce proteasomal degradation of a target protein, as described in detail in the following section.

1.4 Proteolysis Targeting Chimeras (PROTACs)

Proteolysis targeting chimeras (PROTACs) are an emerging strategy in the field of targeted protein degradation (TPD) whose function is to promote the degradation of a target protein of interest (POI) by triggering the physiological ubiquitin-proteasome system (UPS). Unlike classical inhibitors, these molecules don't necessarily need to bind the target in enzymatic active-sites, neither to have high affinity, permitting to address proteins previously considered undruggable. So far, PROTACs demonstrated to be able to selectively degrade several targets associated to different kind of diseases, such as various type of cancers, immune disorders, neurodegenerative conditions, cardiovascular diseases and viral infections.[177, 178]

1.4.1 Ubiquitin Proteasome System (UPS)

In eukaryotic cells, the specific degradation of denatured, misfolded or mutated proteins is a fundamental mechanism for maintaining the cell homeostasis and is achieved mainly via lysosomal degradation and ubiquitin-dependent proteolysis.[179, 180] This second mechanism involves the covalent labelling of the defective protein with ubiquitin (Ub),[181] a highly conserved 76 amino acids ubiquitous protein, and the subsequent recognition and degradation by 26S proteasome.[182] The ubiquitylation process is a post-translational modification that involves a cascade of three enzymes. An E1 ubiquitin-activating enzyme activates ubiquitin as a Ub-adenylate which is then attached to a catalytic cysteine of the E1 by the formation of a thioester bond. E1 subsequently transfers Ub to the catalytic cysteine of an E2 ubiquitin-conjugating enzyme via transthioesterification reaction.

Finally, an E3 substrate-specific ligase promotes the formation of a ternary complex together with the target and the Ub-tagged E2, recruited directly or through a series of other adaptor proteins. Ubiquitin is then transferred on the side chain of a lysine residue of the substrate through the formation of an isopeptide bond with the Ub carboxy terminus or, by repetition of the cascade, on lysines of already attached ubiquitin tags, resulting in poly-ubiquitin chains.[183] Depending on the site of the ligation on the former ubiquitin, poly-ubiquitination can lead to different fates of the target protein. While K48 polyubiquitylation generally encodes for 26S proteasomal degradation, other ubiquitylation patterns are associated with different functions. Upon recognition of K48 linked polyubiquitylated proteins via its 19S subunit, the 26S proteasome catalyses the removal of the ubiquitin units, which are recycled, and the proteolytic degradation of the tagged protein.[184]

1.4.2 PROTACs Principle

PROTACs are heterobifunctional molecules consisting of one ligand that binds to the protein of interest (POI) and another one that recruits an E3 ligase, connected by a linker. The recruitment of both the two proteins into a ternary complex by the PROTAC molecule, results in a drug-induced spatial proximity, promoting ubiquitylation of the POI and its subsequent degradation by the 26S proteasome. Upon ubiquitylation of the POI and disruption of the ternary complex, the PROTAC molecule is released and it can potentially catalyse another cycle (Figure **1.12**).[185]

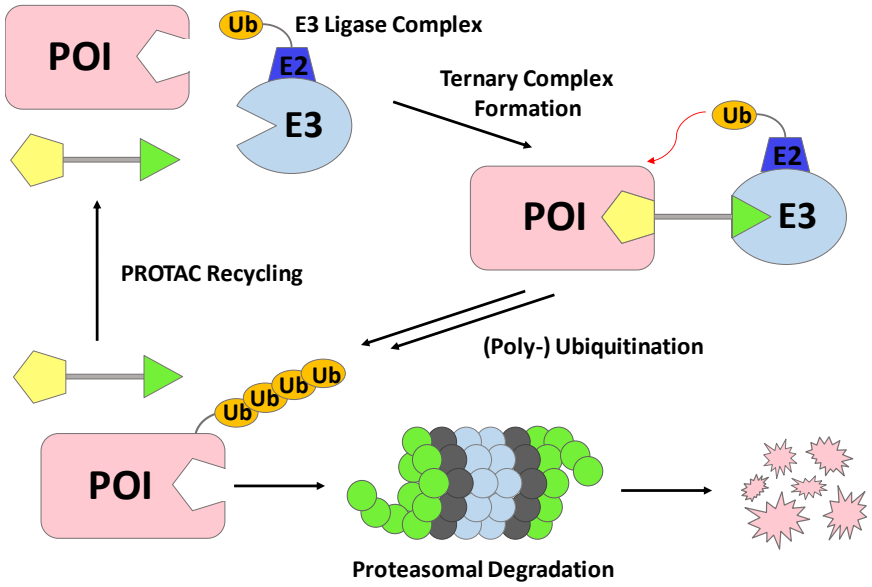

Figure 1.12: General scheme of PROTACs mechanism. The heterobifunctional molecule recruits the protein of interest (POI) and the E3 ligase complex in close proximity in the ternary complex, inducing the transfer of ubiquitin (Ub) to the POI which is subsequently recognized by the 26S proteasome and degraded.

Because of the bivalent nature of PROTACs, the formation of the ternary complex, by simultaneous binding of the POI and the E3 ligase, is strongly influenced by the concentration of the three components. In particular, saturating doses of PROTAC molecules would result in binary non-functional dimers of different PROTAC molecules with either the POI or the E3 ligase, discouraging the formation of the ternary complex and leading to a self-inhibition known as “Hook Effect”.[186, 187] However, this phenomenon is dependent on the specific system (PROTAC, target, E3 ligase recruited and their organ or disease-specific expression levels) and is not always consistently observed.[188]

1.4.3 PROTACs Advantages

Classical small molecule inhibitors rely on continuous occupancy of the active pocket of their target enzyme to exert their pharmacological activity (occupancy-driven mechanism), always competing with endogenous ligands. This results in the requirement of high binding affinity and sufficiently high and frequent dosing for target saturation, often associated with the possible occurrence of undesirable side effects.[189] Long term and prolonged exposition can induce drug resistance via point-mutations in the active site or upregulation of the target protein, decreasing the affinity and impairing the efficacy of the inhibitor.[190] In addition, classic inhibition requires the target protein to have druggable deep groves and active sites for the small molecule to bind besides being able to affect only enzymatic functions, leaving out a great amount of "undruggable proteome".[191-193]

The advantage of PROTACs paradigm relies on the transient nature of the UPS degradation event (event-driven mechanism) and on the permanent reduction of protein levels rather than classical occupancy inhibition of the enzymatic function, rendering a strong and durable interaction with the target not necessary. By complete and fast depletion of the target protein, PROTACs abolish not only enzymatic, but all its biological activities (e.g. scaffolding proteins) and, due to a short drug exposure time and the possibility to occupy non-enzymatic sites, are able to overcome the POI drug resistance mechanisms occurring for small-molecule inhibitors.[194-196] The catalytic nature of non-covalent PROTACs, allows iterative target degradation after the dissociation of the ternary complex, resulting in substoichiometric concentrations for effective POI degradation and reduced off-target toxicity and longer lasting effect.[197] For significant activity, PROTACs don't require long lasting occupancy or high affinity towards POI and E3 ligase, due to the transiency and irreversibility of the single degradation event also in presence of physiological competitors.[198, 199] Also, different binding sites on the POI, not necessarily catalytic pockets only, can be employed for PROTAC-POI interaction, expanding the target protein degradation space to some of the formerly considered "undruggable" goals, such as transcriptional factors, scaffolding and cytoskeletal proteins.[200-202] Finally, the intrinsic modularity of the heterobifunctional PROTAC design allows to fine tune selectivity and specificity, lowering adverse effects and increasing the efficacy, and in general to improve drug physiochemical properties (solubility, oral availability, cell permeability and metabolic stability), by varying the components.

1.4.4 PROTACs Design and Components

The choice of different components forming PROTAC is fundamental for potency and selectivity of the degradation process. Of particular importance is the ability of the PROTAC to induce the formation of a thermodynamically stable ternary complex which promotes the transfer of ubiquitin. This step is mainly influenced by the cooperative protein-protein interactions (PPI) forming between the POI and E3 ligase interfaces once in close proximity, impacting on the degradation efficiency much more than the single affinities between the recruiters and the corresponding POI and E3 ligase. This positive interaction can be regulated by deciding which surface of the POI (depending also on availability of lysine residues for Ub attachment) will interact with the counterpart by targeting different binding sites and/or by different insertion of the linker on the recruiter, as well as by recruiting different E3 ligases.

The development of the POI recruiting unit often starts from the chemical functionalization of existing inhibitors or known substrates. The choice of the warhead has obviously a great impact on the selectivity of the degradation and it can engage the POI via covalent or non-covalent interactions. While covalent POI recruiters have the advantage of reducing the usual three-body into a two-body assembly kinetic with probable better degradation activity in the single event, they lose the catalytic nature of non-covalent PROTACs and are often associated to off-target effects due to the high reactivity.[203] Due to PROTAC transient mode of action, a strong interaction with the target is often not necessarily required, making this strategy a great opportunity to modify known inhibitors that didn't show binding properties strong enough to be efficient as occupancy-driven inhibitors.[197, 204, 205]

Despite more than 600 E3 ligases are encoded in the human proteome,[206] only a few of them have been employed for PROTAC development, because of availability of recruiting molecules as well as their relatively high abundance in different cell lines.[207] Among them, cereblon (CRBN) and Von Hippel-Lindau (VHL) are the most commonly used, followed by inhibitor of apoptosis protein (IAP), mouse double minute 2 (MDM2) and others to a minor extent.[208]

The VHL protein is a member of the VHL E3 ligase complex (VBC) together with the adaptor proteins cullin 2, elongins B and C, and RBX1. Physiologically, it acts as a tumor suppressor by degrading hypoxia-inducible factors (HIFs).[209-211] Recruiters for VHL were initially derived from a small peptide fragment of its natural substrate, hypoxia-inducible factor 1α (HIF-1α) (Figure **1.13, 30**),[212] later optimized via *in silico* fragment-based screening and consequent SAR studies to improve binding properties (**31**).[213-218] Negative controls for validating the mode of action of VHL-dependent PROTACs can be acquired by epimerization of the chiral hydroxyl group in the proline ring (**32**).

CRBN forms together with CUL4, RBX1, and DDB1, the CRL4 E3 ligase complex and has a central role in nervous system development during embryogenesis.[219, 220] This E3 ligase is often chemically recruited by thalidomide (**33**) and its derivatives pomalidomide (**34**), lenalidomide (**35**), also known as immunomodulatory drugs (IMiDs).[219, 221] Negative controls of CRBN-dependent PROTACs can be generated by introducing an *N*-methyl group on glutarimide ring (**36**).

Von Hippel-Lindau (VHL) Recruiters:

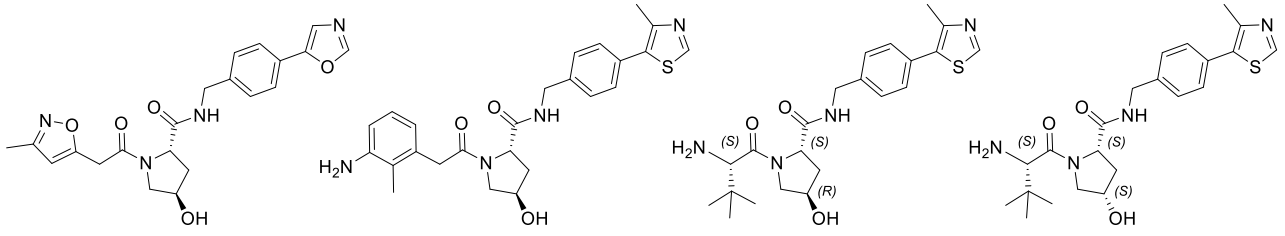

Peptidic fragment of HIF-1α | **First generation VHL recruiter (30)** | **Last generation VHL recruiter (31)** | **Inactive (32)**

Cereblon (CRBN) Recruiters:

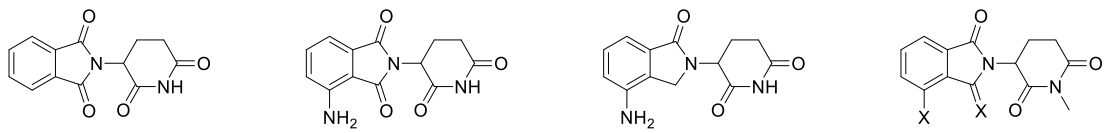

Thalidomide (33) | **Pomalidomide (34)** | **Lenalidomide (35)** | **Inactive (36)**

Figure 1.13: Structure of most common VHL and CRBN recruiters.

Given that different E3 ligases present diverse substrate affinities, as well as subcellular localization, tissue expression levels (e.g. central nervous system specific E3 ligases) and disease-related enrichment profile, varying between them could permit to fine tune selectivity and optimize the efficiency of targeted protein degradation of a specific POI.[222] In addition to pursue target selectivity (resulting in lower off-target effects), the interest in expanding the E3 ligase repertoire is directed to overcome drug resistance, observed in the prolonged treatment of certain tumours, by mutations or reduced expression of the engaged E3 ligase, when this is not essential for cancer cells.[223-227]

Another fundamental aspect of the PROTAC strategy is the design of the linker, whose length and nature are influencing not only the efficiency of the ternary complex formation and therefore of POI degradation, but also the biological and physiochemical properties of the drug, such as target selectivity, cooperativity, bio-distribution, metabolic stability, membrane permeability, and aqueous solubility.[228]

Linker length has a significant effect on the degradation activity of PROTAC by defining the spatial vicinity of the POI with the E3 ligase.[229] If the linker is too short, steric hindrance will impair the formation of the ternary complex, while too long linkers may hinder protein-protein interaction (PPI) and keep them away from each other, apart from reducing membrane permeability due to higher molecular weight. In general, longer linkers are more likely to succeed in the preliminary design of PROTACs, followed by a stepwise shortening to identify the optimal linker length.[230] Once determined the optimal length and the desired orientation also thanks to crystal structure or computational predictions, increasing the linker rigidity can positively influence cooperativity in the formation of the ternary complex by constraining a PROTAC in its bioactive conformation, resulting in higher selectivity and improved protein degradation.[231, 232] After identifying a range of suitable linker lengths, the chemical composition of the linker as well as its flexibility is modulated to produce a finely-tuned balance of target degradation, cellular permeability, and aqueous solubility. The most frequently used linker compositions are flexible polyethylene glycol (PEG) and (un)saturated alkane chains with varying lengths.[233] In comparison to the less polar alkyl linkers, PEG linkers (as well as chains containing nitrogen atoms), present an improved hydrophilicity, solubility and membrane permeability. Linear linkers are then optimized by introducing rigid moieties, such as alkynes, saturated heterocycles (piperazine and piperidine) or aromatic rings, improving solubility, cell permeability and oral bioavailability.[231, 234, 235] Introduction of triazolic rings via click chemistry, often utilized to synthesise modular PROTACs, was shown to additionally improve metabolic stability.[236]

1.4.5 PROTACs History and Future Perspective

The concept of Proteolysis Targeting Chimeras (PROTACs) was first proposed in 2001 by *Crews* and *Deshaies*, reporting a bifunctional molecule able to induce UPS degradation of methionine aminopeptidase 2 (MetAP-2) by combining its covalent inhibitor ovalicin and a peptide ligand for the E3 ligase SCFβ-TRCP.[237] In 2004, the discovery of a peptide derived from the VHL endogenous substrate hypoxia-inducible factor 1α (HIF1α) led to the creation of the first cell penetrating PROTACs against different POIs.[238, 212, 239] Although peptidic PROTACs had the advantage of high biocompatibility and low toxicity, they were associated with limited cell permeability. This guided the development of entirely small molecule PROTACs via recruitment of MDM2 E3 ligase against

androgen receptor (AR) in 2008 and in 2010 recruiting cell inhibitor of apoptosis protein (cIAP).[240, 241] The identification in 2010 of CRBN as the direct target of thalidomide and its analogues,[221] opened the way to the application of IMiDs as CRBN E3 ligase recruiters for PROTAC development.[242] Another milestone has been the discovery in 2012 of the first small molecule ligand for VHL through *in silico* and fragment-based screening and further SAR optimization for the development of potent VHL-recruiting PROTACs.[214, 215, 217, 218, 243, 244] In the last decade, the academic and pharmaceutical interest in this promising technique increased exponentially,[245] leading to the entrance in clinical trials of the first two PROTACs from *Arvinas* against AR (ARV-110, NCT03888612) and ER (ARV-471, NCT04072952), in 2019, as anticancer agents, respectively in phase II and phase III at the moment.[246] Up to date, altogether, 16 protein degraders entered in phase I or phase I/II clinical trials.[246]

Notably, PROTAC technology has been applied also to treat autoinflammatory and autoimmune diseases, targeting different targets such as key proteins in the immune response interleukin-1 receptor-associated kinase 3 and 4 (IRAK3 and IRAK4),[247-250] histone deacetylases (HDACs),[251, 252] indoleamine, 3-dioxygenase 1 (IDO1),[253] sirtuin 2 (Sirt2),[254, 255] RIPk2 and more recently STING (**1.4.6**).[197, 204]

The great interest that PROTACs and targeted protein degradation attracted, together with the promising results from clinical trials lately released, demonstrated the great potential of these emerging technologies in treating different types of diseases. For what concerns the future of PROTAC research, the focus lies on expanding the E3 ligase toolbox for reaching case by case, better selectivity, efficiency and overcoming potential drug resistance.[207] Major challenges associated with the nature of these molecules and their high molecular weight will be related to the improvement of pharmaceutical properties like permeability, solubility, stability and oral bioavailability.[256] Finally, recent advances and application of *in silico* approaches to the PROTAC paradigm, like Rosetta, PRosettaC, PROTAC-Model and others, will enable the computational rationalization of protein-protein interactions and ternary complex formation, improving the optimization of PROTAC design and efficiency.[257-260]

1.4.6 STING-degrading PROTACs

A first example of STING-degrading PROTAC SP-23 (**37**) was developed in 2022 by *Liu et al.* combining a STING recruiting unit based on the covalent palmitoylation inhibitor C-170 and the cereblon (CRBN) E3 ligase ligand pomalidomide (**Figure 1.14**). This compound, with a DC_{50} (half maximal degrading concentration) of 3.2 µM *in vitro*, showed also anti-inflammatory activity in a murine model of acute kidney injury.[261] More recently, *Zhu et al.* designed the STING PROTAC UN9036 (**38**) based on a diABZI STING agonist and recruiting Von Hippel-Lindau (VHL) E3 ligase (**Figure 1.14**). Despite the ability to reduce STING levels in renal cell carcinoma (RCC) cell line and therefore reducing induced inflammation, the agonist-based PROTAC retained partial agonist activity, triggering STING activation before inducing its proteasomal degradation.[262]

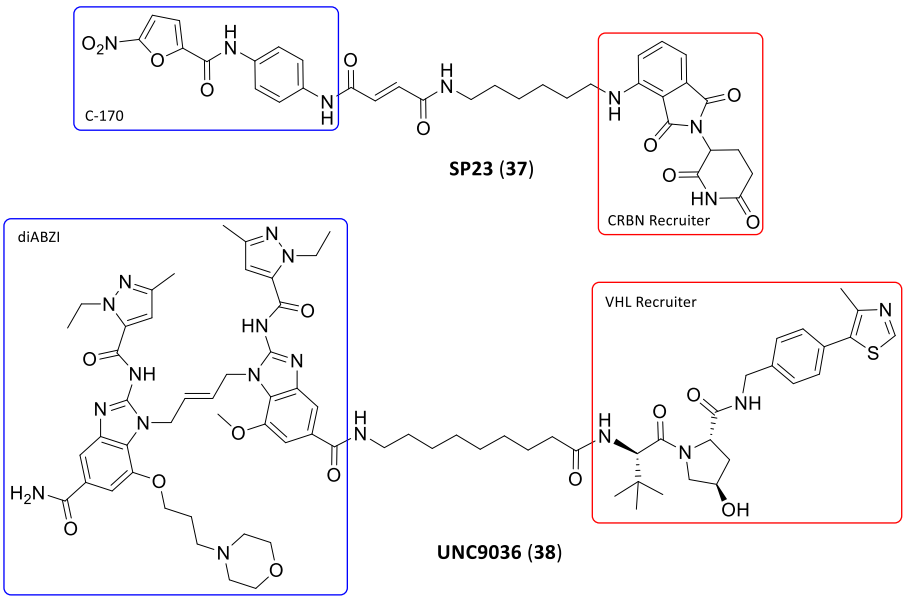

Figure 1.14: STING-degrading PROTACs.

2 Aim of the Project

Due to the central role of the cGAS-STING pathway in several disease contexts, the interest in regulating its activity is constantly rising. Along with the antitumor action of STING agonists, used in cancer immunotherapy or as vaccine adjuvants, efforts in inducing downregulation and consequent reduction of abnormal cGAS-STING -driven inflammation are increasing. As detailed in the introduction, in fact, STING antagonists validated this innate immune pathway as a promising therapeutic target for autoimmune and autoinflammatory diseases, invasive tumour formation and aging-related disorders.

Despite the development of STING covalent and non-covalent inhibitors still remains predominant in the medicinal chemistry research community, the recent rise of targeted protein degradation techniques created novel opportunities to reach efficient and durable downregulation of inflammation. Among these, proteolysis targeting chimeras (PROTACs) represent the most promising strategy, possibly overcoming the disadvantages of classical occupancy-driven inhibition in terms of off-side effects and loss of efficiency due to mutations.

The main goal of this research project is the development of novel STING-degrading PROTACs via design and synthesis of different POI and E3 ligase recruiters to establish, in a second phase, the optimal configuration by comparison of their different biological activities.

Initially the recruitment of STING, as the target of the degradation, will be attempted by designing and synthesising a derivative of its natural substrate cGAMP with the insertion of a linker for the connection with an E3 ligase recruiter. Different linker positions on the cyclic dinucleotide will be tested to hinder as little as possible the interaction with the protein dimer and permit the binding. Alternative options, such as non-CDN STING agonists or inhibitors, will be evaluated for overcoming stability and cellular permeability issues typical of cyclic dinucleotides.

Different E3 ligases will be targeted for recruitment. Besides classical cereblon (CRBN) and Von Hippel-Lindau (VHL), often employed in the PROTAC strategy, the focus will move on the design and synthesis of novel recruiters for other E3 ligases in the effort of optimizing the potency and selectivity of STING degradation.

The design of the linker will start from flexible PEG-based structures to identify the optimal linker length for then progressing, if necessary, to more rigid and pre-organized architectures. The introduction of complementary clickable moieties in the linker, will allow an efficient assembly of the final molecule, simplifying the synthesis of the two halves and permitting to maintain a high degree of modularity. With this design, Cu(I) catalysed click chemistry between a terminal azide and a terminal alkyne will be used to generate an array of novel PROTACs for STING targeted degradation by the fast combination of different POI and E3 ligase recruiters.

3 Results and Discussion

In the following section, the design and synthesis of potential PROTAC molecules will be described. These compounds have the aim of promoting STING degradation through the ubiquitin – proteasome system. Once obtained, this library of compounds was handed over to biochemistry for the evaluation of pharmacological properties.

3.1 Recruiting STING

The first issue to be addressed in order to design a feasible PROTAC degrader, is STING recruitment. As our protein of interest (POI), target of the degradation, it requires a small molecule to interact with, in order to allow the formation of the ternary complex and the consequent transfer of ubiquitin (Figure **3.1**). As previously described, the most important condition is the specificity of this interaction to limit possible side reactions that could impair the effect of the drug or produce undesired effects. In this regard, the current knowledge of STING substrates and non-covalent inhibitors was considered to identify suitable candidates that would be easy to modify synthetically and where the chemical modification would not impair the recognition and interaction with STING.

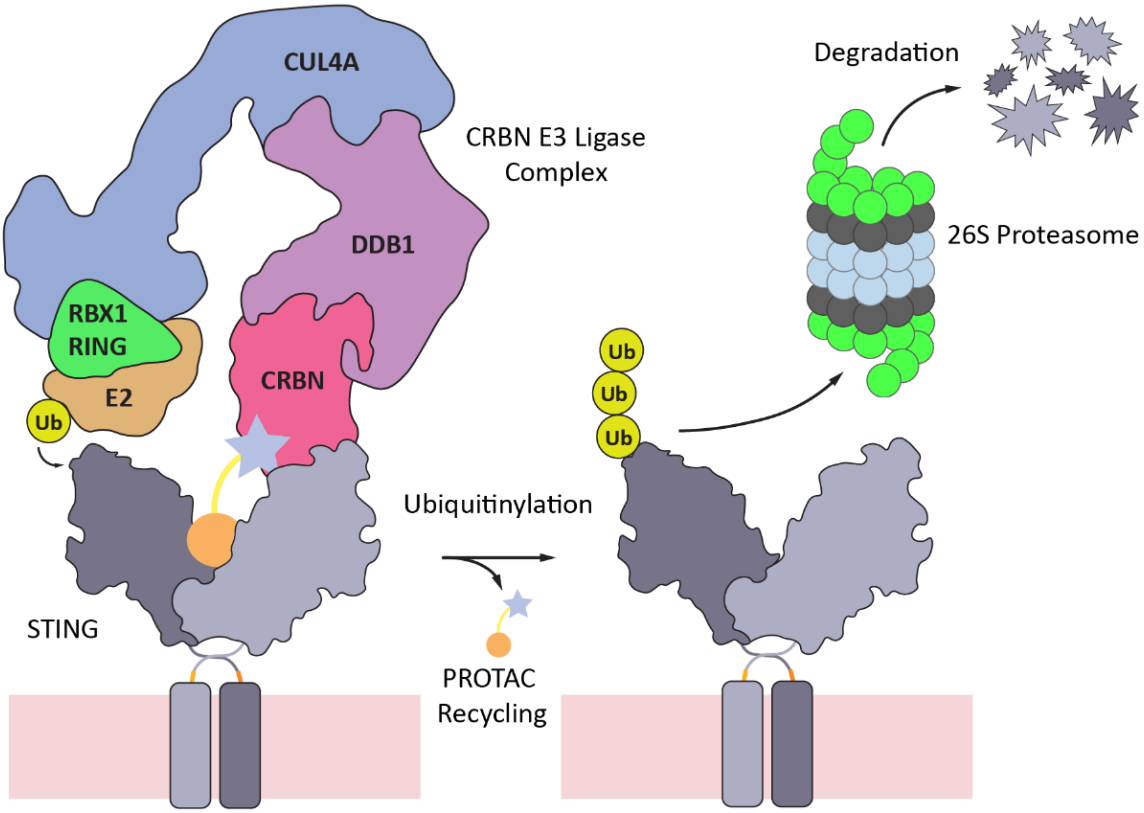

Figure 3.1: Schematic representation of CRBN-based STING PROTACs and induced proteasomal degradation.

3.1.1 Design of cGAMP-Based STING Recruiters

As first choice, cGAMP has been considered as recruiting element for the interaction with STING. The idea is that the modified cGAMP will be recognized by STING in the active site, taking the protein surface in close proximity to the E3 ligase complex recruited by the other side of the PROTAC molecule, promoting the ubiquitination of the POI and the proteasomal degradation.

As the natural substrate of STING, a cGAMP-based PROTAC should provide a high selectivity and a moderately strong binding, depending on the site of the modification. This chemical modification has indeed to be designed to disturb the recognition and the binding in the STING active site as little as possible: the presence of a sterically demanding linker that would hinder and not allow the closure of the two units of the homodimer or the alteration of a relevant group involved in the interaction with the active site, could weaken the binding and prejudice the recognition of the recruiter.

In the work of *Zhang et al.*,[30] the interaction of natural cGAMP with human STING has been described. Therefore, by analysing the crystal structure of the binding complex, shown in Figure **3.2**, it was possible to identify which sites of the CDN would be less hindered and less interacting, hence more accessible for the linker attachment. Modifications on the phosphate were avoided to not reduce the stability of the CDN, as well as the introduction of new alkyl groups on the sugar hydroxyls, which has already proved to heavily reduce the binding.[263]

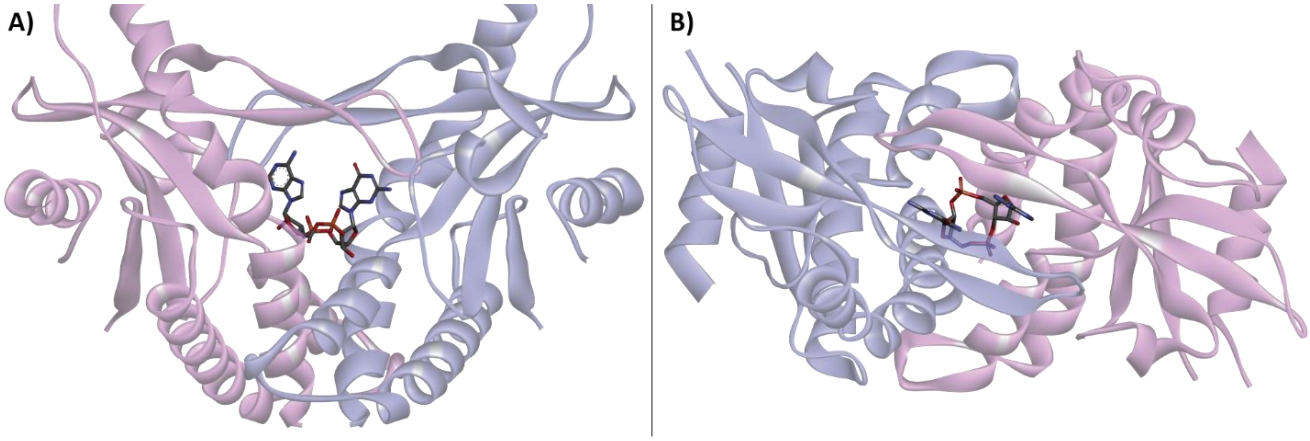

Figure 3.2: Crystal structure of STING in the closed conformation, bound to cGAMP in the active site.[30] **A**) Side view of the complex. **B**) View from above, with nucleobases pointing in between the two STING units.

In conclusion, the position 6 on adenosine and guanosine were identified as the most suitable for the insertion of the chemical modification, pointing in the space between the two monomeric units of the enzyme when complexed, where the linker would cause the least steric clash with the protein. In particular, the functionalization of the amino group of adenosine (Figure **3.3**) would also not affect the formation of hydrogen bond interactions, observed in the crystal structure of the natural cGAMP (chapter **1.2**). Position *C*8 of the two purines or position *N*2 of guanosine, were also taken into consideration as alternative options.

Regarding the nature of the linker, it was decided to focus mainly on polyethylene glycol (PEG) - based structures, due to their flexibility and improved water solubility in comparison to alkane alternatives, nonetheless for the relative ease of chemical modification.

Another feature that was selected for the PROTAC structure is the adoption of clickable moieties. Beyond the general advantages of Cu(I)-catalysed azide-alkyne cycloaddition (CuAAC) in terms of selectivity, specificity, speed and tolerance of other functional groups, this strategy would allow a substantial simplification in the synthesis of two distinct subunits and a high degree of modularity by combining together different recruiters. Moreover, the introduction of triazole ring into the linker has been shown in different cases to improve cell permeability, solubility and stability by influencing the physiochemical properties of the molecule, along with the increase of linker rigidity, potentially resulting in a more stable ternary complex and potent PROTAC.[257, 264-266]

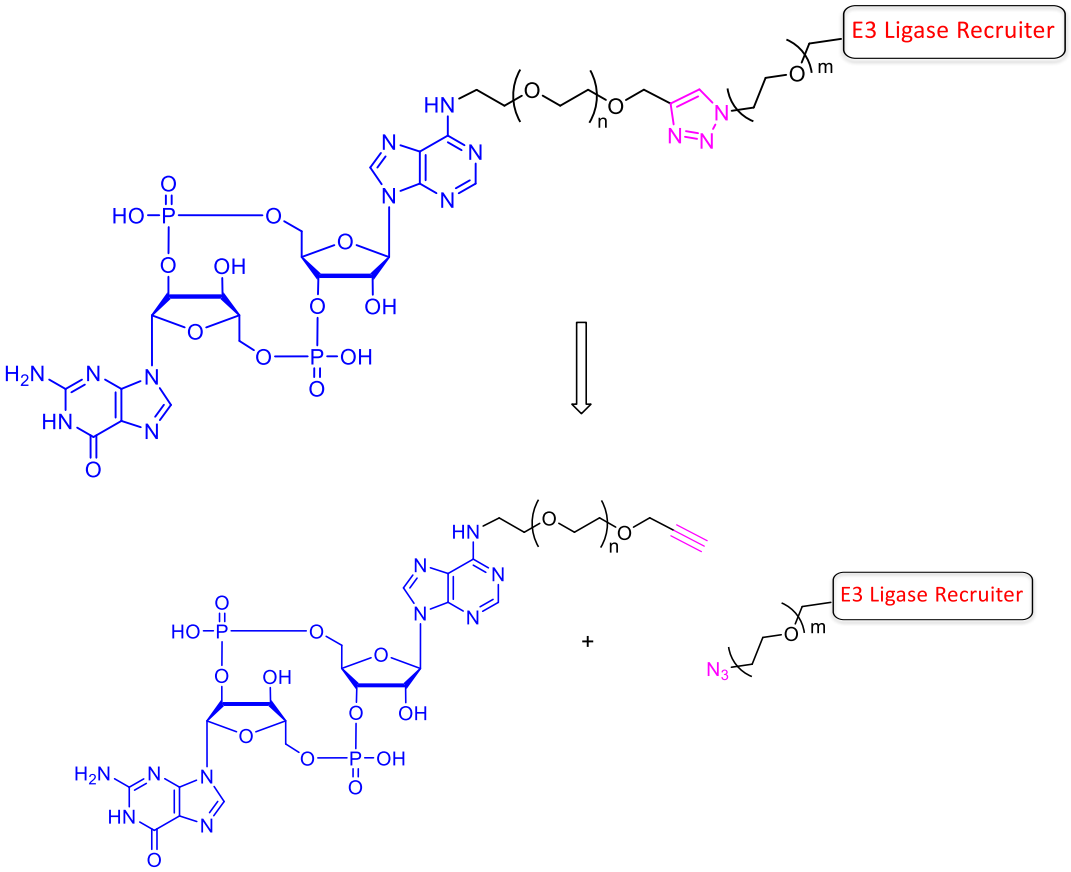

Figure 3.3: Structure of a potential STING degrading PROTAC based on a *N*6A modified cGAMP derivative (blue), connected to an E3 ligase (red) through a PEG linker and via click chemistry (violet).

As a general base for the synthesis of cGAMP derivatives, we relied on phosphoramidite and phosphate chemistry, previously developed in our group with opportune modifications, which allowed to obtain CDNs in moderately high yields, compared to other published procedures.[159, 163, 267-269] As shown in the retrosynthetic scheme in Scheme **3.1**, two appropriately protected nucleoside precursors were respectively converted into a 2'- protected phosphate (guanosine) and a 3'-phosphoramidite (adenosine). These compounds were then coupled to obtain a protected linear dimer which, after the removal of a protecting group on the phosphate, was cyclized applying P(V) chemistry. After the cleavage of the remaining protecting groups, the final products were purified by high-performance liquid chromatography (HPLC) to obtain cGAMP analogues in high purity.

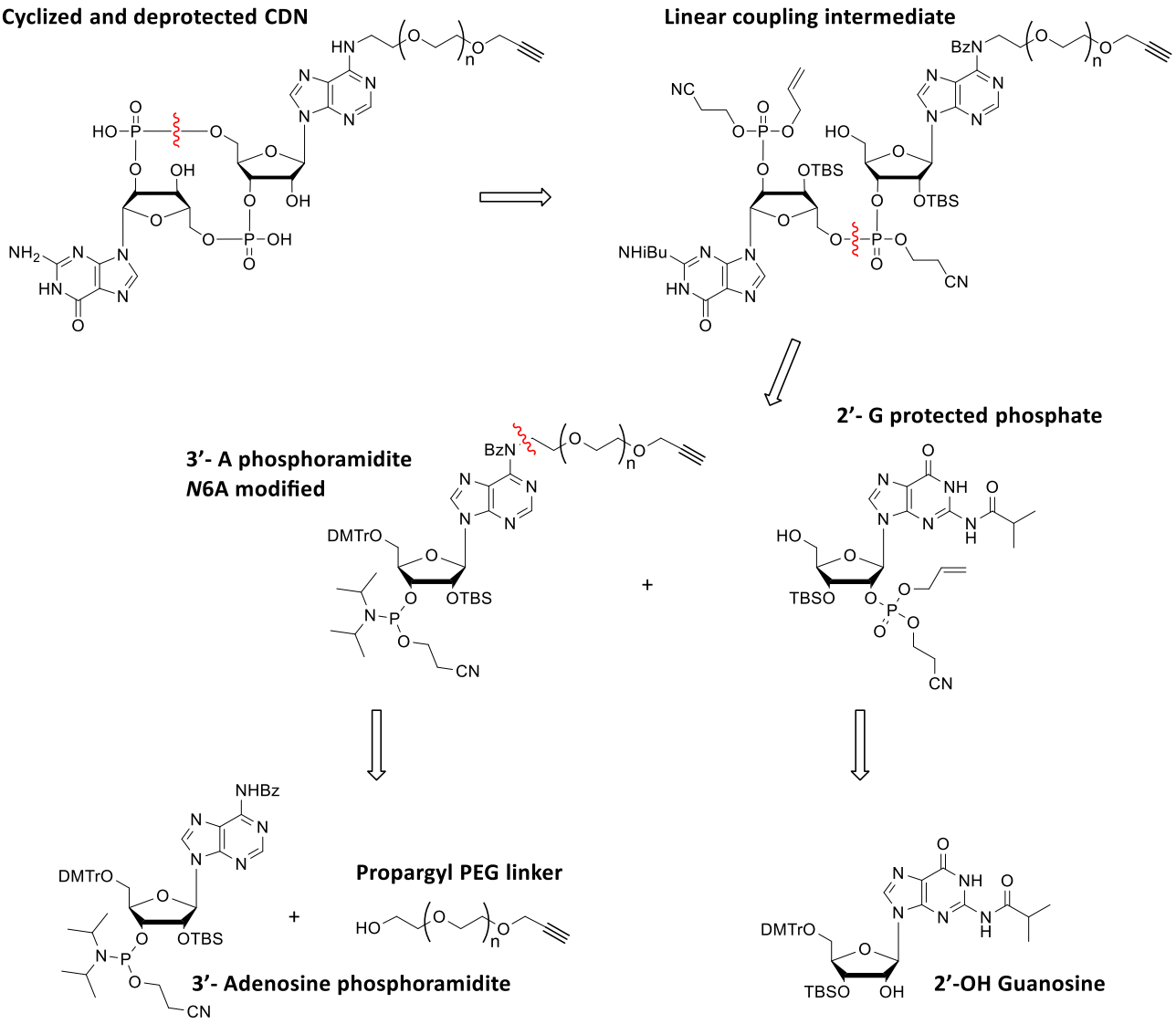

Scheme 3.1: Retrosynthetic analyses for the synthesis of *N*6A cGAMP propargyl PEG STING recruiter.

Another consideration in the direction of a higher variability of the system and reduced complexity of the synthesis, was the ambition of creating a cGAMP derivative that could be further modified after the closure of the dinucleotide. In this way, the CDN synthesis, usually characterized by multiple steps and an overall low yield, could be performed for a single compound later functionalized. Hence, it was initially aimed at a cGAMP modification holding a chlorine atom on the position 6 of the adenosine aromatic ring. This chlorinated version of the CDN would have been the starting point for the insertion of different linkers and E3 ligase recruiters by nucleophilic aromatic substitution.[270-272] As shown in Scheme **3.2**, the synthesis was successful until the cyclization step, which failed probably due to an undesired interaction with the cyclizing agent MSNT.

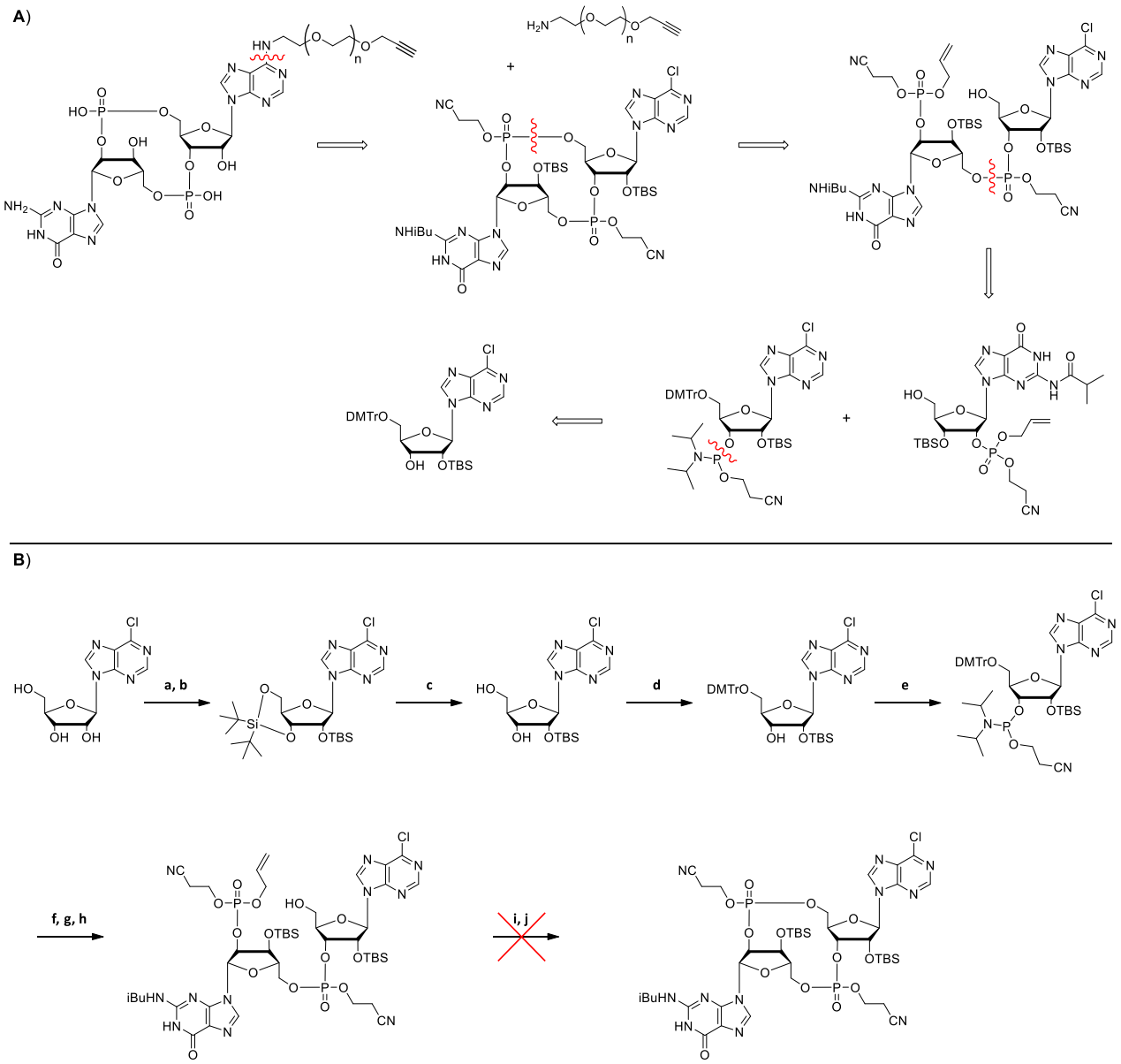

Scheme 3.2: **A**) Retrosynthetic analyses for the synthesis of *N*6A chlorinated cGAMP derivative. **B**) Unsuccessful synthetic procedure for the *N*6A chlorinated cGAMP derivative: **a**) di-*tert*-butylsilyl bis(trifluoromethanesulfonate), DMF, N_2, 0 °C, 1 hour; **b**) TBSCl, imidazole, r.t., overnight, 95 % over two steps; **c**) HF, Py, DCM, 0 °C, 2 hours, 72 %; **d**) DMTrCl, Py, N_2, r.t., overnight, 69 %; **e**) 2-cyanoethyl *N,N,N',N'*-tetraisopropylphosphorodiamidite, PyTFA, MeCN, Ar, r.t., overnight; **f**) **3**, BTT, MeCN, r.t., 2 hours; **g**) tBuOOH, r.t., 40 min; **h**) 3 % DCA/DCM, r.t., 15 min, 50 % over 3 steps; **i**) NaI, acetone, reflux, 5 hours; **j**) MSNT, Py, r.t., 24 hours, no conversion over 2 steps.

This strategy, reported above for informational purposes only and not included in this dissertation, was therefore abandoned in favour of an alternative approach consisting in the insertion via *Mitsunobu reaction* of the PEG linker with a terminal alkyne on adenosine's commercially available phosphoramidite, described in detail in the following section.

3.1.2 Synthesis of cGAMP-Based STING Recruiters

The first part of the synthesis consisted in the conversion of commercially available *N*2-isobutyryl guanosine to the corresponding 2'- protected phosphate (Scheme **3.3**).

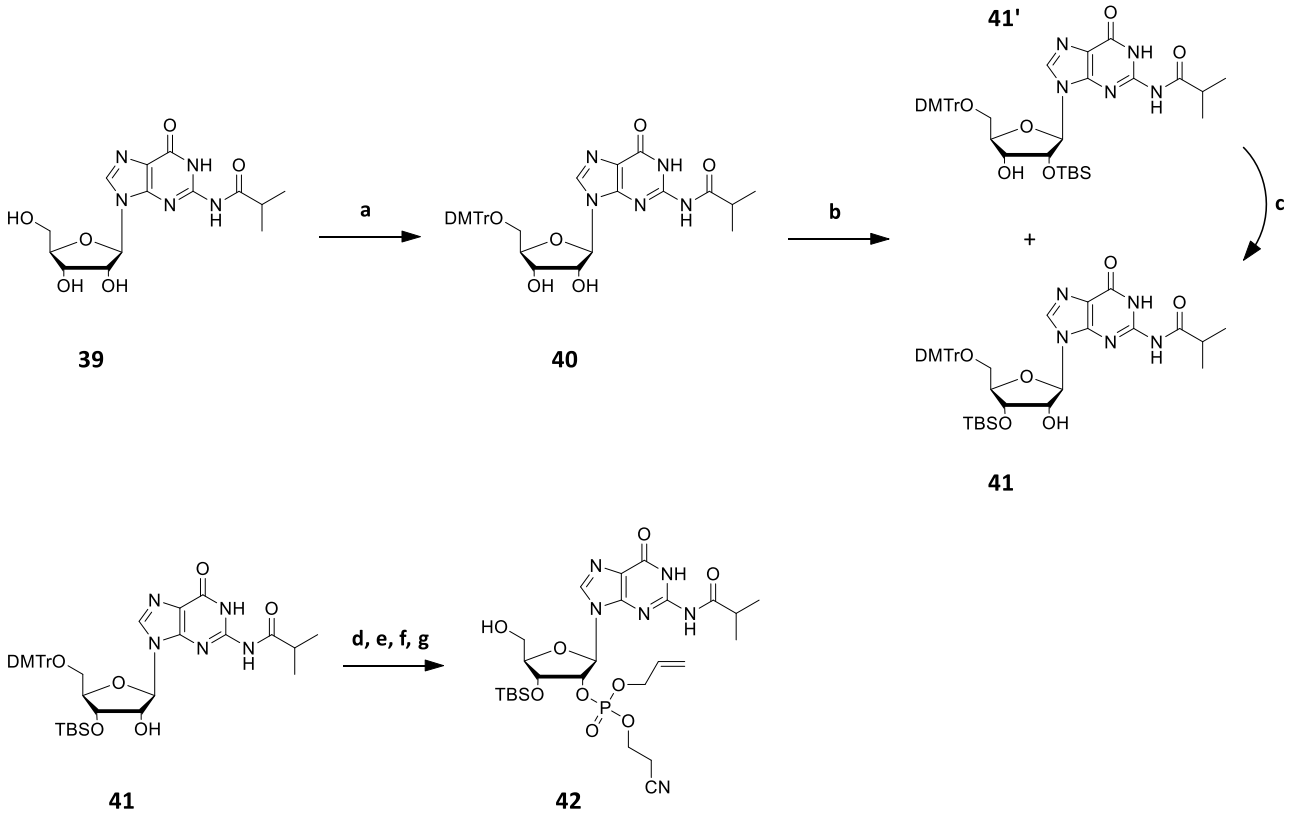

Scheme 3.3: Synthesis of the *N*2-iBu-3'-*O*TBS-guanosine-2'-phosphate **42**. **a**) DMTrCl, pyridine, Ar, r.t., overnight, 70 %; **b**) TBDMSCl (1 eq), imidazole, 1:1:10 Py:DMF:DCM, Ar, r.t., overnight; **c**) Et_3N, MeOH, r.t., 30 min; **d**) 2-cyanoethyl *N,N,N',N'*-tetraisopropylphosphorodiamidite, PyTFA, MeCN, Ar, r.t., overnight; **e**) allyl alcohol, BTT, r.t., 2.5 hours; **f**) tBuOOH, r.t., 40 min; **g**) 3 % DCA/DCM, r.t., 20 min, 87 % over 4 steps.

As shown in the first step of Scheme **3.3**, the 5'-OH group of the commercially available **39** was selectively protected with DMTrCl followed by the reaction of **40** with 1 equivalent of TBDMSCl, yielding a mixture of 3'- and 2'- TBDMS protected isomers **41** and **41'**. After separation, the undesired isomer **41'** was re-isomerized to **41** by using a mixture of triethylamine and methanol. Once obtained the desired isomer, **41** was converted to the 2'- phosphate **42** by a first reaction with 2-cyanoethyl *N,N,N',N'*-tetraisopropylphosphorodiamidite and pyridine trifluoroacetate (PyTFA) as activator for the formation of the 2'-cyanoethyl phosphoramidite. Because of the marked sensitivity towards hydrolysis, the phosphoramidite was directly protected with allyl alcohol using BTT as coupling agent and the P(III) subsequently oxidized to P(V) with tBuOOH. At last, the DMTr group on the 5'-OH was removed with 3 % DCA in DCM, obtaining the desired phosphate **42** in 87 % yield over four steps. In conclusion, the 2'- protected phosphate (**42**) was obtained in a 61 % yield over 6 steps starting from commercially available *N*2-isobutyryl guanosine (**39**), as a mixture of two isomers due to the chirality of the trisubstituted P(V), which was not further purified (Figure **3.4**).

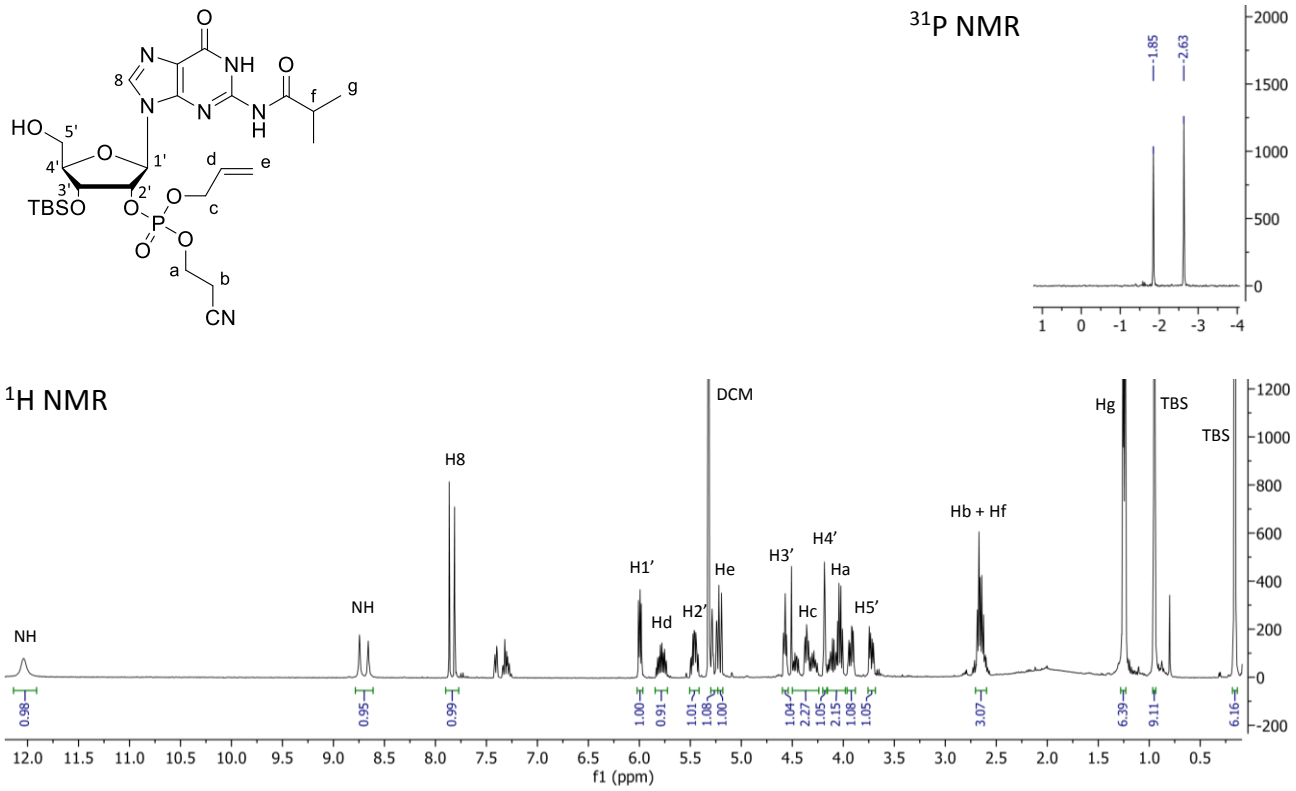

Figure 3.4: Structure, 400 MHz ^{1}H NMR and 162 MHz ^{31}P NMR spectra of **42** (mixture of 2 diastereomers).

On the second half of the CDN (Scheme **3.4**), the commercially available protected adenosine phosphoramidite **43** was selectively labelled through *Mitsunobu reaction* on the benzoyl protected *N*6 position with propargyl PEG alcohols available for click reaction (**44** and **45**). The reagents, together with triphenylphosphine and DEAD, were stirred under inert dry atmosphere to reach conversion to the desired *N*6-PEG propargyl adenosine phosphoramidites **46** and **47** after optimization of the conditions. This intermediates were immediately used in the following coupling step with the 2'- guanosine phosphate **42**, after a fast purification, because of phosphoramidites susceptibility to hydrolysis that would result in an inseparable mixture from the desired product.

In order to cover a wider space in terms of different linker lengths, two different propargyl PEG alcohols were used for this intermediate: propargyl PEG2 (**44**) and propargyl PEG3 (**45**) alcohols, commonly synthesized according to published literature from di- or triethylene glycol in presence of tBuOK followed by a stoichiometric amount of propargyl bromide.

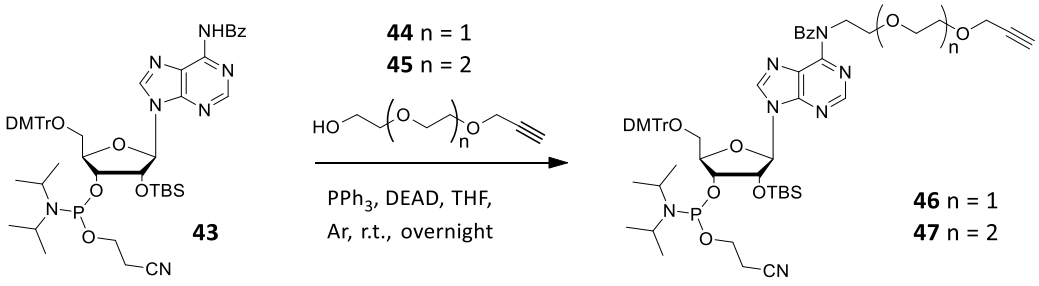

Scheme 3.4: Functionalization of the commercially available *N*6-Bz-2'-*O*TBS-5'-*O*DMTr protected adenosine 3'-phosphoramidite **43** with propargyl PEG2 **44** and PEG3 **45** alcohol via *Mitsunobu reaction* on the benzoyl protected *N*6 position to give **46** and **47**, respectively.

Once obtained, the two halves of the CDN were coupled using BTT as activator for the P(III) of the adenosine phosphoramidite (**46** and **47**), which reacts with the 5'-OH of the guanosine phosphate (**42**), as shown in Scheme **3.5**. The trialkylphosphite intermediate was then oxidised to phosphate with tBuOOH and the DMTr group was removed in 3 % DCA in DCM, to generate the 3'-phosphate-5' connection between A and G. The linear coupled products **48** and **49** were obtained after purification by column chromatography with 86 % and 74 % yield over 3 steps respectively. Due to the chirality of the two phosphotriester moieties, each isolated product resulted in a mixture of four diastereoisomers which, in addition to the large size of the molecule, did not allow the characterization of these intermediates by ^{1}H and ^{13}C NMR spectroscopy, which however was possible by ^{31}P NMR and HRMS.

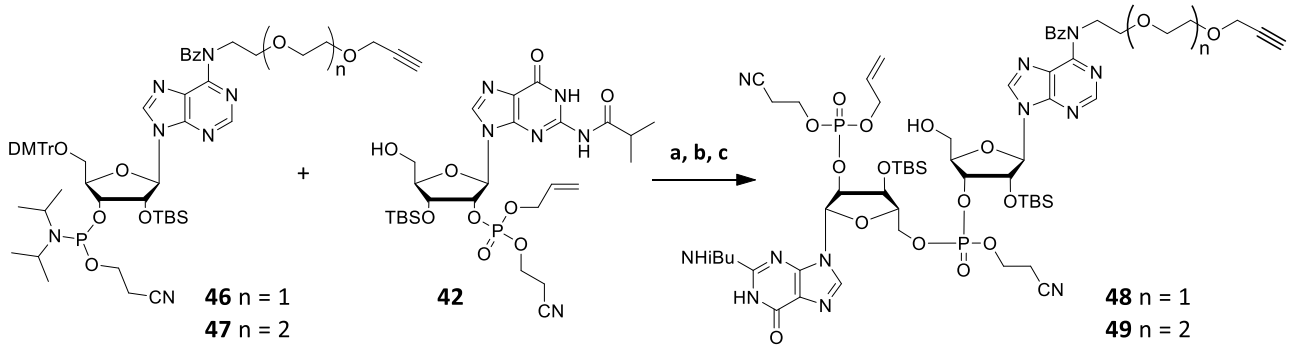

Scheme 3.5: Linear coupling reaction between the *N*6 modified adenosine 3'-phosphoramidites (**46** and **47**) and the protected guanosine 2'-phosphate **42**. **a**) BTT, MeCN, Ar, r.t., 2.5 hours; **b**) tBuOOH, r.t., 40 min; **c**) 3 % DCA/DCM, r.t., 20 min. **48**: 86 %, **49**: 74 % yield over 3 steps.

On the guanosine 2'- phosphate moiety, the allyl protecting group on **48** and **49** was then cleaved using sodium iodide in refluxing acetone (Scheme **3.6**). After a rough purification from the residual iodide, the product was directly used for the cyclization reaction to give **50** and **51**. In this step the phosphate is activated by 1-(mesitylene-2-sulfonyl)-3-nitro-1H-1,2,4-triazole (MSNT) and then attached by the 5'-OH, closing the cycle between the two nucleotides. Once again, the high complexity of the isomeric mixture for the two chiral phosphotriesters made the conventional NMR characterization impossible, despite ^{31}P NMR and HRMS. The final deprotection to **52** and **53** of the nucleobases and phosphates was performed initially by using a 33 % solution of methylamine in absolute EtOH to cleave all the protecting groups except the TBS groups, which were subsequently removed with HF in triethylamine. The crude cGAMP derivatives were precipitated in cold acetone and further purified by reversed phase HPLC to give a yield over four steps of 35 % for the *N*6A propargyl PEG2 cGAMP **52** and 39 % for the *N*6A propargyl PEG3 cGAMP **53** (Figure **3.5**).

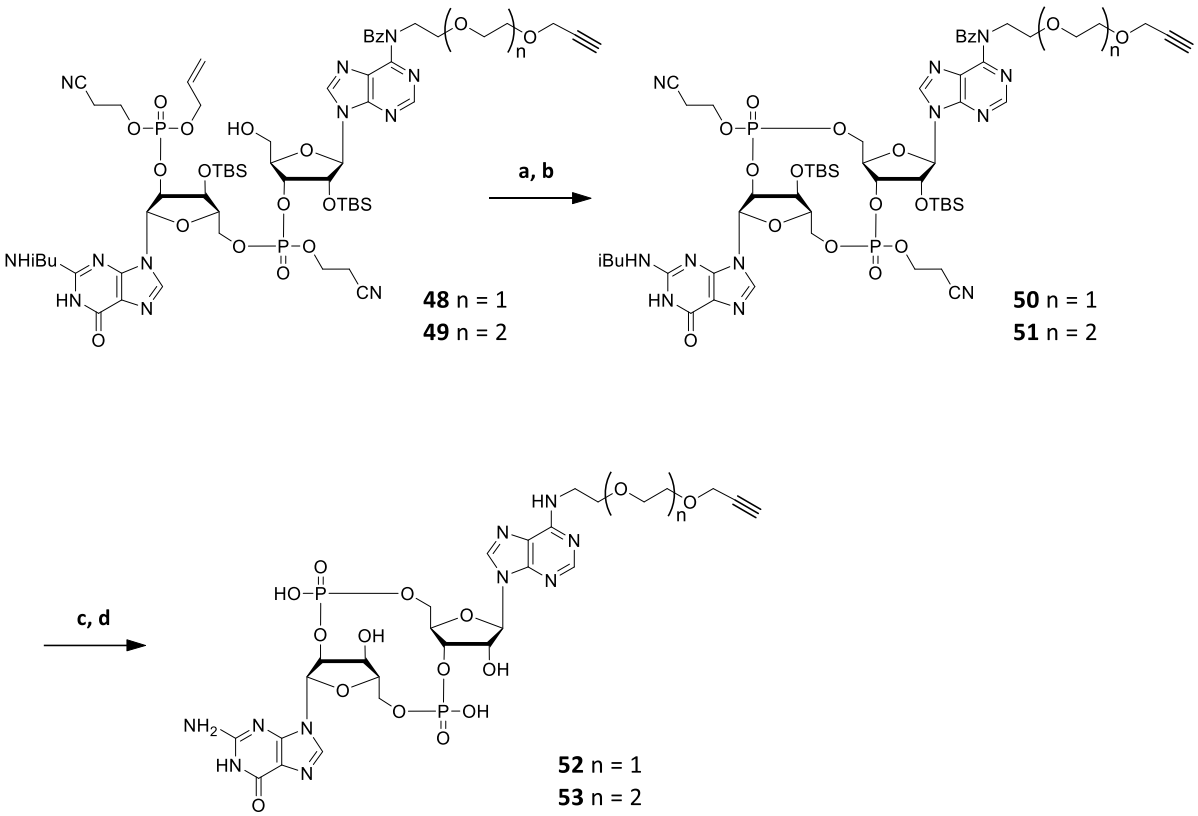

Scheme 3.6: Allyl deprotection, cyclization and final deprotection. **a**) NaI, acetone, reflux, 5 hours; **b**) MSNT, Py, r.t., 24 hours; **c**) 33 % $MeNH_2$ in EtOH, r.t. 2.5 hours; **d**) Et_3N x 3HF, r.t., overnight. **52**: 35 %, **53**: 39 % yield over 4 steps.

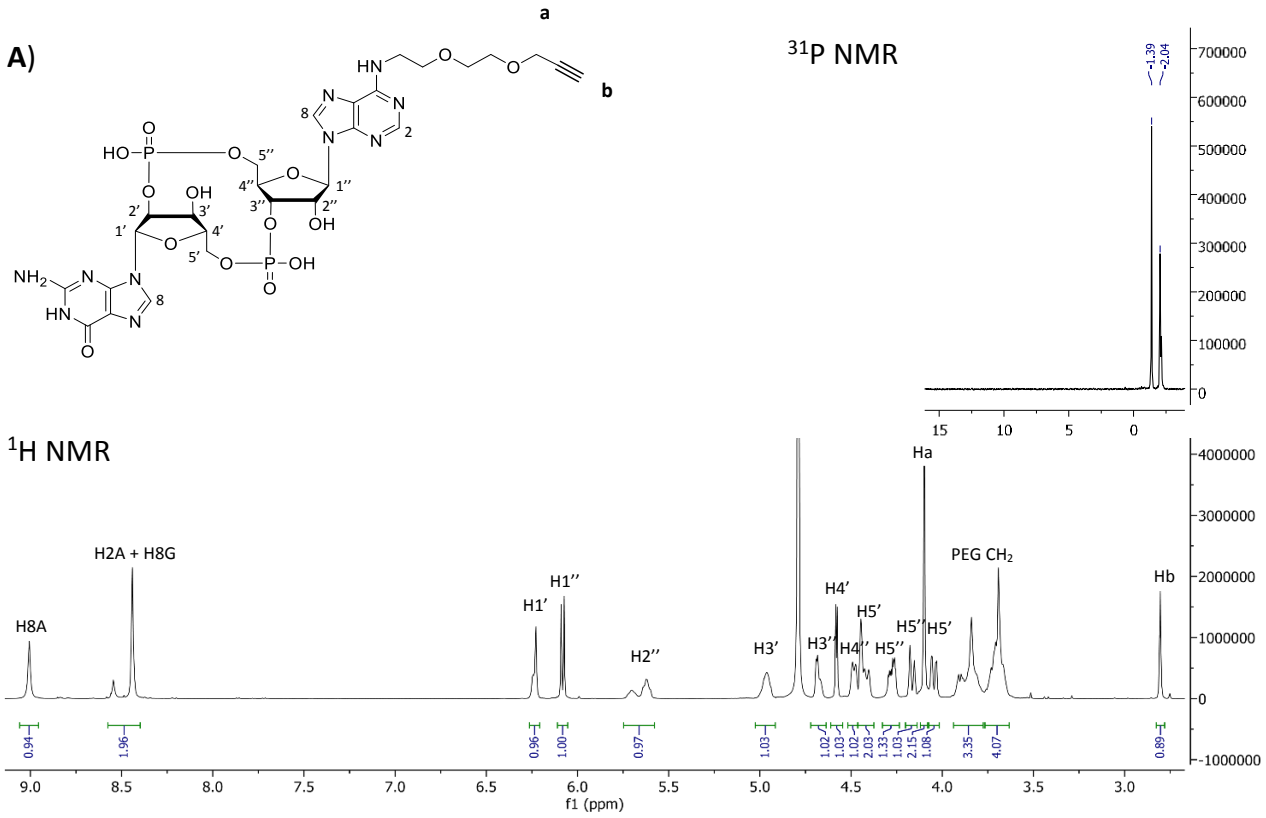

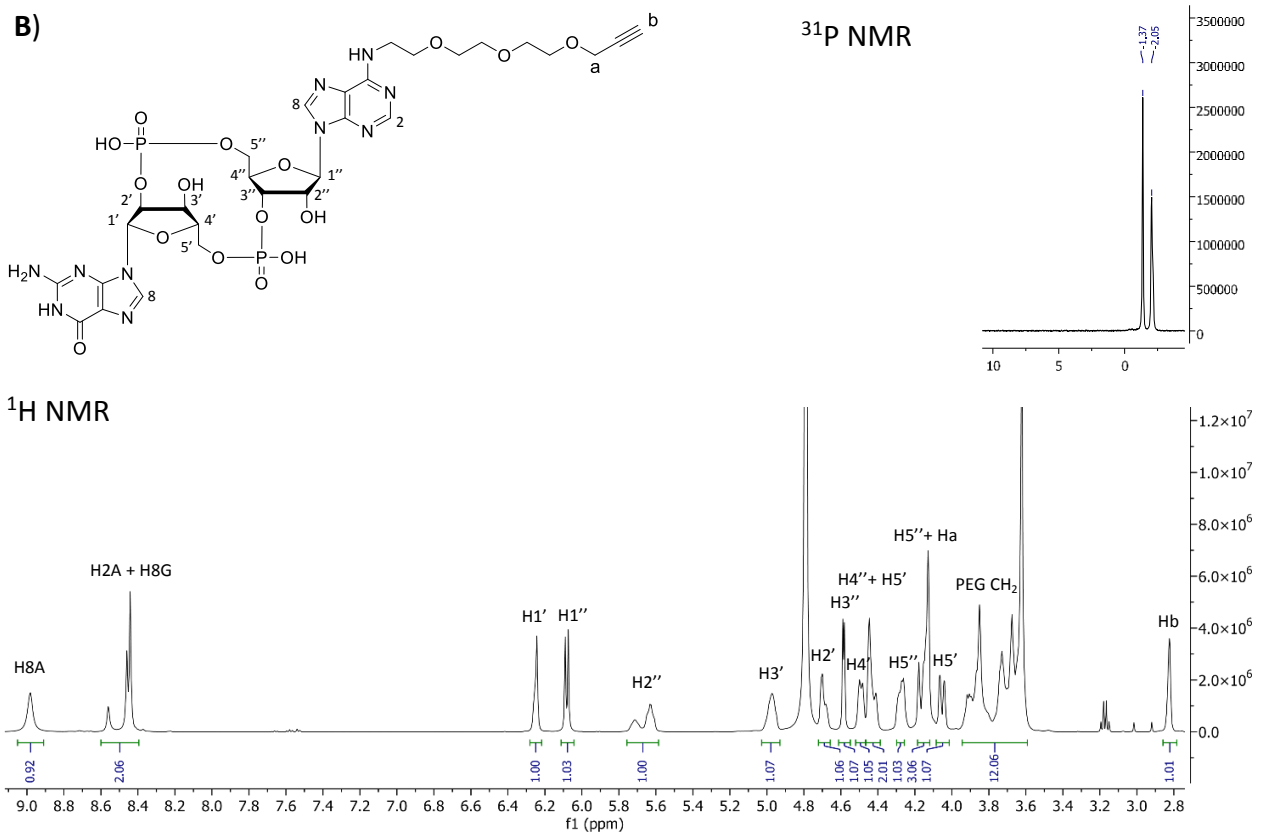

Figure 3.5: **A**) Structure, 500 MHz ^{1}H NMR and 202 MHz ^{31}P NMR spectra of **52** (mixture of 2 diastereomers); **B**) Structure, 500 MHz ^{1}H NMR and 202 MHz ^{31}P NMR spectra of **53** (mixture of 2 diastereomers).

3.1.3 Observations about cGAMP-Based STING Recruiters

The reported strategy represents an interesting foundation for the creation of cGAMP derivatives easily modifiable through click chemistry with a multitude of different bioactive molecules, facilitating the synthetic challenge to produce elaborate modified CDNs in higher yields.

Regarding the purpose of this work, which is the application of modified CDNs in PROTAC strategy as STING recruiters, besides the great advantage of the selectivity given by a direct derivative of the natural substrate of the enzyme, some negative aspects can be pointed out. On the chemical perspective, the complex and multistep synthesis is usually associated to low total yields. This issue has been partially improved by the optimization of the synthetic procedure and the possibility to use click chemistry as a starting point for further modifications of the CDNs. For the biological application of these compounds, the relatively large size of the molecule and the double negative charge of the phosphates, may represent a problem for the delivery and entrance to the cell, despite a relatively good membrane penetration ability of cGAMP derivatives.[159] The stability of the CDN itself, mainly endangered by the action of ENPP1 enzymes on the cell membrane and by nucleases in general, can be reinforced by chemical derivatisation of the phosphodiester such as thiophosphate moieties,[64, 153-155] or by fluorination or dehydroxylation of the sugar of the free -OH groups (Figure **3.6**).[158-160] These modifications could be applied in order to improve the durability of the molecules, possibly without impairing their activity. Unfortunately, the methylation of the sugar 2' or 3'-OH, commonly used to increase the stability of RNA strands towards nucleases, does not represent a valid possibility on the CDN, having shown significantly decreased binding affinity towards STING, probably due to steric hindrance in the active site, as already proven in our group.[263]

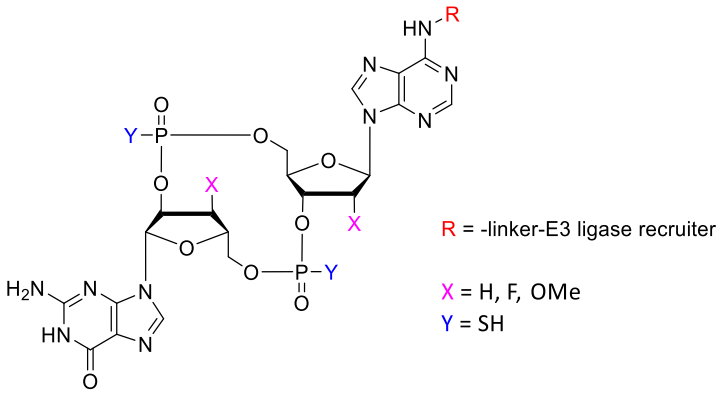

Figure 3.6: Most common modification sites for increasing the stability of CDNs.

Concerning the site of modification, the presence of a relatively bulky group as the linker may negatively influence the binding strength and the recognition. Obviously, a decrease of binding is expected which, however, would not necessarily impair a positive outcome of the derived PROTAC. As discussed in chapter **1**, the formation of the ternary complex does not compulsorily require a strong interaction between the PROTAC and the POI. In addition, the presence of the PEG linker may not permit the complete closure of the two STING subunits, eventually resulting in a lower activation.

Other analogues based on this synthetic strategy worth to be mentioned, are currently being developed by *Johann de Graaff*, as part of the same research project (Figure **3.7**). These derivatives, which also present a propargyl PEG linker available for click chemistry attached on position 6 of one of the guanosines, are based on the 3',3'-c-di-GMP bacterial second messenger, which is known to bind hSTING in the less active open state.[39] In this case, in addition to a simplified chemical synthesis (both the halves come from commercially available phosphoramidites), some advantages could derive from the lower STING activation as well as from the lower sterically hindered conformation of the "open" STING dimer, possibly less disturbed by the presence of the PROTAC linker. Moreover, the presence of a 3',3' connection between the two nucleobases could result in an increased stability towards degradation of the CDNs by the enzyme ENPP1 or viral poxins, due to a less favoured conformation inside the active sites of these nucleases.[64, 65] Additional stability towards nucleases, may be also improved with 2',3' de-oxy cGAMP and c-di-AMP analogues bearing an alkyne-containing linker on the *N*6 position (Figure **3.7**), synthesised by *Aikaterini Pappa* following the same procedure reported in this dissertation, that could be in future investigated as STING recruiters for PROTAC development and compared to their oxy- respectives.

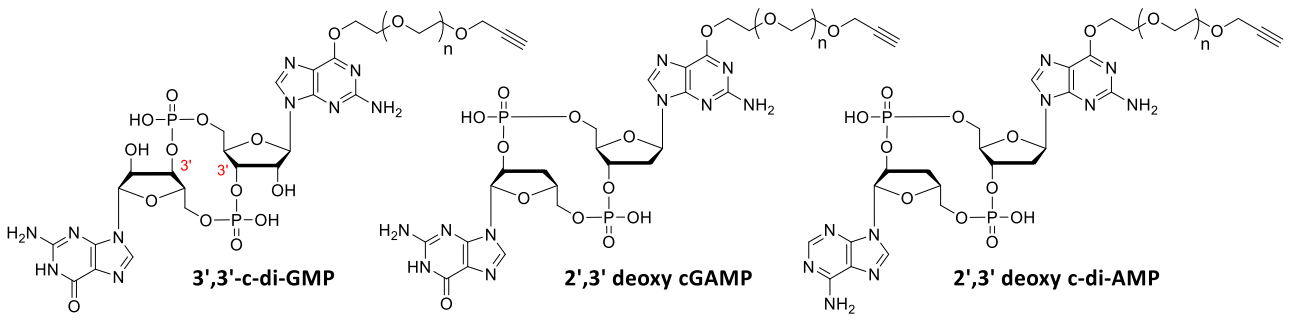

Figure 3.7: Structure of 3',3'-c-di-GMP, 2',3' deoxy cGAMP and 2',3' deoxy c-di-AMP derivatised with a propargyl PEG linker as alternative CDN-based STING recruiters.

3.1.4 Design of Non-Covalent STING Inhibitors POI Recruiters

In order to address in particular, the delivery issues potentially arising from the negative charges and size of the cGAMP derivative, as well as enzymatic instability and the eventual residual agonist activity of the CDN structure, we started considering other possible warheads for recruiting STING. In order to preserve the advantages of non-covalent PROTACs (see chapter **1**), our attention focused on STING antagonists targeting the CDN-binding site which would not react covalently with our POI (Figure **3.8**). To this class belong the natural product Astin C (**21**), Compound 18 (**22**) and the more recent SN-011 (**23**).[121, 170, 171] Other newly discovered STING antagonists, Palbociclib (**24**), Compound 30 (**25**) and HDS1077 (**26**), not yet discovered during the development of this project, represent an interesting opportunity for the creation of new inhibitor-based recruiters for STING targeting PROTACs.[174, 273, 274]

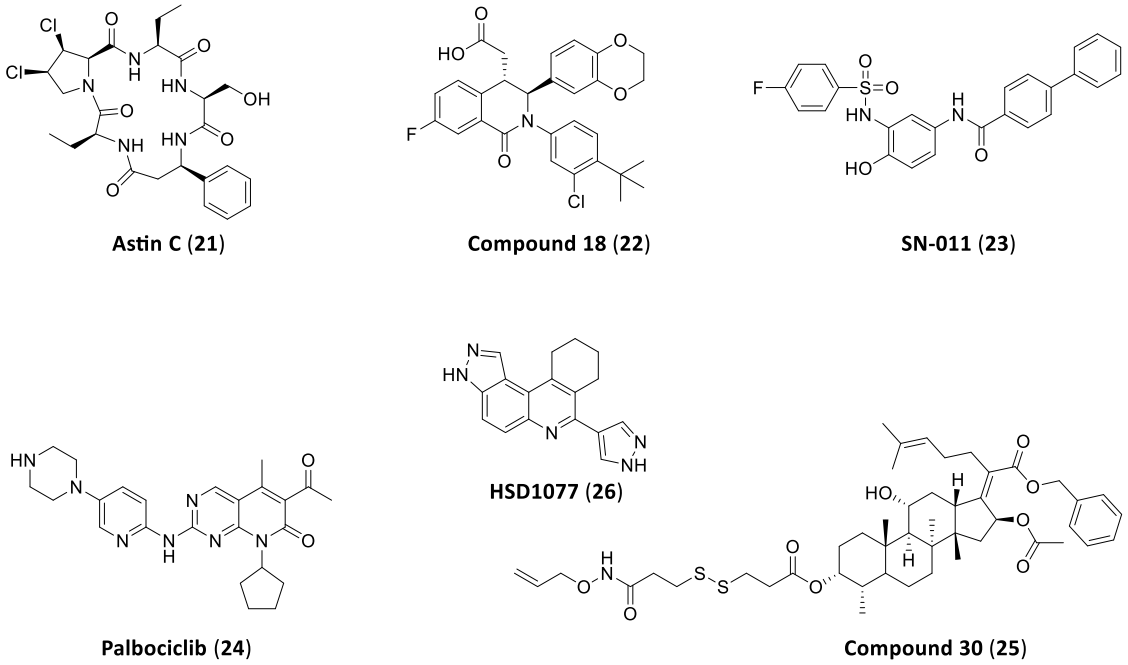

Figure 3.8: Structure of non-covalent STING antagonists targeting the CDN binding pocket.

Among the inhibitors known at the time of this research, SN-011 was chosen for the development of potential STING PROTACs mainly due to the higher chemical accessibility for the derivatisation with propargyl PEG linkers suitable for click chemistry. As already discussed in chapter **1**, SN-011 was identified by *Hong et al.* via *in silico* docking calculations and demonstrated to bind STING in the CDN binding pocket with a higher affinity than 2',3'-cGAMP. The mechanism of inhibition was demonstrated to be related to the ability of the compound to lock STING in an "open", inactive conformation.[121]

In the study of analogue structures of this molecule, it was shown that the introduction of a linker on the phenolic oxygen (SN-012) does not impair too much the capability to bind. Considering this, it was initially planned to functionalize SN-011 with a propargyl PEG linker accessible to click chemistry (Scheme **3.7**).

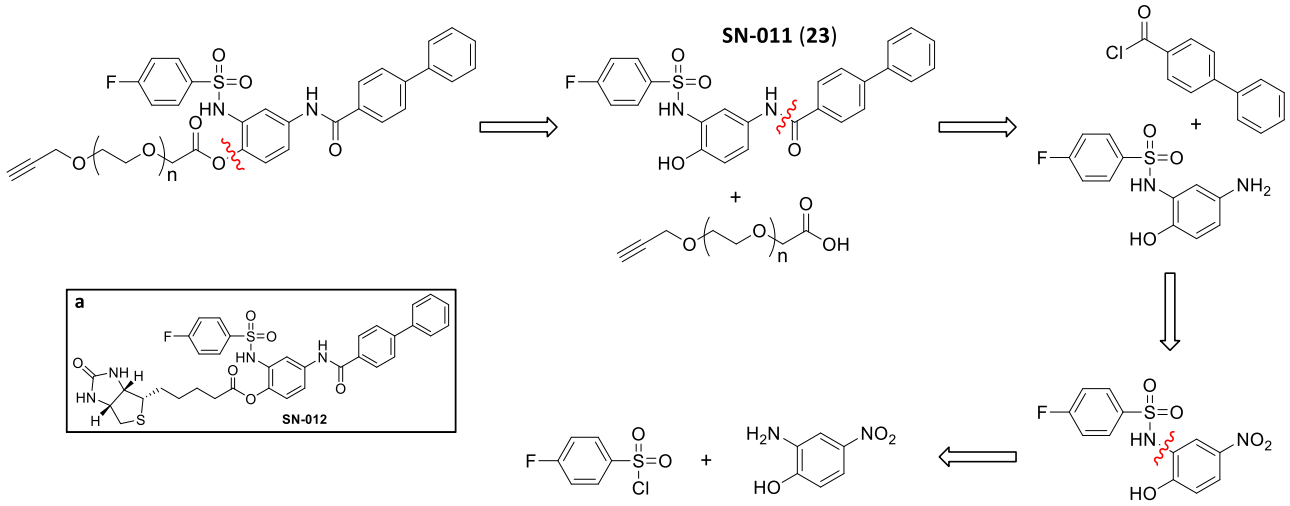

Scheme 3.7: Retrosynthetic analysis for the synthesis of a SN-011 derivative with the introduction of a clickable alkyne moiety through PEG linker. **a**) Structure of SN-012.

The synthesis of SN-011 (**23**), was successfully carried out according to the literature with minor differences, as reported in Scheme **3.8**. The commercially available **54** and **55** were reacted to get **56** whose nitro group was then reduced to amine via hydrogenation to obtain **57**. At this point, the strategy differed from literature in the last step for the coupling of the biphenyl carboxyl group which was introduced as the commercially available acyl chloride (**58**) rather than as carboxylic acid with EDC and HOBt via *Steglich esterification* mechanism, avoiding the necessary TBS protection and subsequent deprotection of the phenolic -OH group. Taking advantage of the higher nucleophilicity of the NH_2 group and adding the acyl chloride in stoichiometric amount at low temperature, it was possible to obtain the final product **23** with a higher yield (50 % over 3 steps versus 13 % over 5 steps of the published work). At the moment of its derivatisation with **59** though, the formation of the ester bond always resulted in very poor yields, despite the different conditions tried, due to the chemical instability of the ester itself, activated towards hydrolysis by the electron withdrawing groups present in the aromatic ring.

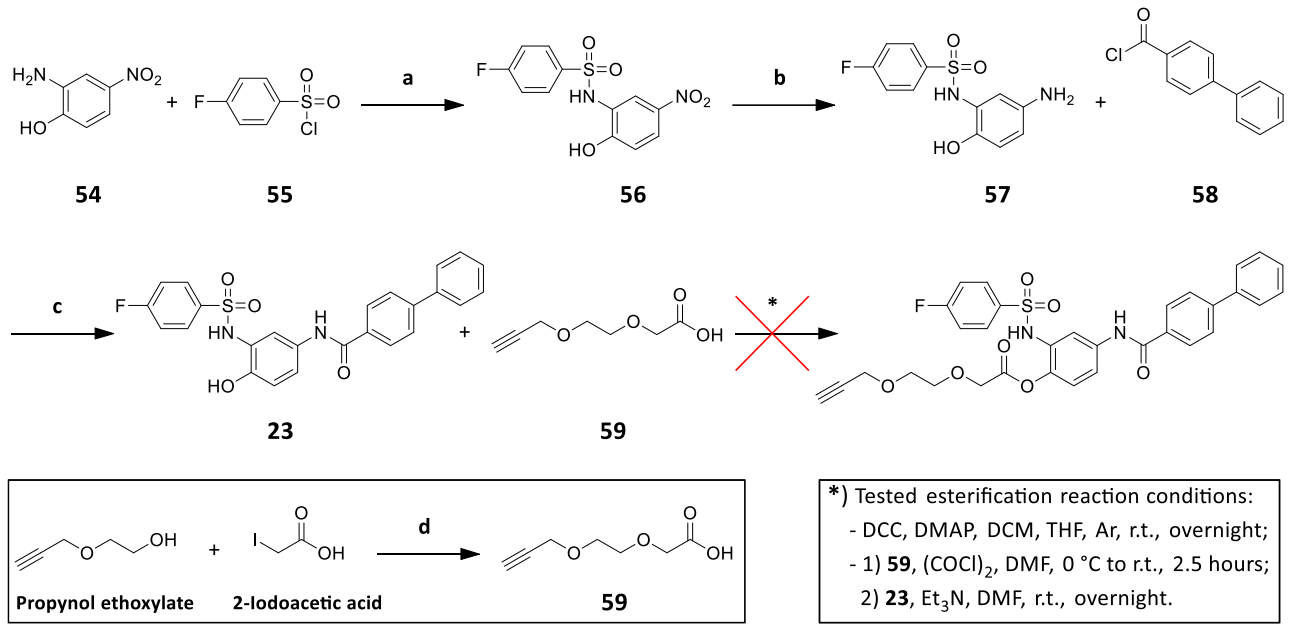

Scheme 3.8: Optimized synthesis of SN-011 (**23**) and failed esterification. **a**) DCM, Py, Ar, r.t, overnight, 60 %; **b**) H_2, 10 % Pd/C, MeOH, r.t., overnight, crude; **c**) Et_3N, DMF, r.t., 30 min, 50 % over 2 steps; ***)** Failed esterification reaction conditions.

3.1.5 Synthesis of non-Covalent STING Recruiters

To improve the stability of the derivative, the labile ester bond was replaced by a more resistant amide moiety, which would improve the durability of the final drug against the esterase enzymes present in the cell. In light of this, the synthetic strategy was adapted to the presence of the new group (Scheme **3.9**).

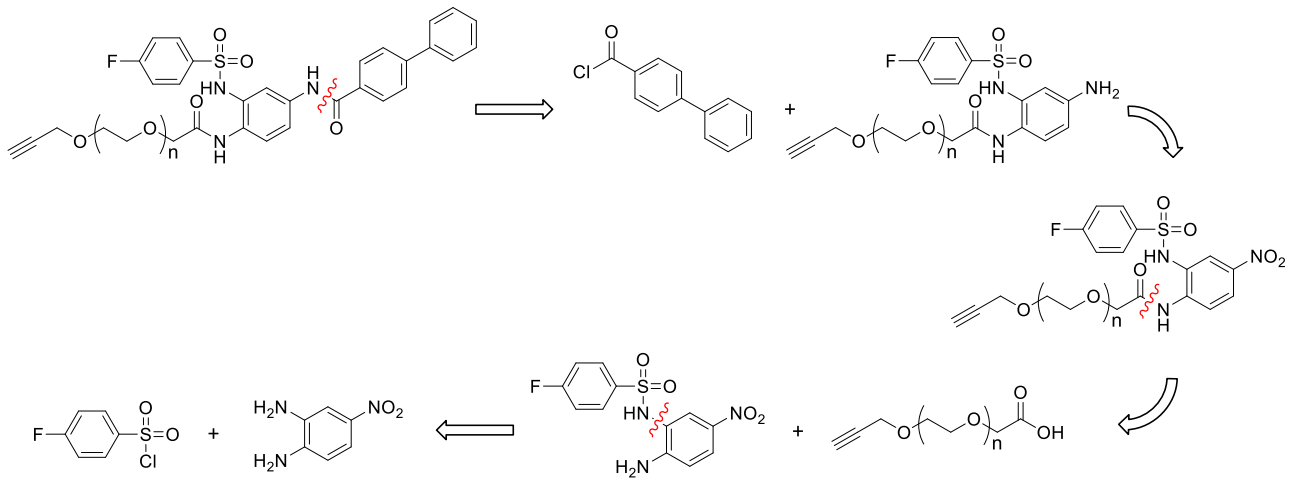

Scheme 3.9: Retrosynthetic analysis for the synthesis of a SN-011 derivative with the substitution of the phenolic -OH group with an aniline for introduction of a clickable alkyne PEG linker through a more stable amide bond.

The new strategy had to face the main challenge to be able to functionalize the two different amino groups selectively, exploiting the different reactivities due to the presence of the electron withdrawing nitro group in para- and meta- position and later, after the insertion of the propargyl PEG linker, the possibility of reducing selectively the nitro to amino group in presence of the alkyne moiety. The solution came by using a mild reducing reaction with zinc powder and acetic acid which permitted to convert the target aromatic nitro group to aniline without reducing the triple bond of the alkyne.

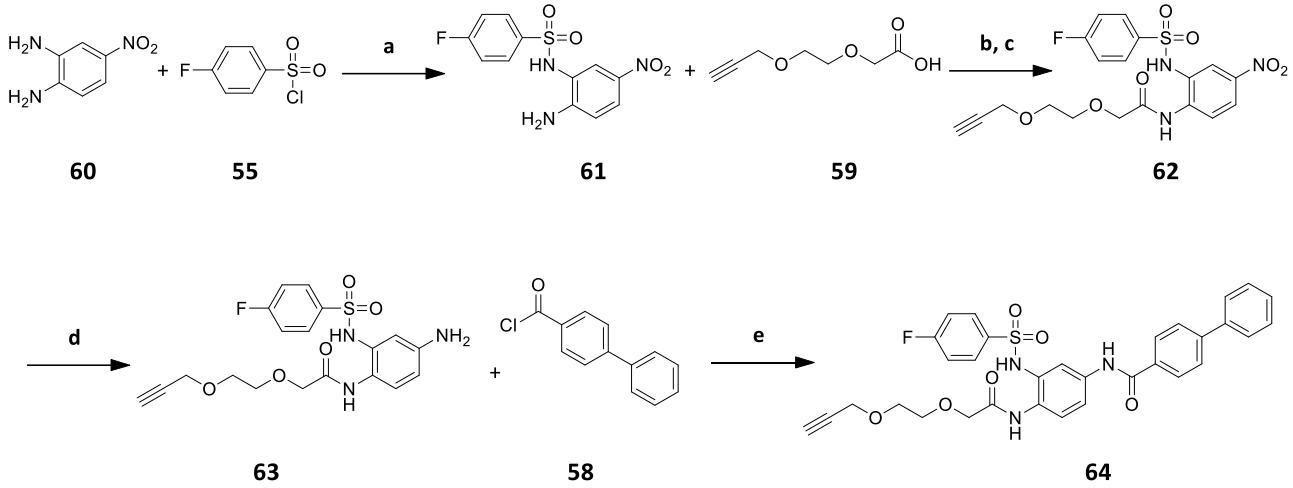

Scheme 3.10: Synthetic procedure for the preparation of **64**. **a**) THF, Py, Ar, r.t., overnight, 91 %; **b**) **58**, $(COCl)_2$, Ar, r.t. 1.5 hours; **c**) **15**, THF, Et_3N, 0 °C, 30 min, 62 % over 2 steps; **d**) Zn dust, DCM, AcOH, r.t., overnight, 88 %; **e**) THF, Py, Ar, 0 °C, 2 hours, 85 %.

In the first step (Scheme **3.10**), the commercially available 1,2-diamino-4-nitrobenzene (**60**) was treated with 1 equivalent of 4-fluorobenzenesulfonyl chloride (**55**) which reacted only with the amino group in meta and therefore less deactivated by the electron withdrawing -NO_2, obtaining **61** with a yield of 91 %. Then, the propargyl PEG carboxylic acid **59**, previously prepared according to literature,[275] was converted to the more reactive acyl chloride by reacting with oxalyl chloride at room temperature. Due to the high sensitivity towards hydrolysis, the chlorinated compound was kept under argon atmosphere and, after having evaporated the residual $(COCl)_2$, was directly added to **61** to obtain **62.** The nitro group of the intermediate was then reduced to amine with zinc dust and acetic acid, leaving untouched the triple bond on the linker and,[276] after purification, **63** was isolated with 88 % yield. The final compound **64** was at last achieved by coupling 4-biphenylcarbonyl chloride (**58**) with the newly formed amino function of **63**, in 85 % yield and subsequently characterized by NMR spectroscopy (Figure **3.9**).

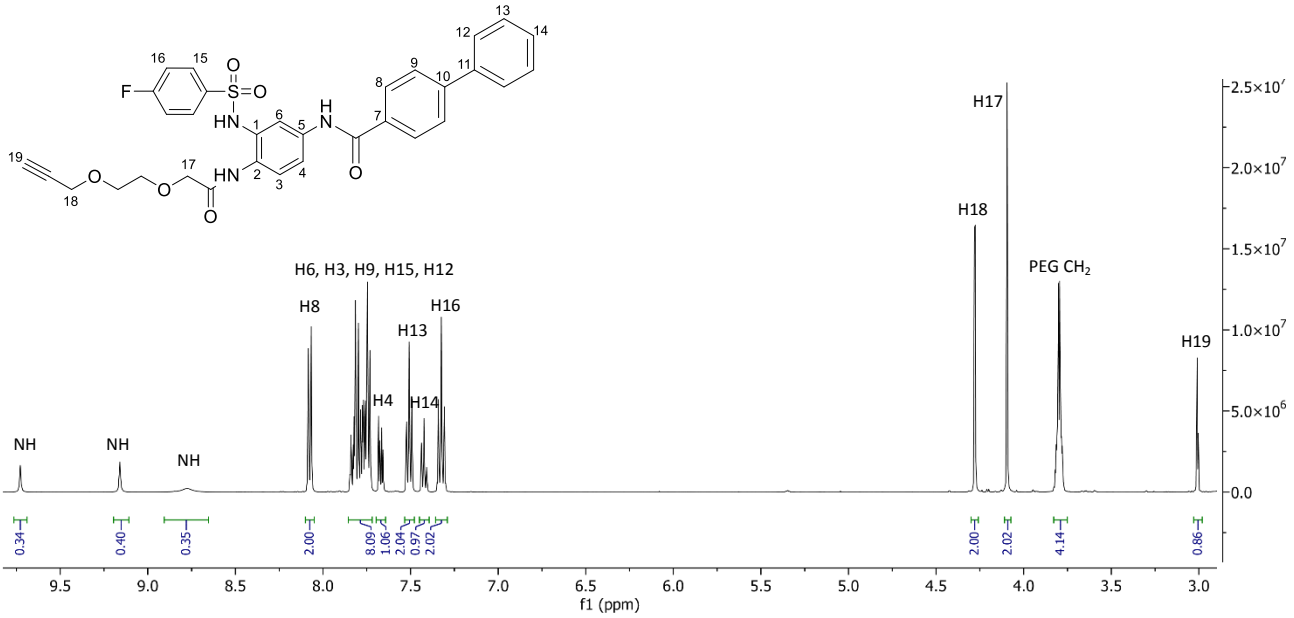

Figure 3.9: Structure, 500 MHz ^{1}H NMR spectrum of **64**.

3.1.6 Observations about STING Recruiter 64

With the realization of compound **64**, a derivative of the STING inhibitor SN-011 bearing an alkyne moiety ready for coupling via click reaction, we created a powerful tool for the progress of STING inhibition related research and, specifically in the interest of this dissertation, a promising recruiting warhead for the development of STING degrading PROTACs.

The choice of starting from compound SN-011 is related to its higher affinity and bioactivity towards STING then other known non-covalent inhibitors (Astin C, Compound 18), comparable, in terms of inhibitory effect, to H-151, a covalent STING antagonist which however presents a lower specificity than SN-011 and may have more off-target effects. SN-011 is also proven to be non-cytotoxic, unlike H-151.

In comparison to the cGAMP -based alternative, this potential STING recruiter could combine to the high specificity, a higher affinity and a strong inhibitory action. Besides this, on the druglikeness point of view, compound **64** presents a lower molecular weight and the absence of CDN's negative charges, often associated with poorer drug uptake through the cell membrane. Using **64** instead of a CDN derivative as a POI recruiter in STING targeting PROTACs would also increase the stability of the potential drug avoiding ENPP1 -promoted phosphodiester cleavage.

As already mentioned, the constant development of research about STING inhibitors gives the possibility of an expanding the number of new antagonists which could be explored, upon chemical modification, as recruiters for potential STING targeting PROTACs.

3.1.7 Design and Synthesis of a cGAMP – Cy3 Fluorescent Derivative

In order to expand the applicability of the clickable design and to gain insights on the cellular entry and distribution of cGAMP derivatives, a fluorescent variant (**65**) was produced. Fluorescent modifications of CDNs represent an interesting tool for the development of assays and emitting probes important for the study of localization and the faith inside the cell of these messengers.[277]

In our case, we focused on studying the influence of the negatively charged phosphates on membrane permeability by following the modified CDN entering the cell via fluorescent microscopy. This was possible by attaching a fluorescent dye to the cGAMP derivative **53** taking advantage of the clickable moiety. Regarding the choice of dye to use, it was important to consider the possibility to perform this assay *in vivo*. The excitation wavelength should fall into the visible range not to harm the viability of cells. Considering this, a version of Cy3® containing an azide available for click reaction (**66**), with a maximum absorption at 555 nm, was purchased and used for functionalization of the modified CDN through click chemistry (Scheme **3.11**).

The click reaction was performed in a mix of H_2O and MeCN to better solubilize both reagents. The catalytic copper species was introduced as $CuSO_4$, *in situ* reduced to Cu(I) by an excess of sodium ascorbate. THPTA was chosen as ligand for Cu(I). After 3 hours at 45 °C, the final product **65** was purified with preparative HPLC and obtained in 86 % yield (Figure **3.10**).

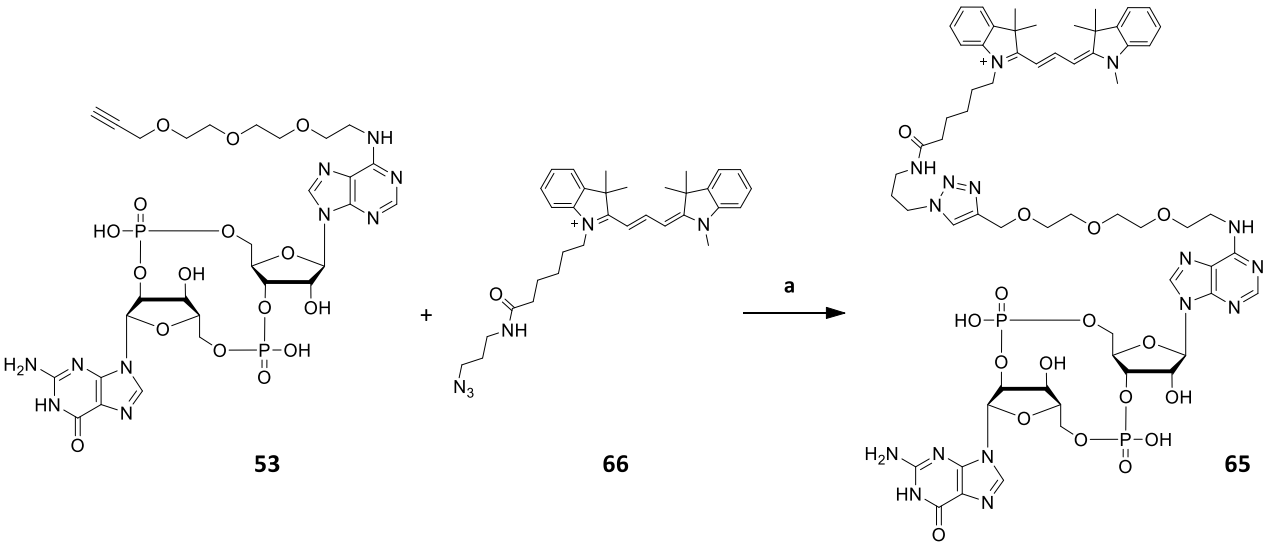

Scheme 3.11: Click reaction between the cGAMP derivative **53** bearing an alkyne and Cy3 azide **66**. **a**) $CuSO_4$, THPTA, Na ascorbate, H_2O, MeCN, Ar, 45 °C, 3 hours, 86 %.

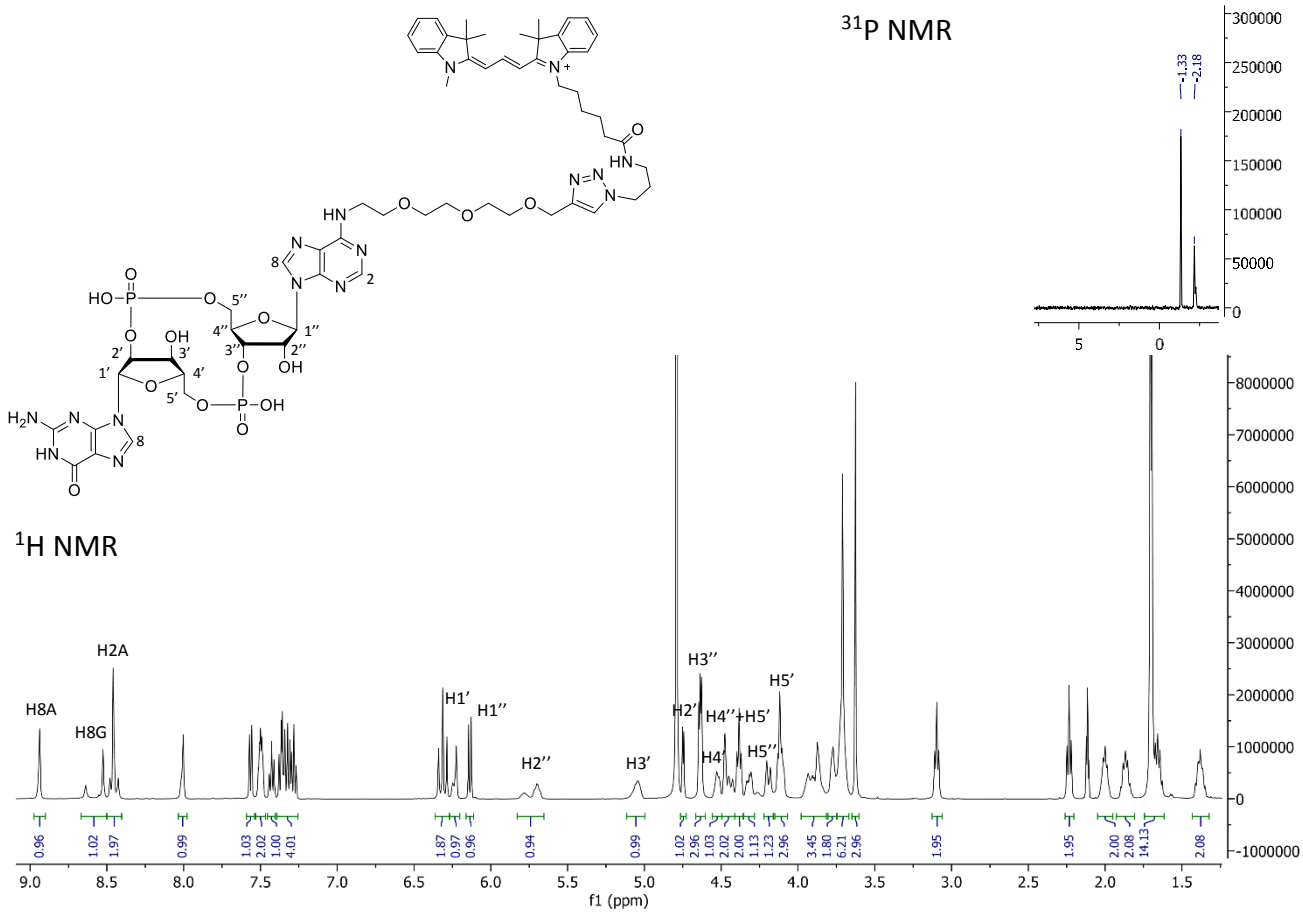

Figure 3.10: Structure, 800 MHz ^{1}H NMR and 202 MHz ^{31}P NMR spectra of **65** (mixture of 2 diastereomers).

The obtained fluorescent derivative of cGAMP **65** was used to study and visualize the entrance and localization in living cells via fluorescent microscopy (**3.4.1**).

3.2 Recruiting E3 Ligases

As second part of the project, we focused on the design and synthesis of molecular recruiters for E3 ligase enzymes, which are responsible for carrying ubiquitin, often in form of a complex with E2 ligases. Among many known enzymes belonging to this class, only few of them have been utilized for the purpose of PROTAC -induced targeted degradation, leaving a great research space unexplored. For the purpose of this work, we decided to initially recruit two of the most commonly used E3 ligases: Cereblon (CRBN), recruited by a group of molecules derived from thalidomide, and Von-Hippel-Lindau (VHL), engaged by a synthetic motif derived from a peptidic sequence, developed by *Crews* and others (see chapter **1**). Later, an attempt was made in the direction of fetching RNF5, a specific E3 ligase known to physiologically regulate the degradation of STING through the UPS.

The relationship between the effectiveness of the degradation and the nature of the E3 ligase, is extremely dependent case by case. Particularly, the efficiency of a PROTAC molecule is strongly related to its ability of forming a stable ternary complex. This depends on the surface - surface interactions between the two proteins in close proximity. The preference for one E3 ligase in terms of degradation, is also dependent on its abundance in different tissues (and on the abundance of the POI as well).

In the following section, the design and synthesis of PEG-based pomalidomide CRBN recruiters bearing a terminal azide moiety available for functionalization through click chemistry will be presented. The azide-PEG-based VHL recruiters were instead purchased from *Merck-Sigma Aldrich*.

3.2.1 Design of Pomalidomide-Based CRBN Recruiters

As already discussed in chapter **1**, cereblon (CRBN) is one of the mostly common E3 ligases recruited for PROTAC technology. Based on the abundant existing literature, a pool of pomalidomide-based CRBN recruiters with different PEG linker lengths with a terminal azide available for click chemistry, were synthesised.

The thalidomide derivative pomalidomide (**34**), also widely used in the field, was chosen as a starting point for the attachment of the PEG linker, due to the easy derivatisation through the formation of an amide bond on its primary amino group reacting with the corresponding acyl chloride. The azide moiety was usually introduced before the coupling step, replacing one of the terminal hydroxyl groups, previously converted to a better leaving group (Scheme **3.12**).

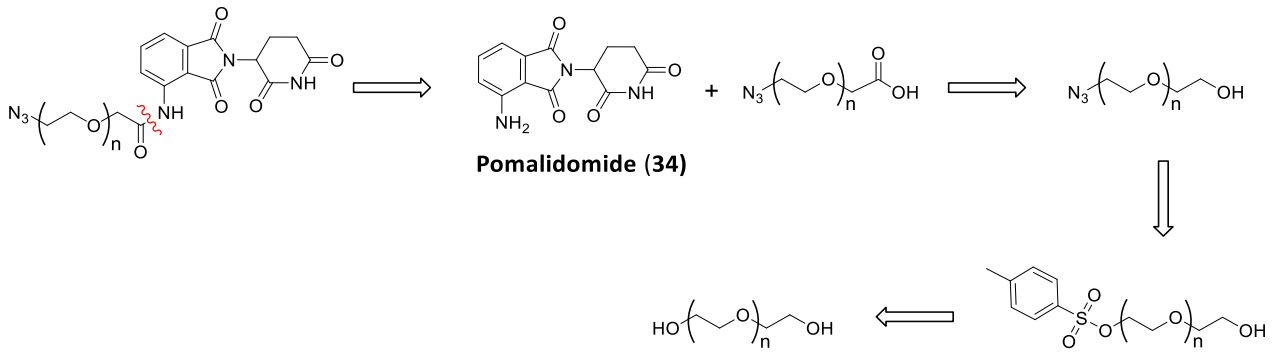

Scheme 3.12: Retrosynthetic analysis for the synthesis of pomalidomide-based CRBN recruiters bearing an azide moiety available for Cu(I) catalysed click reaction at the end of a PEG linker.

3.2.2 Synthesis of Pomalidomide-Based CRBN Recruiters

For synthesising the shortest of the pomalidomide-PEG-azide CRBN recruiters, compound **67**, pomalidomide (**34**) was firstly reacted with 2-chloroacetyl chloride to give the intermediate **68** in 95 % yield. At this point the residual chlorine atom was nucleophilically substituted by sodium azide, yielding the final product **67** in 76 % after purification (Scheme **3.13**).

The rest of the derivatives were synthesised in a similar fashion. The appropriate PEG alcohols (**69** PEG2, **70** PEG3) were reacted with toluene sulfonyl chloride in stoichiometric amount for the functionalization of a single terminal hydroxyl (**71** and **72**). The tosylated -OH, now turned into a good leaving group, was nucleophilically substituted by the attachment of an azide anion introduced as sodium azide in DMF accompanied by strong heating (90 °C) to give **73** and **74**, while **75** (PEG4) was acquired as commercially available. The opposite -OH group was then oxidised via *Jones oxidation* in presence of a solution of CrO_3 in aqueous 1.5 M H_2SO_4 to obtain the correspondent carboxylic acid (**76**, **77** and **78**). These intermediates were further converted to acyl chlorides which were generated *in situ* through the reaction with oxalyl chloride. Due to the high reactivity and sensitivity towards hydrolysis, these compounds were not isolated and directly used in the reaction with pomalidomide (**34**) to which it was added dropwise. The nucleophilic attach of the primary amino group to the acyl chloride, resulted in the formation of the amide bond and the final compounds **79**, **80** and **81** were isolated after purification through silica gel column chromatography and characterized by NMR (Figure **3.11**).

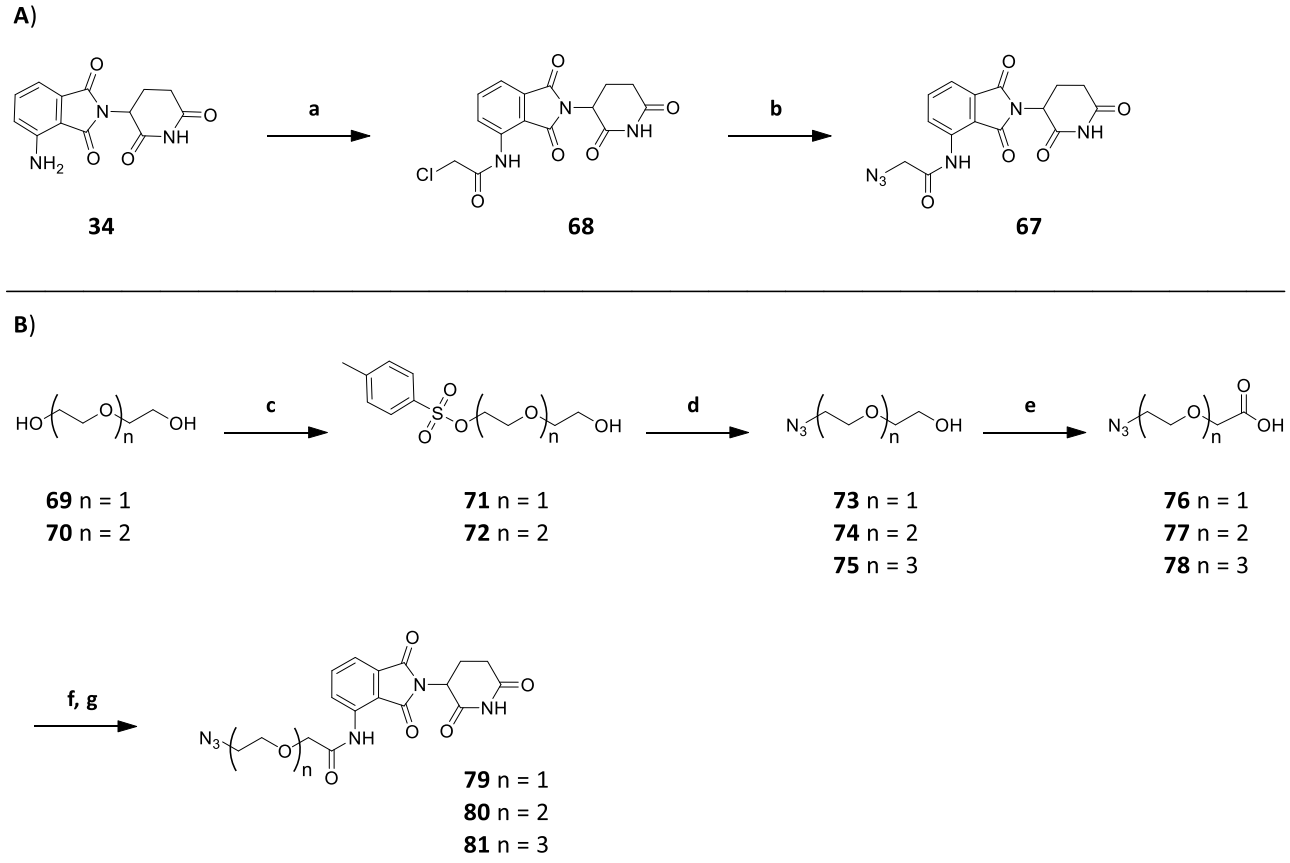

Scheme 3.13: Synthetic procedure for the preparation of pomalidomide-based CRBN recruiters with terminal azide on PEG linker. **A**) Synthesis of **67** (n = 0): **a**) 2-chloroacetyl chloride, THF, Ar, reflux, 2 hours, 95 %; **b**) NaN3, NaI, acetone, Ar, reflux, overnight, 76 %. **B**) General scheme for PEG linkers: **c**) *p*-toluenesulphonylchloride, DCM, Et_3N, N_2, r.t.,

overnight, **71**: 52 %, **72**: 72 %; **d**) NaN_3, DMF, Ar, 90 °C, overnight, **73**: 52 %, **74**: 59 %; **e**) CrO_3, 1.5 M H_2SO_4 in H_2O, acetone, r.t., overnight, **76**: 94 %, **77**: quantitative, **78**: 94 %; **f**) $(COCl)_2$, Ar, r.t., 1.5 hours; **g**) **34**, DMF, Ar, r.t. overnight. Yield over 2 steps **79**: 33 %, **80**: 39 %, **81**: 64 %.

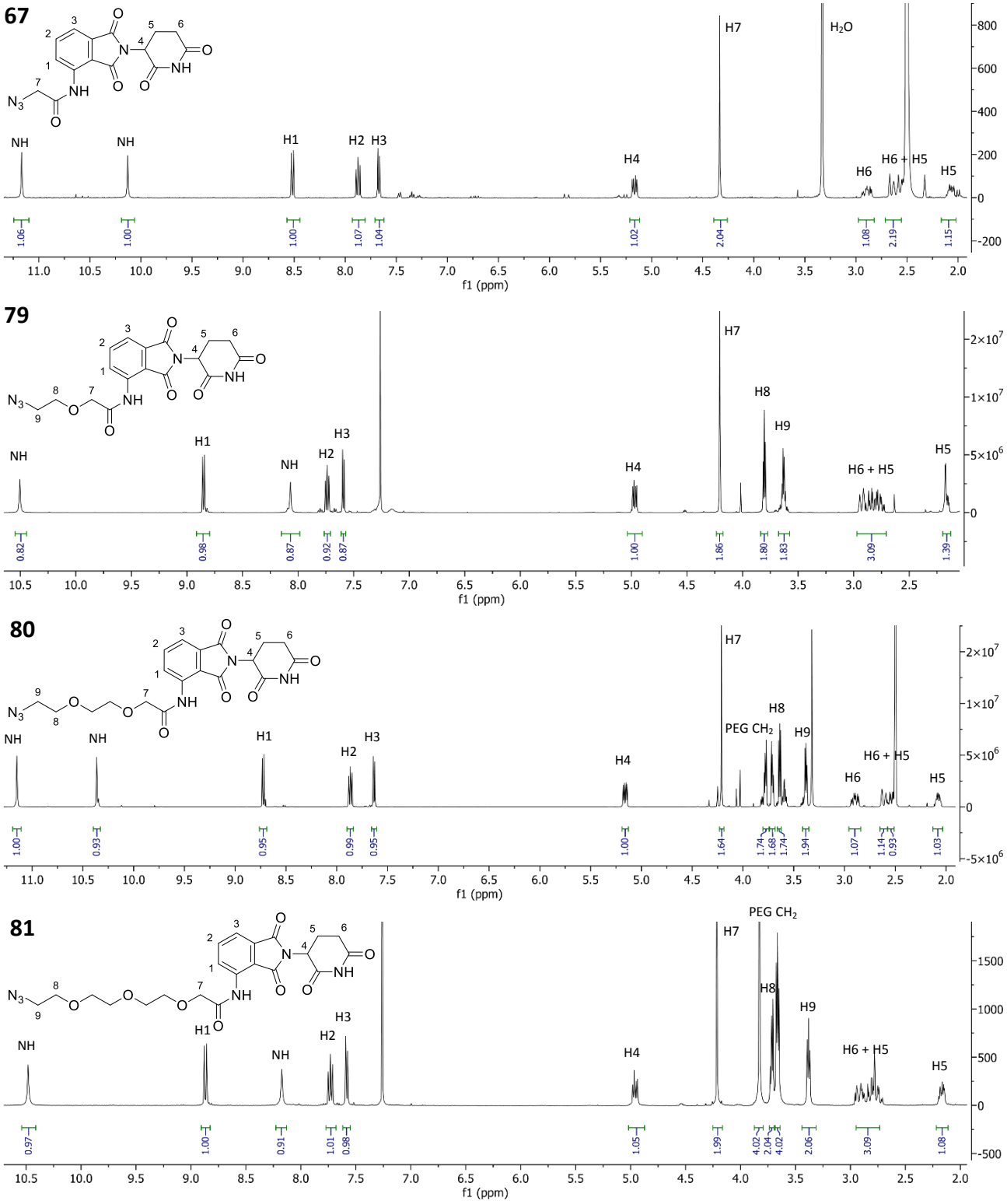

Figure 3.11: Structure and ^1H NMR spectra of azide PEG CRBN recruiters: **67** 400 MHz ^1H NMR in DMSO, **79** 500 MHz ^1H NMR in $CDCl_3$, **80** 500 MHz ^1H NMR in DMSO, **81** 400 MHz ^1H NMR in $CDCl_3$.

3.2.3 Design of RNF5 Recruiters

Referring back to the employment of different E3 ligases in the PROTAC strategy, we already outlined how few of them have been investigated besides the huge number of identified enzymes belonging to this class. In the next paragraph, the attempt to expand the researched space by designing and synthesising a feasible recruiting unit for the yet unexploited E3 ligase RNF5 will be discussed.

One of the possible problems arising from the application of PROTAC technology to degrade STING, is related to the fact that this enzyme presents physiologically multiple ubiquitination sites targeted by different E3 ligases some of which are boosting its activity, and others whose ubiquitination leads to the proteasomal degradation. To this last category belongs RNF5, which targets STING at K150 for K48-linked ubiquitination leading to its degradation.[46]

Despite the absence of known PROTAC recruiters for this E3 ligase, the inspiration came from the research of an inhibitor towards this enzyme by the group of professor *Pedemonte* in 2018.[278] During the design and synthesis of this inhibitor inh-02, they identified a by-product named analog-1 which did not show inhibition properties and was used as a negative control for their purpose. The compound, that after further investigation was recently confirmed as an activator of RNF5,[279] was chosen in this work as a promising starting scaffold for the creation of a recruiter for our purpose (Figure **3.12**).

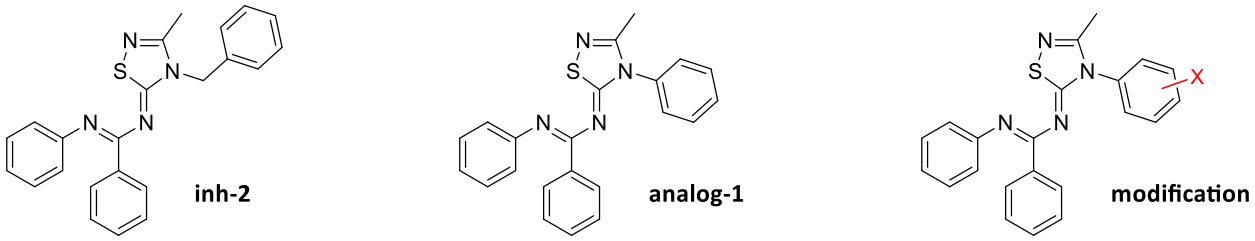

Figure 3.12: Comparison of the structures of inh-2, analog-1 and the proposed site for the insertion of the modification.

A suitable site for the introduction of the clickable azide modification was identified on the aromatic ring which is represents the structural difference between inh-02 and analog-1, assuming the importance of rest of the molecule for the recognition by the enzyme. This variable part instead, fundamental for the modulation of the activity, will have less chances to impair the interaction and to reduce the activation properties.

Analysing retrosynthetically the possible route (Scheme **3.14**), the formation of the [1,2,4] thiadiazolic ring in the last compound can be obtained by the reaction of the suitable thiourea with MeCN. In literature two different options are described to obtain the ring closure selectively on the correct side, exploiting the catalytic properties of phenyliodine (III) diacetate (PIDA) in absence of any solvent,[280] or by a first reaction with Br_2, causing an intramolecular ring closure, followed by the treatment of the intermediate with MeCN and triethylamine, as described in the over mentioned paper.[278] The formation of the desired thiourea is generally achieved by the reaction of the isothiocyanate on one or the other halves of the final structure and the opposite amine.

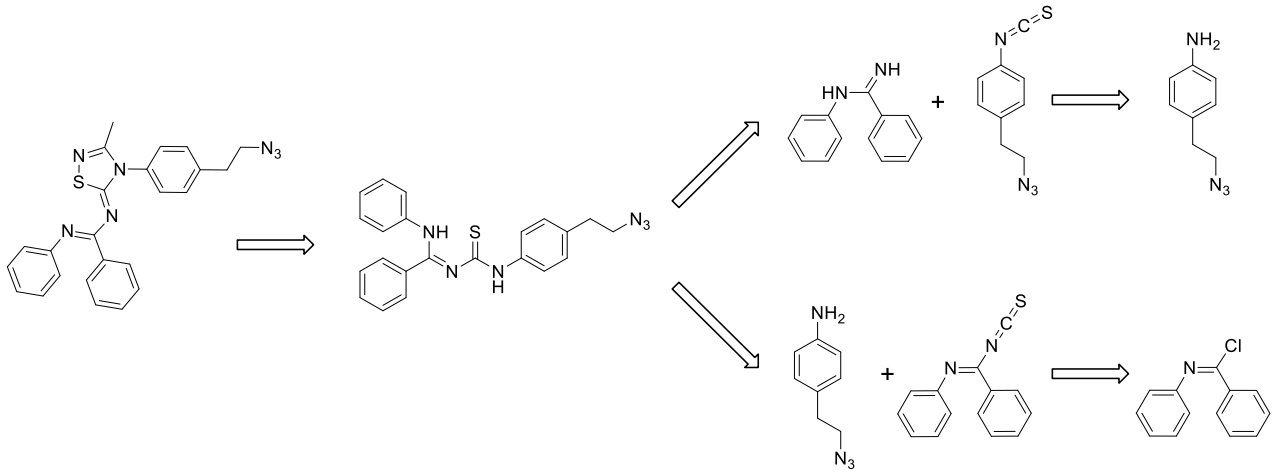

Scheme 3.14: Retrosynthetic analysis for the synthesis of analog-1 derivative with the introduction of an azide moiety, available for Cu(I) catalysed click reaction. The formation of the thiadiazolic ring has to pass through the reaction of the corresponding thiourea and MeCN. The thiourea can be obtained by the addition of an amine to the isothiocyanate on the other half.

4-(2-Azidoethyl)aniline, necessary for both routes for the formation of the thiourea, can be obtained by the substitution of a hydroxyl group by an azide after turning it into a good leaving group with tosyl chloride. A suitable protection of the amine moiety is needed in order to avoid undesired reactivity (Scheme **3.15**).

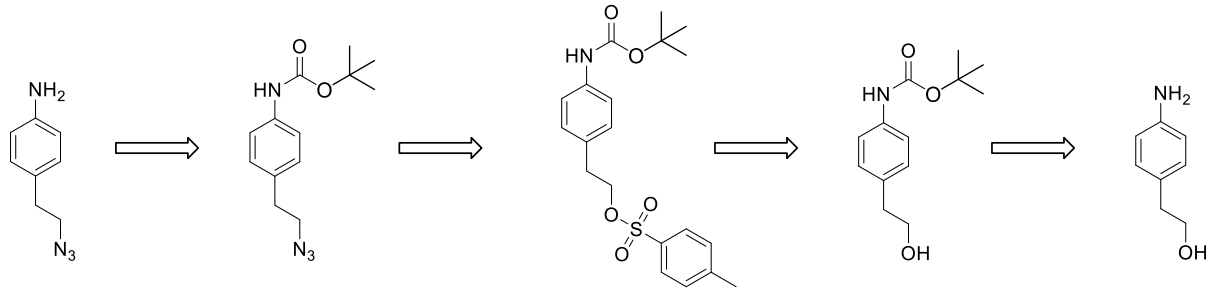

Scheme 3.15: Retrosynthetic analysis for the synthesis of 4-(2-azidoethyl)aniline.

3.2.4 Synthesis of RNF5 Recruiter

The first building block for the synthesis of the desired thiourea was compound **82**, introducing the azidic function necessary for click functionalization of the designed final product (Scheme **3.16**). This was obtained starting from 2-(4-aminophenyl)ethanol (**83**), which was at first instance Boc-protected on the amino group to **84** by reaction with Boc-anhydride, to avoid undesired side reactivity in the following step in which the hydroxyl group was converted into a good leaving group for the later introduction of the azide. Therefore, once reacted with *p*-toluenesulfonyl chloride to **85**, the -OH group was nucleophilically substituted by the azide ion introduced as NaN_3 and stirred at high temperature in DMF to provide **86**. At last, the isolated intermediate was deprotected by removal of the Boc- group from the amine by treatment with 20 % TFA in DCM. The obtained **82**, was used as starting point for the following reactions.

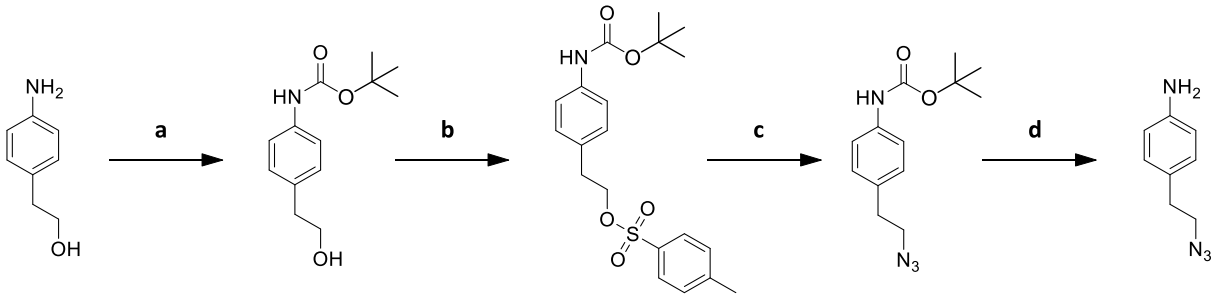

83 **84** **85** **86** **82**

Scheme 3.16: Synthetic procedure for the preparation of 4-(2-azidoethyl)aniline (**82**): **a**) Boc anhydride, THF, r.t., overnight, 93 %; **b**) *p*-toluenesulphonylchloride, DCM, THF, Et_3N, N_2, 0 °C to r.t., overnight, 99 %; **c**) NaN_3, DMF, N_2, 90 °C, overnight, 98 %; **d**) 20 % TFA in DCM, N_2, r.t., 30 min, 94 %.

Initially it was tried to produce the thiourea from the isothiocyanate (**87**) of the newly synthesised 4-(2-azidoethyl)aniline (**82**), which could be easily obtained through the reaction of the amino group with di-2-pyridyl thiono-carbonate (**88**) in 91 % yield (Scheme **3.17**).

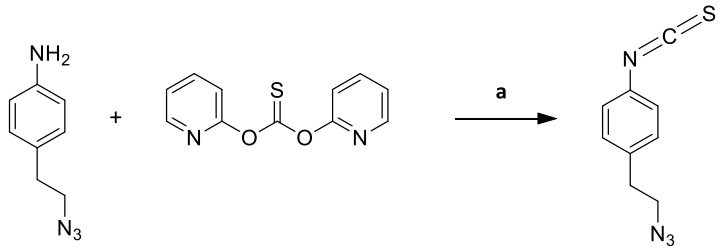

82 **88** **87**

Scheme 3.17: Synthetic procedure for the formation of isothiocyanate **87**: a) DCM, Ar, r.t., overnight, 91 %.

After isolation, the isothiocyanate **87** was used for the coupling with *N*-phenylbenzimidamide. Different conditions for the formation of the desired thiourea **89**, between the most commonly used in literature, were tried as shown in Scheme **3.18**, but all of them resulted in extremely low or no conversion at all, probably due to the high instability of the isothiocyanate towards hydrolysis despite the dry atmosphere used. It was also attempted to generate the isothiocyanate *in situ* and subsequent reaction with the following reagent, without appreciable improvement.

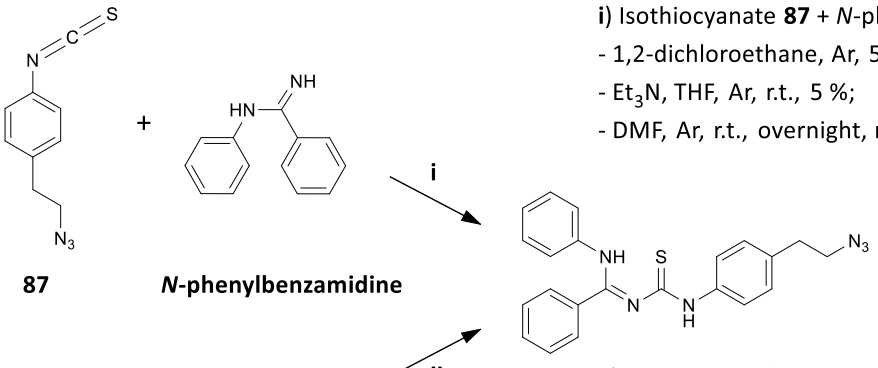

i) Isothiocyanate **87** + *N*-phenylbenzamidine:
- 1,2-dichloroethane, Ar, 55 °C, 19 hours, 8 %;
- Et_3N, THF, Ar, r.t., 5 %;
- DMF, Ar, r.t., overnight, no conversion.

ii) Generation of the isothiocyanate and subsequent reaction:
- 1) **82**, di-2-pyridyl thiono-carbonate, DCM, Ar, 1 hour;
  2) *N*-phenylbenzamidine, r.t., overnight, no conversion;
- 1) **82**, CS_2, DMSO, Ar, 70 °C, overnight;
  2) *N*-phenylbenzamidine, 70 °C, overnight, no conversion;
- 1) *N*-phenylbenzamidine, CS_2, DMSO, Ar, 70 °C, overnight;
  2) **82**, 70 °C, overnight, no conversion;
- 1) *N*-phenylbenzamidine, CS_2, Et_3N, THF, Ar, r.t., overnight;
  2) **82**, r.t., overnight, no conversion.

Scheme 3.18: Summary of conditions tested for the formation of thiourea **89**: **i**) Isothiocyanate **87** reacting with *N*-phenylbenzamidine; **ii**) Generation of the thiocyanate *in situ* on one side and subsequent reaction with the other half.

It was then decided to attempt the opposite route by forming the isothiocyanate on the other half of the structure (Scheme **3.19**). On this regard, the commercially available *N*-phenylbenzimidoyl chloride (**90**) was chosen as a starting reagent for the reaction with a thiocyanate salt (Na^+, K^+, NH_4^+) to form the desired isothiocyanate *in situ* (**91**), before the subsequent coupling with 4-(2-azidoethyl)aniline (**82**) generating the thiourea (**89**). Among the different conditions tested, the combination of potassium thiocyanate in DCM, followed by 4-(2-azidoethyl)aniline (**82**), brought to the formation of compound **89** in 65 % yield after purification by column chromatography (Figure **3.13**).

A

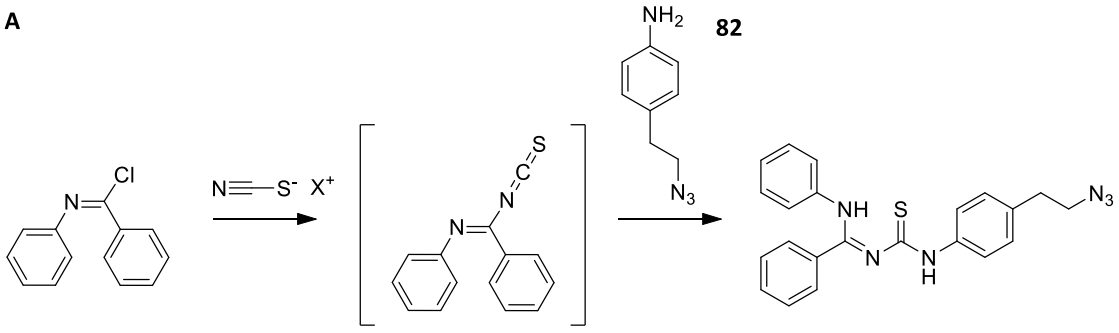

90 **91** **89**

Tested *N*-phenylbenzimidamide isothiocyanate formation conditions:

- 1) NaSCN, acetone, Ar, -15 to 0 °C, 30 min;
  2) **82**, DCM, Ar, r.t., overnight, no convertion;
- 1) NaSCN, acetone, Ar, -15 °C to r.t., overnight;
  2) **82**, DCM, Ar, r.t., overnight, no convertion;
- 1) KSCN, acetone, Ar, -15 to 0 °C, 30 min;
  2) **82**, acetone, Ar, r.t., overnight, no convertion;
- 1) NH_4SCN, DCM, Ar, r.t., 48 hours;
  2) **82**, DCM, Ar, r.t., overnight, low convertion;
- 1) KSCN, DCM, Ar, r.t., 48 hours;
  2) **82**, DCM, Ar, r.t., overnight, 70 %.

B

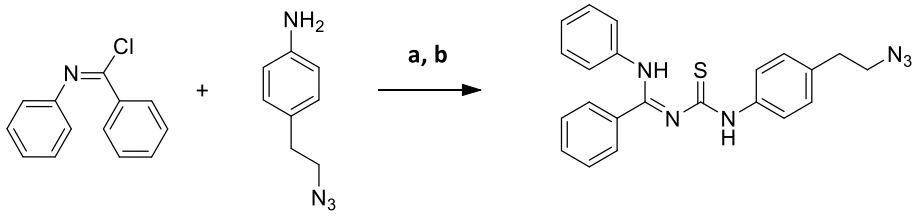

90 **82** **89**

Scheme 3.19: **A**) Tested conditions for the formation of isothiocyanate **91** from *N*-phenylbenzimidoyl chloride (**90**) and subsequent reaction with **82**. **B**) Final conditions for the synthesis of thiourea **89**: **a**) KSCN, DCM, Ar, r.t., overnight; **b**) **82**, DCM, Ar, r.t., 48 hours, 65 % over 2 steps.

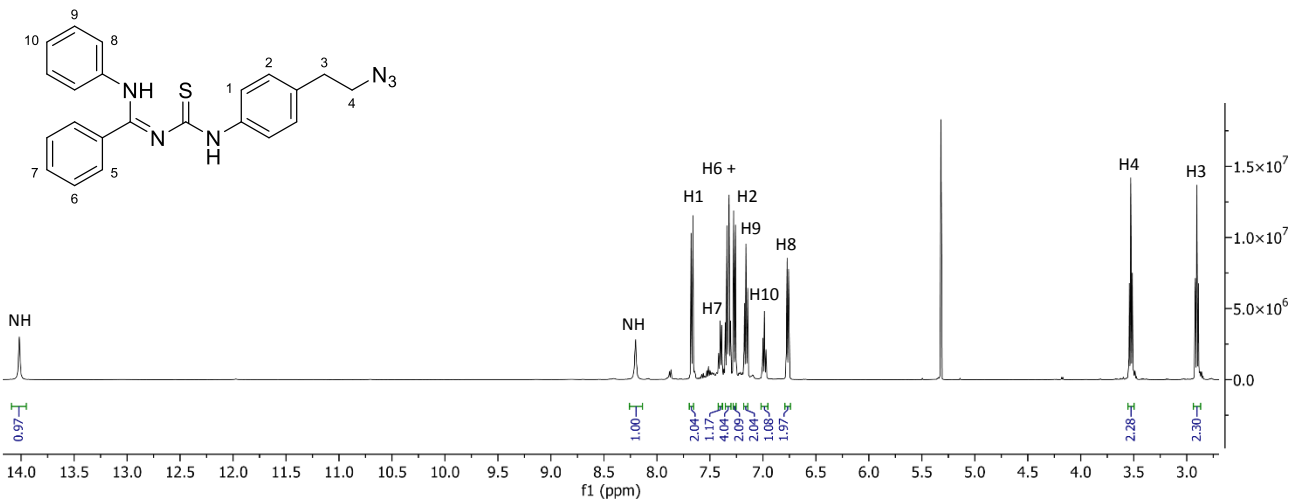

Figure 3.13: Structure, 500 MHz ^{1}H NMR spectrum of **89**.

Once obtained, the thiourea **89** was used to create the desired final product **92** (Scheme **3.20**). As first, the neat reaction with MeCN and the catalyst PIDA was tried, but difficulties arose due to the low amount of material available and the necessity of using high pressure, resulting to be not ideal for our purposes. It was then the alternative investigated pathway consisting of a first reaction with elemental bromine to promote an intramolecular ring closure (**93**) followed by the reaction with MeCN in presence of triethylamine to obtain the final product **92** in 56 % yield over two steps, after purification with column chromatography (Figure **3.14**).

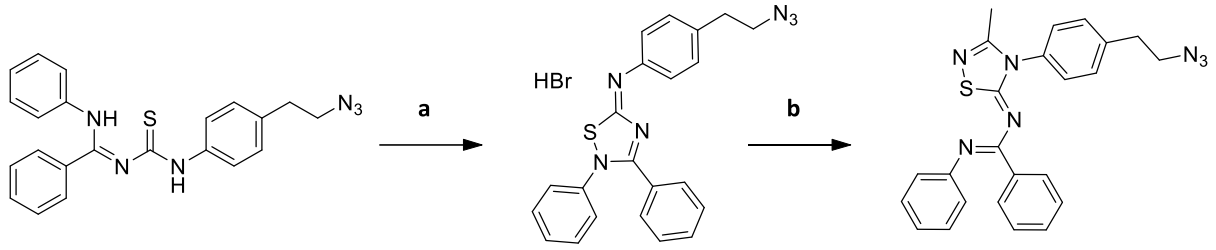

89 **93** **92**

Scheme 3.20: Synthesis of **92** by closure of the thiadiazolic ring: **a**) Br_2, DCM:EtOAc 1:2, r.t., 10 min; **b**) MeCN, Et_3N, refluxed, 2 hours, 56 % over 2 steps.

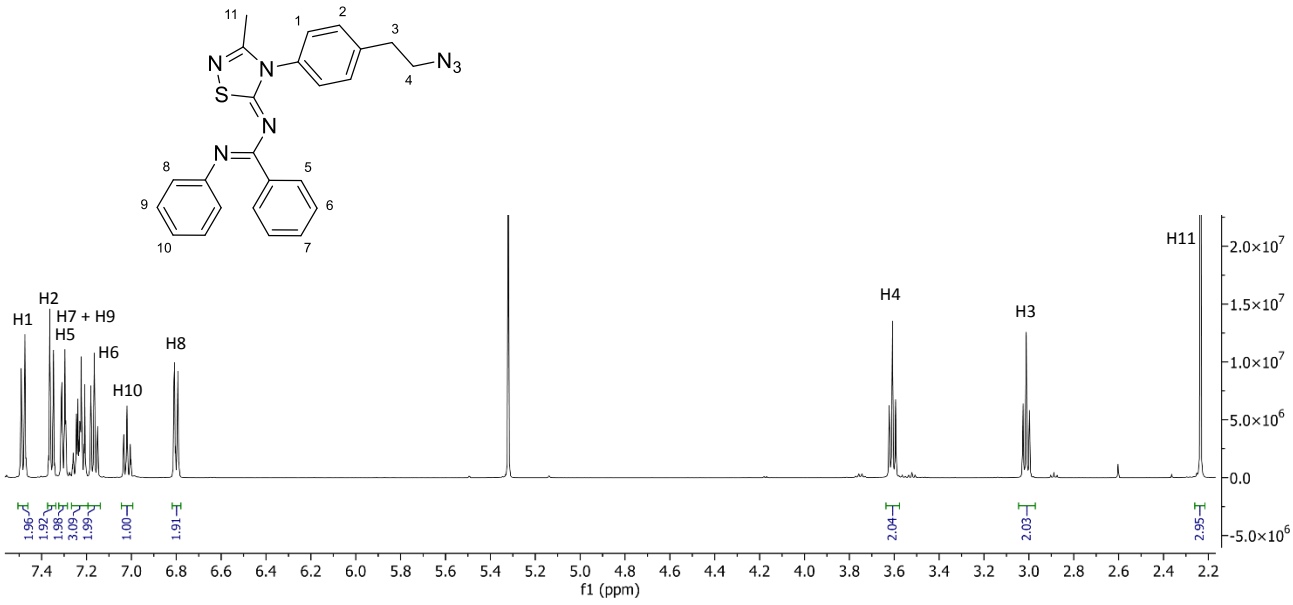

Figure 3.14: Structure, 500 MHz ^{1}H NMR spectrum of **92**.

3.2.5 Observations Regarding the RNF5 Recruiter

Through the previously described method, it was possible to design and synthesise a potential recruiting unit for the E3 ligase RNF5, so far never employed for PROTAC degrading technology. The possibility of recruitment of this particular enzyme could be especially interesting to target STING as physiologically ubiquitinated on lysine 150 by RNF5 in the process of proteasomal degradation. We therefore assume that this POI-E3 ligase combination could rely on a favourable protein-protein interaction, fundamental for the ternary complex formation and for high PROTAC potency.

Beyond the primary scope of this work, due to the strong involvement of RNF5 in different types of cancer, the creation of a modulator for this enzyme easily functionalized by click reaction, could be of great interest. In particular, RNF5 is known for being linked to different pro- or anti- tumoral activity depending on the model. In some malignancies, like hepatocellular carcinoma and acute myeloid leukaemia, an increased expression of the enzyme is correlated with worse prognosis.[281-283] However in breast cancer patients, a higher expression of RNF5 is associated with promoted proteasomal degradation of misfolded proteins generated by chemotherapy-related ER stress, reducing malignant cell proliferation.[284] In other cases, RNF5 exerts an anti-tumoral activity as in the case of neuroblastoma and melanoma, towards which the activity of analog-1 has been proven beneficial for a better outcome, impairing the cellular energy metabolism and inducing oxidative stress without significant side effects on healthy cells.[279]

In light of this, the development of RNF5 modulators represents a promising strategy for the treatment of several illnesses. Moreover, the possibility of an accessible modification through click chemistry, could open new opportunities for enlightening the mechanism of action of this enzyme and its role in different diseases and for the creation of new tools for specific targeting and delivery of the drug to the target cells.

3.2.6 Design and Synthesis of RNF5 Biotinylated Recruiter for Streptavidin Pulldown Assay

In order to verify the ability of the newly synthesised RNF5 recruiter to bind the desired enzyme, **94** a biotinylated version of the recruiter **92** for streptavidin pull down assay was designed and synthesised by exploiting the readily functionalizable azide. To this end, a commercial biotin derivative (**95**) containing a terminal alkyne was reacted with the RNF5 recruiter via Cu(I) catalysed click reaction (Scheme **3.21**).

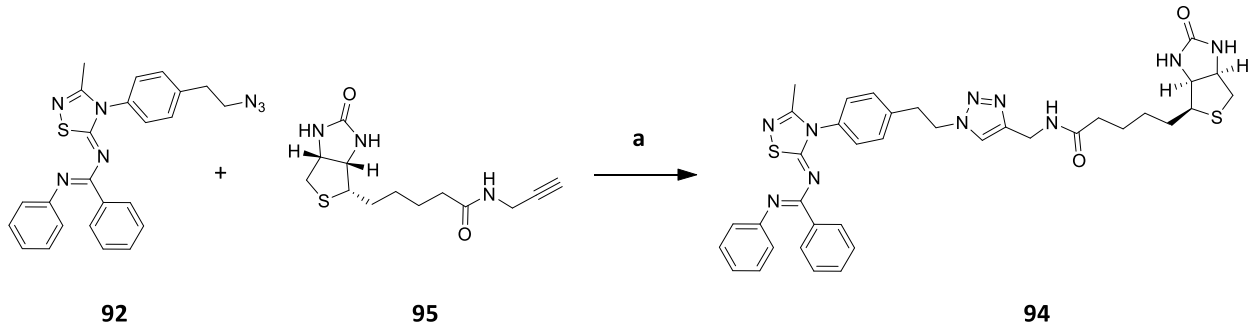

92 **95** **94**

Scheme 3.21: Synthesis of biotinylated derivative **94** via click reaction**: a**) CuBr, TBTA, DMF, 50 °C, 2 hours, 74 %.

As shown in Scheme **3.21**, the two components were reacted in presence of CuBr in oxygen-free conditions reached through degassing via freeze-pump-thaw the solvent DMF and maintaining the reaction mixture under Ar. TBTA was chosen as ligand for the catalytic species Cu(I) to accelerate the reaction. After stirring at 50 °C for 2 hours and purification of the crude via preparative HPLC, the desired product **94** was obtained in 74 % yield (Figure **3.15**).

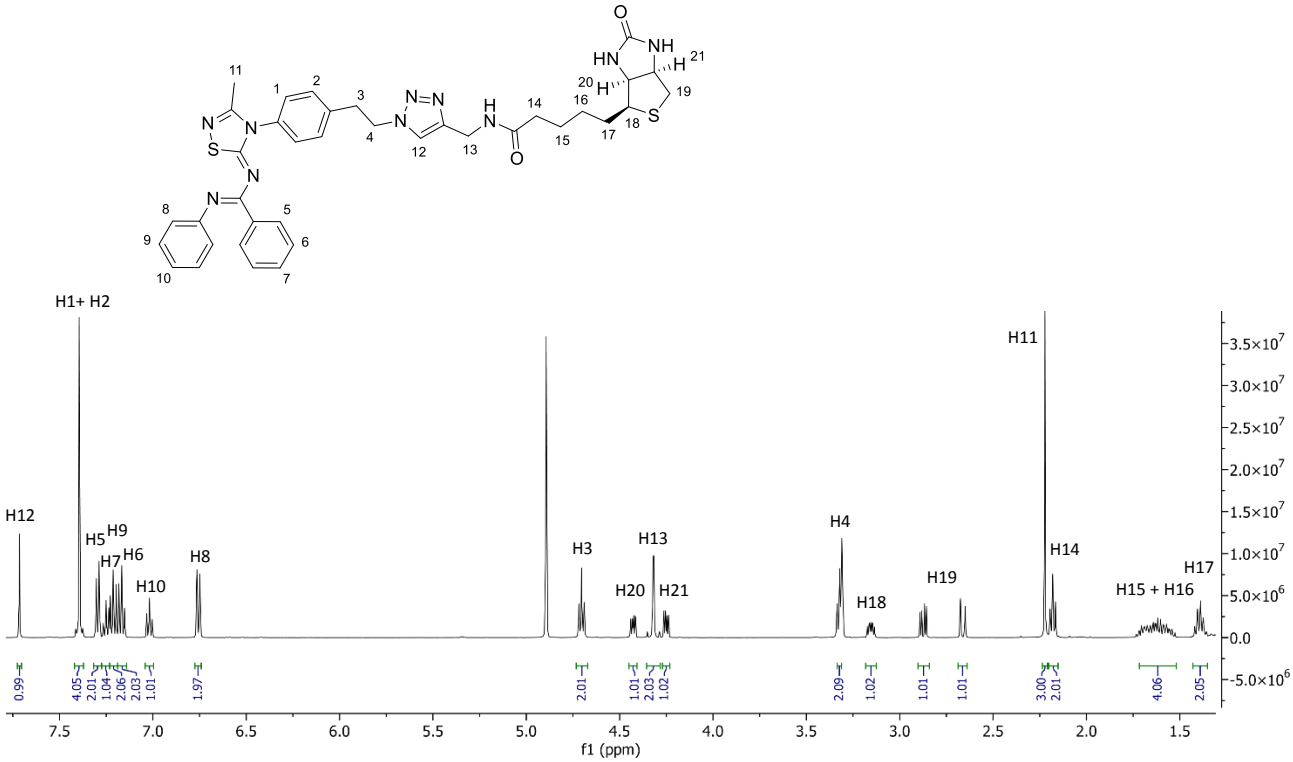

Figure 3.15: Structure, 500 MHz ^{1}H NMR spectrum of **94**.

The obtained compound would then be employed in a biotin - streptavidin protein pull down assay to assess the ability of recruitment of RNF5 by the newly synthesised molecule.

3.3 STING Degrading PROTACs

After all the components were synthesised and characterized, thanks to the versatility of the system, it was possible to produce different classes of potential STING-degrading PROTACs, by combining the individual recruiters and linkers via copper(I)-catalysed azide-alkyne cycloaddition (CuAAC). In addition to the synthesised E3 ligase recruiters, a set of three clickable VHL recruiters with different linker lengths were purchased from *Merck-Sigma Aldrich* (VHL1, VHL2, VHL3, Scheme **3.22**).

Depending on the components and on their solubility, the Cu(I) catalysed click reaction was performed either in water, alone or in combination with other polar solvents (DMSO, MeCN, DMF), or in DMF with the appropriate ligands to solubilize the catalyst.

The PROTAC molecules will be divided in two categories depending on the STING recruiter used, cGAMP and inhibitor-based PROTACs. Each recruiter was coupled to the different E3 ligase counterpart with different linker lengths. The obtained PROTACs can be rationalized in cGAMP – CRBN, cGAMP – VHL, cGAMP – RNF5, inhibitor – CRBN, inhibitor – VHL and inhibitor – RNF5, as shown in Scheme **3.22** and later in Figure **3.22**.

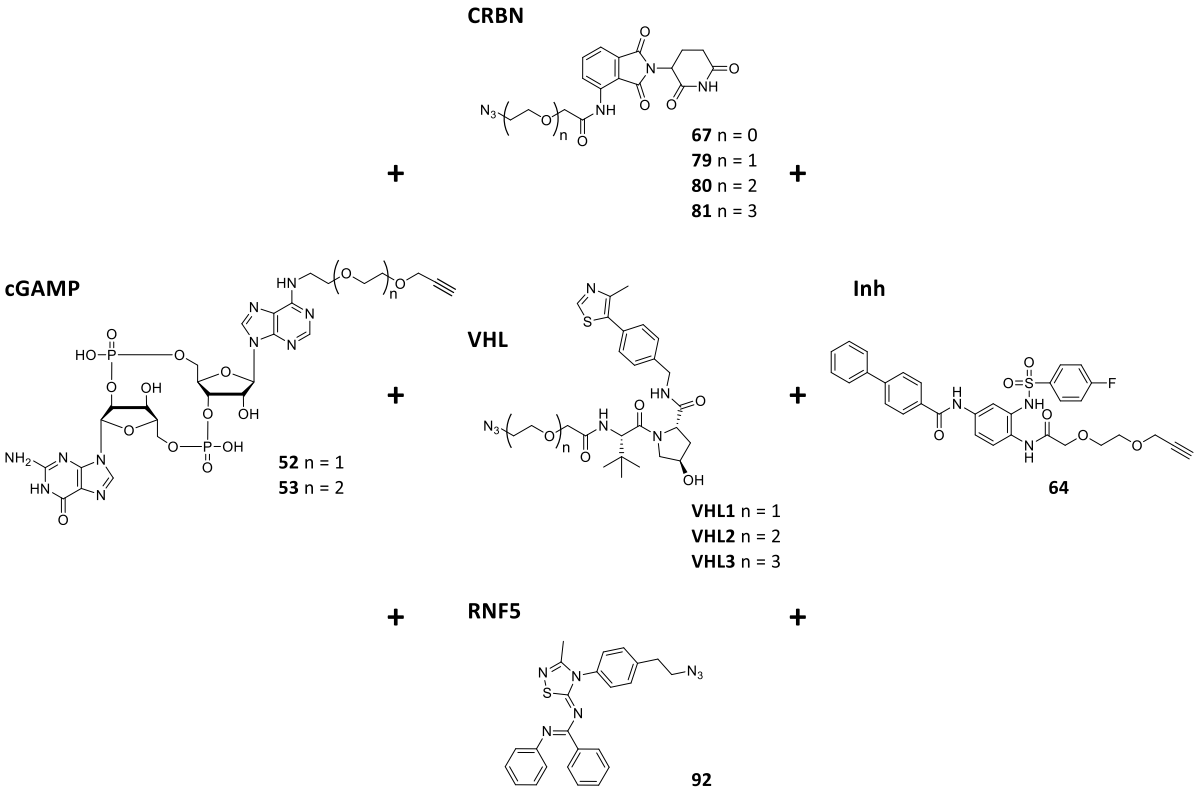

Scheme 3.22: Coupling scheme for the formation of STING PROTACs through Cu(I) catalysed click chemistry by combining an alkyne containing STING recruiter with an E3 ligase recruiter presenting an available azide group.

This pool of potential STING PROTACs will serve as a first important starting point for the investigation and *in vitro* evaluation of STING degradation ability which will give the basis for future activity-based optimization.

3.3.1 Synthesis of cGAMP – CRBN PROTACs

For this first class of STING-targeted PROTACs, we combined the cGAMP-based STING recruiters **52** and **53** bearing a terminal alkyne, and the pomalidomide-based CRBN recruiters **67**, **79** and **81** with different linker lengths and an azide at the end (Scheme **3.23**).

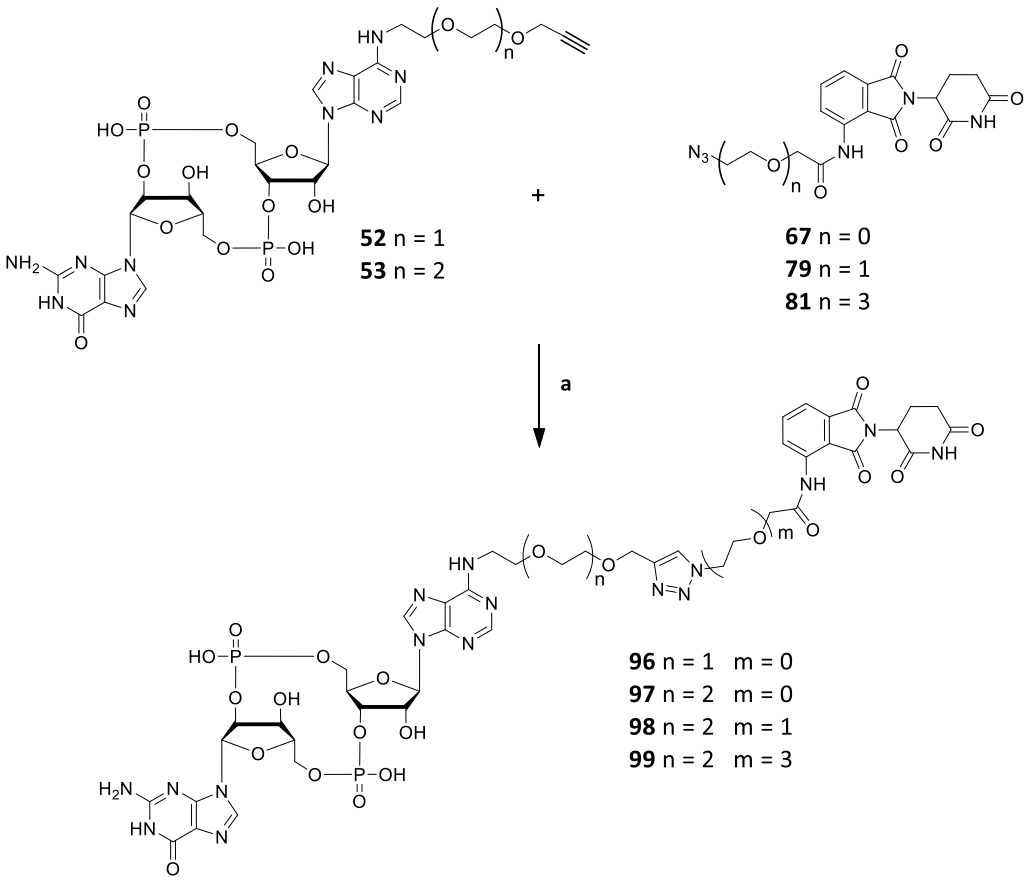

Scheme 3.23: Synthesis of cGAMP - CRBN STING targeting PROTACs: **a**) $CuSO_4$, THPTA, Na ascorbate, H_2O, MeCN, DMSO, Ar, 50 °C, 2.5 hours. Yields: **96**: 87 %, **97**: 67 %, **98**: 90 %, **99**: 62 %.

As shown in Scheme **3.23**, the two halves were coupled through Cu(I)-catalysed click reaction generated *in situ* from $CuSO_4$ reduced to Cu(I) by sodium ascorbate present in high excess. The reaction was performed in H_2O and DMSO and/or MeCN were added to improve the solubility of the pomalidomide derivative, otherwise poorly soluble in H_2O. THPTA was chosen as ligand for the Cu(I) catalyst, improving his solubility and consequently the availability to the reagents. In general, the reported procedure allowed in circa 2 hours at 45°C, to obtain the final products **96**, **97**, **98** and **99** in medium - high yields after the purification with preparative HPLC (Figure **3.16**).

96

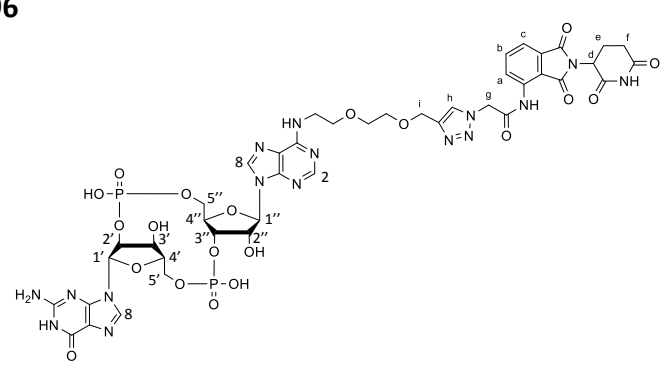

^{31}P NMR

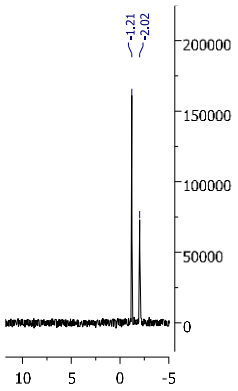

^{1}H NMR

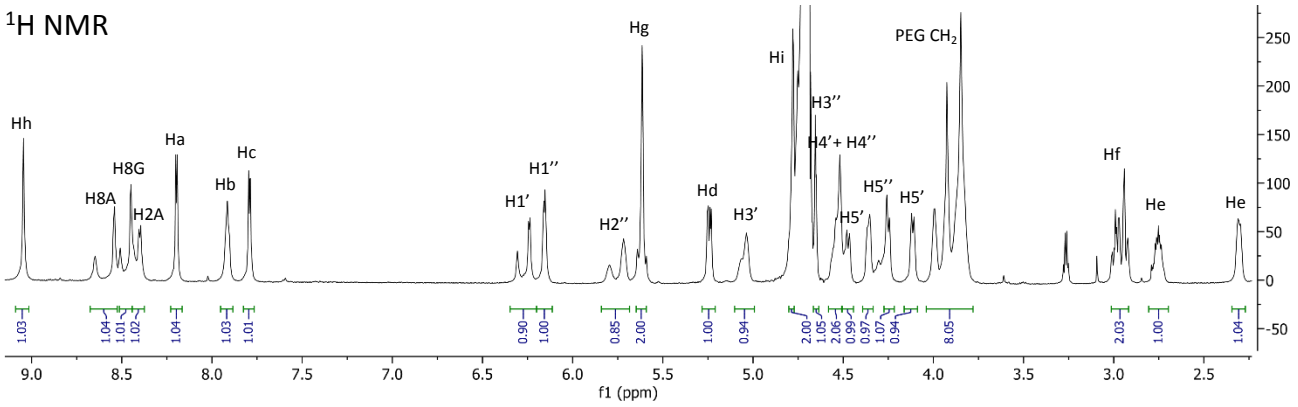

97

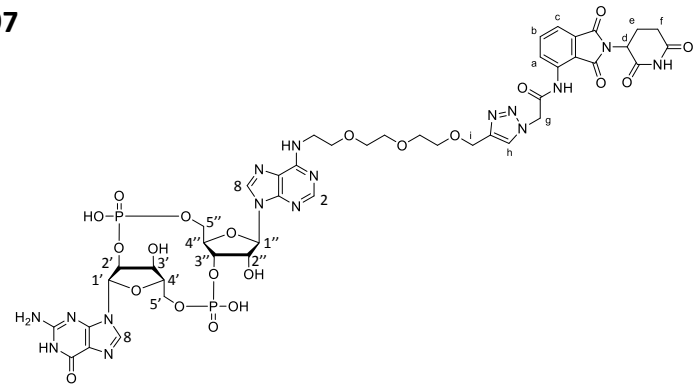

^{31}P NMR

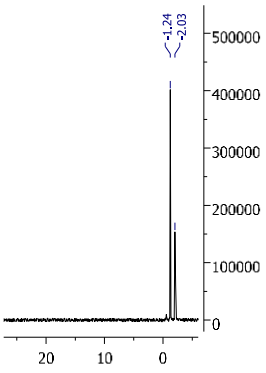

^{1}H NMR

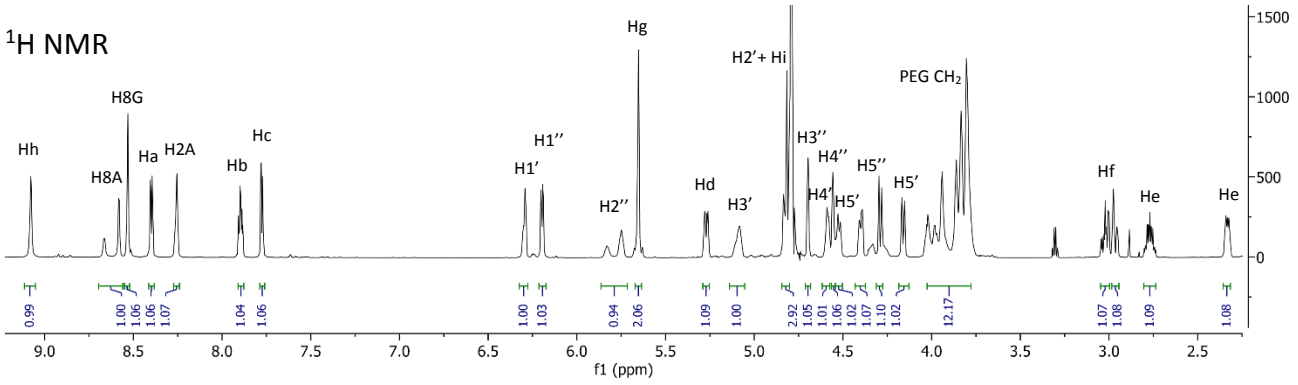

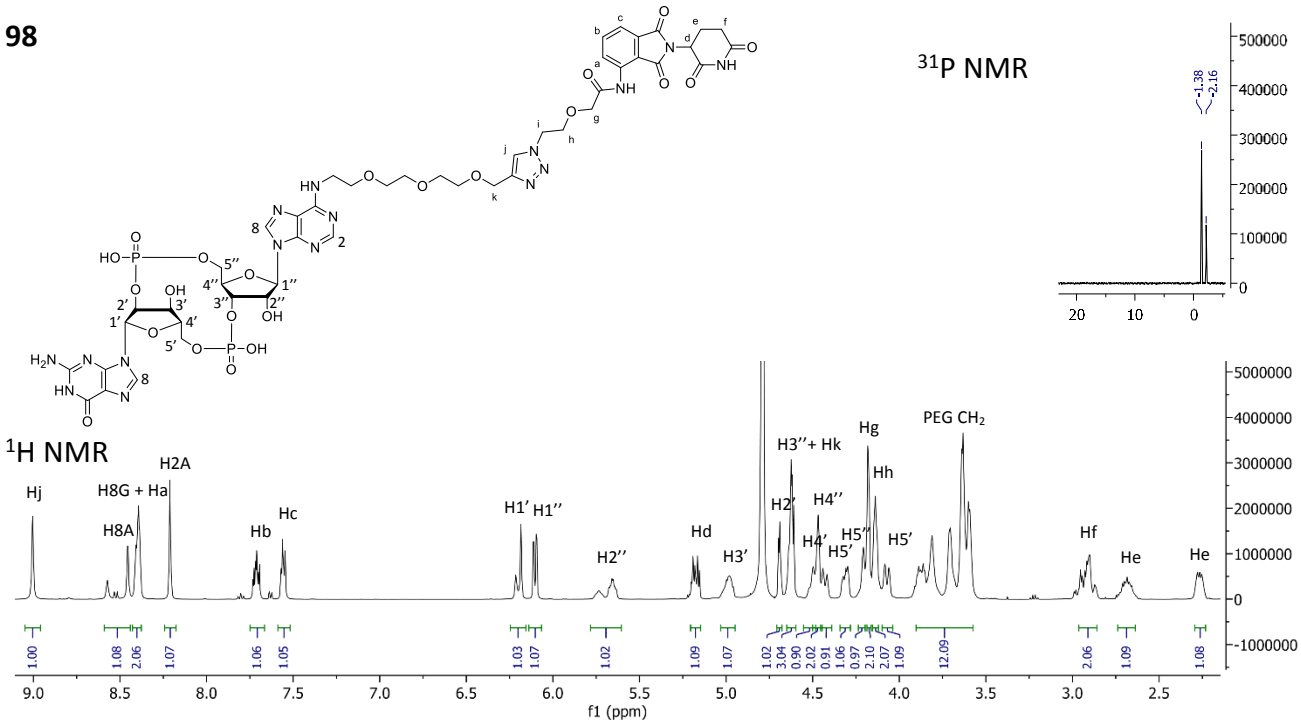

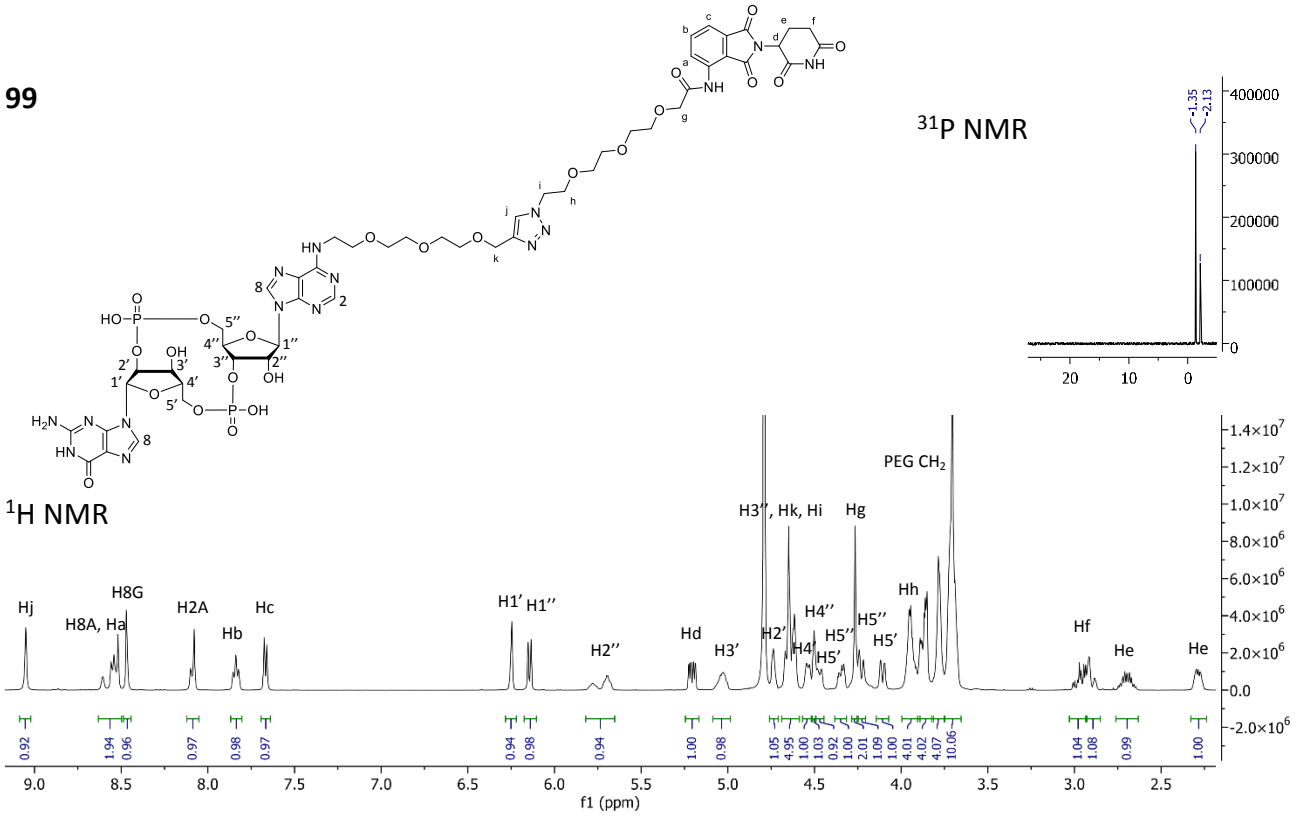

Figure 3.16: Structure, ^{1}H NMR and ^{31}P NMR spectra of cGAMP-CRBN STING PROTACs: **96** 800 MHz ^{1}H NMR, 201 MHz ^{31}PNMR in 9 D_2O : 1 MeCN; **97** 800 MHz ^{1}H NMR, 201 MHz ^{31}PNMR in 9 D_2O : 1 MeCN; **98** 500 MHz ^{1}H NMR, 202 MHz ^{31}PNMR in 9 D_2O : 1 MeCN; **99** 500 MHz ^{1}H NMR, 202 MHz ^{31}PNMR in 9 D_2O : 1 MeCN.

3.3.2 Synthesis of cGAMP – VHL PROTACs

In order to explore different combinations of POI and E3 ligase recruiters to identify the optimal configuration for our purpose, it was purchased a commercially available VHL recruiter with three different PEG linker lengths, with an azide on the terminus. Once again, through click reaction, it was possible to couple them with the two different cGAMP-based STING recruiters for the formation of cGAMP – VHL PROTACs (Scheme **3.24**).

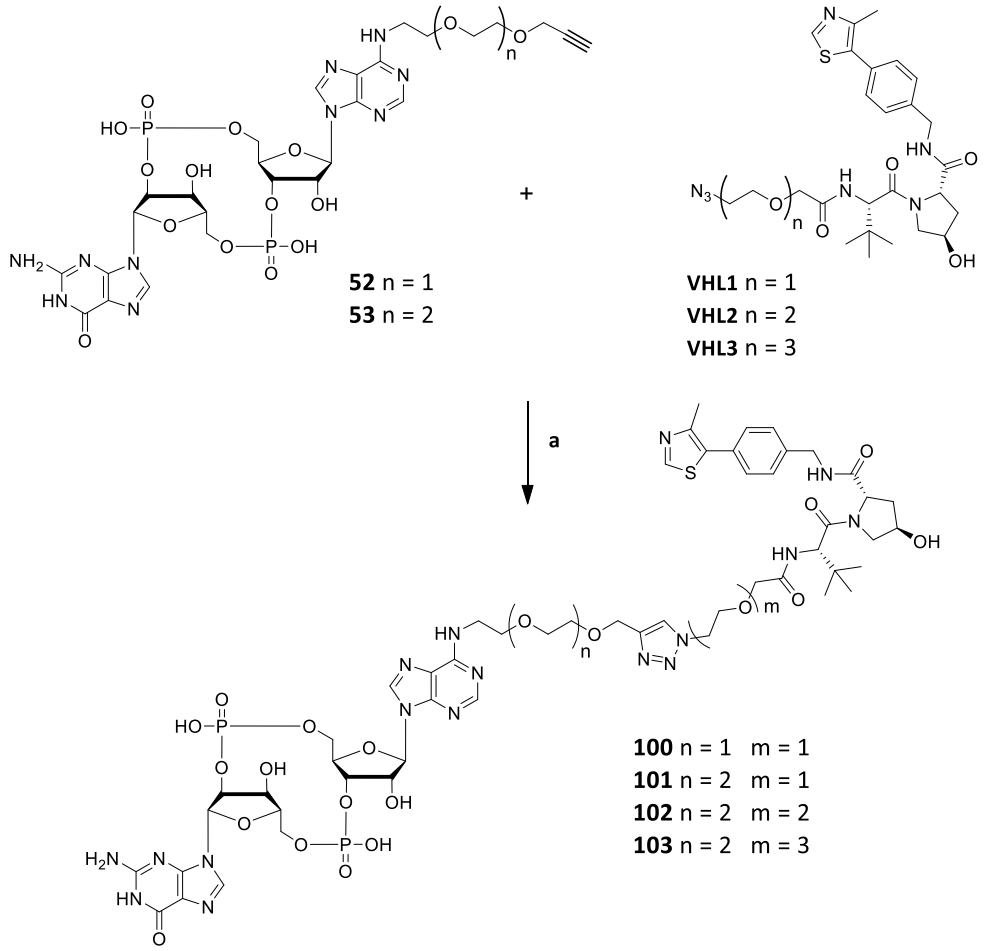

Scheme 3.24: Synthesis of cGAMP - VHL STING targeting PROTACs: **a**) $CuSO_4$, THPTA, Na ascorbate, H_2O, MeCN, Ar, 45 °C, 3.5 hours. Yields: **100**: 83 %, **101**: 90 %, **102**: 88 %, **103**: 91 %.

The click reaction was performed in H_2O with the help of MeCN to solubilize the relative VHL recruiter, introducing the catalytic copper as $CuSO_4$, reduced *in situ* to the active form Cu(I) by an excess of sodium ascorbate. THPTA was chosen as a ligand for Cu(I). After circa 2 hours at 45 °C, the four different final products **100**, **101**, **102** and **103** were isolated in moderately high yields after the purification with preparative HPLC (Figure **3.17**).

100

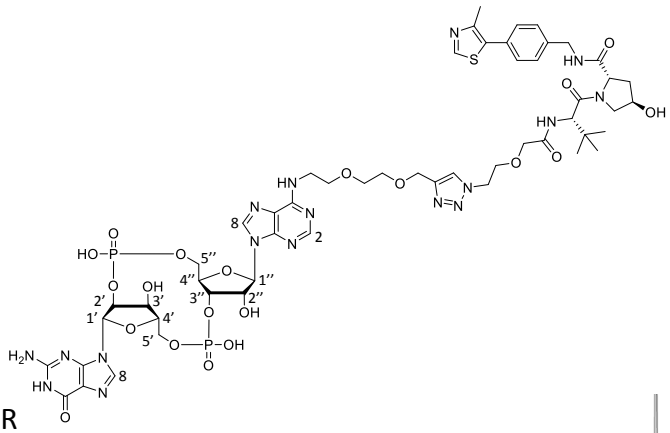

^{31}P NMR

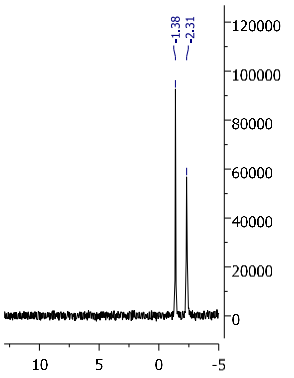

^{1}H NMR

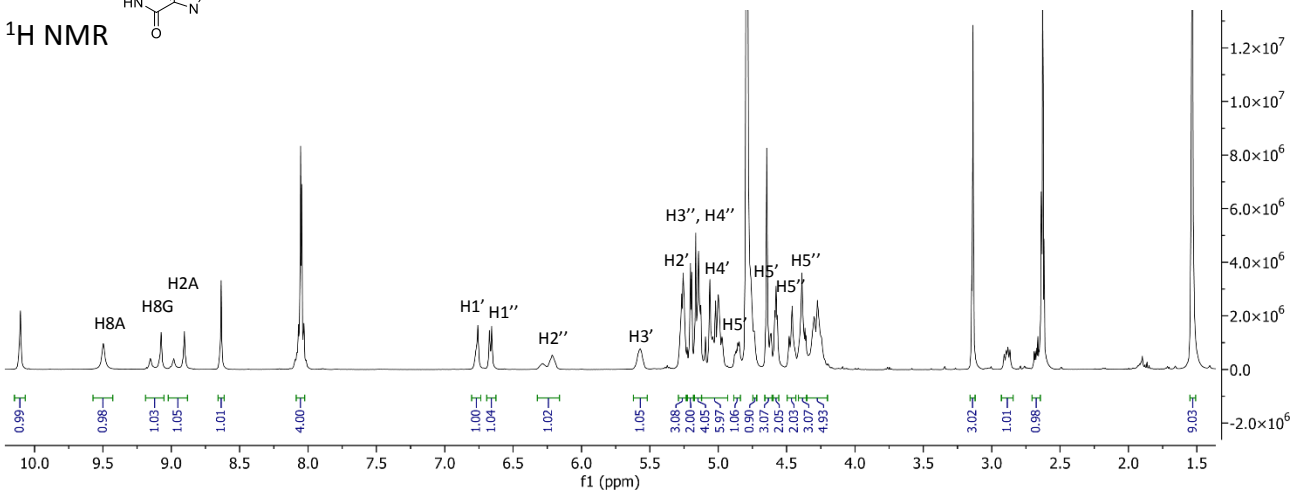

101

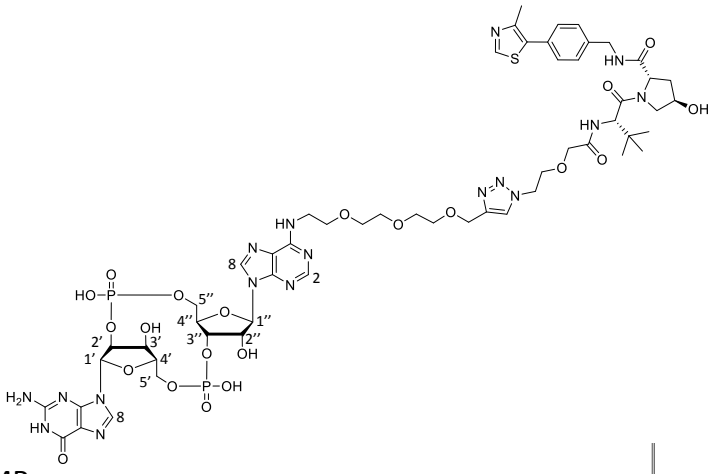

^{31}P NMR

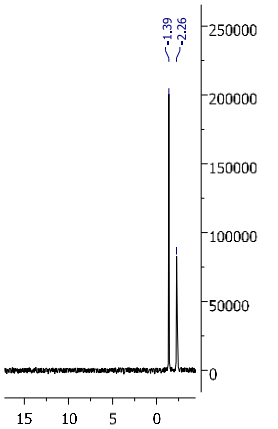

^{1}H NMR

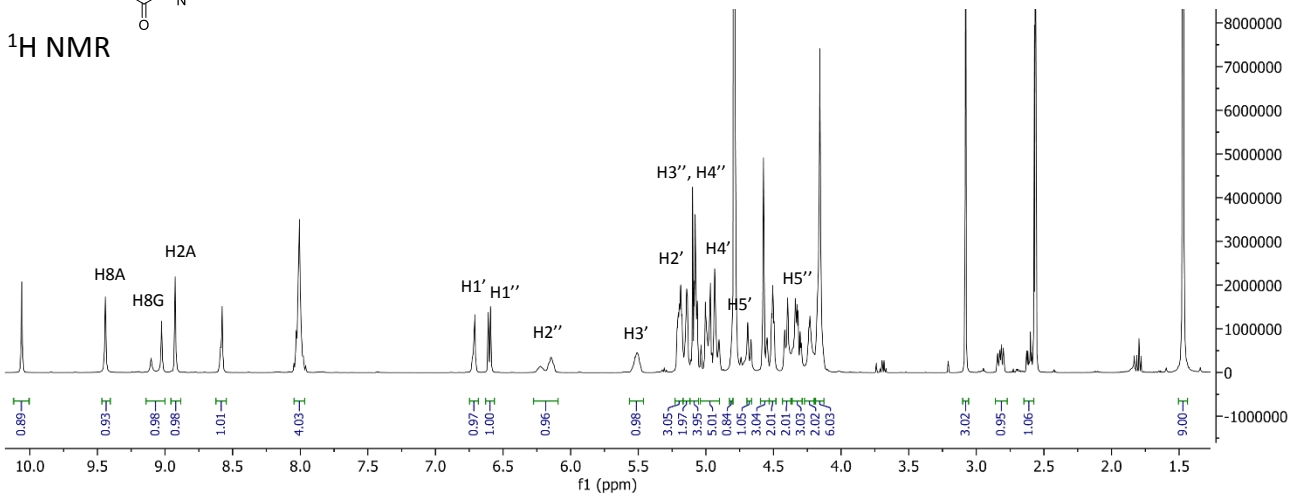

102

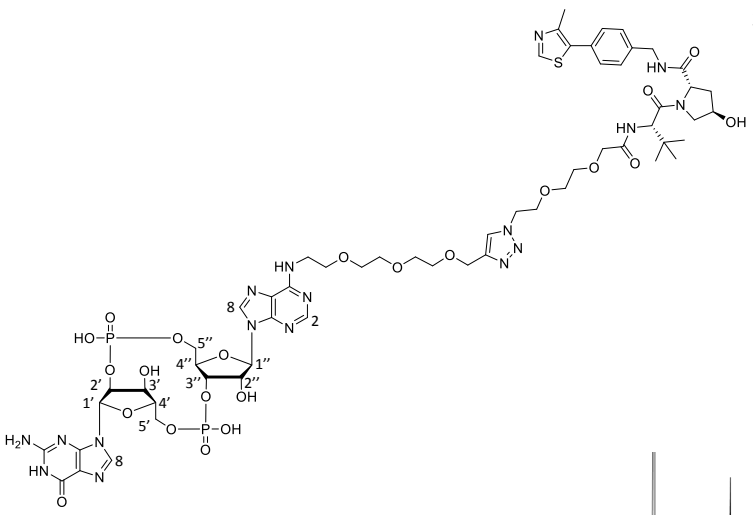

^{31}P NMR

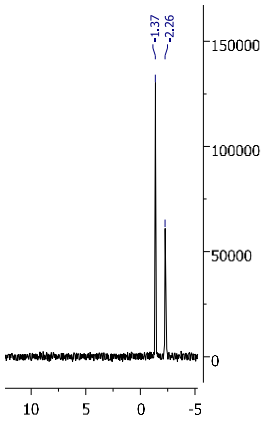

^{1}H NMR

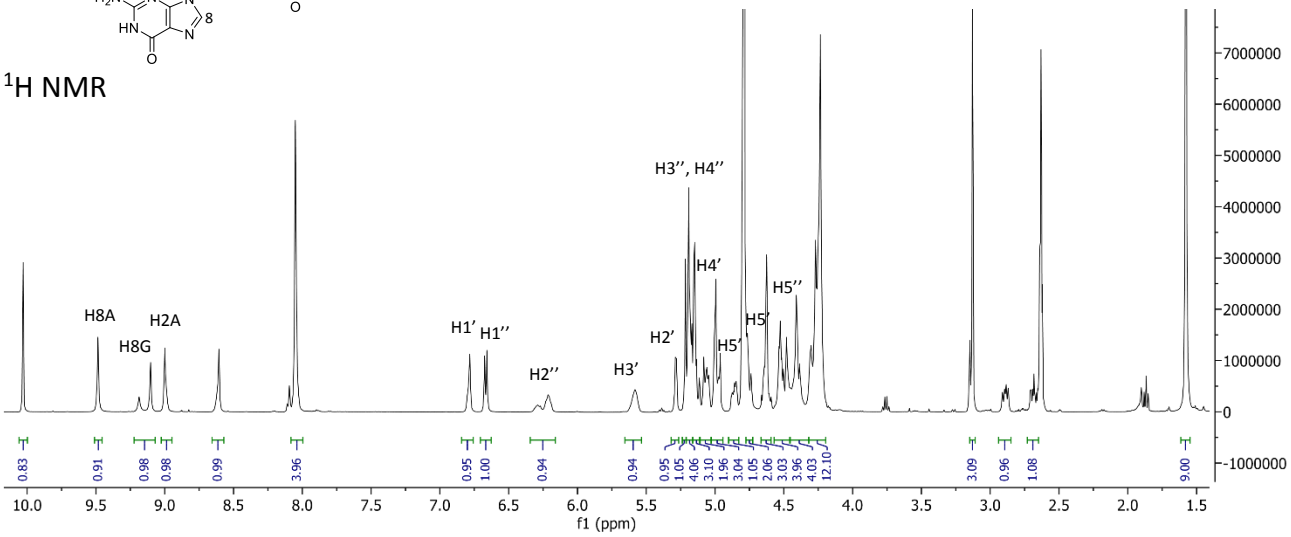

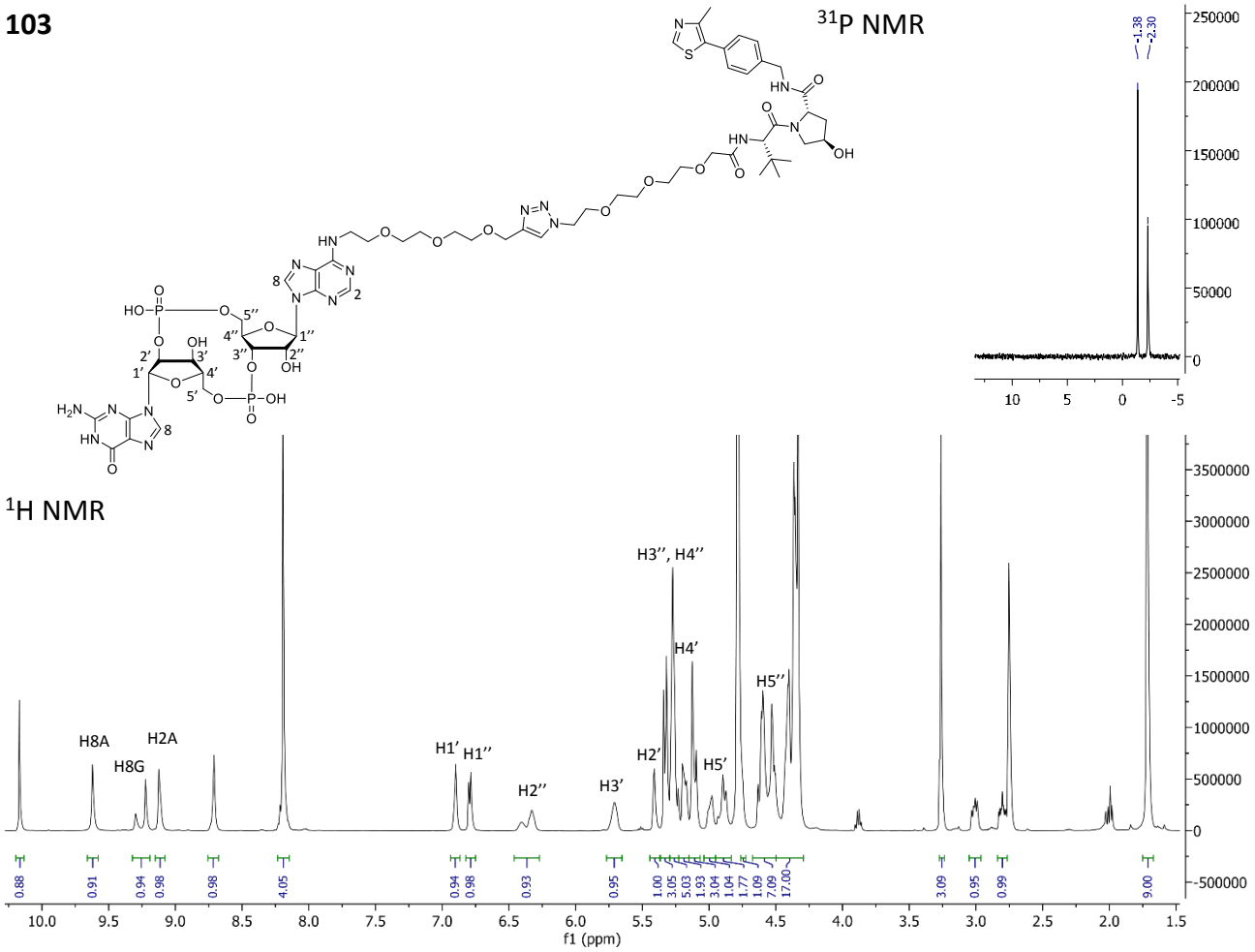

Figure 3.17: Structure, ^{1}H NMR 500 MHz and ^{31}P NMR 202 MHz spectra of cGAMP-VHL STING PROTACs in 9 D_2O : 1 MeCN **100**, **101**, **102**, **103**.

3.3.3 Synthesis of cGAMP – RNF5 PROTACs

Along with the recruitment of the two most common E3 ligases utilized for the PROTAC technology, we produced RNF5 recruiting PROTACs. This was obtained by coupling the newly synthesized compound **92**, whose design is based on a RNF5 activator, to recruit the same ligase responsible for the physiological ubiquitin-directed degradation of STING. The two units were coupled via click reaction between the terminal alkyne on the modified CDN and the azide on the RNF5 recruiter to obtain compounds **104** and **105** (Scheme **3.25**).

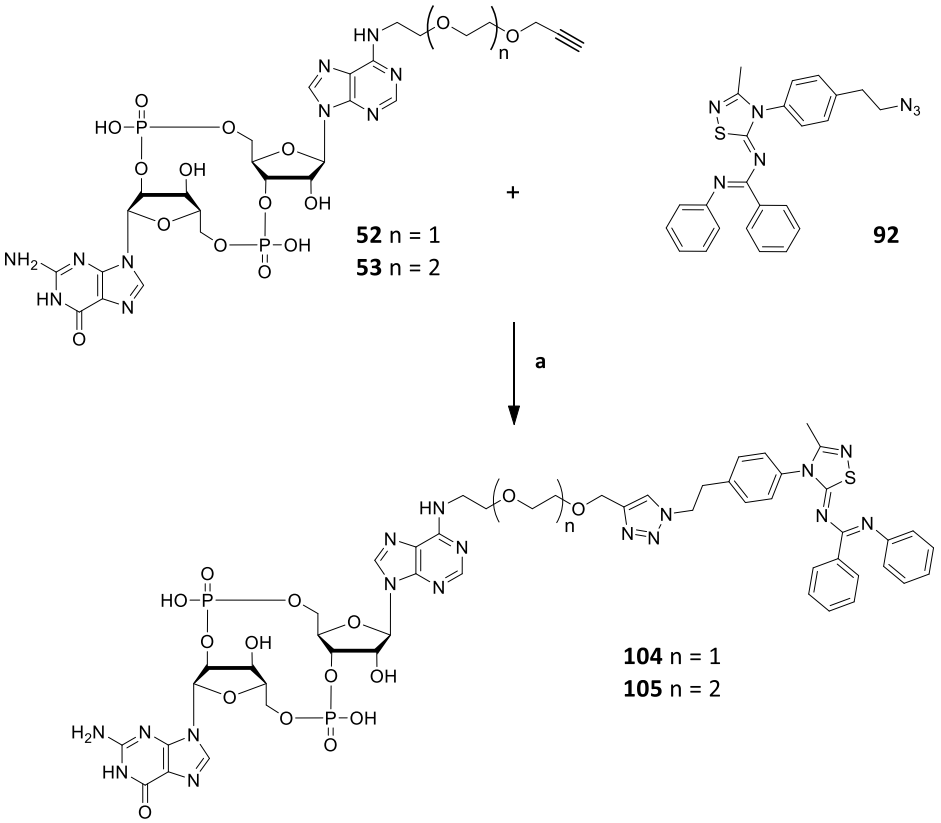

Scheme 3.25: Synthesis of cGAMP – RNF5 STING targeting PROTACs: **a**) $CuSO_4$, THPTA, Na ascorbate, H_2O, DMF, Ar, 45 °C, 2 hours. Yields: **104**: 48 %, **105**: 46 %.

The coupling reaction was performed in H_2O with the addition of DMF to facilitate the solubilisation of the RNF5 recruiter. The catalytic Cu(I), introduced as $CuSO_4$ reduced *in situ* by sodium ascorbate in large excess, is complexed and kept in solution by the ligand THPTA, increasing the reactivity. After stirring at 45 °C for 2 hours circa, the two RNF5 recruiting PROTACs for STING degradation **104** and **105** were isolated after the purification with preparative HPLC (Figure **3.18**).

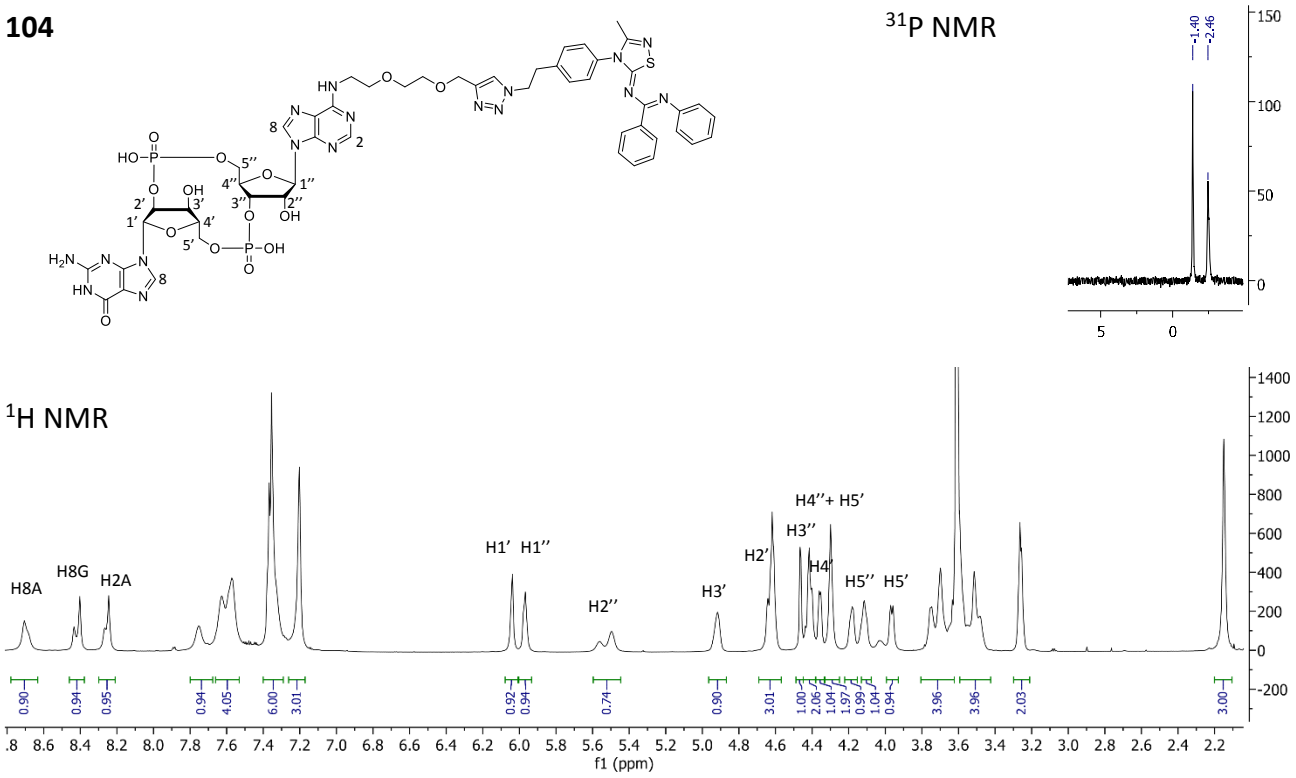

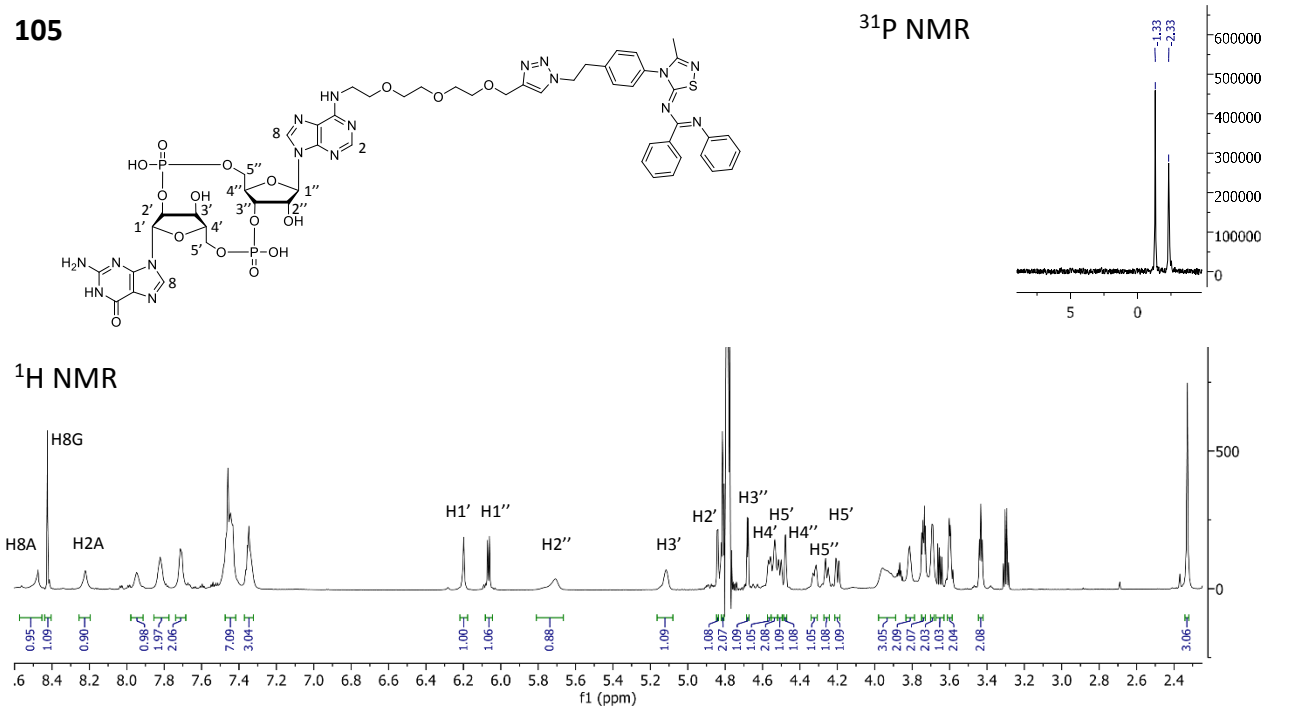

Figure 3.18: Structure, ^{1}H NMR 800 MHz and ^{31}P NMR 201 MHz spectra of cGAMP-RNF5 STING PROTACs **104** in 9 MeCN : 1 D_2O and **105** in 9 D_2O : 1 MeCN.

3.3.4 Synthesis of Inh – CRBN PROTACs

In addition to the cGAMP-based PROTACs, compound **64**, was used to synthesize a new class of PROTACs with which STING would be recruited by a derivative of an inhibitor, avoiding the problem related to CDNs (see section **3.1.3**). This new possible recruiter, bearing an alkyne moiety at the end of the PEG linker, was initially coupled with pomalidomide-based CRBN recruiters via click reaction exploiting their terminal azide to obtain **106**, **107**, **108** and **109** (Scheme **3.26**).

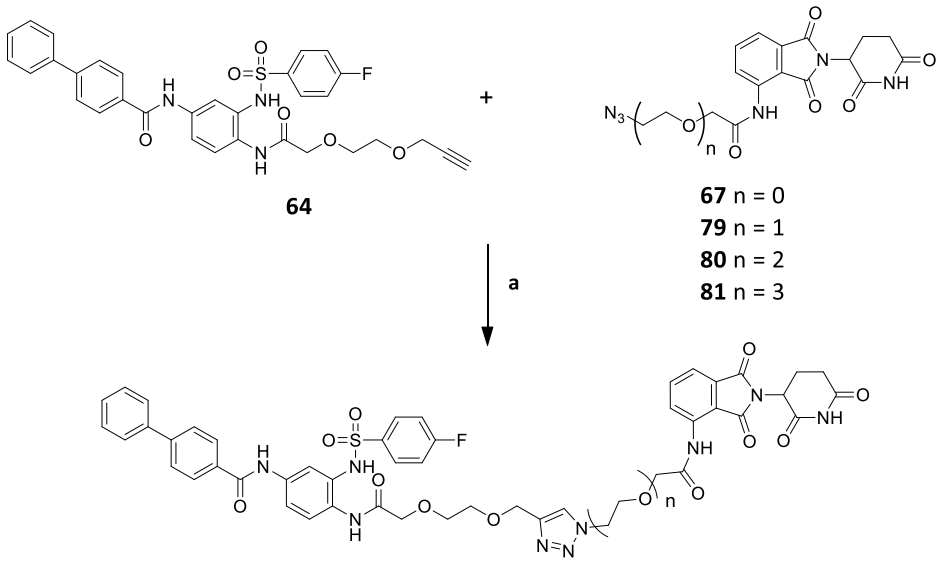

Scheme 3.26: Synthesis of Inh – CRBN STING targeting PROTACs: **a**) CuBr, TBTA, DMF, Ar, 50 °C, 2 hours. Yields: **106**: 47 %, **107**: 81 %, **108**: 92 %, **109**: 97 %.

Differently from the cGAMP derivatives, the reagents in this case were not soluble in H_2O, driving the choice of a suitable solvent for the click reaction towards DMF. In this case, the catalytic Cu(I) is introduced directly in the form of CuBr in presence of TBTA as a ligand. Due to the high sensibility against oxidation, the reaction was carried out under strict oxygen free conditions, under Ar and degassing the DMF by freeze-pump-thaw procedure. In these conditions, after 2 hours at 50 °C there was no evidence of starting material anymore and the four final products **106**, **107**, **108** and **109** were isolated in moderately high yields after purification with preparative HPLC (Figure **3.19**).

106

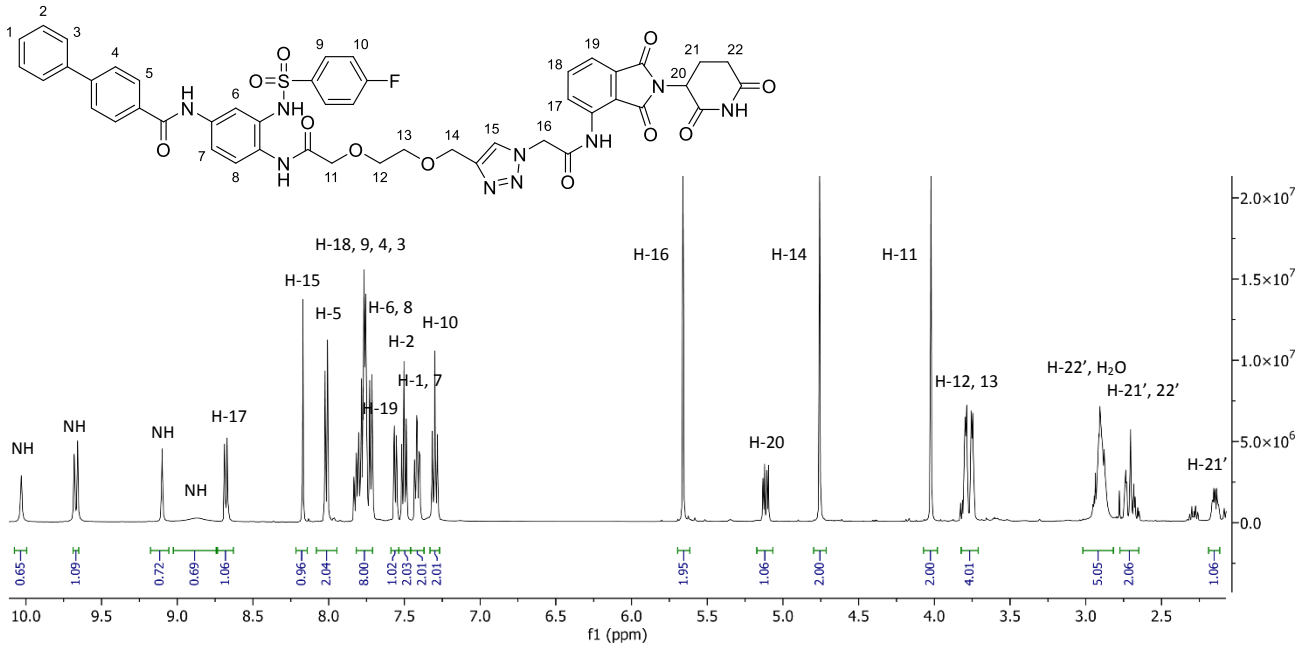
H-18, 9, 4, 3
H-15
H-5
H-6, 8
H-10
H-2
H-1, 7
H-19
H-17
NH
NH
NH
NH
H-16
H-14
H-11
H-20
H-12, 13
H-22', H2O
H-21', 22'
H-21'
f1 (ppm)

107

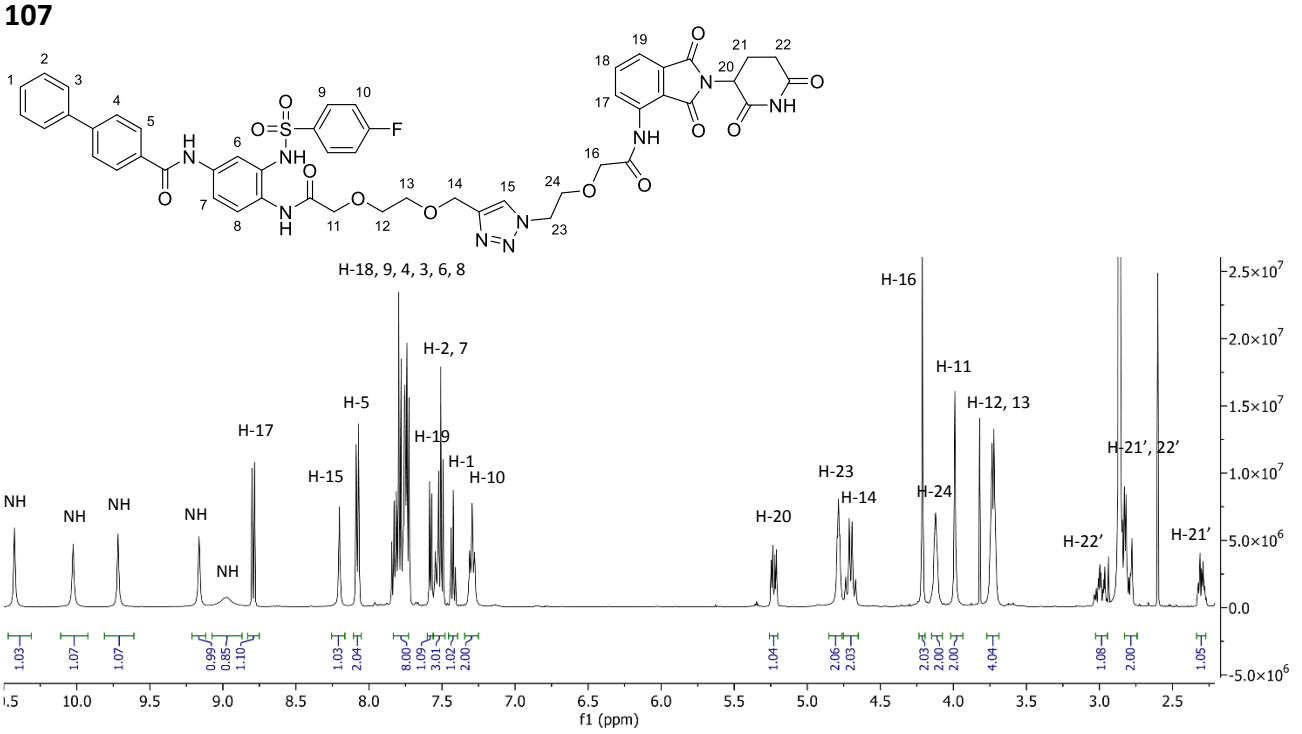
H-18, 9, 4, 3, 6, 8
H-16
H-2, 7
H-11
H-5
H-12, 13
H-17
H-19
H-1
H-15
H-10
H-23
H-14
H-24
H-21', 22'
NH
NH
NH
NH
NH
H-20
H-22'
H-21'
f1 (ppm)

108

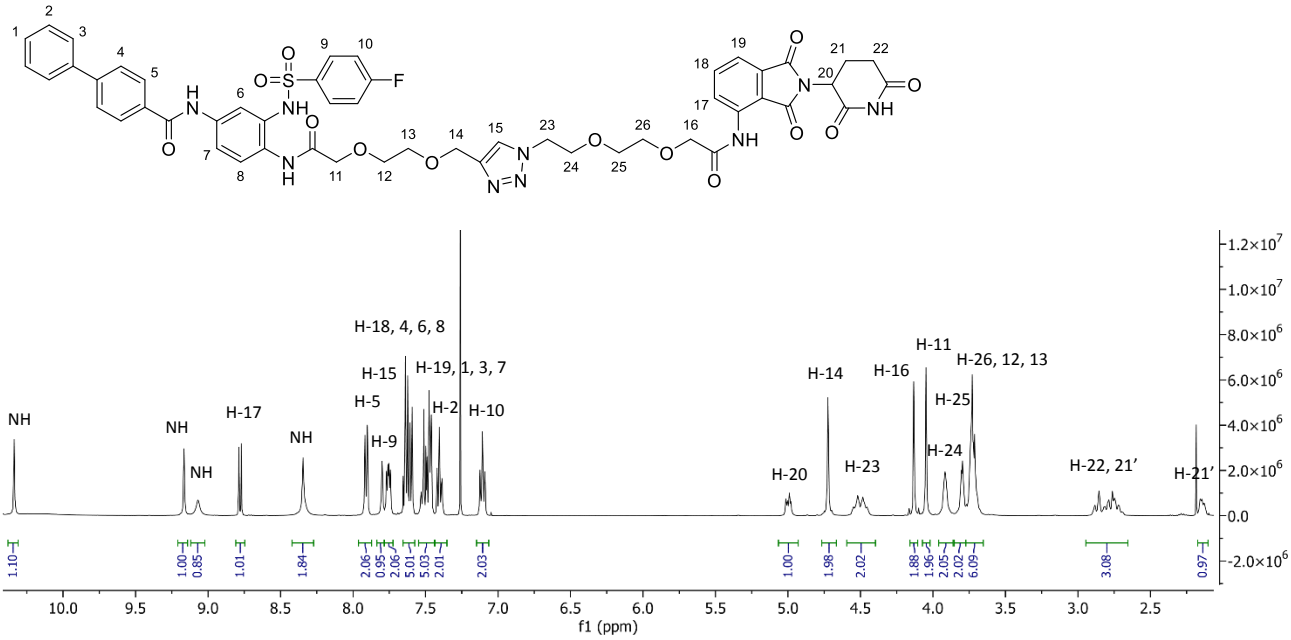

109

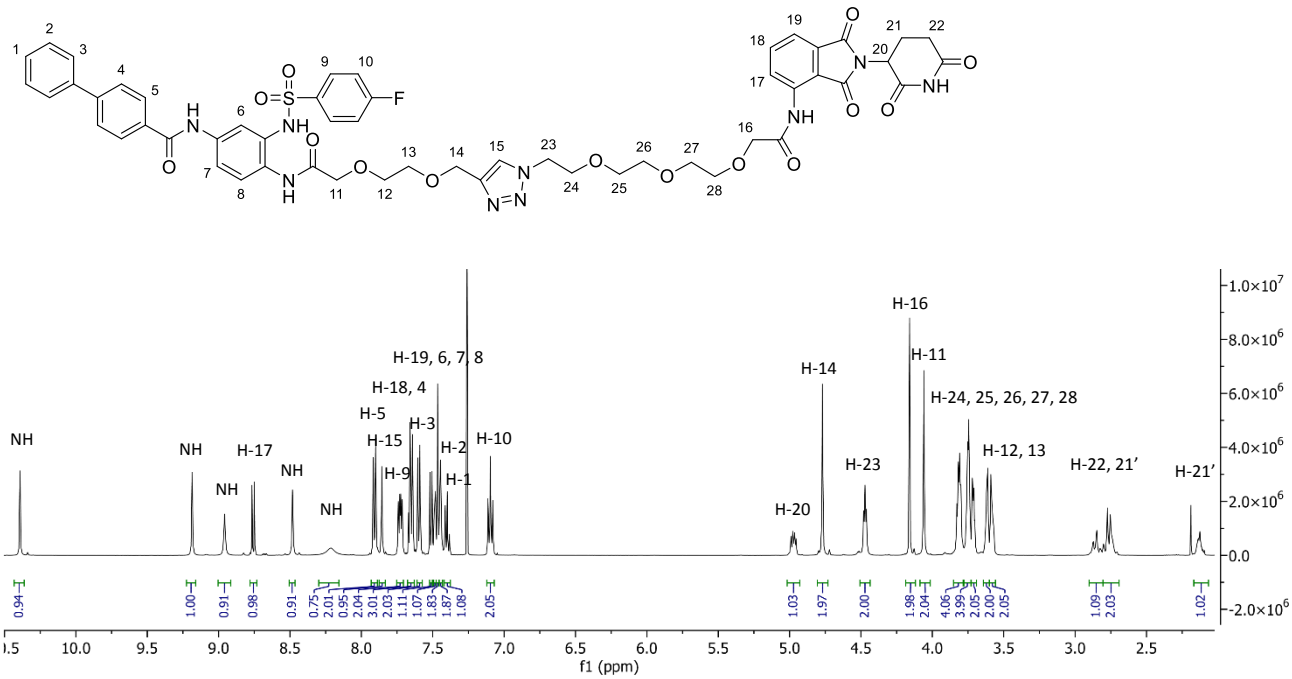

Figure 3.19: Structure and ^{1}H NMR 500 MHz spectra of Inh-CRBN STING PROTACs **106**, **107** in deuterated acetone and **108**, **109** in $CDCl_3$.

3.3.5 Synthesis of Inh – VHL PROTACs

As well as for cGAMP-based PROTACs, exploring the possibility of recruiting different E3 ligases other than CRBN, was investigated. Three different VHL recruiting molecules based on the same motif with different PEG spacers from a terminal azide, were purchased from *Merck-Sigma Aldrich*. Due to the presence of the clickable moiety, it was possible to couple them with the STING recruiter, compound **64**, via copper-catalysed click reaction to obtain **110**, **111** and **112** (Scheme **3.27**).

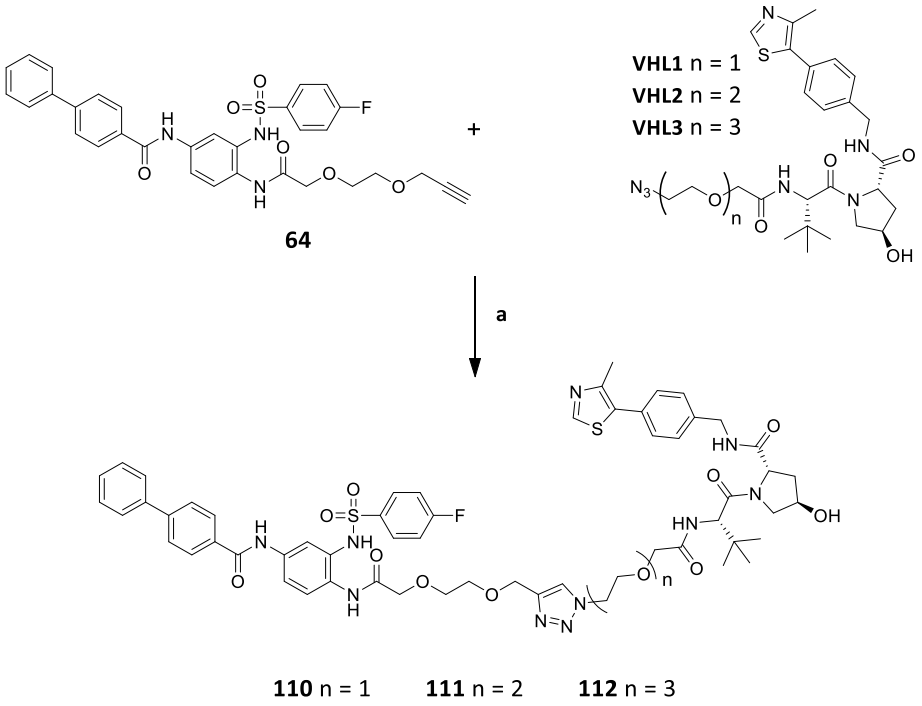

Scheme 3.27: Synthesis of Inh – VHL STING targeting PROTACs: **a**) CuBr, TBTA, DMF, Ar, 50 °C, 2 hours. Yields: **110**: 91 %, **111**: 98 %, **112**: 88 %.

Once again, the choice of the solvent able to solubilize all the reagents, fell on DMF. The strict oxygen free conditions, reached through freeze-pump-thaw and Ar atmosphere, prevented the catalytic copper, introduced as CuBr, to be oxidized to the inactive Cu(II). TBTA was used as ligand for copper and after stirring at 50 °C for two hours, the three final products **110**, **111** and **112** were isolated in high yields after preparative HPLC purification (Figure **3.20**).

110

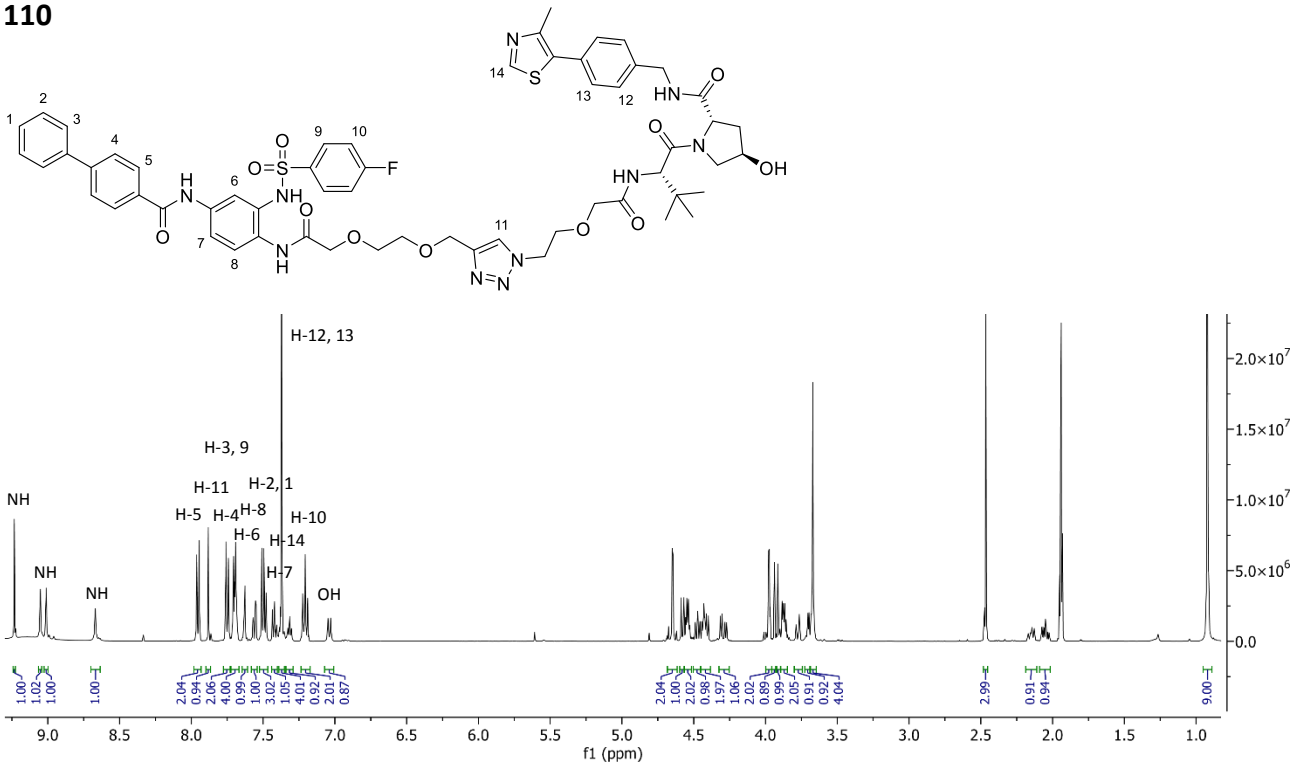
H-12, 13
H-3, 9
H-11
H-2, 1
H-5
H-4
H-8
H-10
H-6
H-14
H-7
NH
NH
NH
OH
f1 (ppm)

111

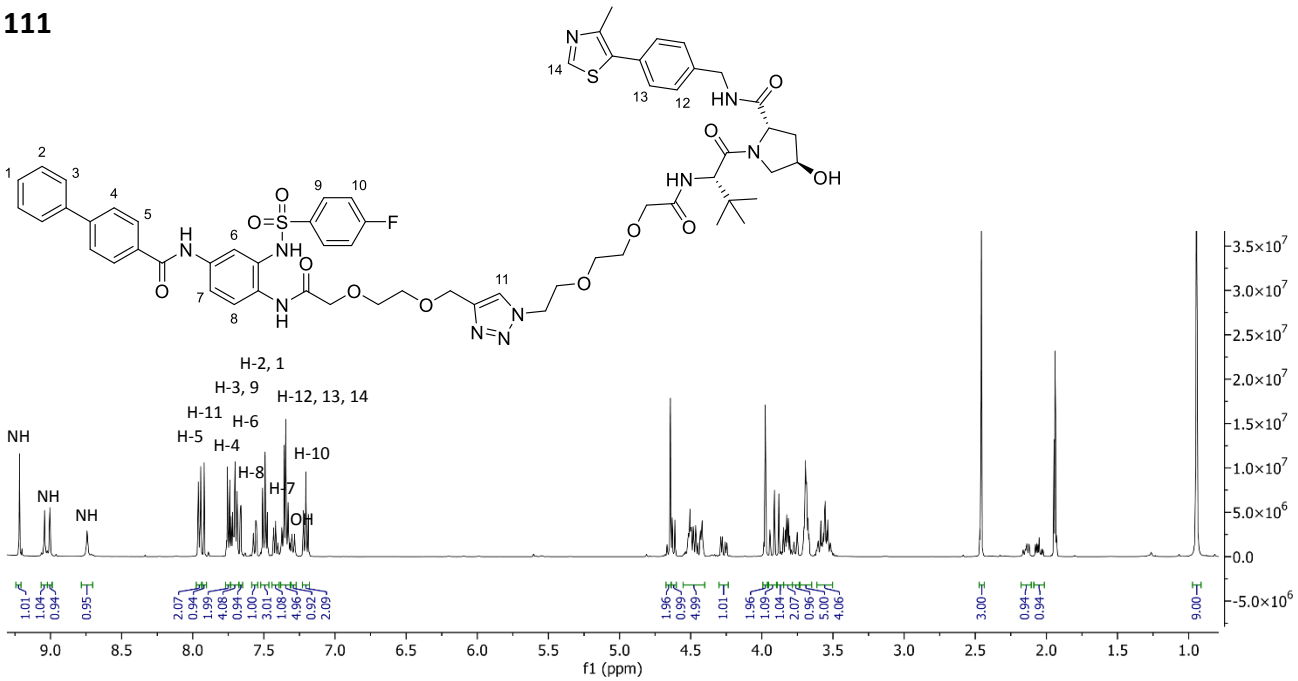
H-2, 1
H-3, 9
H-12, 13, 14
H-11
H-6
H-5
H-4
H-10
H-8
H-7
NH
NH
NH
OH
f1 (ppm)

112

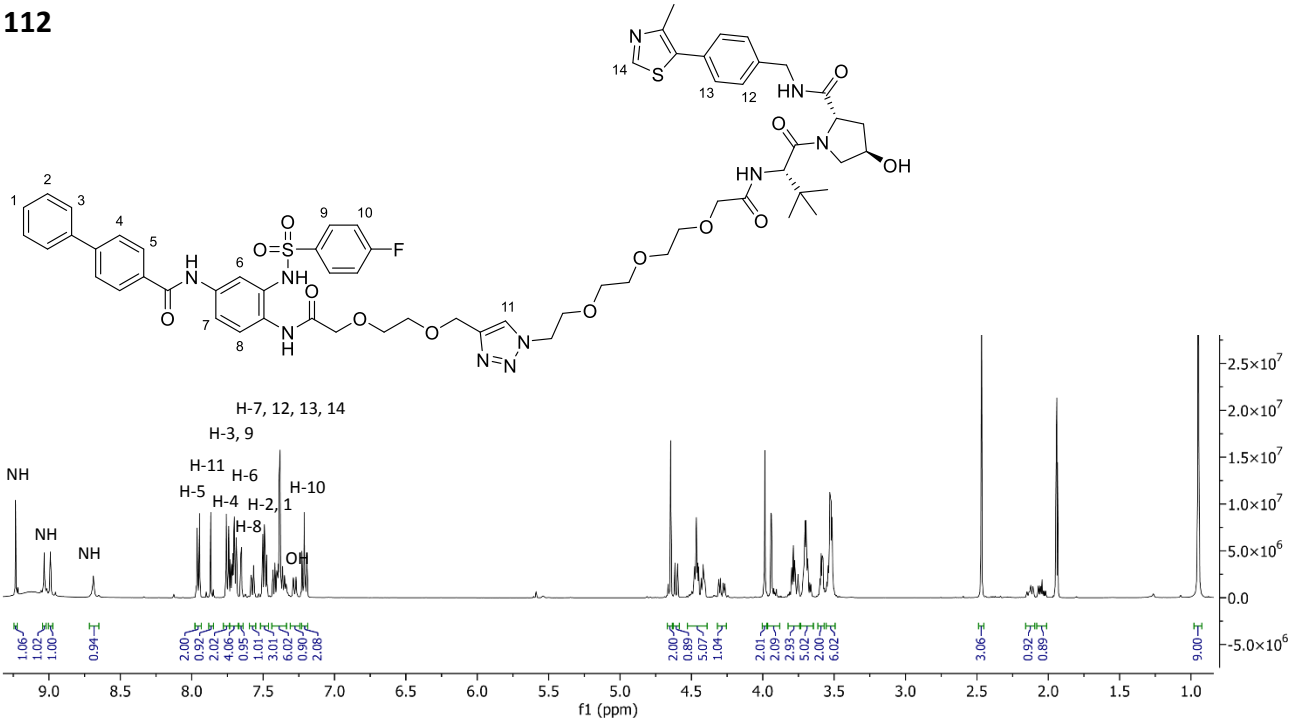

Figure 3.20: Structure and ^{1}H NMR 500 MHz spectra of Inh-VHL STING PROTACs in MeCN **110**, **111**, **112**.

3.3.6 Synthesis of Inh – RNF5 PROTAC

Compound **64** was finally also used for the coupling with RNF5 recruiter **92** in order to synthesize a novel RNF5-recruiting PROTAC targeting STING non-CDN-based. The terminal alkyne was coupled with the azide on the end of the RNF5 recruiter **92** via click reaction, obtaining **113** (Scheme **3.28**).

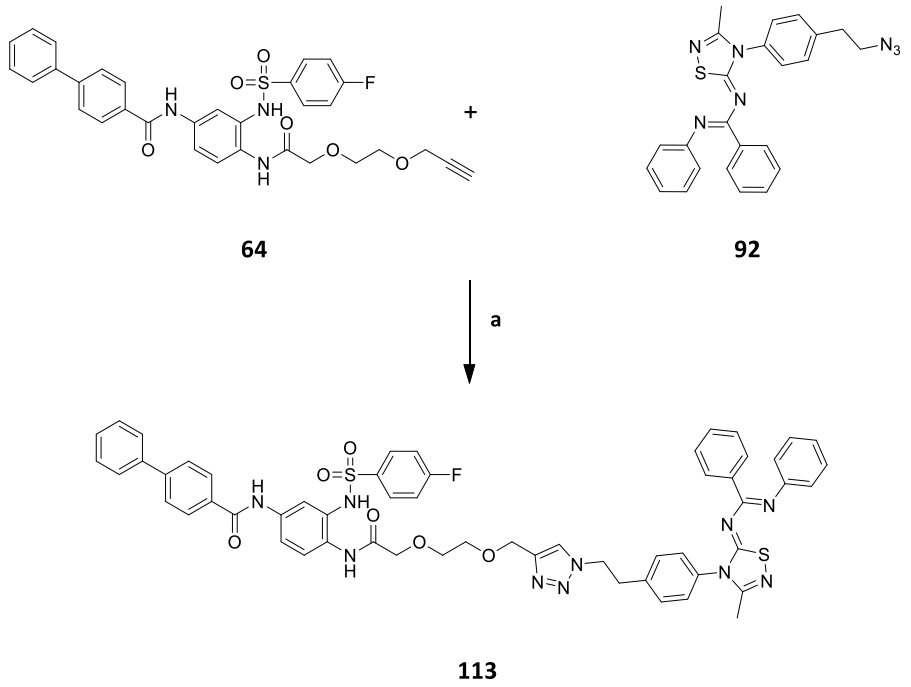

Scheme 3.28: Synthesis of Inh – RNF5 STING targeting PROTAC **113**: **a**) CuBr, TBTA, DMF, Ar, 50 °C, 2 hours, 97 %.

For this click reaction DMF was chosen as the optimal solvent due to the insolubility in water of the starting materials. Because of this, the catalytic Cu(I) was directly introduced as CuBr using TBTA as ligand and to prevent its oxidation to the inactive Cu(II), strict oxygen free conditions were employed (prior degassing by freeze-pump-thaw and Ar atmosphere). After stirring at 50 °C for 2 hours, the product **113** was obtained in 97 % yield after preparative HPLC purification (Figure **3.21**).

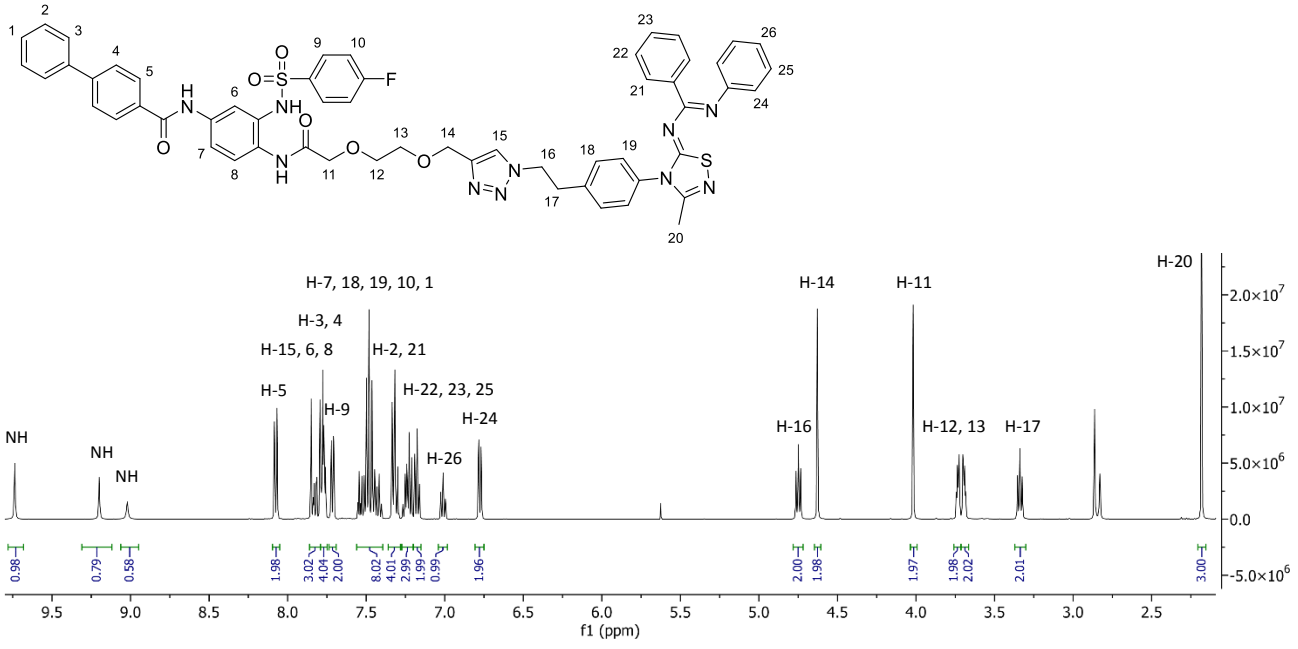

Figure 3.21: Structure, ^{1}H NMR 500 MHz of Inh-RNF5 STING PROTAC **113** in deuterated acetone.

3.3.7 Observations about STING-Targeting PROTACs

In the past chapter, a synthetic strategy for the preparation of a pool of different potential PROTAC molecules targeting STING has been described (Figure **3.22**). The adoption of Cu(I)-catalysed click chemistry, fast, selective and orthogonal towards different functional groups, for the coupling between the POI and the E3 ligase recruiters, permitted to significantly simplify the synthesis which otherwise would encounter a considerably higher degree of difficulty. In addition, this strategy is characterized by great versatility, permitting an easy interchange between the units resulting in the fast generation of different compounds and adjustment of the design according to the subsequent biochemical outcome. This simple concept can function as the basis for the generation of libraries of similar compounds and as a powerful tool for the progress in development of PROTAC technology.

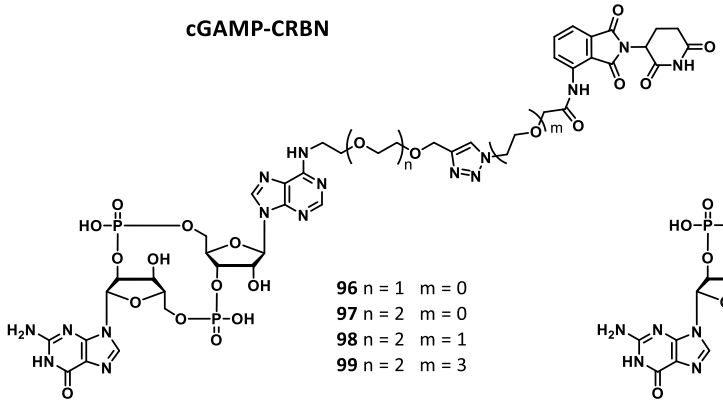

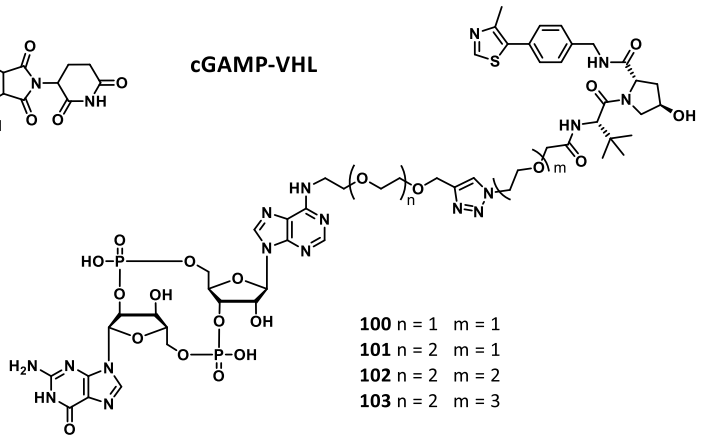

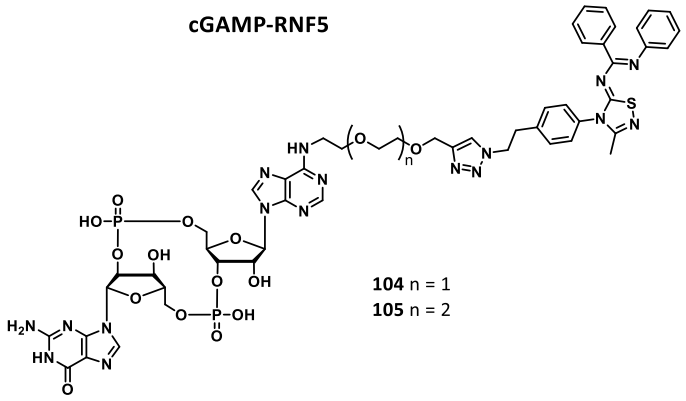

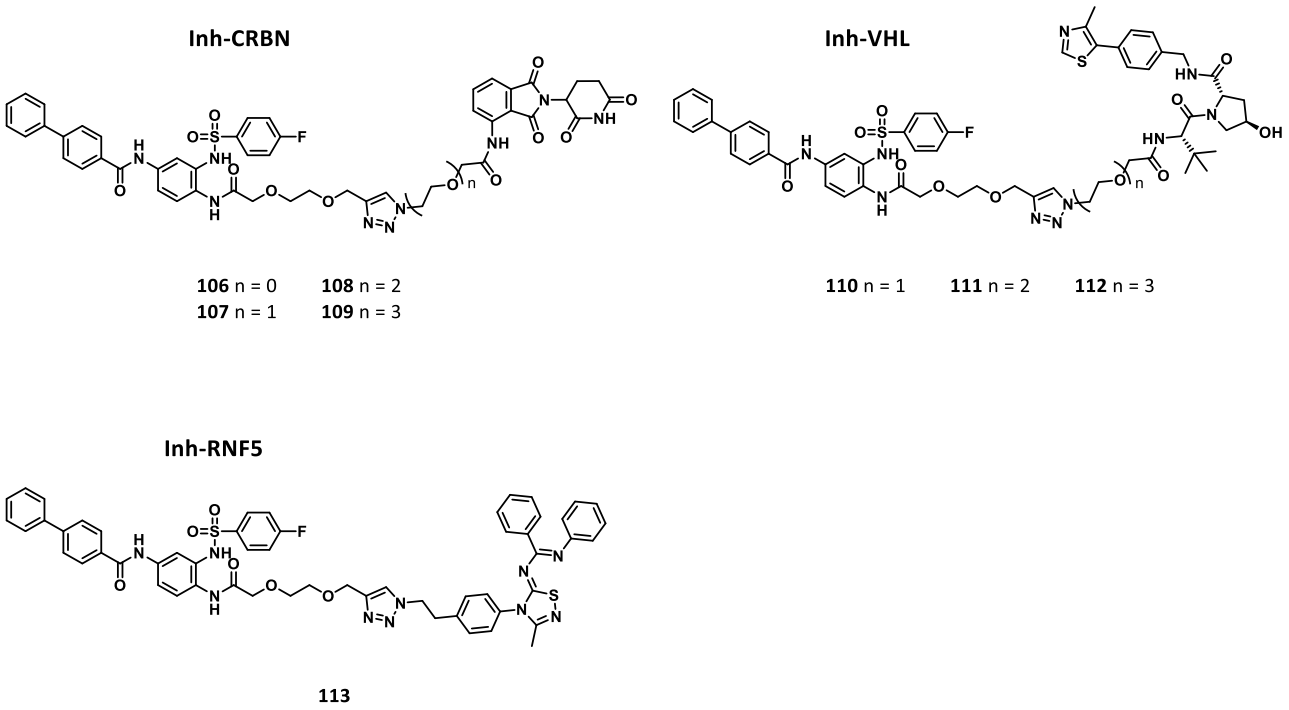

Figure 3.22: Structure of the different STING PROTAC classes investigated in this dissertation.

3.4 Biochemical and Biological Evaluation

Subsequent to the successful synthesis of the different potential STING-targeting PROTAC molecules described above, in collaboration with *Dr. Dilara Özdemir, Yasmin Gärtner* and *Johann de Graaff*, we started to design the experimental biochemical and biological evaluation of their properties. Despite significant progresses have been made on this direction, the establishment of optimal methods for testing the activity of these compounds is still ongoing at the time of writing this dissertation, also due to the novelty of the system investigated.

Therefore, in the following section, a detailed plan for the *in vitro* testing of PROTAC molecules will be reported, together with some preliminary data.

3.4.1 Evaluation of POI and E3 Ligase Recruiters

One important aspect to investigate about POI or E3 ligase recruiters is their capability to interact with the respective target proteins. In details, for the newly synthesised POI recruiters based on 2',3'-cGAMP, compounds **52** and **53**, binding properties towards STING can be studied via thermal shift assays such as Differential Scanning Calorimetry (DSC) and Isothermal Titration Calorimetry (ITC). The first method measures changes in the melting temperature of the C-terminal domain of human STING as a result of the interaction of the protein with a ligand, in the second a solution of the C-terminal domain (CTD) of STING inside the instrument cell is titrated with different concentrations of CDNs. Dissociation constants (K_D) are determined through the obtained thermodynamic parameters (ΔH, ΔS, ΔG).

In order to evaluate the ability of the cGAMP derivatives to cross the cellular membrane and reach the cytosol, fluorescent microscopy can be used to visualize compound **65** (**53** coupled with the fluorophore Cy3® (**66**) via click reaction) after being fed to cells. THP-1 (model cell line for immunological studies, expressing high levels of STING) and HeLa (adherent cell line, easier washing step) cells were treated with **65** 5 μM for 4 hours, the medium was removed and cells were washed to ensure the absence of the compound on the external space, before being imaged. From the acquired pictures (Figure **3.23**) it is possible to observe the presence of fluorescent signal on the inside of treated cells, suggesting the ability of cGAMP clickable derivatives to cross the cellular membrane without need of transfection, despite the double negative charge on the phosphates.

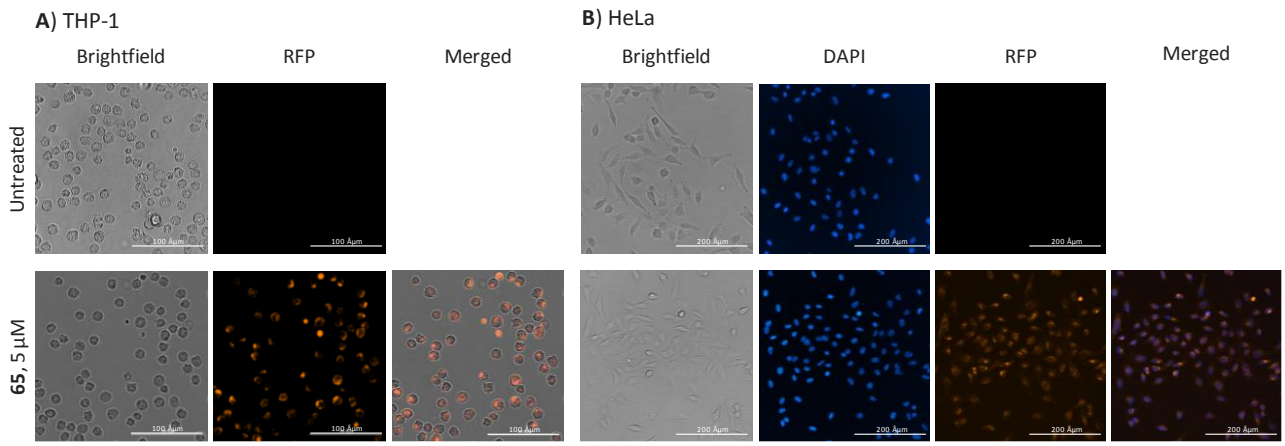

Figure 3.23: Fluorescence microscopy pictures of **A**) THP-1 cells untreated and treated with 5 µM of **65**, visualized under brightfield illumination, compound **65** fluorescing in red fluorescent protein (RFP) channel and merged pictures (scale bar 100 Âµm); **B**) HeLa cells untreated and treated with 5 µM of **65**, visualized under brightfield illumination, Hoechst fluorescent nuclear staining (DAPI channel), compound **65** fluorescing in red fluorescent protein (RFP) channel and merged pictures (scale bar 200 Âµm). Assay and microscopy provided by *Yasmin Gärtner*.

Inhibition properties of compound **64** can be determined *in vitro* by measuring the interferon response after stimulation of the commercially available reporter cell line THP-1 Dual™. These cells, derived from THP-1 monocytes, contain a Lucia luciferase gene under the control of a promoter in conjunction with 5 IFN-stimulated response elements, allowing to study the activation of the STING-dependent IRF production by simply measuring luminescence after stimulating cells with cGAMP. In this case, in order to measure the inhibition of this pathway, the cell line would be treated with different concentrations of **64**, stimulated with cGAMP and the interferon production measured after a defined time to obtain an inhibition curve and determine the relative IC_{50}. Known STING inhibitors as H-151 and particularly SN-011,[121, 165] from which the design of **64** was derived, can be used as positive controls.

Finally, the ability of compound **92** to recruit the E3 ligase RNF5 can be studied via a biotin-streptavidin pull-down assay with compound **94** (**92** coupled with biotin through click reaction). The biotinylated derivative is supposed to interact with the enzyme RNF5 and the complex extracted from the cellular pool exploiting the highly specific interaction between biotin and streptavidin, present on the surface of coated magnetic beads. The isolated enzyme is then visualized on SDS-PAGE via Western blotting.

3.4.2 Evaluation of PROTAC Stability in Cellular Media

During the establishment of a testing method for the degradation activity of PROTACs, the choice of a suitable cellular medium for the incubation with the compound is a fundamental step. This, together with the optimal incubation time, has to be determined by ensuring the stability of the tested compound. The molecules in exam are incubated in different media at 37°C and fractions of the solution are injected at different time points in the HPLC to observe the eventual decrease of the compound signal.

An initial investigation about the stability of CDN and non-CDN - pomalidomide PROTACs in cellular medium composed of RPMI 1640 + 10% FBS, showed a substantial decrease of the compounds signals already after 4 hours, unlike the unclicked cGAMP-PEG3-Alk, compound **53**, which on the contrary remained stable (Figure **3.24**). The instability could be partially recovered for 3',3'-c-di-GMP3-CRBN1 by the addition of 0.1 M EDTA to the medium, suggesting the possible role of double charged metal cations or metal-dependent nucleases in the serum in inducing degradation.

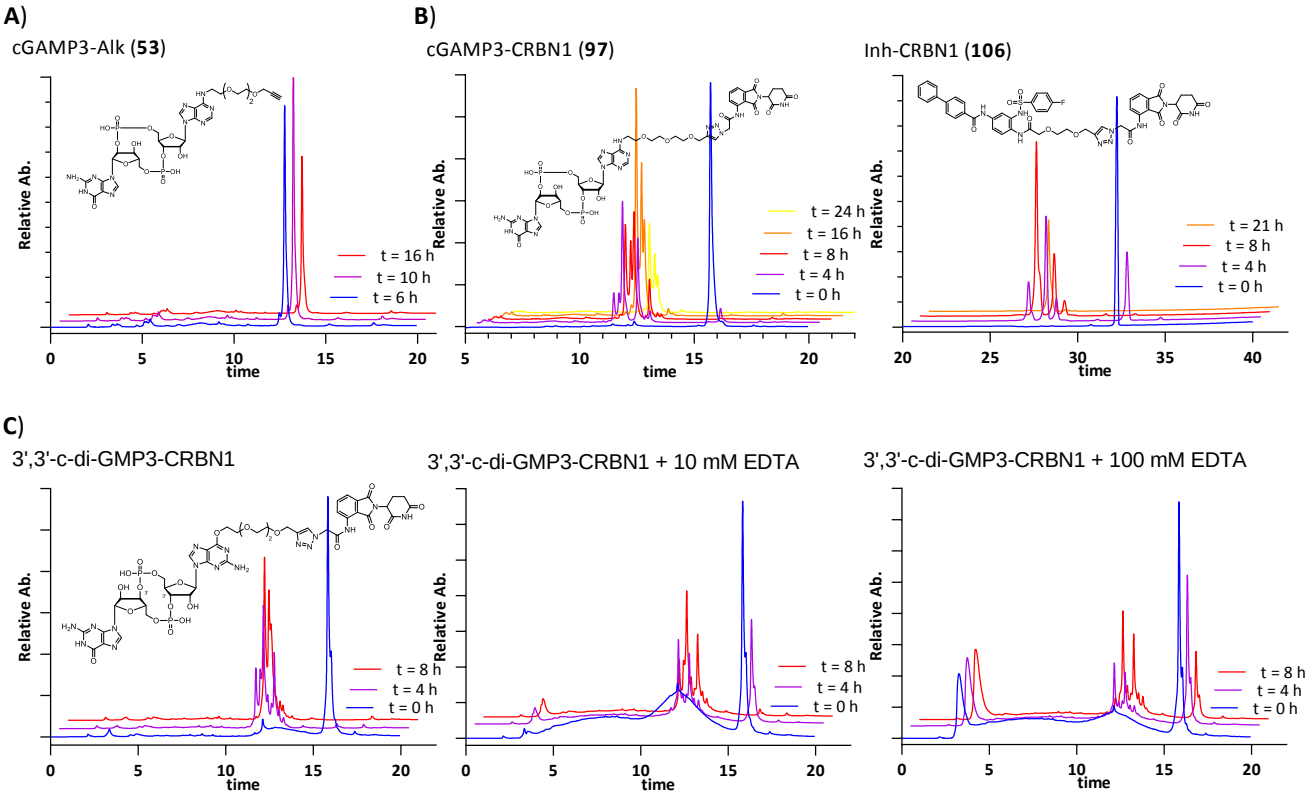

Figure 3.24: Stability studies in which the chromatogram at analytical HPLC is reported at different times of incubation with different colours. **A**) Stability studies of cGAMP3-Alk (**53**) (peak at 12.7 min) showing no degradation over 16 hours. **B**) cGAMP3-CRBN1 (**97**) (peak at 15.7 min) and Inh-CRBN1 (**106**) (peak at 32.2 min) show complete degradation after 4 hours. **C**) Comparison between 3',3'-c-di-GMP based CRBN PROTAC (peak at 16.0 min) in normal RPMI 1640 and medium supplemented with 10 and 100 mM EDTA showing a slowdown of the degradation process (raw data provided by *Johann de Graaff*).

PROTAC molecules based on VHL recruiters (CDN and non-CDN) resulted in higher stability (over 20 hours) under the same conditions, indicating that the pomalidomide may be subject to a certain degree of deterioration (Figure **3.25**). Despite the use of this warhead in different CRBN-recruiting PROTACs, thalidomide derivatives are known to hydrolyse in basic conditions.[285] This instability could be eventually influenced by moieties present in the rest of the PROTAC structure, resulting in enhanced decay at physiological pH. If this last hypothesis would be confirmed, culturing cells at a slightly lower buffered pH could bypass the problem. More detailed studies will be therefore required to clarify the degradation mechanism (e.g. mass and NMR analysis of fragments) and different media compositions tested. Stability studies were done together with *Johann de Graaff* and *Yasmin Gärtner*.

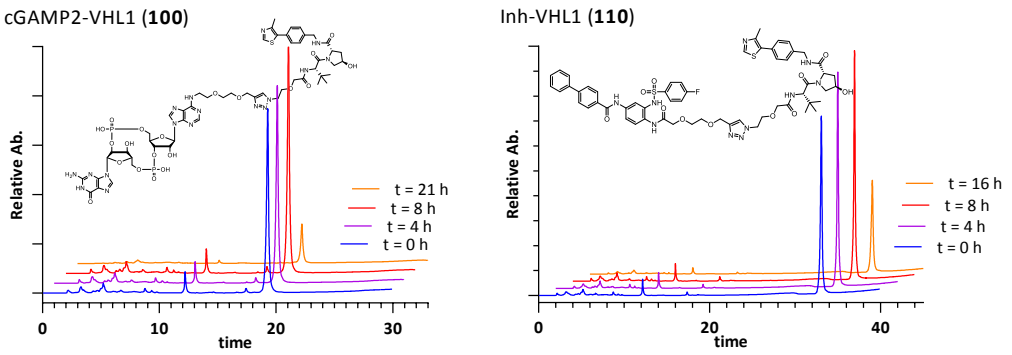

Figure 3.25: Stability studies of cGAMP2-VHL1 (**100**) (peak at 19.1 min) and Inh-VHL1 (**110**) (peak at 33.1 min) PROTAC representatives. The chromatogram at analytical HPLC is reported at different times of incubation with different colours. (t = 21 h for cGAMP2-VHL1 (**100**) and t = 16 h for Inh-VHL1 (**110**) show lower intensity because of injection problem occurred. The absence of degradation products peaks validates the retained stability).

3.4.3 Evaluation of PROTAC Degradation Activity

In order to study PROTACs degradation activity it is essential to select an appropriate system. For *in vitro* tests, cell lines with an appreciable expression of both the POI and the employed E3 ligase, are eligible models. Leukaemia THP-1 monocytic cells express high STING levels and significative CRBN, VHL and RNF5 amounts. The reduction of the POI can be evaluated by treating the selected cell line with different concentrations of the PROTAC molecule and STING levels are analysed by Western blotting, along with an appropriate loading control (e.g. CoxIV). Alternatively, after the incubation with PROTAC, cells can be triggered with cGAMP and interferon mRNA levels determined via qPCR.

For all the experiments, recruiters alone will have to be confirmed as negative controls while existing STING-degrading PROTACs (SP23 **37**, UNC9036 **38**) may be used as positive controls to validate the method.[261, 262] Additional negative controls can be obtained by utilizing the inactive versions of CRBN and VHL recruiters (respectively by *N*-methylation of pomalidomide on glutarimide ring and the epimerized diasteromer on the chiral hydroxyl group in the proline ring of VHL recruiter, **1.4.4**).

3.4.4 Validation Studies of Degradation Mechanism

To validate PROTACs modality of action highjacking the UPS system towards the target protein, a simple experiment consists in blocking the 26S proteasome with the known inhibitor MG132 to evaluate if the degradation is dependent on the ubiquitin-proteasome system. When the co- or pre-treatment of the cells with MG132 abrogates degradation subsequent to incubation of the formerly active PROTAC and induces an increase in the STING ubiquitinated species, the UPS pathway is confirmed, excluding other possible degradation routes (e.g. lysosomal). In addition, the expression of different STING isoforms in a model cell line (e.g. HEKT293T), each bearing a point mutation on different lysine residues (site directed mutagenesis to replace it with a glycine) and the observation for which of these the degradation is suppressed, can elucidate on which site the ubiquitination is occurring, providing important insight on the PROTAC mechanism of action.

3.4.5 Toxicity Studies

For each new potential drug tested, eventual toxicity or undesired side effects have to be investigated on different healthy cell lines e.g. via MTT assay.

4 General Conclusions and Outlook

The increasing evidences that an aberrant over-activation of STING plays a fundamental role in the development of numerous autoimmune and autoinflammatory diseases, as well as metastatic invasion and senescence-related disorders, represented a significant impulse for the development of new immunomodulating drugs by both academic and pharmaceutical research.[150] As already discussed in chapter **1.3.2**, the amount of covalent and non-covalent inhibitors, aiming to downregulate STING activity, is constantly growing. More recently, the innovative approach for protein targeted degradation, PROTACs (proteolysis targeting chimeras), has been proposed as a valid alternative to classical inhibition techniques, potentially overcoming some of the drawbacks associated to them, leading to the development of the first two examples of STING-degrading PROTACs.[261, 262]

In the present dissertation, a library of potential STING-targeting PROTACs was successfully designed and synthesised. As STING-recruiting unit, 2',3'-cGAMP derivatives bearing a clickable PEG linker on the *N*6 position of adenosine, **52** and **53**, were initially produced via phosphoramidite-phosphate chemistry approach. In order to overcome the possible disadvantages deriving from the negatively charged phosphates of the CDN in terms of cell delivery and stability, together with a potential residual agonist activity, an alternative POI recruiter was derived from a rather recently discovered STING inhibitor, SN-011.[121] The chemical structure was modified by the insertion of a PEG linker with a terminal alkyne for further coupling with different E3 ligase recruiters, to obtain **64**.

Regarding this second component of the PROTAC structure, along with the commonly used CRBN and VHL recruiting units, a potential RNF5 recruiter **92** based on its activator analog-1, was developed.[278, 279] All these structures were chemically designed as suitable for click chemistry, by the addition of PEG linkers with different lengths, carrying an azidic moiety on one terminus.

The adoption of Cu(I)-catalysed click chemistry provided a fast, selective and robust coupling between STING and E3 ligase recruiters, simplifying the synthetic route to the final compound and providing a high degree of versatility to the system, beneficial in the stage of screening for potential PROTAC structures by the combination of different POI and E3 ligase recruiters and linkers (Scheme **4.1**).

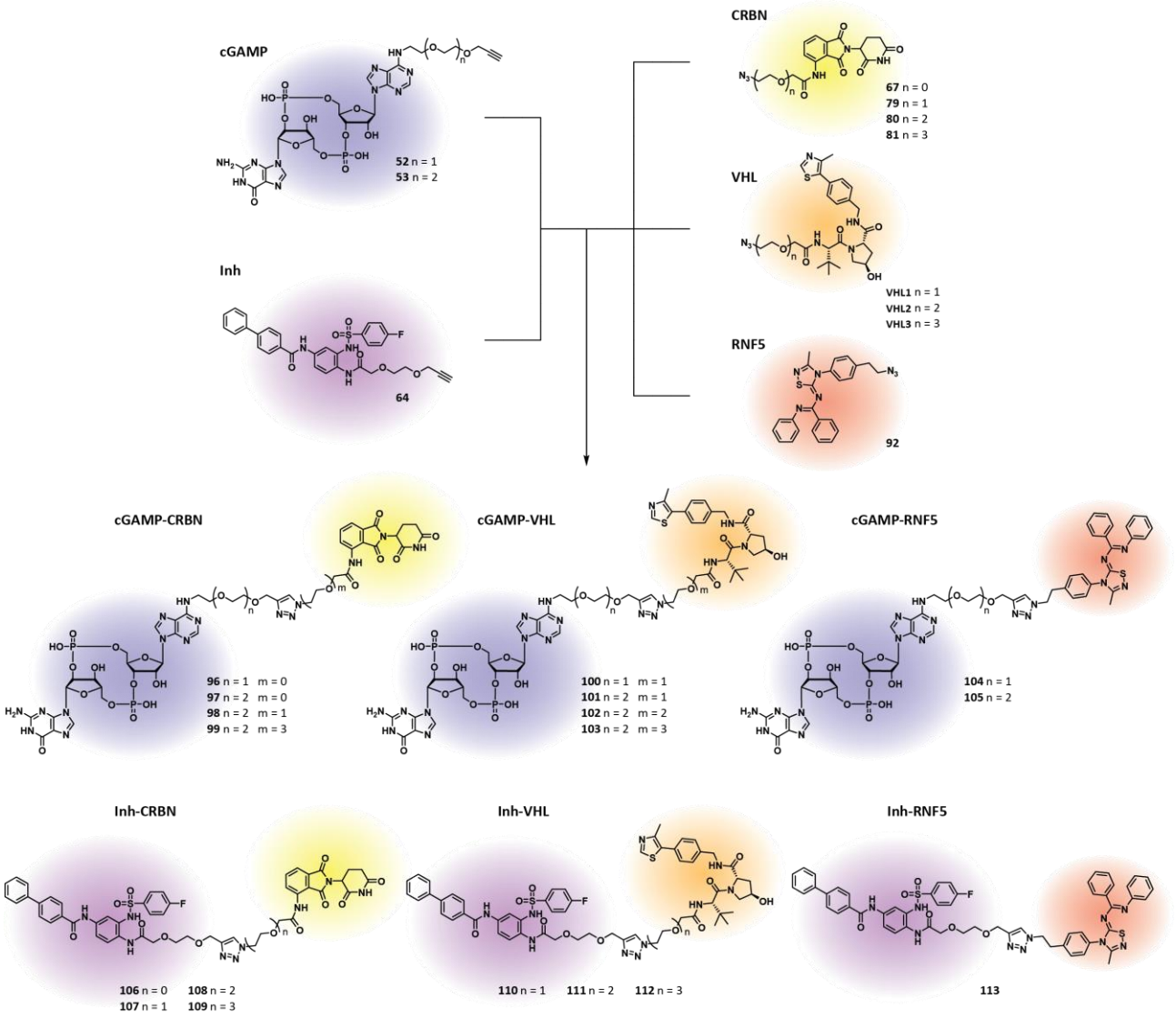

Scheme 4.1: Combination of different STING and E3 ligase recruiters via Cu(I)-catalysed click chemistry for the synthesis of a library of potential STING-degrading PROTACs.

The currently ongoing evaluation of their biological activity will possibly lead to the optimization of their potency through structure-activity relationship (SAR) studies. Despite the defined workflow, difficulties have still to be solved in identifying a suitable system for testing the obtained PROTAC molecules *in vitro* and their ability to induce STING degradation. Depending on the outcome, future improvements could be achieved by varying the site of modification of the different recruiters, as well as the recruiters themselves.

Possible variations of CDN-based recruiters to improve the chemo-pharmacological properties of the corresponding PROTACs in terms of stability, activity and membrane crossing ability, would consist of the chemical modification of phosphates and hydroxyl groups on the sugar. As previously discussed in sections **1.3.1** and **3.1.3**, stability and cell delivery of CDNs are often improved by the conversion of phosphate groups into thiophosphates or by the substitution of free hydroxyls on the sugar with fluorine atoms, as well as by their removal (deoxy CDNs). Moreover, the negative charge of the phosphates can be masked in the form of phosphotriester, improving the membrane permeability, which would then be converted to the active phosphodiester form of the CDN once

inside the cell.[286] For what concerns the near future of this research project, the evaluation and comparison of oxy- and deoxy versions of 2',3'-cGAMP and c-di-AMP, along with 3',3'-c-di-GMP, all carrying a clickable PEG linker on the 6th position of the nucleobases, will lead to important insights about the influence on the activity of STING-degrading PROTACs of different CDN-based POI recruiters. Other insertion points for the linker (*C*8 position of guanosine) will be also tested soon.

Besides CDN-based recruiters, the growing research on classical STING inhibitors, provides great opportunities to expand the pool of possible recruiting units, by the conversion of existing or newly discovered molecules into PROTAC warheads, as shown in this dissertation for compound **64**.

Broadening the choice of E3 ligases to recruit can also lead to the improvement of PROTAC's potency. A stronger degradation is believed to be directly related to the stability of the ternary complex and therefore to the strength of protein-protein interactions between the surfaces of the POI and E3 ligase. Moreover, exploiting the different expression profiles of E3 ligases in cells, tissues or even diseases (e.g. cancers) could greatly increase the specificity of the treatment. Despite the great number of existing ubiquitinating enzymes (over 600), only few of them have been exploited for targeted protein degradation. The attempt to recruit RNF5 for inducing the ubiquitination of STING goes in this direction, taking advantage of its physiological role in the degradation of the target and representing an example generally applicable for the development of new PROTACs.

Finally, the optimization of the linker in terms of length and flexibility, is a crucial step in the process of PROTAC development. From literature, the most common strategy is to start from longer PEG linkers to identify the best E3 ligase to induce degradation of the target and gradually shorten the length. Once identified the most effective length, a set of bivalent molecules with less polar and/or rigid linkers, with different pre-organized orientations, are synthesised, achieving the final optimization of the PROTAC.

The work reported in this dissertation is intended as a valid basis for addressing STING over-activation and related disorders via the PROTAC approach. Further optimization of the reported molecules could represent a promising alternative to classical inhibition of this enzyme.

4 Experimental

4.1 Materials and Methods

4.1.1 General Methods

Chemicals and dry solvents for organic synthesis were purchased from commercial suppliers such as *Sigma-Aldrich*, *Carbosynth*, *TCI*, *ABCR*, *Alfa Aesar, Acros Organics* or *WVR* and used without further purification. The solvents were of reagent grade or purified by distillation. Water was purified by a Milli-Q Plus system from *Merck Millipore*. All chemical reactions were carried out with magnetic stirring, and, when necessary, in oven-dried glassware (> 12 h, 120 °C) under dry argon or nitrogen atmosphere. The temperature of reactions (except r.t.) was adjusted with a solvent/dry ice-, solvent/ice-mixture or an oil bath and the temperature monitored with a thermometer outside the flask. The literature references indicated for known compounds regard the available analytical data. Synthetic procedures were optimized and adapted for each compound as described.

Chromatographic purification of products was accomplished using flash column chromatography on *Merck Geduran* or *Macherey-Nagel* Si 60 (40 – 63 µm) silica gel (normal phase) or by reversed-phase high-performance liquid chromatography (RP-HPLC) with conditions described below. Thin layer chromatography (TLC) was performed on *Merck* 60 (silica gel F254) plates and visualized under UV light (λ = 254 and 366 nm) and staining with potassium permanganate (1.5 g $KMnO_4$, 10.0 g K_2CO_3, 125 mg NaOH in 200 mL water), *p*-anisaldehyde (3.7 mL *p*-anisaldehyde, 135 mL EtOH, 5 mL conc. H_2SO_4, 1.5 mL conc. AcOH) or ceric ammonium molybdate (10.0 g ammonium molybdate tetrahydrate, 2.0 g $Ce(SO_4)_2 \cdot 4H_2O$, 180 mL H_2O, 20 mL conc. H_2SO_4).

^1H, ^{13}C and ^{31}P NMR spectra were recorded in deuterated solvents on *Varian Oxford 200 (200 MHz)*, *Bruker ARX 300 (300 MHz)*, *Varian VXR400S (400 MHz)*, *Varian INOVA 400 (400 MHz)*, *Bruker Avance III 400 (400 MHz)*, *Bruker Ascend 500 (500 MHz), Bruker AMX 600 (600 MHz)* and *Bruker Avance III HD 800 (800 MHz)* spectrometers and calibrated to the residual solvent peak using reported values. ^1H NMR shifts were calibrated to the residual solvent resonances: DMSO-d_6 (2.50 ppm), D_2O (4.79 ppm), CD_3CN (1.94 ppm), CD_3OD (4.87 ppm), Acetone-d_6 (2.05 ppm), CD_2Cl_2 (5.32 ppm) or $CDCl_3$ (7.26 ppm). ^{13}C NMR shifts were calibrated to the residual solvent: DMSO-d_6 (39.52 ppm), CD_3CN (1.32 ppm), CD_3OD (49.00 ppm), CD_2Cl_2 (53.84 ppm), $CDCl_3$ (77.16 ppm), Acetone-d_6 (29.84 ppm). All NMR spectra were analyzed using the program MestReNOVA 10.0.1 from Mestrelab Research. NMR data are reported as follows: chemical shift (multiplicity, coupling constants where applicable, number of hydrogens, assignment where applicable). The chemical shifts are given in ppm, the coupling constants (J) in Hz. Multiplicities are abbreviated as follows: s = singlet, d = doublet, t = triplet, q = quartet, m = multiplet, br = broad and combinations of these. For assignment of the structures, additional 2D-NMR spectra (such as COSY, HSQC, HMBC) were measured. When the amount of compound obtained was not sufficient for a ^{13}C-NMR with a high signal-to-noise ratio, 2D-NMR spectra were used to detect ^{13}C peaks when possible.

High resolution electrospray ionization mass spectra (HRMS-ESI) were recorded on a *Thermo Finnigan LTQ-FT* (ESI-FTICR), and high-resolution electron impact ionization mass spectra (HRMS-EI) were recorded on a *Thermo Finnigan MAT 95* by the analytical section of the Department of Chemistry of the Ludwig-Maximilians-Universität München. Alternatively, it was utilized *Thermo Scientific Vanquish* LC system coupled to a *Thermo Scientific QExactive HF* mass spectrometer. The LC was performed on an *Interchim Uptisphere* 150-21 3HDO C18 column with a flow of 0.15 ml/min and a constant column temperature of 30 °C. Eluting buffers were buffer A (5 mM NH_4OAc in H_2O (pH 4.9)) and buffer B (2 mM NH_4HCO_2 in H_2O/MeCN 20/80 (pH 5.5)).

LC-MS and ESI-MS were measured on a *Dionex UltiMate 3000* micro UHPLC-System (pump, auto sampler, column compartment and diode array detector) coupled to a *Thermo Fischer* MSQ-single quadrupole spectrometer allowing direct injections and RP-column chromatography methods using a *Hypersil GoldC18 selectivity* column (100 × 2.1mm). As mobile phases water and acetonitrile with 0.01 % formic acid were used.

IR measurements were performed on a *Perkin Elmer BX FT-IR* spectrometer with a diamond ATR unit or a *Shimadzu IR Spirit FT-IR* instrument. Band frequencies in the region between 4400 and 1400 cm^{-1} are reported to the nearest cm^{-1}. Signal intensities are reported as strong (s), medium (m), weak (w), broad (br). Substances were applied as a film or directly as solids on the ATR unit.

For the reverse-phase HPLC analysis and purification the following instruments were used:

Analytical HPLC: *Agilent Technologies 1260 Infinity II* consisting of *1260 flexible pumps*, *1260 vial sampler* and *1260 MWD* equipped with a *Macherey-Nagel* EC 250/4 *NUCLEOSIL* 120-3 C18 or *Macherey-Nagel* EC 250/4 *NUCLEODUR* 120-3 C18ec column with a flow rate of 0.5 mL/min.

Analytical HPLC: *Shimadzu LC-2060C 3D* equipped with a *Macherey-Nagel* EC 250/4 *NUCLEODUR* 120-3 C18ec column with a flow rate of 1.0 mL/min.

Semi-preparative HPLC: *Agilent Technologies 1260 Infinity II* consisting of *1260 Quat Pump VL*, *1260 man. inj.* and *1260 MWD* equipped with a *Macherey-Nagel* VP 250/10 *NUCLEOSIL* 100-7 C18 or *Macherey-Nagel* VP 250/10 *NUCLEODUR* 100-7 C18 column with a flow rate of 5.0 mL/min.

Preparative HPLC: *Shimadzu Nexera Prep LC-20AP* consisting of *DGU-405 degassing unit*, *FCV-200AL prep quaternary valve pump*, *SPD-40 UV-Vis detector* and *CB-40 system controller* equipped with a *Shim-pack Scepter* 120-5 C18 column with a flow rate of 45.0 mL/min.

Gradients of unbuffered and buffered solutions of H_2O and MeCN were used as mobile phases. For unbuffered gradients were used pure H_2O and MeCN or H_2O + 0.1% TFA and MeCN + 0.1% TFA as A and B buffers. For buffered gradients 0.1 M NEt_3/AcOH in H_2O and 0.1 M NEt_3/AcOH in 80% MeCN were used as A and B buffers. Buffer compositions and elution methods were optimized for each product with analytical HPLCs and then the same methods were used for purification.

4.1.2 Biochemical Methods

4.1.2.1 Cell Culture

THP-1 monocytic cells (male) were purchased from *Cell Lines Service (CLS)*. They were cultured according to the manufacturer's instructions using RPMI-1640 (Sigma-Aldrich, R0883) supplemented with 10 % (v/v) inactivated FBS (*Gibco*, 10500-064), 2 mM Alanyl-glutamine (*Sigma-Aldrich*, G8541), and 1 mM sodium pyruvate solution (*Sigma-Aldrich*, S8636). The cells were kept between 0.1 x 10^6/mL and 1 x 10^6/mL either by addition of fresh medium or complete medium replacement every 2 to 3 days.

HeLa cells were purchased from *Cell Lines Service (CLS)* and cultured according to the manufacturer's guidelines in DMEM (*Sigma-Aldrich*, D6546) with 10 % (v/v) inactivated FBS (*Gibco*, 10500-064) + 2 mM Alanyl-glutamine (*Sigma-Aldrich*, G8541). When cells reached a confluency of 80 - 90%, they were split 1:10 – 1:20 either by addition of fresh medium or complete medium replacement every 3 to 5 days.

4.1.2.2 Fluorescence Microscopy

1 x 10^5 THP-1 cells were seeded in 200 µL medium in 96-well plates (*Sarstedt*, 83.3924.500) and treated with 5 µM compound **65** for 4h. Cells were transferred into 1.5 mL Eppendorf tubes to remove the compound that was not taken up. The wells were washed 2 x with 200 µL pre-warmed HBSS (*Sigma-Aldrich*, H9269) to ensure complete transfer of all cells. After spinning at 150 rcf for 5 min, the pellets were washed with 2 x 200 µL HBSS before the cells were resuspended in 200 µL medium without phenol red (RPMI, *Gibco*, 32404) and transferred into µ-slides (*ibidi*, 80826-90).

2 x 10^4 HeLa cells were seeded in 200 µL medium in µ-slides (*ibidi*, 80826-90) 16-24h before the treatment. 5 µM compound **65** was added to the medium for 4h before washing the cells with 2 x 200 µL HBSS (*Sigma-Aldrich*, H9269). Medium without phenol red was added (DMEM, *Gibco*, 11880) after the washing as well as Hoechst 33342 (*Sigma-Aldrich*, 382065) to a final concentration of 5 µg/mL 30 minutes before imaging.

The treated cells were imaged with *Cytation 5* (*Agilent*). Channels: DAPI 377, 447 (filter set), RFP 531, 593 (filter set) and BrightField High Contrast. Data were processed with the *Gen5 3.14* software.

4.1.2.3 Stability Studies in Media

The compound in exam was incubated with a final concentration of 0.25 mM in RPMI-1640 (*Sigma-Aldrich*, R0883) supplemented with 10 % (v/v) inactivated FBS (*Gibco*, 10500-064), 2 mM Alanyl-glutamine (*Sigma-Aldrich*, G8541), and 1 mM sodium pyruvate solution (*Sigma-Aldrich*, S8636) at 37 °C in the heated sample tray compartment of the analytical HPLC *Shimadzu LC-2060C 3D*. The analysis was performed by injecting 20 µL each time per different time points and eluted with a gradient of 0 to 100 % B in 45 minutes with a *Macherey-Nagel* EC 250/4 *NUCLEODUR* 120-3 C18ec column and a flow rate of 1.0 mL/min. A buffer: 0.1 M Et_3N/HOAc in H_2O, B buffer: 0.1 M Et_3N/HOAc in 80 % MeCN. Data from these measurements were analysed using *GraphPad Prism 8*.

4.2 Synthetic Procedures

4.2.1 STING Recruiters

4.2.1.1 cGAMP-Based STING Recruiters

*N*2-Isobutyryl-*O*5'-DMTr-Guanosine (**40**)

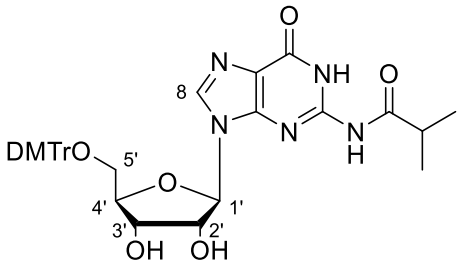

To a solution of *N*2-isobutyryl-guanosine (**39**) (10.00 g, 28.30 mmol, 1.00 eq.) in dry pyridine (200 mL), DMTrCl (12.47 g, 36.80 mmol, 1.30 eq.) was added. After the addition, the solution was stirred under Ar at r.t. overnight, during which time the colour changed from orange to yellow. The mixture was then washed with saturated $NaHCO_3$ solution (150 mL) and extracted with DCM (3 x 300 mL). The combined organic layers were dried over anhydrous Na_2SO_4 and concentrated *in vacuo*. The residue was dissolved in DCM and added dropwise to a stirred solution of Et_2O/iHex (1 L/300 mL). The white precipitate was filtered and dried under vacuum overnight. The solid was purified by column chromatography on silica gel (2 to 10 % MeOH/DCM + 0.1 % pyridine) to afford compound **40** (12.99 g, 19.81 mmol, 70 %) as a white foam.

^{1}H NMR (400 MHz, CD_2Cl_2): δ (ppm) = 12.06 (s, 1H, NH-1), 9.02 (s, 1H, NH-2), 8.57 (s, 1H, H-8), 7.37 - 7.31 (m, 4H, DMTr MeO-Ph-*m*-C*H*), 7.29 (d, 2H, DMTr Ph-*o*-C*H*), 7.26 - 7.21 (m, 2H, DMTr Ph-*m*-C*H*), 7.20 - 7.13 (m, 1H, DMTr Ph-*p*-C*H*), 6.84 - 6.74 (m, 4H, DMTr MeO-Ph-*o*-C*H*), 6.26 (s, 1H, OH-3'), 5.84 (d, *J* = 6.3 Hz, 1H, H-1'), 5.07 (t, *J* = 5.9 Hz, 1H, H-2'), 4.49 (dd, *J* = 5.5, 2.6 Hz, 1H, H-3'), 4.25 (dd, *J* = 3.8, 2.5 Hz, 1H, H-4'), 4.12 (s, 1H, OH-2'), 3.73 (d, *J* = 2.8 Hz, 6H, DMTr *Me*O-Ph), 3.42 (dd, *J* = 10.7, 2.7 Hz, 1H, H-5'), 3.18 (dd, *J* = 10.6, 4.1 Hz, 1H, H-5'), 2.06 (q, *J* = 6.8 Hz, 1H, iBu C*H*), 0.89 (d, 6H, iBu CH_3).

^{13}C NMR (101 MHz, CD_2Cl_2): δ (ppm) = 180.12 (iBu *C*=O), 159.26 (DMTr MeO-Ph-*p*-*C*), 155.93 (C-6), 150.27 (C-2/C-4), 145.43 (DMTr Ph-*C*), 139.31 (DMTr MeO-Ph-*C*), 136.82 - 136.19 (DMTr MeO-Ph-*o*-*C*/C-8), 130.54 (DMTr Ph-*m*-*C*), 128.57 (DMTr Ph-*o*-*C*), 124.27 (DMTr Ph-*p*-*C*), 121.49 (C-5), 113.70 (DMTr MeO-Ph-*m*-*C*), 86.72 (DMTr *C*-Ph(PhOMe)$_2$), 85.58 (C-1'), 74.33 (C-2'), 72.00 (C-3'), 64.39 (C-4'/C-5'), 55.72 (DMTr *Me*O-Ph), 36.54 (iBu *C*H), 18.94 (iBu *C*H$_3$).

HR-ESI-MS: m/z calc. for $[C_{35}H_{38}O_8N_5]^+$ $[M+H]^+$: 656.27149; found: 656.27150.

FT-IR: $\tilde{\nu}$ (cm^{-1}) = 3146.9 (w), 2929.2 (w), 1672.5 (s), 1605.4 (s), 1556.8 (m), 1506.0 (s), 1463.0 (m), 1439.5 (m), 1491.5 (m), 1299.6 (m), 1247.4 (s), 1174.2 (m), 1031.2 (s), 826.9 (m).

Rf = 0.41 (2 % MeOH/DCM).

*N*2-Isobutyryl-*O*3'-TBS-*O*5'-DMTr-Guanosine (41)

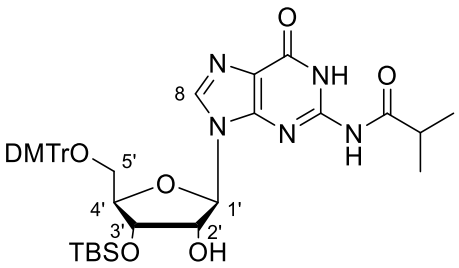

40 (12.99 g, 19.81 mmol, 1.00 eq.) was pre-dried by co-evaporation with pyridine and dissolved in dry DCM (80 mL) under Ar. Pyridine (8 mL) and DMF (8 mL) were added after dissolving. After stirring for 10 minutes, the reaction mixture was cooled down to 0 °C. Imidazole (3.370 g, 49.54 mmol, 2.50 eq.) was added and the reaction was stirred for another 30 min. TBSCl (2.990 g, 19.81 mmol, 1.00 eq.) was added, the ice bath removed and the reaction mixture was stirred under Ar at r.t. overnight. The mixture was then washed with saturated $NaHCO_3$ solution (150 mL) and extracted with DCM (3 x 200 mL), the combined organic layers were washed with brine (200 mL) and dried over anhydrous Na_2SO_4 and then concentrated *in vacuo*. The residue was purified via column chromatography on silica gel (30/70 % EtOAc/DCM + 0.1 % pyridine) in order to obtain the two isomers, which were then separated via column chromatography on silica gel (10/20/70 to 30/0/70 % acetone/toluene/DCM + 0.1 % pyridine) to obtain the desired isomer **41** as a white foam. The conversion of the single reaction to the two isomers was estimated around 1:1. The undesired isomer **41'** was dissolved in a solution 10 % triethylamine in MeOH (final concentration of the isomer 0.03 M) and stirred at r.t. foe 30 min. The solvent was evaporated *in vacuo* and the two isomers separated again via column chromatography on silica gel (10/20/70 to 30/0/70 % acetone/toluene/DCM + 0.1 % pyridine) to obtain the desired isomer **2** as a white foam.

^{1}H NMR (400 MHz, CD_2Cl_2): δ (ppm) = 11.90 (s, 1H, NH-1), 8.13 (s, 1H, NH-2), 7.97 (s, 1H, H-8), 7.54 - 7.47 (m, 2H, DMTr Ph-*o*-C*H*), 7.42 - 7.35 (m, 4H, DMTr MeO-Ph-*m*-C*H*), 7.33 - 7.20 (m, 3H, DMTr Ph-*m*-C*H* / DMTr Ph-*p*-C*H*), 6.89 - 6.76 (m, 4H, DMTr MeO-Ph-*o*-C*H*), 5.76 (d, *J* = 5.6 Hz, 1H, H-1'), 4.75 - 4.71 (m, 1H, H-2'), 4.45 (d, *J* = 1.7 Hz, 1H, H-3'), 4.11 (td, *J* = 3.8, 2.4 Hz, 1H, H-4'), 3.72 (d, *J* = 3.4 Hz, 6H, DMTr *Me*O-Ph), 3.51 (dd, *J* = 10.8, 2.4 Hz, 1H, H-5'), 3.12 (dd, *J* = 10.8, 3.8 Hz, 1H, H-5'), 3.08 (s, 1H, OH-2'), 1.96 (dtd, *J* = 8.7, 6.7, 5.0 Hz, 1H, iBu C*H*), 1.02 (d, *J* = 6.9 Hz, 6H, iBu C*H*$_3$), 0.86 (d, *J* = 2.9 Hz, 9H, TBS CH-C*H*$_3$), 0.06 - - 0.09 (m, 6H, TBS Si-C*H*$_3$).

^{13}C NMR (101 MHz, CD_2Cl_2): δ (ppm) = 178.91 (iBu *C*=O), 159.09 (DMTr MeO-Ph-*p*-*C*), 155.58 (C-6), 148.43 (C-2), 147.60 (C-4), 145.11 (DMTr Ph-*C*), 138.18 (DMTr MeO-Ph-*C*), 136.02 (C-8 / DMTr MeO-Ph-*o*-*C*), 130.24 (DMTr Ph-*m*-*C*), 128.30, (DMTr Ph-*o*-*C*), 122.35 (C-5 / DMTr Ph-*p*-*C*), 113.40 (DMTr MeO-Ph-*m*-*C*), 89.41 (DMTr *C*-Ph(PhOMe)$_2$), 86.59 (C-1'), 84.78 (C-3'), 74.07 (C-4'), 71.74 (C-2'), 63.09 (C-5'), 55.51 (DMTr *Me*O-Ph), 36.48 (iBu *C*H), 31.30 (TBS CH-*C*H$_3$), 25.71 (iBu *C*H$_3$), 18.15 (TBS *C*H-*C*H$_3$), - 4.77 (TBS Si-*C*H$_3$).

HR-ESI-MS: m/z calc. for $[C_{41}H_{52}O_8N_5Si]^+$ $[M+H]^+$: 770.35797, found: 770.35812.

Rf = 0.27 (50/50 % EtOAc/iHex).

*N*2-Isobutyryl-O2'-TBS-O5'-DMTr-Guanosine (41')

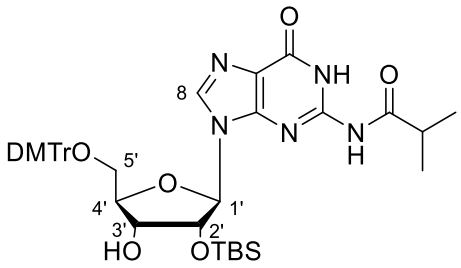

^{1}H NMR (400 MHz, CD_2Cl_2): δ (ppm) = 11.89 (s, 1H, NH-1), 7.81 (s, 1H, H-8), 7.48 - 7.39 (m, 4H, DMTr Ph-*o*-C*H* / DMTr Ph-*m*-C*H*), 7.31 - 7.20 (m, 4H, DMTr MeO-Ph-*m*-C*H*), 7.20 - 7.11 (m, 1H, DMTr Ph-*p*-C*H*), 6.87 - 6.77 (m, 4H, DMTr MeO-Ph-*o*-C*H*), 5.77 (d, *J* = 7.0 Hz, 1H, H-1'), 5.22 - 5.18 (m, 1H, H-2'), 4.35 (dt, *J* = 5.3, 1.9 Hz, 1H, H-3'), 4.21 (dt, *J* = 4.1, 2.0 Hz, 1H, H-4'), 3.76 (d, *J* = 5.5 Hz, 6H, DMTr *Me*O-Ph), 3.55 (dd, *J* = 10.8, 2.0 Hz, 1H, H-5'), 3.10 (dd, *J* = 10.8, 3.1 Hz, 1H, H-5'), 2.79 (q, *J* = 2.1 Hz, 1H, OH-3'), 1.50 (m, 1H, iBu C*H*), 0.89 - 0.80 (m, 9H, TBS CH-C*H$_3$*), 0.62 (d, 6H, iBu C*H$_3$*), 0.62 - 0.04 (m, 6H, TBS Si-C*H$_3$*).

Rf = 0.50 (50/50 % EtOAc/iHex).

*N*2-Isobutyryl-*O*2'-phosphotriester-*O*3'-TBS-*O*5'-DMTr-Guanosine (**42**)

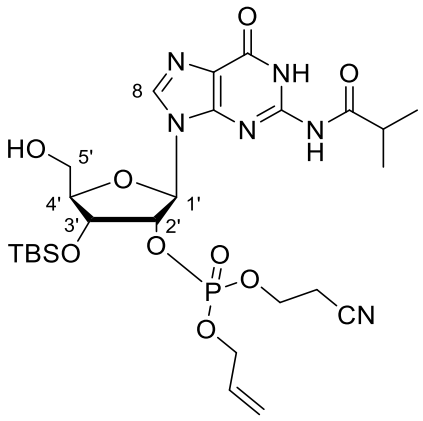

*N*2-Isobutyryl-*O*3'-TBS-*O*5'-DMTr-guanosine **41** (4.37 g, 5.67 mmol, 1.00 eq.) was pre-dried by co-evaporation with pyridine (1x), toluene (3x) and MeCN (3x) and dissolved in dry MeCN (22 mL) under Ar. 2-Cyanoethyl *N*,*N*,*N*',*N*'-tetraisopropylphosphorodiamidite (3.60 mL, 11.4 mmol, 2.00 eq.) and PyTFA (1.64 g, 8.51 mmol, 1.50 eq.) were added to the solution. The mixture was stirred for 2.5 hours at r.t.. Allyl alcohol (7.72 mL, 113 mmol, 20.0 eq.) was added, followed, after 10 minutes, by BTT (56.7 mL, 17.0 mmol, 3.00 eq., 0.3 M in MeCN) and stirred for 2.5 hours at r.t. After this time, tBuOOH (3.40 mL, 17.0 mmol, 3.00 eq., 5 M) was added to the reaction mixture and stirred for further 40 minutes. The mixture was quenched with a $NaHSO_3$ solution (15 mL, 0.50 g/mL) and extracted with EtOAc (200 mL), the organic layer was washed with brine (150 mL) and then concentrated *in vacuo*. The residue was added to a mixture of DCA (4.75 mL) and dry DCM (152 mL), stirred at r.t. for 20 minutes, during which the color changed from colorless to orange. After this time, the solution was quenched with saturated $NaHCO_3$ solution (150 mL) at 0 °C and extracted with EtOAc (3 x 250 mL), washed with brine, dried over Na_2SO_4 and evaporated *in vacuo*. The residue was purified by column chromatography on silica gel (2 to 15 % MeOH/DCM) yielding the desired product **42** (3.18 g, 4.96 mmol, 87 %) as a pale yellow foam.

Mixture of two phosphate isomers:

^{1}H NMR (400 MHz, CD_2Cl_2): δ (ppm) = 12.04 (s, 1H, NH-1), 8.70 (d, J = 34.4 Hz, 1H, NH-2), 7.84 (d, J = 21.1 Hz, 1H, H-8), 6.00 (dd, J = 6.8, 4.4 Hz, 1H, H-1'), 5.85 – 5.72 (m, 1H, PO-CH_2-C*H*=CH_2), 5.46 (tdd, J = 8.7, 6.8, 4.7 Hz, 1H, H-2'), 5.26 (ddq, J = 17.2, 3.0, 1.5 Hz, 1H, PO-CH_2-CH=C*H*$_2$), 5.21 (dt, J = 10.4, 1.2 Hz, 1H, PO-CH_2-CH=C*H*$_2$), 4.57 (ddd, J = 6.5, 4.7, 2.0 Hz, 1H, H-3'), 4.51 (s, 1H, OH), 4.50 – 4.24 (m, 2H, PO-C*H*$_2$-CH=CH_2), 4.19 (t, J = 2.1 Hz, 1H, H-4'), 4.16 – 3.99 (m, 2H, PO-C*H*$_2$-CH_2-CN), 3.92 (ddd, J = 12.7, 6.0, 2.2 Hz, 1H, H-5'), 3.72 (ddd, J = 12.7, 5.2, 1.8 Hz, 1H, H-5'), 2.74 – 2.57 (m, 3H, iBu C*H* / PO-CH_2-C*H*$_2$-CN), 1.24 (ddd, J = 6.9, 3.3, 1.6 Hz, 6H, iBu C*H*$_3$), 0.95 (d, J = 1.3 Hz, 9H, TBS C-C*H*$_3$), 0.16 (d, J = 4.3 Hz, 6H, TBS Si-C*H*$_3$).

^{13}C NMR (101 MHz, CD_2Cl_2): δ (ppm) = 179.08 (iBu *C*=O), 154.98 (C-6), 147.86 (C-4), 139.02 (C-8),

131.75 (PO-CH_2-*C*H=CH_2), 129.02 (C-2), 122.48 (*C*N), 118.63 (PO-CH_2-CH=*C*H_2), 116.48 (C-5), 87.79 (C-1'), 87.52 (C-4'), 77.34 (C-2'), 71.79 (C-3'), 69.02 (PO-*C*H_2-CH=CH_2), 62.20 (PO-*C*H_2-CH_2-CN), 62.02 (C-5'), 36.37 (iBu *C*H), 25.46 (TBS CH-*C*H_3), 19.67 (PO-CH_2-*C*H_2-CN), 18.70 (iBu *C*H_3), 18.02 (TBS *C*H), -5.21 (TBS Si-*C*H_3).

^{31}P NMR (162 MHz, CD_2Cl_2): δ (ppm) = -1.85, -2.63.

HR-ESI-MS: m/z calc. for $[C_{26}H_{42}O_9N_6PSi]^+$ $[M+H]^+$: 641.25147, found: 641.25151.

Rf = 0.53 (5 % MeOH/DCM).

*N*6-Propargyl-PEG$_2$-*N*6-Bz-*O*2'-TBS-*O*3'- phosphoramidite-*O*5'-DMTr-Adenosine (46)

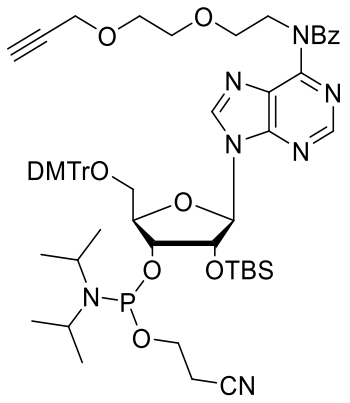

The reaction was carried out under oxygen free conditions with Schlenk technique. Propargyl diethylene glycol (**44**) was co-evaporated with toluene (3x) and dried under high vacuum. To a solution of propargyl diethylene glycol (678 mg, 4.71 mmol, 1.55 eq.) in THF (36 mL), *N*6-Bz-*O*2'-TBS-*O*3'-phosphoramidite-*O*5'-DMTr-Adenosine (**43**) (3.00 g, 3.04 mmol, 1.00 eq.), triphenylphosphine (1.27 g, 4.86 mmol, 1.60 eq.) and DEAD (2.80 mL, 4.55 mmol, 1.50 eq.) were added. The reaction mixture was stirred under Ar at r.t. for 3 hours. The mixture was concentrated in vacuo and major impurities were removed via fast column chromatography on silica gel (10 to 20 % EtOAc/DCM + 0.1 % pyridine) to isolate the crude phosphoramidite as a white foam. Due to the high instability of the product towards hydrolysis, it was considered pure enough and used in the next reaction.

Mixture of two isomers.

^{31}P NMR (162 MHz, CD_2Cl_2): δ (ppm) = 151.03, 148.95.

HR-ESI-MS: m/z calc. for $[C_{60}H_{76}N_7NaO_{10}PSi]^+$ $[M+Na]^+$: 1136.50528, found: 1136.50712.

Rf = 0.76, 0.87 (30 % EtOAc/DCM).

*N*6-PEG$_2$-Propargyl-Adenosine-*O*3'-Phosphate-*O*5'-Guanosine Phosphate (**48**)

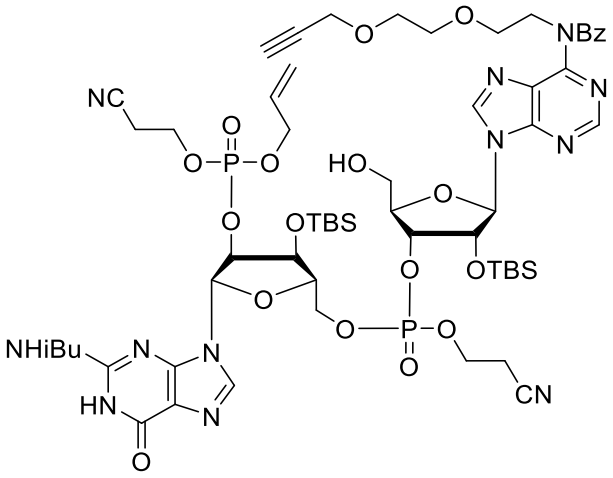

*N*6-iBu Guanosine phosphate (**42**) (900 mg, 1.40 mmol, 1.00 eq.) was pre-dried with toluene (3x) and then dissolved in dry MeCN (5 mL) together with *N*6-PEG$_2$-propargyl adenosine phosphoramidite (**46**) (3.13 g, 2.81 mmol, 2.00 eq.) under Ar. BTT (18.73 mL, 5.62 mmol, 4.00 eq., 0.3 M in MeCN) was added and the mixture was stirred for 3 hours at r.t. under Ar. tBuOOH (1.69 mL, 8.43 mmol, 6.00 eq., 5 M in decane) was added to the mixture and stirred for further 40 minutes. The mixture was quenched with a $NaHSO_3$ solution (13 mL, 0.5 g/mL) and extracted with EtOAc (150 mL), the organic layer was washed with brine and then concentrated *in vacuo*. The residue was redissolved in a solution of DCA (3 mL) in dry DCM (97 mL) and stirred for 15 minutes, during which time the solution changed from colourless to orange. The mixture was quenched with saturated solution of $NaHCO_3$ (200 mL) at 0 °C and extracted with EtOAc (3 x 150 mL), washed with brine and dried over Na_2SO_4 and evaporated *in vacuo*. The residue was purified by column chromatography on silica gel (2 to 5 % MeOH/DCM) to afford a mixture of four isomers of the desired compound **48** (1.65 mg, 1.21 mmol, 86 %) as a pale yellow grease.

Due to the high complexity of the isomeric mixture, the product was only characterized by HR-MS and ^{31}P NMR.

^{31}P NMR (202 MHz, CD_2Cl_2): δ (ppm) = -1.87, -2.05, -2.26, -2.44, -2.92, -3.00, -3.06, -3.18.

HR-ESI-MS: m/z calc. for $[C_{59}H_{85}N_{12}O_{18}P_2Si_2]^+$ $[M+H]^+$: 1367.51131, found: 1367.51509.

Rf = 0.30 (4 % MeOH/DCM).

*N*6-PEG$_2$-Propargyl-Adenosine-Guanosine (**48b**)

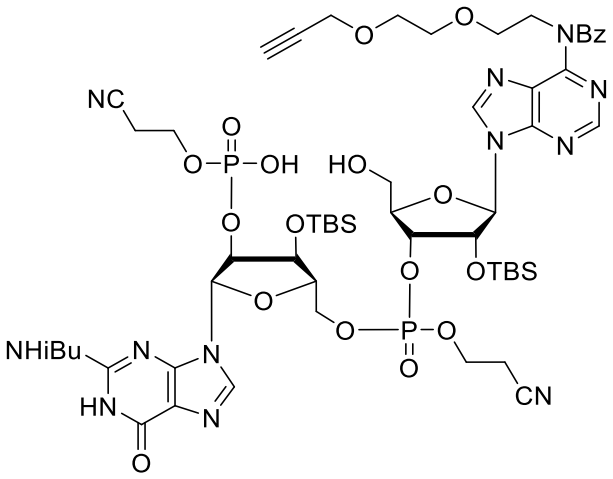

The *N*6-PEG$_2$-propargyl adenosine – guanosine linear product **48** (1.50 g, 1.10 mmol, 1.00 eq.) was suspended in acetone (200 mL) and NaI (1.64 g, 10.97 mmol, 10.00 eq.) was added. The mixture was vigorously stirred and refluxed for 5 hours. After this time, the solvents were removed *in vacuo* and the crude was roughly purified in a short column chromatography (10 to 20 % MeOH/DCM). The intermediate (954 mg, 0.719 mmol, 66 % assessed yield) was obtained in a mixture of two isomers as a pale yellow foam and directly used for the next reaction.

Due to the high complexity of the isomeric mixture, the intermediate was only characterized with HR-MS and ^{31}P NMR.

^{31}P NMR (202 MHz, MeOD): δ (ppm) = -1.39 (two P peaks fused together), -2.50, -2.62.

HR-ESI-MS: m/z calc. for $[C_{58}H_{85}N_{12}O_{19}P_2Si_2]^+$ $[M+H]^+$: 1371.50622, found: 1371.50657.

Rf = 0.14 (20 % MeOH/DCM).

*N*6A-PEG$_2$-Propargyl protected cGAMP (**50**)

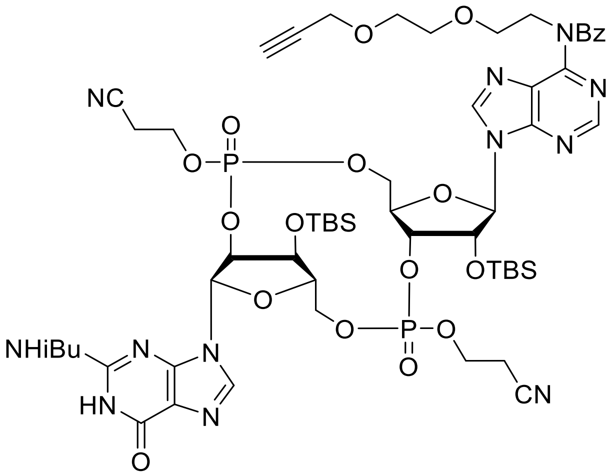

After co-evaporation with pyridine (3x), the intermediate **48b** (950 mg, 716 µmol, 1.00 eq.) was redissolved in dry pyridine (150 mL) and MSNT (1.06 g, 3.58 mmol, 5.00 eq.) was added. The mixture was stirred 24 hours at r.t. in the dark protected with aluminium foil. After this time the solvents were removed *in vacuo* and the crude roughly purified via short column chromatography (3 to 10 % MeOH/DCM) to separate the mixture of four isomers of the cyclized intermediate **50** (700 mg, 535 µmol, 75 % assessed yield of the step) as a pale yellow foam.

Due to the high complexity of the isomeric mixture, the intermediate was only characterized with HR-MS and ^{31}P NMR.

^{31}P NMR (202 MHz, Acetone): δ (ppm) = 2.78, 2.23, -0.02, -2.03, -3.12, -4.09, -4.22, -4.67.

HR-ESI-MS: m/z calc. for $[C_{56}H_{79}N_{12}O_{17}P_2Si_2]^+$ $[M+H]^+$: 1309.46944, found: 1309.46996.

Rf = 0.24 (5 % MeOH/DCM).

*N*6A-PEG$_2$-Propargyl cGAMP (**52**)

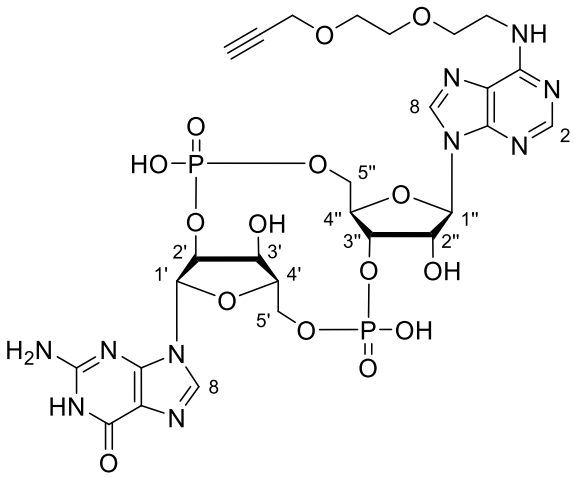

50 (500 mg, 0.382 mmol) was dissolved in a solution of 33% $MeNH_2$ in absolute ethanol (100 mL) under Ar. The solution was stirred for 2.5 hours at r.t., after which time LC-MS showed no more starting material present. The solvent was evaporated and the residue co-evaporated twice with pyridine and dried under high vacuum. The solid was then redissolved in dry pyridine (3.6 mL), transferred in a falcon tube under Ar and dry THF (18mL) was added. After the addition of Et_3N x 3HF (3.64 mL), the mixture was stirred at r.t. overnight. When LC-MS showed no more starting material present, the reaction was quenched with TMSOMe (9.3 mL) and concentrated *in vacuo*. The residue was redissolved in a minimal amount of methanol and precipitated by dropping it slowly in a falcon tube containing cold acetone. The precipitate was collected after centrifugation and purified by preparative HPLC (0 to 60 % B in 45 minutes. Buffer A = H_2O + 0.1 % TFA, buffer B = MeCN + 0.1 % TFA) to obtain the desired product **52** (213 mg, 266 µmol, 70 %) as a white solid.

^{1}H NMR (500 MHz, D_2O): δ (ppm) = 9.01 (s, 1H, H-8A), 8.49 (d, J = 51.9 Hz, 2H, H-8G / H-2A), 6.24 (d, J = 9.1 Hz, 1H, H-1'), 6.08 (d, J = 8.3 Hz, 1H, H-1"), 5.74 – 5.58 (m, 1H, H-2"), 4.97 (d, J = 9.8 Hz, 1H, H-3'), 4.71 – 4.65 (m, 1H, H-2'), 4.58 (d, J = 4.2 Hz, 1H, H-3"), 4.48 (d, J = 9.0 Hz, 1H, H-4'), 4.45 (s, 1H, H-4"), 4.41 (d, J = 11.6 Hz, 1H, H-5'), 4.28 (ddd, J = 11.9, 5.8, 2.9 Hz, 1H, H-5"), 4.19 – 4.14 (m, 1H, H-5"), 4.10 (d, J = 2.4 Hz, 2H, O-C*H*$_2$-C≡CH), 4.05 (dd, J = 11.7, 3.0 Hz, 1H, H-5'), 3.95 – 3.76 (m, 4H, PEG CH_2), 3.75 – 3.63 (m, 4H, PEG CH_2), 2.80 (t, J = 2.4 Hz, 1H, O-CH_2-C≡C*H*).

^{13}C NMR (126 MHz, D_2O): δ (ppm) = 163.56 (C-6A), 163.27 (C=O), 155.72 (Ar), 155.26 (Ar), 150.76 (Ar), 149.84 (Ar), 146.52 (Ar), 145.25 (C-2A), 141.61 (C-8G), 139.23 (C-8A), 90.50 (C-1'), 88.34 (C-1"), 85.00 (C-4"), 80.78 (C-4'), 79.73 (*C*≡CH), 76.48 (C≡*C*H), 74.95 (C-2'), 74.82 (C-2"), 72.07 (C-3"), 71.09 (C-3'), 70.29 (PEG CH_2), 70.15 (PEG CH_2), 69.27 (PEG CH_2 / NH-*C*H_2-PEG), 66.21 (C-5"), 62.61 (C-5'), 58.42 (O-*C*H_2-C≡CH).

^{31}P NMR (202 MHz, D_2O): δ (ppm) = -1.39, -2.04.

HR-ESI-MS: m/z calc. for $[C_{27}H_{35}N_{10}O_{15}P_2]^+$ $[M+H]^+$: 801.17531, found: 801.17525.

FT-IR: $\tilde{\nu}$ (cm^{-1}) = 1672.75 (m), 1638.26 (m), 1602.33 (m), 1485.93 (w), 1458.62 (w), 1352.28 (w), 1202.82 (m), 1066.30 (s), 994.45 (m), 886.67 (m), 856.49 (m), 797.57 (m), 781.76 (m), 721.41 (m), 676.86 (m), 642.37 (m), 606.44 (m), 538.90 (m), 508.72 (s), 467.05 (s), 431.12 (s).

Rf = product elution time LC-MS 2.6 min. (5 to 80% B in 7 min., 600 µL/min).

Propargyl-PEG3-OH (45)

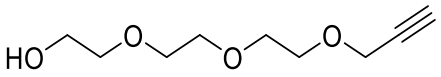

To a suspension of tBuOK (3.77 g, 33.60 mmol, 1.00 eq.) in dry THF (150 mL), triethylene glycol (10.1 g, 67.26 mmol, 2.00 eq.) was added at 0 °C under N_2 atmosphere. The reaction mixture was stirred for 30 minutes at r.t. Through a dropping funnel, propargyl bromide (5.00 g, 33.60 mmol, 1.00 eq.) in dry THF (25 mL) was added dropwise. The reaction mixture was stirred under Ar at r.t. overnight. The precipitate was filtered through Celite and the solution was concentrated in vacuo. The residue was purified by column chromatography on silica gel (EtOAc) to give the desired product **45** (4.95 g, 26.26 mmol, 78 %) as a pale yellow oil.

^{1}H NMR (400 MHz, $CDCl_3$): δ (ppm) = 4.20 (d, J = 2.4 Hz, 2H, O-C*H*$_2$-C≡CH), 3.74 – 3.63 (m, 10H, HO-CH_2-C*H*$_2$ / O-C*H*$_2$-C*H*$_2$-O), 3.63 – 3.59 (m, 2H, HO-C*H*$_2$), 2.72 – 2.46 (s, 1H, OH), 2.43 (t, J = 2.4 Hz, 1H, C≡C*H*).

^{13}C NMR (101 MHz, $CDCl_3$): δ (ppm) = 79.68 (*C*≡CH), 74.74 (C≡*C*H), 72.58 (C-2), 70.75 (C-3), 70.49 (C-4 / C-6), 69.19 (C-5), 61.88 (C-1), 58.54 (O-*C*H_2-C≡CH).

HR-ESI-MS: m/z calc. for $[C_9H_{17}O_4]^+$ $[M+H]^+$: 189.11214, found: 189.11221.

Rf = 0.43 (EtOAc).

*N*6-Propargyl-PEG$_3$-*N*6-Bz-*O*2'-TBS-*O*3'- phosphoramidite-*O*5'-DMTr-Adenosine (**47**)

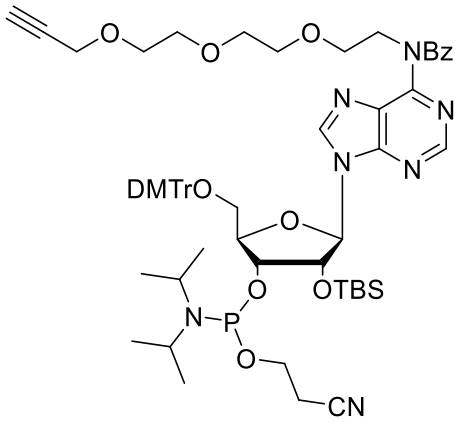

The reaction was carried out under oxygen free conditions with Schlenk technique. Propargyl PEG$_3$ alcohol (**45**) was co-evaporated with toluene (3x) and dried under high vacuum. To a solution of propargyl PEG$_3$-OH (propargyl-triethylene glycol) (1.18 g, 6.27 mmol, 1.55 eq.) in THF (48 mL), *N*6-Bz-*O*2'-TBS-*O*3'-phosphoramidite-*O*5'-DMTr-adenosine (**43**) (4.00 g, 4.05 mmol, 1.00 eq.), triphenylphosphine (1.70 g, 6.48 mmol, 1.60 eq.) and DEAD (2.07 mL, 6.15 mmol, 1.50 eq.) were added. The reaction mixture was stirred under Ar at r.t. for 2.5 hours. The mixture was concentrated in vacuo and major impurities were removed via fast silica gel column chromatography (30 to 70 % EtOAc/DCM + 0.1 % pyridine) to isolate the crude phosphoramidite as a white greasy foam. Due to the high instability of the product towards hydrolysis, it was considered pure enough and used in the next reaction.

Mixture of two isomers.

^{31}P NMR (162 MHz, CD_2Cl_2): δ (ppm) = 151.00, 148.92.

HR-ESI-MS: m/z calc. for $[C_{62}H_{81}O_{11}N_7PSi]^+$ $[M+H]^+$: 1158.54955, found: 1158.54754.

Rf = 0.48, 0.57 (30 % EtOAc/DCM).

N6-PEG$_3$-Propargyl-Adenosine-*O*3'-Phosphate-*O*5'-Guanosine Phosphate (**49**)

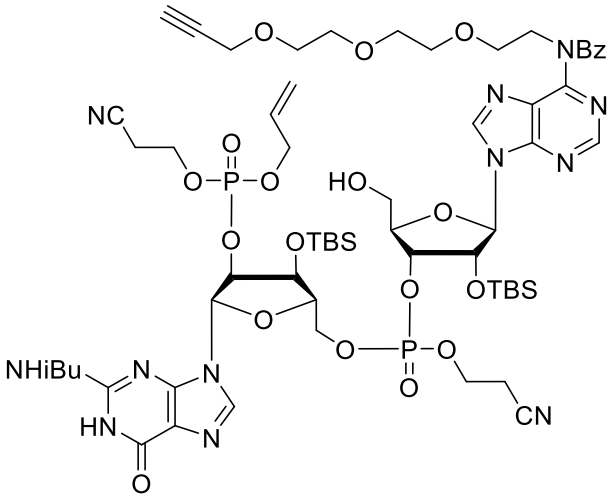

*N*2-iBu Guanosine phosphate (**42**) (700 mg, 0.60 mmol, 1.00 eq.) was pre-dried with toluene (3x) and then dissolved in dry MeCN (2 mL) together with *N*6-PEG$_3$-propargyl adenosine phosphoramidite (**47**) (426 mg, 0.66 mmol, 1.10 eq.) under Ar. BTT (4.03 mL, 1.21 mmol, 2.00 eq., 0.3 M in MeCN) was added and the mixture was stirred for 2.5 hours at r.t. under Ar. tBuOOH (423 µL, 2.11 mmol, 3.50 eq., 5 M in decane) was added to the mixture and stirred for further 40 minutes. The mixture was quenched with a $NaHSO_3$ solution (1.75 mL, 0.5 g/mL) and extracted with EtOAc (80 mL), the organic layer was washed with brine and then concentrated *in vacuo*. The residue was redissolved in a solution of DCA (0.5 mL) in dry DCM (16.2 mL) and stirred for 20 minutes, during which time the solution changed from colourless to orange. The mixture was quenched with saturated solution of $NaHCO_3$ (38 mL) at 0 °C and extracted with EtOAc (3 x 80 mL), washed with brine and dried over Na_2SO_4 and evaporated *in vacuo*. The residue was purified by column chromatography on silica gel (2 to 5 % MeOH/DCM) to afford a mixture of four isomers of the desired compound **49** (632 mg, 0.45 mmol, 74 %) as a pale yellow grease.

Due to the high complexity of the isomeric mixture, the product was only characterized by HR-MS and ^{31}P NMR.

^{31}P NMR (202 MHz, CD_2Cl_2): δ (ppm) = -1.99, -2.12, -2.40, -2.54, -2.91, -3.00, -3.04, -3.19.

HR-ESI-MS: m/z calc. for $[C_{61}H_{89}N_{12}O_{19}P_2Si_2]^+$ $[M+H]^+$: 1411.53752, found: 1411.53845.

Rf = 0.50 (4 % MeOH/DCM).

*N*6-PEG$_3$-Propargyl-Adenosine-Guanosine (**49b**)

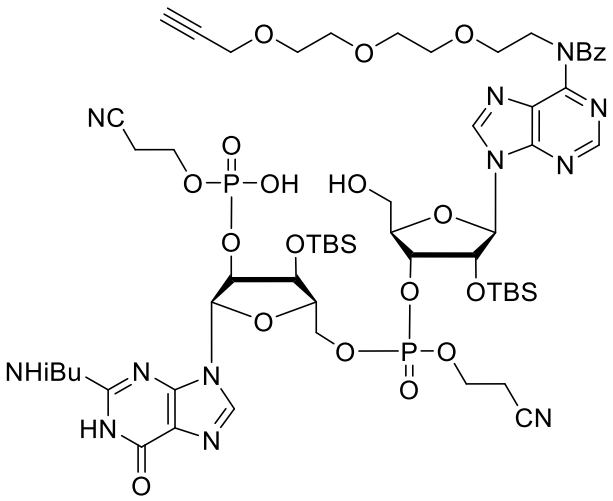

The *N*6-PEG$_3$-propargyl adenosine – guanosine linear product **49** (2.22 g, 1.57 mmol, 1.00 eq.) was suspended in acetone (250 mL) and NaI (2.36 g, 15.73 mmol, 10.00 eq.) was added. The mixture was vigorously stirred and refluxed for 5 hours. After this time, the solvents were removed *in vacuo* and the crude was roughly purified in a short column chromatography (10 to 20 % MeOH/DCM). The intermediate (1.50 g, 1.09 mmol, 70 % assessed yield) was obtained in a mixture of two isomers as a pale yellow foam and directly used for the next reaction.

Due to the high complexity of the isomeric mixture, the intermediate was only characterized with HR-MS and ^{31}P NMR.

^{31}P NMR (202 MHz, DMSO): δ (ppm) = -2.14, -2.55, -4.35, -6.04.

HR-ESI-MS: m/z calc. for $[C_{58}H_{85}N_{12}O_{19}P_2Si_2]^+$ $[M+H]^+$: 1371.50622, found: 1371.50657.

Rf = 0.3, 0.1 (20 % MeOH/DCM).

*N*6A-PEG$_3$-Propargyl protected cGAMP (**51**)

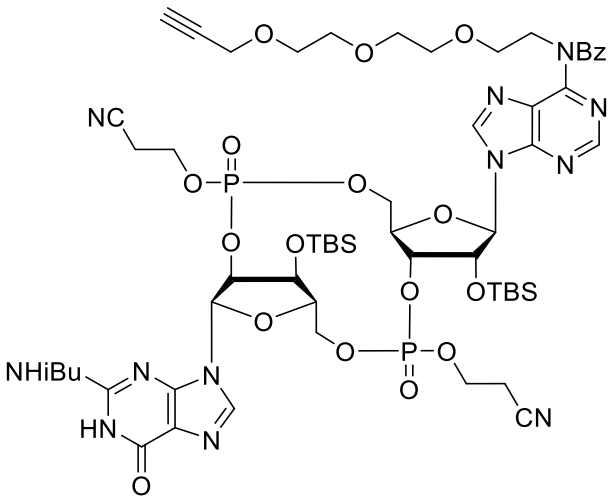

After co-evaporation with pyridine (3x), the intermediate **49b** (1.50 g, 1.09 mmol, 1.00 eq.) was redissolved in dry pyridine (200 mL) and MSNT (1.62 g, 5.47 mmol, 5.00 eq.) was added. The mixture was stirred 36 hours at r.t. in the dark protected with aluminium foil. After this time the solvents were removed *in vacuo* and the crude roughly purified via short column chromatography (0 to 10 % MeOH/DCM) to separate the mixture of four isomers of the cyclized intermediate **51** (1.29 g, 953 µmol, 87 % assessed yield of the step) as a pale yellow foam.

Due to the high complexity of the isomeric mixture, the intermediate was only characterized with HR-MS and ^{31}P NMR.

^{31}P NMR (202 MHz, CD_2Cl_2): δ (ppm) = 2.15, -0.76, -2.79, -2.89, -3.35, -3.82, -4.44, -5.06.

HR-ESI-MS: m/z calc. for $[C_{58}H_{83}N_{12}O_{18}P_2Si_2]^+$ $[M+H]^+$: 1353.49566, found: 1353.49721.

Rf = 0.39, 0.34 (5 % MeOH/DCM).

*N*6A-PEG$_3$-Propargyl cGAMP (**53**)

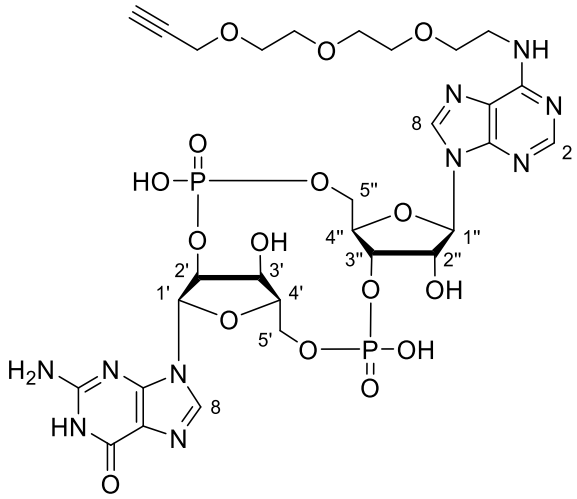

51 (500 mg, 0.369 mmol) was dissolved in a solution of 33% $MeNH_2$ in absolute ethanol (125 mL) under Ar. The solution was stirred for 3.5 hours at r.t., after which time LC-MS showed no more starting material present. The solvent was evaporated and the residue co-evaporated twice with pyridine and dried under high vacuum. The solid was then redissolved in dry pyridine (3.5 mL), transferred in a falcon tube under Ar and dry THF (17.33 mL) was added. After the addition of Et_3N x 3HF (3.53 mL), the mixture was stirred at r.t. overnight. When LC-MS showed no more starting material present, the reaction was quenched with TMSOMe (9 mL) and concentrated *in vacuo*. The residue was redissolved in a minimal amount of methanol and precipitated by dropping it slowly in a falcon tube containing cold acetone. The precipitate was collected after centrifugation and purified by preparative HPLC (0 to 20 % B in 45 minutes. Buffer A = H_2O + 0.1 % TFA, buffer B = MeCN + 0.1 % TFA) to obtain the desired product **53** (198 mg, 0.234 mmol, 64 %) as a white solid.

^{1}H NMR (500 MHz, D_2O): δ (ppm) = 8.98 (s, 1H, H-8A), 8.51 (d, J = 50.2 Hz, 1H, H-8G), 8.44 (s, 1H, H-2A), 6.25 (d, J = 6.5 Hz, 1H, H-1'), 6.08 (d, J = 8.3 Hz, 1H, H-1"), 5.74 – 5.59 (m, 1H, H-2"), 4.98 (d, J = 9.4 Hz, 1H, H-3'), 4.73 – 4.65 (m, 1H, H-2'), 4.59 (d, J = 4.1 Hz, 1H, H-3"), 4.49 (d, J = 9.0 Hz, 1H, H-4'), 4.43 (d, J = 18.2 Hz, 3H, H-4" / H-5'), 4.32 – 4.24 (m, 1H, H-5"), 4.20 – 4.10 (m, 3H, H-5" / O-C*H*$_2$-C≡CH), 4.05 (dd, J = 11.8, 3.0 Hz, 1H, H-5'), 3.94 – 3.58 (m, 12H, PEG CH_2), 2.82 (d, J = 2.7 Hz, 1H, O-CH_2-C≡C*H*).

^{13}C NMR (126 MHz, D_2O): δ (ppm) = 164.07 (C-6A), 163.78 (C=O), 156.33 (Ar), 155.65 (Ar), 150.26 (Ar), 146.94 (Ar), 146.35 (Ar), 145.77 (C-2A), 142.04 (C-8G), 139.81 (C-8A), 90.97 (C-1'), 88.73 (C-1"), 85.41 (C-4"), 81.22 (C-4'), 80.25 (*C*≡CH), 76.93 (C≡*C*H), 75.38 (C-2'), 75.20 (C-2"), 72.50 (C-3"), 71.50 (C-3'), 70.90 (PEG CH_2), 70.51 (PEG CH_2), 70.43 (PEG CH_2), 69.60 (PEG CH_2), 66.68 (C-5"), 63.00 (C-5'), 58.87 (O-*C*H_2-C≡CH), 43.49 (NH-*C*H_2-PEG).

^{31}P NMR (202 MHz, D_2O): δ (ppm) = -1.37, -2.05.

HR-ESI-MS: m/z calc. for $[C_{29}H_{37}N_{10}O_{16}P_2]^-$ $[M-H]^-$: 843.18697, found: 843.18634.

FT-IR: $\tilde{\nu}$ (cm^{-1}) = 1684.24 (m), 1654.06 (m), 1636.82 (m), 1559.22 (m), 1457.19 (w), 1418.38 (w), 1353.72 (w), 1201.39 (m), 1130.97 (m), 1070.61 (s), 997.32 (m), 948.46 (m), 799.01 (m), 780.33 (m), 719.97 (m), 668.24 (m), 639.49 (m), 514.47 (m), 472.79 (m), 429.68 (m).

Rf = product elution time 22 minutes HPLC (0 to 20% B in 45 minutes).

4.2.1.2 Non-Covalent Inhibitor-Based STING Recruiters

4-Fluoro-*N*-(2-hydroxy-5-nitrophenyl)benzenesulfonamide (56)

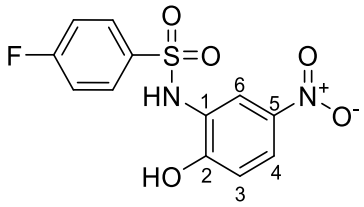

To a solution of 2-amino-4-nitrophenol (**54**) (2.10 g, 13.63 mmol, 1.00 eq) and pyridine (1.65 mL, 20.44 mmol, 1.50 eq) in dry DCM (40 mL) under Ar, was added dropwise at 0 °C, 4-fluorobenzenesulfonyl chloride (**55**) (3.18 g, 16.35 mmol, 1.20 eq) in dry DCM (20 mL) over 30 minutes and the mixture stirred at r.t. overnight. After this time the solvents were evaporated *in vacuo* and the residue was purified by silica gel column chromatography (2 % MeOH/DCM) to obtain the desired product **56** (2.54 g, 8.13 mmol, 60 %) as a yellow solid.

^{1}H NMR (400 MHz, MeOD): δ (ppm) = 9.85 (d, J = 2.8 Hz, 1H, H-6), 9.46 (dd, J = 9.0, 2.8 Hz, 1H, H-4), 9.43 – 9.37 (m, 2H, SO_2-Ar-F *o*-CH), 8.81 – 8.73 (m, 2H, SO_2-Ar-F *m*-CH), 8.37 (d, J = 9.0 Hz, 1H, H-3).

^{13}C NMR (101 MHz, MeOD): δ (ppm) = 167.92 (Ar C-F), 165.41 (Ar C-S), 157.27 (C-2), 141.46 (C-5), 131.37 / 131.28 (SO_2-Ar-F *o*-CH), 126.33 (C-1), 123.35 (C-4), 120.75 (C-3), 117.11 / 116.88 (SO_2-Ar-F *m*-CH), 115.75 (C-6).

HR-ESI-MS: m/z calc. for $[C_{12}H_8FN_2O_5S]^-$ $[M-H]^-$: 311.01434; found: 311.01440.

Rf = 0.49 (5% MeOH/DCM).

N-(5-Amino-2-hydroxyphenyl)-4-fluorobenzenesulfonamide (**57**)

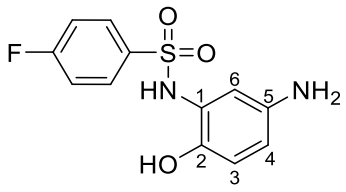

To a solution of 4-fluoro-*N*-(2-hydroxy-5-nitrophenyl)benzenesulfonamide (**56**) (1.58 g, 5.06 mmol) in dry MeOH (20 mL), was added Pd/C (140 mg, 10 %) under H_2 atmosphere and the mixture stirred at r.t. overnight. The mixture was then filtered through Celite™ and the solvent removed *in vacuo* to afford the crude product (1.47 g, 5.21 mmol, > 100 %) as a yellow solid. The product **57** was considered pure enough and directly used in the next step without further purification.

^{1}H NMR (400 MHz, THF): δ (ppm) = 7.99 – 7.79 (m, 2H, NH / OH), 7.76 (dt, J = 8.7, 4.0 Hz, 2H, SO_2-Ar-F *m*-CH), 7.13 (td, J = 8.9, 3.1 Hz, 2H, SO_2-Ar-F *o*-CH), 6.70 (q, J = 3.1 Hz, 1H, H-6), 6.36 (dd, J = 8.6, 3.1 Hz, 1H, H-3), 6.15 (dq, J = 6.5, 3.0 Hz, 1H, H-4), 4.07 (s, 2H, NH_2).

^{13}C NMR (101 MHz, THF): δ (ppm) = 166.99 (Ar C-F), 164.49 (Ar C-S), 142.66 (C-2), 141.22(C-5), 130.92 / 130.83 (SO_2-Ar-F *o*-CH), 126.12 (C-1), 116.49 (C-4), 116.29 / 116.07 (SO_2-Ar-F *m*-CH), 112.55 (C-3), 110.96 (C-6).

HR-ESI-MS: m/z calc. for $[C_{12}H_{12}FN_2O_3S]^+$ $[M+H]^+$: 283.05472, found: 283.05489.

Rf = 0.41 (5 % MeOH/DCM).

N-(3-((4-Fluorophenyl)sulfonamido)-4-hydroxyphenyl)-[1,1'-biphenyl]-4-carboxamide (**23**)

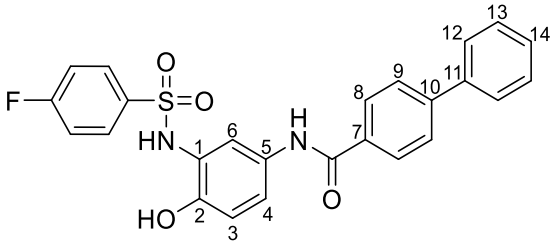

To a solution of *N*-(5-amino-2-hydroxyphenyl)-4-fluorobenzenesulfonamide (**57**) (970 mg, 3.44 mmol, 1.00 eq) in dry DMF (50 mL), was added Et_3N (478 µL, 3.44 mmol, 1.00) at 0 °C under Ar and the mixture stirred for 1 hour. A solution of 1,1'-biphenyl-4-carbonyl chloride (**58**) (819 mg, 4.78 mmol, 1.10 eq) in dry DMF (30 mL) was added dropwise at 0 °C and the mixture stirred at r.t. for 30 minutes. After quenching with MeOH (20 mL), the solvents were removed *in vacuo*. The residue was then treated with a saturated solution of NH_4Cl (20 mL) and extracted with EtOAc (3 x 40 mL). The combined organic phases were washed with brine, dried over Na_2SO_4 and the solvent evaporated through rotatory evaporation. The crude mixture was purified via silica gel column chromatography (0 to 5 % EtOAc/DCM) to obtain the desired product **23** (789 mg, 1.71 mmol, 50 %) as a light pink-brown solid.

^{1}H NMR (400 MHz, THF): δ (ppm) = 9.38 (s, 1H, OH), 8.38 (s, 2H, $NH_{a/b}$), 8.02 (dd, J = 8.3, 3.1 Hz, 2H, H-8), 7.87 – 7.79 (m, 2H, SO_2-Ar-F *o*-CH), 7.77 – 7.66 (m, 5H, H-6 / H-13, H-9), 7.63 (q, J = 3.1 Hz, 1H, H-3), 7.45 (td, J = 7.6, 2.8 Hz, 2H, H-12), 7.35 (t, J = 7.5 Hz, 1H, H-4), 7.16 (td, J = 8.8, 3.1 Hz, 2H, SO_2-Ar-F *o*-CH), 6.62 (dd, J = 8.9, 3.2 Hz, 1H, H-14).

^{13}C NMR (101 MHz, THF): δ (ppm) = 167.11(Ar C-F), 165.33 (C=O), 164.61 (Ar C-S), 146.38 (C-5), 144.56 (C-7), 141.06 (C-11), 135.50 (C-10), 133.18 (C-1), 131.06 / 130.96 (SO_2-Ar-F *o*-CH), 129.64 (C-12), 128.83 (C-8), 128.62 (C-4), 127.86 (C-9), 127.40 (C-13), 125.63 (C-2), 118.95 (C-6), 116.93 (C-3), 116.42 / 116.20 (SO_2-Ar-F *m*-CH), 115.59 (C-14).

HR-ESI-MS: m/z calc. for $[C_{25}H_{20}FN_2O_4S]^+$ $[M+H]^+$: 463.11223, found: 463.11202.

Rf = 0.42 (15 % EtOAc/DCM).

2-(2-(Prop-2-yn-1-yloxy)ethoxy)acetic acid (**59**)

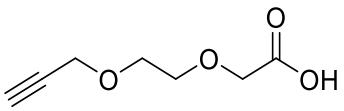

To NaH (60 % in mineral oil, 3.20 g, 79.91 mmol, 4.00 eq), dry THF (25 mL) was added at 0 °C under Ar. After dissolving 2-(prop-2-yn-1-yloxy)ethan-1-ol (2.00 mL, 19.98 mmol, 1.00 eq) in dry THF (10 mL), the solution was added to the reaction mixture dropwise at 0 °C. After stirring 15 minutes, a solution of 2-iodoacetic acid (3.71 g, 19.98 mmol, 1.00 eq.) in dry THF (10 mL) was added to the mixture dropwise at 0 °C. After the addition, the solution was stirred at r.t. overnight. The mixture was quenched with MeOH (30 mL) and concentrated via rotary evaporation. After that, a Na_2CO_3 solution (5 %, 100 mL) was added and the aqueous phase washed with EtOAc (3 x 50 mL). Solid $Na_2S_2O_3$ was added to the aqueous phase to decolorize, followed by acidification with HCl (conc.) until pH 1. The aqueous phase was then extracted with EtOAc (3 x 40mL) and the combined organic phases washed with a saturated solution of $Na_2S_2O_3$ until turned from yellow to colourless. The solution was then dried over anhydrous Na_2SO_4 and the solvent concentrated *in vacuo*. The crude product **59** was obtained as a yellow oil (2.71 g, 17.11 mmol, 86 %). No further purification was necessary and the crude product was directly used for the following step.

^{1}H NMR (400 MHz, MeOD): δ (ppm) = 4.20 (d, J = 2.4 Hz, 2H, C*H*$_2$-C≡CH), 4.12 (s, 2H, C*H*$_2$-COOH), 3.71 (m, 4H, PEG CH_2), 2.85 (t, J = 2.4 Hz, 1H, C≡CH).

4.19 (d, J = 2.4 Hz, 2H, H-6), 4.12 (t, J = 3.1 Hz, 2H, H- 3), 3.74 – 3.68 (m, 4H, H- 4, 5), 2.85 (t, J = 2.5 Hz, 1H, H-1)

^{13}C NMR (101 MHz, MeOD): δ (ppm) = 174.02 (C=O), 80.47 (*C*≡CH), 75.95 (C≡*C*H), 71.51 (PEG *C*H_2), 70.11 (PEG *C*H_2), 68.98 (*C*H_2-COOH), 58.99 (*C*H_2-C≡CH).

HR-ESI-MS: m/z calc. for $[C_7H_9O_4]^-$ $[M-H]^-$: 157.05063, found: 157.05055.

FT-IR: $\tilde{\nu}$ (cm^{-1}) = 3267.5 (w), 2920.9 (w), 2363.6 (w), 2116.8 (w), 1730.8 (s), 1147.7 (m), 1094.4 (s), 1027.4 (m).

Rf = 0.25 (10 % EtOAc/DCM).

N-(2-Amino-5-nitrophenyl)-4-fluorobenzenesulfonamide (**61**)

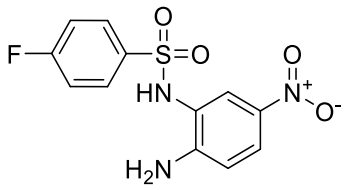

4-fluorobenzenesulfonyl chloride (**55**) (2.58 g, 13.26 mmol, 1.00 eq) in dry THF (30 mL) was added dropwise over 1 hour at 0 °C under Ar, to a solution of 4-nitrobenzene-1,2-diamine (**60**) (2.02 g, 13.19 mmol, 1.00 eq) and pyridine (1.05 mL, 13.06 mmol, 1.00 eq) in dry THF (30 mL). The mixture was then stirred at r.t. overnight, after which time the solvents were evaporated. Water (30 mL) was added to the residue and the mixture extracted with EtOAc (3 x 100 mL), the combined organic layers were washed with brine (50 mL) and dried over Na_2SO_4. After the solvent had been removed under vacuum, the crude product was purified by flash column chromatography (0 to 20 % EtOAc/DCM) to obtain the desired product **61** (3.74 g, 12.01 mmol, 91 %) as a yellow solid.

^{1}H NMR (400 MHz, DMSO): δ (ppm) = 9.59 (s, 1H, NH), 7.84 (dd, J = 9.1, 2.7 Hz, 1H, H-4), 7.80 – 7.72 (m, 2H, SO_2-Ar-F *o*-CH), 7.54 (d, J = 2.6 Hz, 1H, H-6), 7.41 (t, J = 8.8 Hz, 2H, SO_2-Ar-F *m*-CH), 6.68 (d, J = 9.1 Hz, 1H, H-3), 6.50 (s, 2H, NH_2).

^{13}C NMR (101 MHz, DMSO): δ (ppm) = 165.77 (Ar C-F), 163.27 (Ar C-S), 151.39 (C-2), 135.28 (C-5), 130.15 / 130.06 (SO_2-Ar-F *o*-CH), 124.51 (C-1), 123.51 (C-4), 118.86 (C-3), 116.57 / 116.34 (SO_2-Ar-F *m*-CH), 113.93 (C-6).

HR-ESI-MS: m/z calc. for $[C_{12}H_{11}FN_3O_4S]^+$ $[M+H]^+$: 312.0454; found: 312.0450.

FT-IR: $\tilde{\nu}$ (cm^{-1}) = 3492.5 (w), 3388.9 (w), 1623.0 (m), 1586.9 (m), 1486.3 (m), 1302.0 (s), 1293.0 (s), 1267.2 (m), 1235.9 (m) 1163.7 (m), 832.7 (m), 747.8 (m), 668.5 (m).

Rf = 0.52 (20% EtOAc/DCM).

N-(2-((4-Fluorophenyl)sulfonamido)-4-nitrophenyl)-2-(2-(prop-2-yn-1-yloxy)ethoxy)acetamide (**62**)

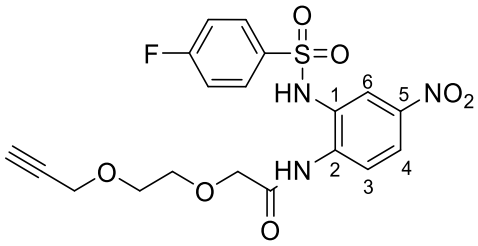

To 2-(2-(prop-2-yn-1-yloxy)ethoxy)acetic acid (**59**) (4.32 g, 27.31 mmol, 1.70 eq), oxalyl chloride (20.66 mL, 240.93 mmol, 15.00 eq) were added under Ar at 0 °C. The solution was left stirring at r.t. for 1.5 hours. After concentrating via rotary evaporation, the precipitate was dissolved in dry THF (30 mL). This solution was added dropwise at 0 °C under Ar to a previously prepared one containing *N*-(2-amino-5-nitrophenyl)-4-fluorobenzenesulfonamide (**61**) (5.00 g, 16.06 mmol, 1.00 eq) and Et_3N (3.81 mL, 27.31 mmol, 1.70 eq) in dry THF (50 mL). The mixture was stirred under the same conditions for 30 minutes until LC-MS showed no more starting material, the reaction was then quenched with MeOH (50 mL) and the solvents evaporated. The residue was dissolved in a saturated solution of NH_4Cl (75 mL) and extracted with EtOAc (3x 150 mL). The combined organic phases were then washed with brine, dried over anhydrous Na_2SO_4, filtered and evaporated. The crude was purified via silica gel chromatography (0 to 10 % EtOAc/DCM) giving the final product **62** (4.50 g, 9.97 mmol, 62 %) as a yellow-orange solid.

^{1}H NMR (400 MHz, CD_2Cl_2): δ (ppm) 9.18 (s, 1H, NH), 8.11 (dd, J = 8.9, 2.6 Hz, 1H, H-4), 8.06 (d, J = 2.5 Hz, 1H, H-6), 7.85 (d, J = 8.9 Hz, 1H, H-3), 7.76 – 7.65 (m, 2H, SO_2-Ar-F *m*-CH), 7.17 (t, J = 8.6 Hz, 2H, SO_2-Ar-F *o*-CH), 4.26 (d, J = 2.4 Hz, 2H, CH_2-C≡CH), 4.07 (s, 2H, O-CH_2-C=O), 3.80 – 3.73 (m, 4H, PEG CH_2), 2.51 (t, J = 2.4 Hz, 1H, CH_2-C≡C*H*).

^{13}C NMR (101 MHz, CD_2Cl_2): δ (ppm) = 170.05 (C=O), 167.20 (Ar C-F), 164.66 (Ar C-S), 145.05 (C-1), 139.01 (C-5), 130.32 / 130.23 (SO_2-Ar-F *m*-CH), 128.10 (C-2), 124.03 (C-6), 123.56 (C-4), 123.26 (C-3), 117.09 / 116.87 (SO2-Ar-F *o*-CH), 79.49 (*C*≡CH), 75.46 (C≡*C*H), 71.74 (PEG CH_2), 70.59 (O-*C*H_2-C=O), 69.39 (PEG CH_2), 58.98 (*C*H_2-C≡CH).

HR-ESI-MS: m/z calc. for $[C_{19}H_{19}FN_3O_7S]^+$ $[M+H]^+$: 452.09223, found: 452.09226.

FT-IR: $\tilde{\nu}$ (cm^{-1}) = 3338.7 (m), 3275.9 (m), 2255.4 (w), 2112.9 (w), 1710.5 (s), 1591.1 (s), 1537.6 (s), 1511.1 (s), 1494.2 (m), 1339.7 (s), 1281.8 (m), 1242.3 (m), 1166.2 (s), 1154.8 (s), 1095.9 (s), 1085.8 (s), 915.2 (m), 840.5 (s), 819.9 (m).

Rf = 0.42 (15 % EtOAc/DCM).

N-(4-Amino-2-((4-fluorophenyl)sulfonamido)phenyl)-2-(2-(prop-2-yn-1-yloxy)ethoxy) acetamide (**63**)

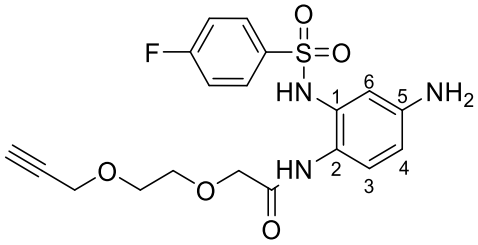

N-(2-((4-Fluorophenyl)sulfonamido)-4-nitrophenyl)-2-(2-(prop-2-yn-1-yloxy)ethoxy)acetamide (**62**) (90 mg, 199 µmol, 1.00 eq) was dissolved in dry DCM (6 mL) under N_2. Zinc dust (12 mg, 184 µmol, 0.92 eq) and AcOH (11 µmL, 183 µmol, 0.92 eq) were added to the solution which was then left stirring at r.t. overnight. The solution was then washed with water (40 mL) and the aqueous phase was extracted with EtOAc (5 x 20 mL). After drying the organic phase over Na_2SO_4 the solvent was removed via rotary evaporation and the crude product was purified via silica gel chromatography (10 to 20 % EtOAc/ DCM) giving the final product **63** (74 mg, 176 µmol, 88 %) as a yellow-brown liquid.

^{1}H NMR (400 MHz, CD_2Cl_2): δ (ppm) = 8.30 (s, 1H, NH_a), 8.22 (s, 1H, NH_b), 7.66 – 7.58 (m, 2H, SO_2-Ar-F *m*-CH), 7.11 (t, J = 8.7 Hz, 2H, SO_2-Ar-F *o*-CH), 6.86 (d, J = 8.5 Hz, 1H, H-3), 6.75 (d, J = 2.6 Hz, 1H, H-6), 6.52 (dd, J = 8.5, 2.6 Hz, 1H, H-4), 4.19 (d, J = 2.4 Hz, 2H, C*H*$_2$-C≡CH), 3.96 (s, 2H, O-C*H*$_2$-C=O), 3.85 (b s, 2H, NH_2), 3.71 – 3.61 (m, 4H, PEG CH_2), 2.51 (t, J = 2.4 Hz, 1H, C≡C*H*).

^{13}C NMR (101 MHz, CD_2Cl_2): δ (ppm) = 169.55 (C=O), 166.76 (Ar C-F), 164.24 (Ar C-S), 146.57 (C-1), 131.14 (C-2), 129.77 / 129.67 (SO_2-Ar-F *m*-CH), 125.54 (C-6), 122.06 (C-5), 116.57 / 116.35 (SO_2-Ar-F *o*-CH), 114.06 (C-4), 113.76 (C-3), 79.49 (*C*≡CH), 75.30 (C≡*C*H), 71.45 (PEG CH_2), 70.28 (O-*C*H_2-C=O), 69.17 (PEG CH_2), 58.81 (*C*H_2-C≡CH).

HR-ESI-MS: m/z calc. for $[C_{19}H_{21}FN_3O_5S]^+$ $[M+H]^+$: 422.11805, found: 422.11801.

Rf = 0.11 (15 % EtOAc/DCM).

N-(3-((4-Fluorophenyl)sulfonamido)-4-(2-(2-(prop-2-yn-1-yloxy)ethoxy)acetamido) phenyl)-[1,1'-biphenyl]-4-carboxamide (**64**)

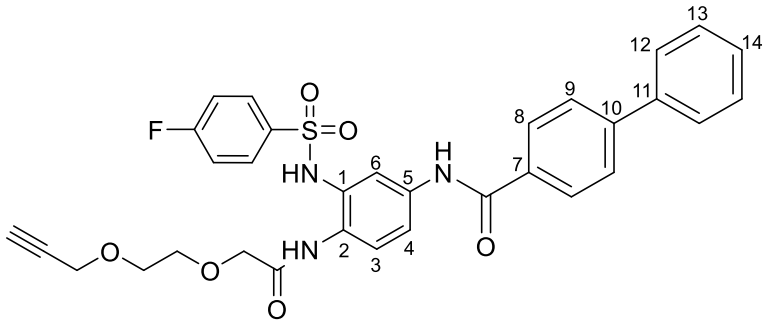

After the co-evaporation with toluene (3 x), *N*-(4-amino-2-((4-fluorophenyl)sulfonamido)phenyl)-2-(2-(prop-2-yn-1-yloxy)ethoxy) acetamide (**63**) (1.07 g, 2.53 mmol, 1.00 eq) was dissolved in dry THF (100 mL) under Ar and pyridine (224 µL, 2.78 mmol, 1.10 eq) was added. Though a dropping funnel, a solution of 4-phenylbenzoyl chloride (**58**) (603 mg, 2.78 mmol, 1.10 eq) in dry THF (80 mL) was added slowly to the mixture at 0 °C and stirred for 2 hours. After this time, the reaction was quenched with MeOH (40 mL) and the solvents evaporated *in vacuo*. The residue was redissolved in DCM (100 mL) and the organic phase washed with a saturated solution of NH_4Cl (50 mL), brine (20 mL) and then dried with Na_2SO_4. After removal of the solvents through rotatory evaporation, the crude was purified by silica gel column chromatography (20 % EtOAc/DCM) to obtain the desired product **64** (1.52 g, 2.14 mmol, 85 %) as a light yellow solid.

^{1}H NMR (500 MHz, Acetone): δ (ppm) = 9.73 (s, 1H, NH_a), 9.16 (s, 1H, NH_b), 8.78 (s, 1H, NH_c), 8.08 (d, J = 8.3 Hz, 2H, H-8), 7.86 – 7.71 (m, 8H, H-6 / H-3 / H-9 / SO_2-Ar-F *o*-CH / H-12), 7.67 (dd, J = 8.8, 3.7 Hz, 1H, H-4), 7.51 (dd, J = 8.4, 6.9 Hz, 2H, H-13), 7.45 – 7.39 (m, 1H, H-14), 7.32 (t, J = 8.8 Hz, 2H, SO_2-Ar-F *m*-CH), 4.28 (d, J = 2.4 Hz, 2H, CH_2-C≡CH), 4.09 (s, 2H, O-CH_2-C=O), 3.84 – 3.75 (m, 4H, PEG CH_2), 3.01 (t, J = 2.4 Hz, 1H, C≡C*H*).

^{13}C NMR (126 MHz, Acetone): δ (ppm) = 169.69 / 169.61 (C=O), 167.10 (Ar C-F), 165.86 / 165.79 (C=O), 165.09 (Ar C-S), 144.94 (C-7), 140.68 (C-11), 137.95 (C-2), 137.87 (C-5), 136.88 (C-1), 134.66 (C-10), 130.96 / 130.88 (SO_2-Ar-F *m*-CH), 129.88 (C-13), 129.01 (C-8), 128.94 (C-14), 127.92 (C-12), 127.71 (C-9), 124.33 / 124.23 (C-4), 120.20 / 120.11 (C-6), 119.93 / 119.84 (C-3), 117.21 / 117.03 (SO_2-Ar-F *o*-CH), 80.64 (*C*≡CH), 76.26 (C≡*C*H), 71.72 (PEG CH_2), 71.00 (O-*C*H_2-C=O), 69.74 (PEG CH_2), 58.82 (*C*H_2-C≡CH).

HR-ESI-MS: m/z calc. for $[C_{32}H_{29}FN_3O_6S]^+$ $[M+H]^+$: 602.17556, found: 602.17597.

FT-IR: $\tilde{\nu}$ (cm^{-1}) = 3368.48 (w), 3276.51 (w), 2922.99 (w), 2852.58 (w), 2358.23 (m), 2330.92 (m), 1734.54 (m), 1717.29 (m), 1684.24 (m), 1669.87 (m), 1654.06 (m), 1590.83 (s), 1541.97 (m), 1521.85

(m), 1507.48 (w), 1488.80 (m), 1457.19 (m), 1419.82 (m), 1388.21 (m), 1326.41 (m), 1291.92 (m), 1235.88 (w), 1164.02 (m), 1153.96 (m), 1097.92 (m), 1086.42 (m), 1030.38 (w), 1007.38 (w), 987.26 (w), 893.86 (m), 837.81 (m), 817.69 (m), 740.09 (m), 691.23 (s), 669.67 (m), 613.63 (m), 571.95 (m), 538.90 (s), 481.42 (m), 456.99 (m).

Rf = 0.61 (40 % EtOAc/DCM).

4.2.2 cGAMP Fluorescent Probe

cGAMP$_3$-Cy3 (65)

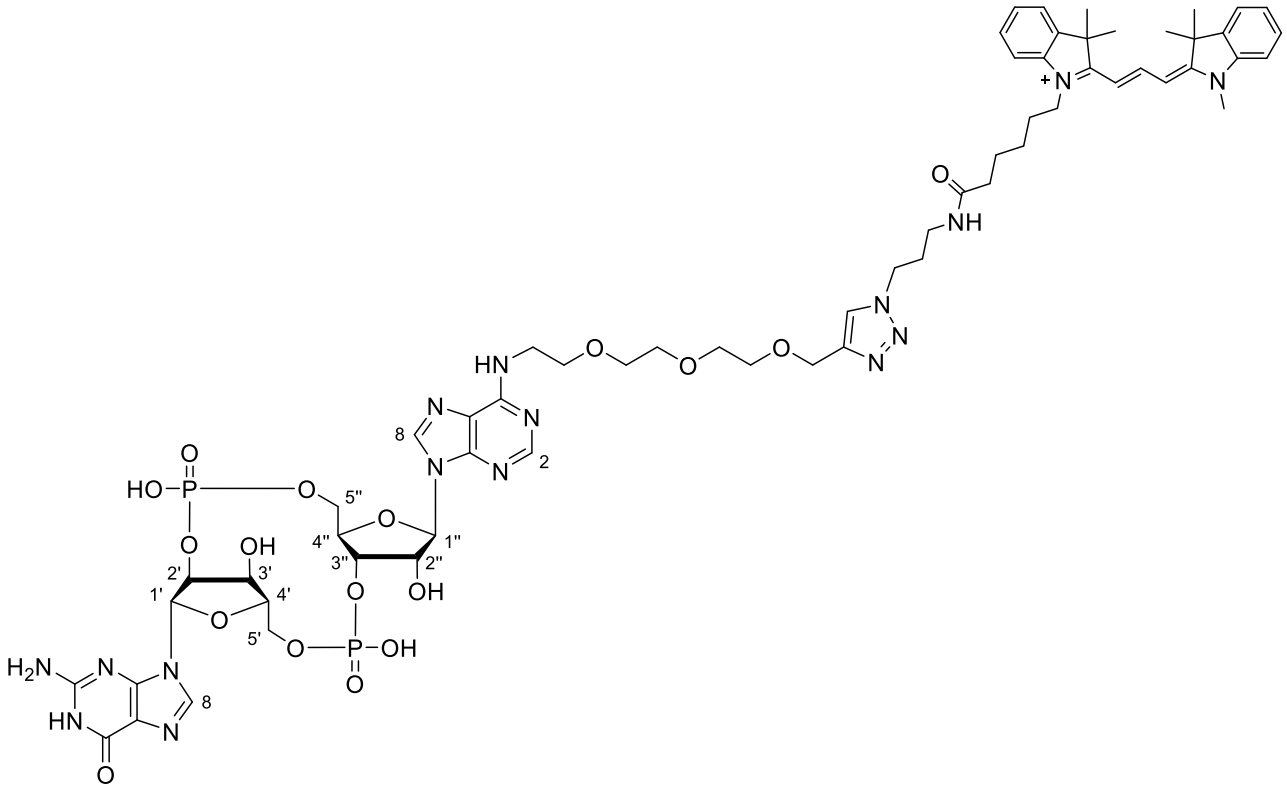

To a solution of **53** (9 mg, 11 µmol, 1.20 eq) and THPTA (11 mg, 26 µmol, 3.00 eq) in H_2O (300 µL), was added a 0.1 M water solution of $CuSO_4$ (87 µL, 9 µmol, 1.00 eq) and Cyanine3® azide (**66**) (5 mg, 9 µmol, 1.00 eq) previously dissolved in MeCN (300 µL) and the mixture was vortexed for a couple of minutes to ensure complete dissolution of the reagents. After this, a 1 M water solution of sodium ascorbate (87 µL, 87 µmol, 10.00 eq) and the red mixture was agitated at 45 °C for 3 hours under Ar. After this time, the crude mixture was directly purified via preparative HPLC (10 to 60 % B in 45 minutes. Buffer A = H_2O + 0.1 % TFA, buffer B = MeCN + 0.1 % TFA) to obtain the desired product **65** (11 mg, 8 µmol, 86 %) as a dark red solid.

^{1}H NMR (800 MHz, 9 D_2O : 1 MeCN): δ (ppm) = 8.95 (s, 1H, H-8A), 8.59 (d, J = 90.6 Hz, 1H, H-8G), 8.50 – 8.44 (m, 2H, H-2A), 8.02 (d, J = 12.0 Hz, 1H), 7.60 – 7.56 (m, 1H), 7.51 (q, J = 4.9, 3.3 Hz, 2H), 7.44 (t, J = 7.7 Hz, 1H), 7.40 – 7.35 (m, 2H), 7.33 (d, J = 8.0 Hz, 1H), 7.30 (tt, J = 7.3, 1.1 Hz, 1H), 6.33 (dd, J = 21.7, 13.3 Hz, 1H), 6.28 – 6.22 (m, 1H, H-1'), 6.15 (d, J = 8.3 Hz, 1H, H-1"), 5.83 – 5.68 (m, 1H, H-2"), 5.12 – 5.02 (m, 1H, H-3'), 4.76 (dd, J = 4.9, 4.0 Hz, 1H, H-2'), 4.67 – 4.63 (m, 3H, H-3"), 4.53 (d, J = 9.4 Hz, 1H, H-4'), 4.49 (d, J = 3.6 Hz, 1H, H-4"), 4.45 (d, J = 11.6 Hz, 1H, H-5'), 4.40 (t, J = 6.9 Hz, 2H), 4.36 – 4.27 (m, 1H,), 4.21 (d, J = 11.9 Hz, 1H, H-5"), 4.13 (t, J = 7.0 Hz, 3H, H-5'), 3.98 – 3.86 (m, 4H), 3.82 – 3.68 (m, 8H), 3.64 (s, 3H), 3.11 (t, J = 6.8 Hz, 2H), 2.25 (t, J = 7.1 Hz, 2H), 2.05 – 1.99 (m, 2H), 1.88 (p, J = 7.2 Hz, 2H), 1.72 (d, J = 7.6 Hz, 12H), 1.67 (p, J = 7.3 Hz, 2H), 1.39 (p, J = 8.3 Hz, 2H).

^{13}C NMR (201 MHz, 9 D_2O : 1 MeCN): δ (ppm) = 176.62, 175.80, 175.75, 175.19, 175.14, 163.42, 163.24, 163.07, 162.89, 156.01, 154.98, 150.90, 149.93, 146.50, 144.47, 143.14, 142.54, 141.31, 129.42, 129.32, 129.31, 129.20, 126.17, 126.02, 125.86, 125.42, 125.34, 122.94, 122.86, 122.80, 122.74, 119.55, 119.26, 119.17, 117.72, 116.27, 114.82, 111.89, 111.75, 111.61, 110.50, 102.66, 102.45, 90.51, 90.28, 84.80, 80.76, 74.89, 70.18, 69.56, 69.17, 63.59, 49.70, 49.68, 48.53, 44.33, 36.77, 35.91, 29.48, 27.87, 27.77, 27.67, 27.57, 27.25, 26.06, 25.54.

^{31}P NMR (202 MHz, 9 D_2O : 1 MeCN): δ (ppm) = -1.33, -2.18.

HR-ESI-MS: m/z calc. for $[C_{62}H_{81}N_{16}O_{17}P_2]^+$ $[M+H]^+$: 1383.5435, found: 1383.5427.

FT-IR: $\tilde{\nu}$ (cm^{-1}) = 2356.79 (w), 2335.23 (w), 1771.90 (w), 1734.54 (w), 1717.29 (m), 1684.24 (m), 1654.06 (m), 1646.88 (m), 1636.82 (m), 1616.70 (m), 1602.33 (m), 1559.22 (s), 1507.48 (m), 1472.99 (m), 1457.19 (s), 1418.38 (s), 1373.84 (m), 1199.95 (s), 1174.08 (m), 1153.96 (s), 1112.29 (s), 1018.88 (m), 965.71 (m), 925.47 (m), 856.49 (m), 793.26 (s), 757.33 (m), 719.97 (m), 681.17 (m), 668.24 (m), 538.90 (m), 494.35 (m), 469.92 (m), 455.55 (m), 429.68 (m), 409.56 (m).

Rf = 5.90 min (LC-MS: 5 to 80 % B in 7 min).

4.2.3 E3 Ligases Recruiters

4.2.3.1 Pomalidomide-Based CRBN Recruiters

2-Chloro-*N*-pomalidomide acetamide (68)

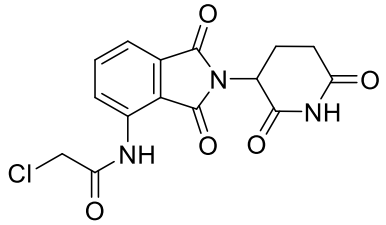

To a solution of pomalidomide (**34**) (1.00 g, 3.66 mmol, 1.00 eq) in dry THF (60 mL) was added 2-chloroacetyl chloride (583 µL, 7.32 mmol, 2.00 eq) and the mixture heated to reflux for 2 hours under Ar. After this time, the solvent was evaporated *in vacuo* and the resulting solid slurried in diethyl ether (40 mL) and filtered to give the desired product **68** (1.21 g, 3.46 mmol, 95 %) as a light brown solid.

^{1}H NMR (400 MHz, DMSO): δ (ppm) = 11.18 (s, 1H, NH_b), 10.32 (s, 1H, NH_a), 8.59 – 8.48 (m, 1H, NH-Ar *o*-CH), 7.89 (dd, J = 8.4, 7.3 Hz, 1H, NH-Ar *m*-CH), 7.69 (dd, J = 7.3, 0.8 Hz, 1H, NH-Ar *p*-CH), 5.18 (dd, J = 12.8, 5.4 Hz, 1H, N-C*H*), 4.55 (s, 2H, CO-CH_2-Cl), 2.90 (ddd, J = 17.0, 13.7, 5.4 Hz, 1H, $CH_{2b'}$), 2.68 – 2.54 (m, 2H, $CH_{2b'/a'}$), 2.08 (dtd, J = 12.8, 5.5, 5.0, 2.0 Hz, 1H, $CH_{2a'}$).

^{13}C NMR (101 MHz, DMSO): δ (ppm) = 172.80 (C=O), 169.79 (C=O), 167.83 (C=O), 166.62 (C=O), 165.74 (C=O), 136.46 (NH-Ar *m*-CH), 135.61 (NH-Ar CH), 131.51 (Ar), 125.61 (NH-Ar *o*-CH), 119.09 (NH-Ar *p*-CH), 117.35 (Ar), 48.99 (N-*C*H), 43.18 (CO-*C*H_2-Cl), 30.95 (CH_2), 21.97 (CH_2).

HR-ESI-MS: m/z calc. for $[C_{15}H_{11}ClN_3O_5]^-$ $[M-H]^-$: 348.03927, found: 348.03940.

FT-IR: $\tilde{\nu}$ (cm^{-1}) = 3094.1 (w), 1769.7 (w), 1704.0 (s), 1620.1 (m), 1536.5 (m), 1399.0 (s), 1349.7 (m), 1259.6 (m), 1199.3 (s), 1177.0 (m), 1120.0 (m), 823.4 (m).

Rf = 0.64 (3 % MeOH/DCM).

2-Azido-*N*-pomalidomide acetamide (**67**)

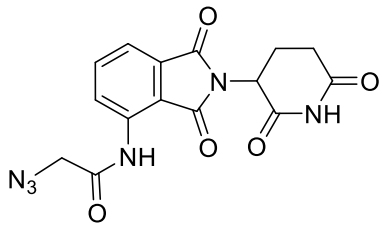

NaN_3 (132 mg, 2.03 mmol, 2.00 eq) was slowly added under Ar to a suspension of 2-chloro-*N*-pomalidomide acetamide (**68**) (355 mg, 1.02 mmol, 1.00 eq) and NaI (76 mg, 508 µmol, 0.50 eq) in acetone (10 mL), then the mixture was kept stirring under reflux overnight during which time the colour turned red. The precipitate was filtered, washed with acetone and the filtrate concentrated *in vacuo*. The residue was purified by silica gel column chromatography (50 to 100 % EtOAc/iHex) to afford the desired product **67** (274 mg, 769 µmol, 76 %) as a yellow solid.

^{1}H NMR (400 MHz, DMSO): δ (ppm) = 11.17 (s, 1H, NH_a), 10.13 (s, 1H, NH_b), 8.52 (d, J = 8.4 Hz, 1H, NH-Ar *o*-CH), 7.87 (dd, J = 8.4, 7.4 Hz, 1H, NH-Ar *m*-CH), 7.67 (d, J = 7.2 Hz, 1H, NH-Ar *p*-CH), 5.17 (dd, J = 12.8, 5.4 Hz, 1H, N-C*H*), 4.33 (s, 2H, CO-CH_2-N_3), 2.89 (ddd, J = 16.8, 13.7, 5.4 Hz, 1H, $CH_{2b'}$), 2.71 – 2.57 (m, 2H, $CH_{2b'/a'}$), 2.14 – 2.01 (m, 1H, $CH_{2a'}$).

^{13}C NMR (101 MHz, DMSO): δ (ppm) = 172.80 (C=O), 169.80 (C=O), 167.70 (C=O), 167.13 (C=O), 166.64 (C=O), 136.38 (NH-Ar *m*-CH), 135.62 (NH-Ar C), 131.55 (Ar), 125.98 (NH-Ar *o*-CH), 118.94 (NH-Ar *p*-CH), 117.36 (Ar), 51.87a(CO-*C*H_2-N_3), 48.98 (N-*C*H), 30.96 (CH_2), 21.98 (CH_2).

HR-ESI-MS: m/z calc. for $[C_{15}H_{11}N_6O_5]^-$ [M-H]$^-$: 355.07964, found: 355.07941.

FT-IR: $\tilde{\nu}$ (cm^{-1}) = 3221.9 (w), 2112.6 (m), 1777.8 (w), 1704.0 (s), 1619.9 (m), 1535.4 (m), 1478. 7 (w), 1394.5 (s), 1347.6 (m), 1257.8 (m), 1192.8 (s), 1177.8 (m), 823.4 (m), 740.6 (s).

Rf = 0.65 (5 % MeOH/DCM).

2-(2-Hydroxyethoxy)ethyl 4-methylbenzenesulfonate (**71**)

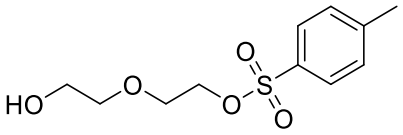

Diethylene glycol (**69**) (6.58 mL, 69.43 mmol, 2.00 eq) and Et_3N (5.32 mL, 28.19 mmol, 1.10 eq) were dissolved in dry DCM (60 mL) under N_2. Toluene sulfonyl chloride (6.62 g, 34.71 mmol, 1.00 eq) was added carefully and the reaction mixture was stirred at r.t. overnight. The reaction was then quenched with 1.0 M HCl (40 mL), H_2O (40 mL) and treated with brine (60 mL). The resulting aqueous phase was extracted with DCM (3 x 100 mL) and the combined organic layers were dried over Na_2SO_4, filtered and the solvent was removed under vacuum. The crude product was purified via silica gel column chromatography (0 to 4 % MeOH/DCM) to obtain the desired product **71** (4.70 g, 18.04 mmol, 52 %) as a colourless oil.

^{1}H NMR (400 MHz, $CDCl_3$): δ (ppm) = 7.84 – 7.75 (m, 2H, Tos. SO_3-Ar *o*-CH), 7.34 (d, J = 8.0 Hz, 2H, Tos. SO_3-Ar *m*-CH), 4.25 – 4.13 (m, 2H, SO_3-CH_2), 3.74 – 3.62 (m, 4H, CH_2-O-CH_2), 3.58 – 3.48 (m, 2H, HO-CH_2), 2.44 (s, 3H, Tos. CH_3), 2.06 (s, 1H, OH).

^{13}C NMR (101 MHz, $CDCl_3$): δ (ppm) = 145.09 (Tos. SO_3-Ar C), 133.01 (Tos. SO_3-Ar *p*-C), 129.96 (Tos. SO_3-Ar *m*-CH), 128.06 (Tos. SO_3-Ar *o*-CH), 72.56 (HO-*C*H_2-CH_2), 69.29 (SO_3-*C*H_2), 68.66 (SO_3-CH_2-*C*H_2), 61.74 (HO-CH_2-*C*H_2), 21.77 (Tos. CH_3).

HR-ESI-MS: m/z calc. for $[C_{11}H_{17}O_5S]^+$ $[M+H]^+$: 261.07912, found: 261.07914.

FT-IR: $\tilde{\nu}$ (cm^{-1}) = 2924.43 (w), 2872.70 (w), 2359.66 (m), 2343.86 (m), 1598.02 (w), 1451.44 (w), 1350.84 (s), 1291.92 (w), 1189.89 (m), 1172.65 (s), 1132.41 (m), 1096.48 (m), 1067.74 (m), 1008.82 (m), 916.85 (s), 814.82 (s), 773.14 (s), 705.60 (w), 689.79 (w), 661.05 (s), 582.01 (m), 551.83 (s).

Rf = 0.67 (4 % MeOH/DCM).

2-(2-Azidoethoxy)ethan-1-ol (**73**)

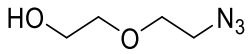

To a solution of 2-(2-hydroxyethoxy)ethyl 4-methylbenzenesulfonate (**71**) (4.70 g, 18.04 mmol, 1.00 eq) in dry DMF (60 mL), NaN_3 (1.99 g, 30.66 mmol, 1.70 eq) was added under Ar and the reaction was stirred at 90 °C overnight. After adding water (50 mL), the reaction mixture was cooled to r.t. and the water phase was then extracted with EtOAc (3 x 100 mL). The combined organic layers were dried over Na_2SO_4 and the solvent was removed *in vacuo*. The residue was purified via silica gel column chromatography (2 % MeOH/DCM) to obtain the target product **73** (1.23 g, 9.38 mmol, 52 %) as a light yellow oil.

^{1}H NMR (500 MHz, $CDCl_3$): δ (ppm) = 3.78 – 3.74 (m, 2H, HO-C*H*$_2$), 3.70 (td, J = 5.0, 0.8 Hz, 2H, N_3-CH_2-C*H*$_2$), 3.62 (dd, J = 5.0, 4.0 Hz, 2H, HO-CH_2-C*H*$_2$), 3.41 (t, J = 5.0 Hz, 2H, N_3-C*H*$_2$), 2.00 (s, 1H, OH).

^{13}C NMR (126 MHz, $CDCl_3$): δ (ppm) = 72.53 (HO-CH_2-*C*H_2), 70.27 (N_3-CH_2-*C*H_2), 61.96 (HO-*C*H_2), 50.86 (N_3-*C*H_2).

LC-ESI-MS: m/z calc. for $[C_4H_{10}N_3O_2]^+$ $[M+H]^+$: 132.07675, found: 132.2.

FT-IR: $\tilde{\nu}$ (cm^{-1}) = 3377.11 (w), 2925.87 (w), 2869.82 (w), 2359.66 (m), 2343.86 (m), 2093.81 (s), 1717.29 (w), 1654.06 (w), 1559.22 (w), 1540.54 (w), 1507.48 (w), 1457.19 (w), 1346.53 (w), 1284.74 (m), 1261.74 (m), 1123.79 (s), 1061.99 (s), 1030.38 (m), 913.97 (s), 888.11 (m), 847.87 (w), 804.76 (m), 744.40 (s), 668.24 (m), 648.12 (m), 554.71 (m).

Rf = 0.53 (2 % MeOH/DCM).

2-(2-Azidoethoxy)acetic acid (**76**)

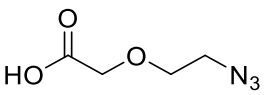

To a solution of 2-(2-azidoethoxy)ethan-1-ol (**73**) (400 mg, 3.05 mmol, 1.00 eq) in acetone (35 mL) at 0° C, was added a solution of CrO_3 (915 mg, 9.15 mmol, 3.00 eq) in 1.5 M H_2SO_4 in H_2O (18.72 mL) dropwise by an additional funnel. After addition, the reaction was allowed to stir at r.t. overnight. During this time the solution turns from red-orange to dark green colour. The reaction was then

quenched by addition of isopropanol (22 mL) and concentrated under vacuum. The aqueous phase was extracted with EtOAc (4 x 60 mL). The organic layers were combined, wash brine, dried over Na_2SO_4 and concentrated under vacuum. The residue was purified by silica gel column chromatography (10 % MeOH/DCM) to obtain the desired product **76** (415 mg, 2.86 mmol, 94 %) as a colourless oil.

^{1}H NMR (500 MHz, $CDCl_3$): δ (ppm) = 4.22 (s, 2H, COOH-C*H*$_2$), 3.78 – 3.73 (m, 2H, N_3-CH_2-C*H*$_2$), 3.51 – 3.44 (m, 2H, N_3-C*H*$_2$).

^{13}C NMR (126 MHz, $CDCl_3$): δ (ppm) = 175.36 (C=O), 70.59 (N_3-CH_2-*C*H_2), 68.12 (COOH-*C*H_2), 50.81 (N_3-*C*H_2).

HR-ESI-MS: m/z calc. for $[C_4H_6N_3O_3]^-$ $[M-H]^-$: 144.04146, found: 144.04149.

FT-IR: $\tilde{\nu}$ (cm^{-1}) = 2918.68 (w), 2359.66 (s), 2343.86 (m), 2102.43 (s), 1733.10 (s), 1559.22 (w), 1507.48 (w), 1437.07 (w), 1347.97 (w), 1289.05 (m), 1258.87 (s), 1224.38 (m), 1135.28 (s), 1097.92 (m), 1053.37 (w), 1020.32 (w), 870.86 (w), 797.57 (w), 678.30 (w), 668.24 (m), 659.61 (w), 556.14 (w).

Rf = 0.19 (2 % MeOH/DCM).

Pomalidomide-PEG$_2$-Azide (79)

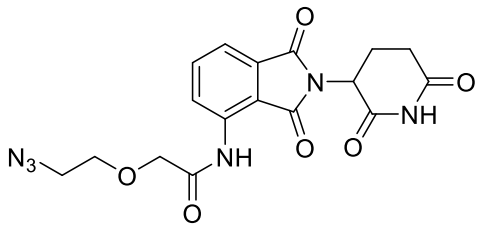

To 2-(2-azidoethoxy)acetic acid (**76**) (100 mg, 689 µmol, 1.00 eq), was added dropwise oxalyl chloride (827 µL, 9.65 mmol, 14.00 eq) at 0 °C under Ar and the mixture was stirred at r.t. for 1.5 hours, during which time the colour turned from yellow to orange-red. After this time, the solution was concentrated *in vacuo* and under Ar, dry DMF (1.5 mL) and pomalidomide (**34**) (282 mg, 1.03 mmol, 1.50 eq) were added and the solution stirred at r.t. overnight. The mixture was quenched with H_2O (2.5 mL) and extracted with EtOAc (3 x 10 mL). The combined organic phases were washed with brine, dried over Na_2SO_4 and concentrated *in vacuo*. The residue was purified via silica gel column chromatography (5 % acetone/toluene) to obtain the desired product **79** (90 mg, 225 µmol, 33 %) as a white solid.

^{1}H NMR (500 MHz, $CDCl_3$): δ (ppm) = 10.50 (s, 1H, NH_a), 8.85 (d, J = 8.4 Hz, 1H, NH-Ar *o*-CH), 8.07 (s, 1H, NH_b), 7.74 (dd, J = 8.5, 7.3 Hz, 1H, NH-Ar *m*-CH), 7.59 (dd, J = 7.4, 0.8 Hz, 1H, NH-Ar *p*-CH), 4.97 (dd, J = 12.4, 5.4 Hz, 1H, N-C*H*), 4.20 (s, 2H, CO-C*H*$_2$), 3.81 (t, J = 5.0 Hz, 2H, N_3-CH_2-C*H*$_2$), 3.63 (q, J = 4.8 Hz, 2H, N_3-C*H*$_2$), 2.96 – 2.72 (m, 3H, $CH_{2b'/a'}$), 2.17 (dq, J = 9.9, 2.8, 2.4 Hz, 1H, $CH_{2a'}$).

^{13}C NMR (126 MHz, $CDCl_3$): δ (ppm) = 170.81 (C=O), 168.75 (C=O), 168.59 (C=O), 167.87 (C=O), 166.87 (C=O), 136.77 (NH-Ar C), 136.53 (NH-Ar *m*-CH), 131.48 (Ar), 125.31 (NH-Ar *o*-CH), 119.10 (NH-Ar *p*-CH), 116.36 (Ar), 70.87 (CO-*C*H$_2$), 70.78 (N_3-CH_2-*C*H$_2$), 50.92 (N_3-*C*H$_2$), 49.40 (N-*C*H), 31.53 (CH_2), 22.69 (CH_2).

HR-ESI-MS: m/z calc. for $[C_{17}H_{15}N_6O_6]^-$ $[M-H]^-$: 399.10586, found: 399.10566.

FT-IR: $\tilde{\nu}$ (cm^{-1}) = 3309.56 (w), 3231.96 (w), 2956.05 (w), 2925.87 (w), 2856.89 (w), 2359.66 (s), 2343.86 (s), 2109.61 (m), 1773.34 (w), 1702.92 (s), 1622.45 (w), 1540.54 (m), 1533.35 (m), 1480.18 (w), 1396.83 (m), 1350.84 (m), 1323.54 (w), 1297.67 (w), 1261.74 (m), 1198.51 (m), 1120.91 (w), 1028.94 (w), 823.44 (w), 741.53 (m), 668.24 (m).

Rf = 0.43 (50 % EtOAc/iHex).

2-(2-(2-Hydroxyethoxy)ethoxy)ethyl 4-methylbenzenesulfonate (**72**)

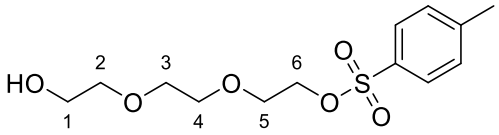

Triethylene glycol (**70**) (14.07 mL, 104.91 mmol, 2.00 eq) and Et_3N (8.04 mL, 57.70 mmol, 1.10 eq) were dissolved in dry DCM (50 mL) under N_2. Toluene sulfonyl chloride (10.00 g, 52.45 mmol, 1.00 eq) dissolved in dry DCM (50 mL) was added carefully and the reaction mixture was stirred at r.t. overnight. The reaction was then quenched with 1.0 M HCl (40 mL), H_2O (40 mL) and treated with brine (60 mL). The resulting aqueous phase was extracted with DCM (3 x 150 mL) and the combined organic layers were dried over Na_2SO_4, filtered and the solvent was removed under vacuum. The crude product was purified via silica gel column chromatography (0 to 2 % MeOH/DCM) to obtain the desired product **72** (11.47 g, 37.69 mmol, 72 %) as a pale yellow oil.

^{1}H NMR (500 MHz, MeOD): δ (ppm) = 7.80 (d, J = 8.3 Hz, 2H, Tos. SO_3-Ar *o*-CH), 7.48 – 7.41 (m, 2H, Tos. SO_3-Ar *m*-CH), 4.19 – 4.09 (m, 2H, H-6), 3.69 – 3.62 (m, 4H, H-5 / H-2), 3.56 (s, 4H, H-3 / H-4), 3.52 (dd, J = 5.5, 4.2 Hz, 2H, H-1), 2.46 (s, 3H, Tos. CH_3).

^{13}C NMR (126 MHz, MeOD): δ (ppm) = 146.48 (Tos. SO_3-Ar C), 134.46 (Tos. SO_3-Ar *p*-C), 131.05 (Tos. SO_3-Ar *m*-CH), 129.05 (Tos. SO_3-Ar *o*-CH), 73.68 (C-1), 71.58 (C-3), 71.37 (C-4), 70.86 (C-6), 69.76 (C-5), 62.20 (C-2), 21.56 (Tos. CH_3).

HR-ESI-MS: m/z calc. for $[C_{13}H_{21}O_6S]^+$ $[M+H]^+$: 305.10534, found: 305.10531.

FT-IR: $\tilde{\nu}$ (cm^{-1}) = 3431.71 (w), 2874.13 (w), 2359.66 (m), 2343.86 (m), 1598.02 (w), 1452.87 (w), 1350.84 (s), 1291.92 (w), 1189.89 (m), 1174.08 (s), 1120.91 (m), 1096.48 (s), 1067.74 (m), 1011.69 (m), 915.41 (s), 816.25 (m), 773.14 (m), 661.05 (s), 582.01 (m), 553.27 (s).

Rf = 0.43 (2 % MeOH/DCM).

2-(2-(2-Azidoethoxy)ethoxy)ethan-1-ol (**74**)

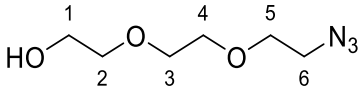

To a solution of 2-(2-(2-hydroxyethoxy)ethoxy)ethyl 4-methylbenzenesulfonate (**72**) (10.00 g, 32.86 mmol, 1.00 eq) in dry DMF (120 mL), NaN_3 (4.27 g, 65.71 mmol, 2.00 eq) was added under Ar and the reaction was stirred at 90 °C overnight. After adding water (100 mL), the reaction mixture was cooled to r.t. and the water phase was then extracted with EtOAc (3 x 200 mL). The combined organic layers were dried over Na_2SO_4 and the solvent was removed *in vacuo*. The residue was purified via silica gel column chromatography (2 % MeOH/DCM) to obtain the target product **74** (3.42 g, 19.52 mmol, 59 %) as a pale yellow oil.

^{1}H NMR (500 MHz, $CDCl_3$): δ (ppm) = 3.77 – 3.72 (m, 2H, H-6), 3.71 – 3.65 (m, 6H, H-2 / H-3 / H-4), 3.64 – 3.60 (m, 2H, H-5), 3.40 (t, J = 5.0 Hz, 2H, H-1), 2.20 (t, J = 6.1 Hz, 1H, OH).

^{13}C NMR (126 MHz, $CDCl_3$): δ (ppm) = 72.58 (C-1), 70.80 (C-3), 70.54 (C-4), 70.22 (C-5), 61.92 (C-2), 50.77 (C-6).

HR-ESI-MS: m/z calc. for $[C_6H_{13}N_3NaO_3]^+$ $[M+Na]^+$: 198.08491, found: 198.08497.

FT-IR: $\tilde{\nu}$ (cm^{-1}) = 3414.47 (m), 2920.12 (m), 2871.26 (m), 2102.43 (s), 1667.00 (w), 1452.87 (w), 1346.53 (w), 1286.17 (m), 1120.91 (s), 1067.74 (s), 932.66 (w), 886.67 (w), 852.18 (w), 829.19 (w), 648.12 (w), 554.71 (w).

Rf = 0.27 (2 % MeOH/DCM).

2-(2-(2-Azidoethoxy)ethoxy)acetic acid (**77**)

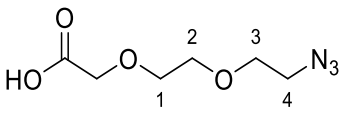

To a solution of 2-(2-(2-azidoethoxy)ethoxy)ethan-1-ol (**74**) (3.42 g, 19.52 mmol, 1.00 eq) in acetone (205 mL) at 0° C, was added a solution of CrO_3 (5.86 g, 58.57 mmol, 3.00 eq) in 1.5 M H_2SO_4 in H_2O (120 mL) dropwise by an additional funnel. After addition, the reaction was allowed to stir at r.t. overnight. During this time the solution turns from red-orange to dark green colour. The reaction was then quenched by addition of isopropanol (150 mL) and concentrated under vacuum. The aqueous phase was extracted with EtOAc (4 x 100 mL). The organic layers were combined, wash brine, dried over Na_2SO_4 and concentrated under vacuum. The residue was purified by silica gel column chromatography (10 % MeOH/DCM) to obtain the desired product **77** (3.90 g, 20.62 mmol, quantitative) as a pale yellow oil.

^{1}H NMR (500 MHz, MeOD): δ (ppm) = 4.14 (s, 2H, COOH-C*H*$_2$), 3.74 – 3.70 (m, 2H, H-1), 3.69 – 3.66 (m, 4H, H-2 / H-3), 3.40 – 3.36 (m, 2H, H-4).

^{13}C NMR (126 MHz, $CDCl_3$): δ (ppm) = 174.10 (C=O), 71.84 (C-2), 71.57 (C-1), 71.10 (C-3), 69.16 (COOH-*C*H_2), 51.76 (C-4).

72.58 (C-1), 70.80 (C-3), 70.54 (C-4), 70.22 (C-5), 61.92 (C-2),

175.36, 70.59 (N_3-CH_2-*C*H_2), 68.12 (COOH-*C*H_2), 50.81 (N_3-*C*H_2).

HR-ESI-MS: m/z calc. for $[C_6H_{10}N_3O_4]^-$ [M-H]$^-$: 188.06768, found: 188.06765.

FT-IR: $\tilde{\nu}$ (cm^{-1}) = 2927.30 (w), 2875.57 (w), 2359.66 (s), 2343.86 (m), 2102.43 (s), 1724.48 (s), 1646.88 (m), 1437.07 (w), 1382.46 (m), 1347.97 (m), 1283.30 (m), 1227.25 (s), 1109.42 (s), 1018.88 (m), 928.34 (m), 852.18 (m), 668.24 (s), 556.14 (w).

Rf = 0.38 (10 % MeOH/DCM).

Pomalidomide-PEG$_3$-Azide (**80**)

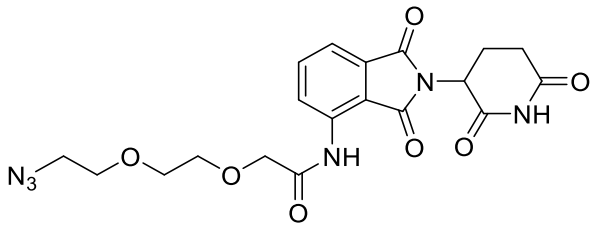

To 2-(2-(2-azidoethoxy)ethoxy)acetic acid (**77**) (500 mg, 2.64 mmol, 1.00 eq), was added dropwise oxalyl chloride (3.40 mL, 39.65 mmol, 15.00 eq) at 0 °C under Ar and the mixture was stirred at r.t. for 2 hours, during which time the colour turned from yellow to orange-red. After this time, the solution was concentrated *in vacuo* and under Ar, dry DMF (8 mL), pomalidomide (**34**) (795 mg, 2.91 mmol, 1.10 eq) and pyridine (234 µL, 2.91 mmol, 1.10 eq) were added and the solution stirred at r.t. overnight. The mixture was quenched with H_2O (25 mL) and extracted with EtOAc (3 x 50 mL). The combined organic phases were washed with brine, dried over Na_2SO_4 and concentrated *in vacuo*. The residue was purified via silica gel column chromatography (0 to 5 % MeOH/DCM) to obtain the desired product **80** (461 mg, 1.04 mmol, 39 %) as a pale brown solid.

^{1}H NMR (500 MHz, DMSO): δ (ppm) = 11.15 (s, 1H, NH_a), 10.36 (s, 1H, NH_b), 8.72 (dd, J = 8.5, 0.7 Hz, 1H, NH-Ar *o*-CH), 7.87 (dd, J = 8.5, 7.3 Hz, 1H, NH-Ar *m*-CH), 7.63 (dd, J = 7.3, 0.8 Hz, 1H, NH-Ar *p*-CH), 5.16 (dd, J = 12.9, 5.4 Hz, 1H, N-C*H*), 4.21 (s, 2H, CO-CH_2), 3.80 – 3.76 (m, 2H, PEG CH_2), 3.73 – 3.69 (m, 2H, PEG CH_2), 3.64 (dd, J = 5.5, 4.4 Hz, 2H, N_3-CH_2-CH_2), 3.38 (dd, J = 5.6, 4.3 Hz, 2H, N_3-CH_2), 2.90 (ddd, J = 17.1, 13.8, 5.4 Hz, 1H, $CH_{2b'}$), 2.65 – 2.58 (m, 1H, $CH_{2b'}$), 2.57 – 2.51 (m, 1H, $CH_{2a'}$), 2.08 (dtd, J = 12.9, 5.4, 2.3 Hz, 1H, $CH_{2a'}$).

^{13}C NMR (126 MHz, $CDCl_3$): δ (ppm) = 172.73 (C=O), 169.72 (C=O), 169.31 (C=O), 168.25 (C=O), 166.68 (C=O), 136.53 (NH-Ar C), 135.97 (NH-Ar *m*-CH), 131.31 (Ar), 124.37 (NH-Ar *o*-CH), 118.33 (NH-Ar *p*-CH), 116.07 (Ar), 70.81 (PEG CH_2), 70.24 (CO-*C*H_2), 69.59 (PEG CH_2), 69.35 (N_3-CH_2-*C*H_2), 50.02 (N_3-*C*H_2), 48.96 (N-*C*H), 30.93 (CH_2), 21.95 (CH_2).

HR-ESI-MS: m/z calc. for $[C_{19}H_{19}N_6O_7]^-$ $[M-H]^-$: 443.13207, found: 443.13229.

FT-IR: $\tilde{\nu}$ (cm^{-1}) = 3224.78 (w), 2925.87 (w), 2856.89 (w), 2361.10 (s), 2343.86 (s), 2102.43 (w), 1780.53 (w), 1717.29 (s), 1701.49 (s), 1622.45 (w), 1540.54 (m), 1396.83 (m), 1350.84 (w), 1323.54 (w), 1300.55 (w), 1260.31 (m), 1198.51 (m), 1118.04 (m), 824.88 (w), 741.53 (m), 668.24 (s), 538.90 (w).

Rf = 0.86 (10 % MeOH/DCM).

2-(2-(2-(2-Azidoethoxy)ethoxy)ethoxy)acetic acid (**78**)

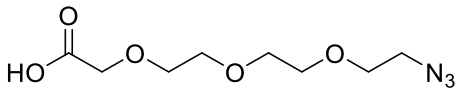

To a solution of HO-PEG$_4$-N$_3$ (**75**) (100 mg, 456 µmol, 1.00 eq) in acetone (5 mL) at 0° C, was added a solution of CrO_3 (137 mg, 1.37 mmol, 3.00 eq) in 1.5 M H_2SO_4 in water (2.8 mL) [5 mL solution: 4.582 mL H_2O, 0.418 mL H_2SO_4 96 %] dropwise by a dropping funnel. After the addition, the reaction was allowed to stir at r.t. overnight. During this time the solution turned from red-orange to dark green colour. The reaction was then quenched by addition of isopropanol (3 mL) and concentrated under vacuum. The aqueous residue was extracted by DCM (4 x 10 mL), the organic layers were combined, dried over Na_2SO_4, and concentrated under vacuum. The residue was purified by silica gel column chromatography (10 % MeOH/DCM) to obtain the desired product **78** (100 mg, 429 µmol, 94 %) as a colourless oil.

The analytical data corresponded to the reported literature:[287]

^{1}H NMR (400 MHz, $CDCl_3$): δ (ppm) = 8.04 (s, 1H, OH), 4.16 (d, J = 3.6 Hz, 2H, O-C*H$_2$*-COOH), 3.80 – 3.60 (m, 10H, PEG CH_2), 3.40 (q, J = 5.6, 5.0 Hz, 2H, O-CH_2-C*H$_2$*-N_3).

Rf = 0.41 (10 % MeOH/DCM).

Pomalidomide-PEG$_4$-Azide (**81**)

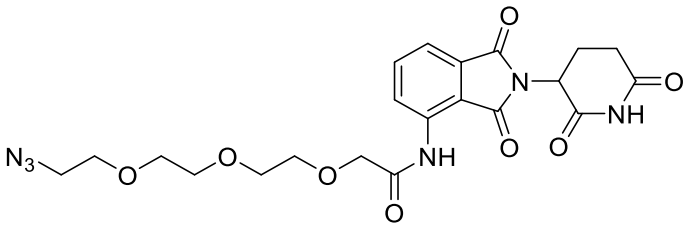

To N_3-PEG$_4$-COOH (**78**) (100 mg, 429 µmol, 1.00 eq), was added dropwise oxalyl chloride (515 µL, 6.00 mmol, 14.00 eq) at 0 °C under Ar and the mixture was stirred at r.t. for 1.5 hours, during which time the colour turned from yellow to orange-red. After this time, the solution was concentrated *in vacuo* and under Ar, dry DMF (1 mL) and pomalidomide (**34**) (129 mg, 472 µmol, 1.10 eq) were added and the solution stirred at r.t. overnight. The mixture was quenched with H_2O (2.5 mL) and extracted with EtOAc (3 x 10 mL). The combined organic phases were washed with brine, dried over Na_2SO_4 and concentrated *in vacuo*. The residue was purified via silica gel column chromatography (50 to 80 % EtOAc/iHex) to obtain the desired product **81** (134 mg, 274 µmol, 64 %) as a white solid.

^{1}H NMR (400 MHz, $CDCl_3$): δ (ppm) = 10.48 (s, 1H, NH_a), 8.92 – 8.82 (d, J = 8.1 Hz, 1H, NH-Ar *o*-CH), 8.17 (s, 1H, NH_b), 7.73 (dd, J = 8.5, 7.3 Hz, 1H, NH-Ar *m*-CH), 7.58 (dd, J = 7.3, 0.8 Hz, 1H, NH-Ar *p*-CH), 4.96 (dd, J = 12.3, 5.4 Hz, 1H, N-C*H*), 4.21 (s, 2H, CO-C*H*$_2$), 3.83 (s, 4H, PEG CH_2), 3.74 – 3.69 (m, 2H, PEG CH_2), 3.66 (dd, J = 5.6, 3.9 Hz, 4H, PEG CH_2), 3.38 (t, J = 5.0 Hz, 2H, C*H*$_2$-N_3), 2.97 – 2.85 (m, 1H, $CH_{2b'}$), 2.86 – 2.67 (m, 2H, $CH_{2b'/a'}$), 2.22 – 2.10 (m, 1H, $CH_{2a'}$).

^{13}C NMR (101 MHz, CDCl3): δ (ppm) = 170.84 (C=O), 169.59 (C=O), 168.54 (C=O), 167.91 (C=O), 166.91 (C=O), 136.92 (NH-Ar *m*-CH), 136.49 (NH-Ar C), 131.49 (Ar), 125.41 (NH-Ar *o*-CH), 118.97 (NH-Ar *p*-CH), 116.26 (Ar), 71.73 (PEG CH_2), 71.17 (PEG CH_2), 70.93 (PEG CH_2), 70.86 (PEG CH_2), 70.80 (PEG CH_2), 70.19 (PEG CH_2), 50.82 (CO-*C*H_2-N_3), 49.36 (N-*C*H), 31.51 (CH_2), 22.80 (CH_2).

HR-ESI-MS: m/z calc. for $[C_{21}H_{28}N_7O_8]^+$ $[M+NH_4]^+$: 506.19939, found: 506.1994.

FT-IR: $\tilde{\nu}$ (cm^{-1}) = 3302.38 (w), 3229.09 (w), 3106.94 (w), 2922.99 (m), 2855.45 (m), 2108.18 (m), 1777.65 (m), 1698.61 (s), 1618.14 (s), 1530.48 (s), 1478.74 (w), 1427.01 (w), 1393.95 (s), 1347.97 (s), 1322.10 (m), 1296.23 (w), 1257.43 (s), 1194.20 (s), 1112.29 (s), 1039.00 (m), 840.68 (m), 765.96 (s), 620.81 (m), 559.02 (m), 481.42 (s).

Rf = 0.52 (80 % EtOAc/iHex).

4.2.3.2 RNF5 Recruiter

N-Boc 2-(4-aminophenyl)ethanol (**84**)

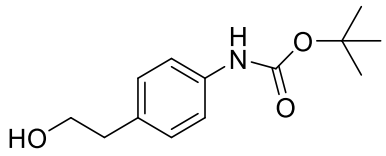

Di-tert-butyl dicarbonate (3.68 mL, 16.04 mmol, 1.10 eq) was added into a solution of 2-(4-aminophenyl)ethanol (**83**) (2.00 g, 14.58 mmol, 1.00 eq) in dry THF (50 mL) and the mixture was stirred at r.t. overnight. After concentrating under reduced vacuum, the residue was purified by silica gel column chromatography (40 % iHex/EtOAc) to afford the desired product **84** (3.20 g, 13.47 mmol, 93 %) as a light brown solid.

^{1}H NMR (400 MHz, $CDCl_3$): δ (ppm) = 7.30 (d, J = 8.1 Hz, 2H), 7.15 (d, J = 8.5 Hz, 1H), 6.43 (s, 1H), 3.82 (q, J = 6.4 Hz, 2H), 2.82 (t, J = 6.5 Hz, 2H), 1.51 (s, 9H), 1.34 (t, J = 6.0 Hz, 1H).

^{13}C NMR (101 MHz, $CDCl_3$): δ (ppm) = 152.96 (C=O), 136.92 (Ar C), 133.18 (Ar C), 129.69 (Ar CH_2), 119.02 (Ar CH_2), 80.65 (Boc C), 63.89 (CH_2), 38.63 (CH_2), 28.48 (Boc CH_3).

HR-ESI-MS: m/z calc. for $[C_{13}H_{18}NO_3]^-$ $[M-H]^-$: 236.12922, found: 236.12933.

FT-IR: $\tilde{\nu}$ (cm^{-1}) = 3322.50 (w), 2977.60 (w), 2933.05 (w), 2877.01 (w), 2361.10 (w), 2343.86 (w), 1807.83 (w), 1697.18 (s), 1596.58 (m), 1523.29 (s), 1411.20 (m), 1368.09 (m), 1316.35 (m), 1241.63 (m), 1156.84 (s), 1118.04 (m), 1051.93 (s), 1017.44 (m), 832.06 (m), 525.97 (m).

Rf = 0.58 (40 % iHex/EtOAc).

N-Boc-*O*-Tosyl-2-(4-aminophenyl)ethanol (**85**)

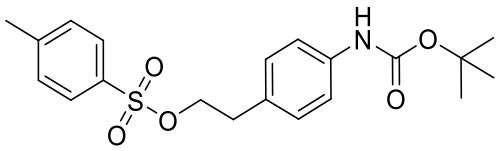

N-Boc-2-(4-aminophenyl)ethanol (**84**) (5.02 g, 21.15 mmol, 1.00 eq) and triethylamine (9.70 mL, 69.81 mmol, 3.30 eq) were dissolved in dry DCM (150 mL) under N_2 and cooled down to 0°C. *p*-Toulenesulfonylchloride (12.10 g, 63.46 mmol, 3.00 eq) in dry THF (150 mL) was added dropwise using dropping funnel at 0° C and stirred for 1 hour. Then the reaction mixture was stirred at r.t. overnight. The solvents were evaporated *in vacuo* and the residue was re-dissolved in DCM (50 mL), washed with a saturated solution of $NaHCO_3$ (50 mL). The water phase was extracted with DCM (3 x 100 mL) and the combined organic phases were washed with brine, dried over Na_2SO_4 and the solvent evaporated *in vacuo*. The crude was then purified via silica gel column chromatography (100 % DCM) to obtain the desired product **85** (8.20 g, 20.95 mmol, 99 %) as a light yellow oil.

^{1}H NMR (400 MHz, $CDCl_3$): δ (ppm) = 7.72 – 7.63 (m, 2H, Tos Ar CH), 7.30 – 7.26 (m, 2H, Tos Ar CH), 7.23 (d, J = 8.3 Hz, 2H, Ar CH), 7.05 – 6.97 (m, 2H, Ar CH), 6.42 (s, 1H, NH), 4.16 (t, J = 7.0 Hz, 2H, O-C*H*$_2$-CH$_2$), 2.89 (t, J = 7.0 Hz, 2H, O-CH$_2$-C*H*$_2$), 2.43 (s, 3H, Tos CH_3), 1.51 (s, 9H, Boc CH_3).

^{13}C NMR (101 MHz, $CDCl_3$): δ (ppm) = 152.82 (C=O), 144.81 (Tos Ar C), 137.28 (Ar C), 133.01 (Ar C), 130.86 (Tos Ar C), 129.92 (Tos Ar CH_2), 129.58 (Ar CH_2), 127.96 (Tos Ar CH_2), 118.78 (Ar CH_2), 80.72 (Boc C), 70.85 (CH_2), 34.80 (CH_2), 28.47 (Boc CH_3), 21.77 (Tos CH_3).

HR-ESI-MS: m/z calc. for $[C_{20}H_{26}NO_5S]^+$ $[M+H]^+$: 392.15262, found: 392.15339.

FT-IR: $\tilde{\nu}$ (cm^{-1}) = 2924.43 (w), 2361.10 (s), 2343.86 (m), 1514.67 (w), 1356.59 (w), 1174.08 (m), 1161.15 (s), 1122.35 (m), 1095.04 (m), 1033.25 (m), 1008.82 (m), 967.15 (w), 905.35 (w), 814.82 (m), 682.61 (s), 668.24 (m), 567.64 (m), 554.71 (m).

Rf = 0.35 (80 % iHex/EtOAc).

N-Boc-4-(2-azidoethyl)aniline (**86**)

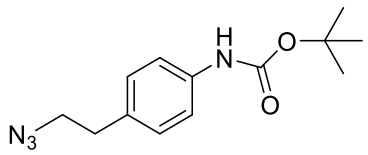

NaN_3 (15.57 g, 239.47 mmol, 2.50 eq) was added to a solution of *N*-Boc-*O*-Tosyl-2-(4-aminophenyl)ethanol (**85**) (37.50 g, 95.79 mmol, 1.00 eq) in dry DMF (500 mL) under N_2 and the reaction mixture was stirred at 90 °C overnight. The mixture was cooled down to r.t. and the solvent evaporated *in vacuo*. The residue was treated with water (100 mL) and extracted with EtOAc (3x 200 mL). The organic layer was washed with brine, dried over Na_2SO_4, and evaporated under vacuum. The crude was purified via silica gel column chromatography (100 % DCM) to afford the desired product **86** (24.66 g, 94.01 mmol, 98 %) as a yellowish oil which became a white solid after co-evaporation with toluene.

^{1}H NMR (500 MHz, $CDCl_3$): δ (ppm) = 7.31 (d, J = 8.0 Hz, 2H, NH-Ar-*o*-CH), 7.13 (d, J = 8.5 Hz, 2H, NH-Ar-*m*-CH), 6.54 (s, 1H, NH), 3.46 (t, J = 7.3 Hz, 2H, N_3-C*H*$_2$-CH_2), 2.83 (t, J = 7.3 Hz, 2H, N_3-CH_2-C*H*$_2$), 1.51 (s, 9H, Boc CH_3).

^{13}C NMR (126 MHz, $CDCl_3$): δ (ppm) = 152.89 (C=O), 137.17 (Ar *C*-CH_2), 132.65 (Ar *C*-NH), 129.37 (NH-Ar-*m*-CH), 118.88 (NH-Ar-*o*-CH), 80.60 (Boc C), 52.64 (N_3-*C*H_2-CH_2), 34.77 (N_3-CH_2-*C*H_2), 28.43 (Boc CH_3).

HR-ESI-MS: m/z calc. for $[C_{13}H_{17}N_4O_2]^-$ $[M-H]^-$: 261.13570, found: 261.13589.

FT-IR: $\tilde{\nu}$ (cm^{-1}) = 3335.43 (w), 2977.60 (w), 2930.18 (w), 2359.66 (s), 2343.86 (s), 2095.24 (m), 1717.29 (m), 1701.49 (m), 1595.14 (w), 1523.29 (s), 1507.48 (m), 1412.64 (m), 1366.65 (m), 1316.35 (m), 1234.44 (m), 1158.28 (s), 1053.37 (m), 1017.44 (w), 836.37 (w), 668.24 (m).

Rf = 0.77 (80 % iHex/EtOAc).

4-(2-Azidoethyl)aniline (**82**)

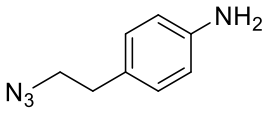

N-Boc-4-(2-azidoethyl)aniline (**86**) (1.08 g, 4.12 mmol, 1.00) was treated with 20 % TFA in DCM (v/v, 20 mL) at r.t. for 30 minutes under N_2. After concentrating under vacuum, the residue was dissolved in water (20 mL), treated with a saturated solution of $NaHCO_3$ (30 mL) and the pH adjusted to 8 with 2 drops of 4 M NaOH, before extracting with EtOAc (3 x 100 mL). The organic layers were combined, washed with brine, dried over Na_2SO_4 and evaporated *in vacuo* to obtain the desired product (626 mg, 3.86 mmol, 94 %) as a light brown oil. The product **82** was considered pure enough and directly used in the next reaction without any further purification.

^{1}H NMR (400 MHz, $CDCl_3$): δ (ppm) = 7.06 – 6.96 (m, 2H, NH_2-Ar *m*-CH), 6.69 – 6.61 (m, 2H, NH_2-Ar *o*-CH), 3.62 (bs, 2H, NH_2), 3.44 (t, J = 7.3 Hz, 2H, N_3-C*H*$_2$-CH_2), 2.79 (t, J = 7.3 Hz, 2H, N_3-CH_2-C*H*$_2$).

^{13}C NMR (101 MHz, $CDCl_3$): δ (ppm) = 145.21 (Ar *C*-NH_2), 129.70 (NH_2-Ar *m*-CH), 127.92 (Ar *C*-CH_2), 115.44 (NH_2-Ar *o*-CH), 52.91 (N_3-*C*H_2-CH_2), 34.61 (N_3-CH_2-*C*H_2).

HR-ESI-MS: m/z calc. for $[C_8H_{11}N_4]^+$ $[M+H]^+$: 163.09782, found: 163.09803.

FT-IR: $\tilde{\nu}$ (cm^{-1}) = 3447.52 (w), 3361.30 (w), 2925.87 (w), 2871.26 (w), 2361.10 (s), 2342.42 (s), 2089.49 (s), 1623.89 (m), 1516.11 (s), 1457.19 (w), 1437.07 (w), 1347.97 (w), 1273.24 (m), 1251.68 (m), 1179.83 (m), 823.44 (m), 668.24 (m), 648.12 (m), 550.40 (m), 537.46 (m), 501.54 (m).

Rf = 0.25 (80 % iHex/EtOAc).

1-(2-Azidoethyl)-4-isothiocyanatobenzene (87)

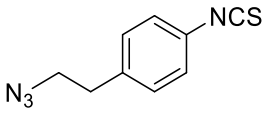

4-(2-Azidoethyl)aniline (**82**) (575 mg, 3.55 mmol, 1.00 eq) was dissolved in dry DCM (70 mL) under Ar atmosphere and to this, di-2-pyridyl thiono-carbonate (**88**) (823 mg, 3.55 mmol, 1.00 eq) was added. The reaction mixture was stirred under Ar at r.t. overnight. After removal of the solvent *in vacuo*, the crude product was purified by silica gel column chromatography (100 % DCM) to obtain the desired product **87** (660 mg, 3.23 mmol, 91 %) as pale yellow crystalline solid.

Due to the fast hydrolysation rate IR and HRMS were not possible to record.

^{1}H NMR (400 MHz, $CDCl_3$): δ (ppm) = 7.21 (d, J = 8.8 Hz, 2H), 7.18 (d, J = 8.8 Hz, 2H), 3.51 (t, J = 7.0 Hz, 2H, N_3-C*H*$_2$-CH_2-Ph), 2.88 (t, J = 7.0 Hz, 2H, N_3-CH_2-C*H*$_2$-Ph).

^{13}C NMR (101 MHz, CDCl3): δ (ppm) = 137.69 (NCS), 130.10 (Ph CH), 126.11 (Ph CH), 52.26 (N_3-CH_2-*C*H_2-Ph), 35.11 (N_3-*C*H_2-CH_2-Ph).

Rf = 0.98 (50 % iHex in EtOAc)

N'-((4-(2-Azidoethyl)phenyl)carbamothioyl)-*N*-phenylbenzimidamide (89)

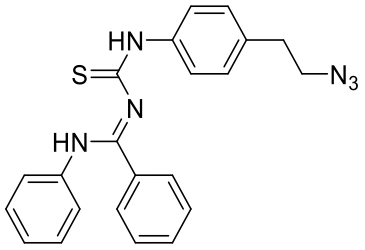

To a solution of *N*-phenylbenzimidoyl chloride (**90**) (5.00 g, 23.18 mmol, 1.00 eq) in dry DCM (78 mL), potassium thiocyanate (2.70 g, 27.82 mmol, 1.20 eq) was added under Ar and the reaction was stirred at r.t. overnight, during which the colour turned to red. After this time, the reaction mixture was filtered under Ar and added dropwise to a solution of 4-(2-azidoethyl)aniline (**82**) (4.14 g, 25.50 mmol, 1.10 eq) in dry DCM at 0 °C under Ar. After the addition, the mixture was allowed to reach r.t. and was stirred for 48 hours. Once the LC-MS didn't show anymore presence of the intermediate, the solvent was evaporated *in vacuo*. In order to purify the product, a first silica gel column chromatography (10 % EtOAc/iHex) was performed, followed by the precipitation of the product by re-dissolving it in the minimum amount of DCM and adding it dropwise to a large amount of iHex stirring. After removal of the solvents, the desired product **89** (6.00 g, 14.98 mmol, 65 %) was obtained as a yellow foam.

^{1}H NMR (500 MHz, CD_2Cl_2): δ (ppm) = 14.02 (s, 1H, NH_a), 8.20 (s, 1H, NH_b), 7.69 – 7.65 (m, 2H, CSNH-Ar *o*-CH), 7.40 (ddt, J = 7.8, 6.2, 1.8 Hz, 1H, Ar_a *p*-CH), 7.36 – 7.30 (m, 4H, Ar_a *o*/*m*-CH), 7.29 – 7.24 (m, 2H, CSNH-Ar *m*-CH), 7.19 – 7.13 (m, 2H, NH-Ar_b *m*-CH), 7.01 – 6.96 (m, 1H, NH-Ar_b *p*-CH), 6.78 – 6.75 (m, 2H, NH-Ar_b *o*-CH), 3.53 (t, J = 7.2 Hz, 2H, N_3-C*H*$_2$-CH_2), 2.90 (t, J = 7.2 Hz, 2H, N_3-CH_2-C*H*$_2$).

^{13}C NMR (126 MHz, CD_2Cl_2): δ (ppm) = 179.44 (C=S), 156.53 (NNHAr_a-C), 146.85 (NH-Ar_b C), 137.66 (CSNH-Ar C), 137.00 (N_3-CH_2-CH_2-Ar C), 132.65 (Ar_a C), 131.13 (Ar_a *p*-CH), 129.58 (CSNH-Ar *m*-CH), 129.31 (NH-Ar_b *m*-CH), 129.25 (Ar_a *m*-CH), 128.74 (Ar_a *o*-CH), 124.86 (CSNH-Ar *o*-CH), 124.45 (NH-Ar_b *p*-CH), 123.00 (NH-Ar_b *o*-CH), 52.90 (N_3-*C*H_2-CH_2), 35.31 (N_3-CH_2-*C*H_2).

HR-ESI-MS: m/z calc. for $[C_{22}H_{21}N_6S]^+$ $[M+H]^+$: 401.15429, found: 401.15428.

FT-IR: $\tilde{\nu}$ (cm^{-1}) = 3465.61 (s), 2957.48 (w), 2922.99 (w), 2852.58 (w), 2359.66 (s), 2343.86 (s), 2098.12 (w), 1698.61 (m), 1635.38 (m), 1507.48 (m), 1362.34 (m), 1237.31 (m), 1152.53 (m), 1093.61 (w), 1021.75 (w), 668.24 (s).

Rf = 0.52 (10 % EtOAc/iHex).

N-(4-(2-Azidoethyl)phenyl)-2,3-diphenyl-1,2,4-thiadiazol-5-imine (93)

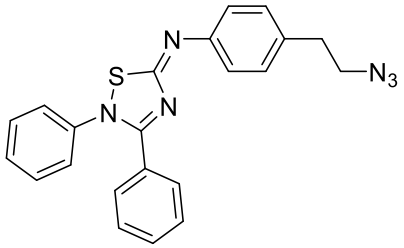

N'-((4-(2-Azidoethyl)phenyl)carbamothioyl)-*N*-phenylbenzimidamide (**89**) (130 mg, 325 µmol, 1.00 eq) was dissolved in a mixture of DCM/EtOAc (1:2, 2 mL DCM, 4 mL EtOAc) and a 0.5 M solution of Br_2 in EtOAc (1.30 mL, 649 µmol, 2.00 eq) was added dropwise at r.t. during which the hydrobromide salt of the product started precipitating. After the addition, iHex (15 mL) was added and the mixture was left at 3 °C overnight to complete the precipitation. The precipitate was then filtered, washed with additional iHex and dried under high vacuum to afford the desired intermediate **93** (156 mg circa, complete conversion) as a yellow solid which was directly used in the next step without any further purification.

HR-ESI-MS: m/z calc. for $[C_{22}H_{19}N_6S]^+$ $[M+H]^+$: 399.13864, found: 399.13880.

FT-IR: $\tilde{\nu}$ (cm^{-1}) = 3356.99 (m), 2956.05 (m), 2921.56 (m), 2852.58 (m), 2361.10 (s), 2342.42 (s), 2095.24 (w), 1654.06 (m), 1457.19 (m), 1260.31 (m), 1021.75 (s), 801.88 (m), 668.24 (s).

N-(4-(4-(2-Azidoethyl)phenyl)-3-methyl-1,2,4-thiadiazol-5-ylidene)-*N*'-phenylbenzimidamide (**92**)

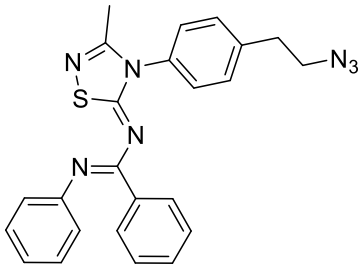

To a suspension of the intermediate bromide salt **93** (156 mg, 325 µmol, 1.00 eq) in dry MeCN (4 mL), Et_3N (400 µL, 2.93 mmol, 9.00 eq) was added and the reaction was refluxed for 2 hours during which time the colour turned dark green. The solvents were removed *in vacuo* and the crude was purified via silica gel column chromatography (100 % DCM) to afford the desired product **92** (80 mg, 182 µmol, 56 %) as a green solid.

^{1}H NMR (500 MHz, CD_2Cl_2): δ (ppm) = 7.52 – 7.45 (m, 2H, N-Ar *o*-CH), 7.39 – 7.33 (m, 2H, N-Ar *m*-CH), 7.33 – 7.28 (m, 2H, Ar_a *o*-CH), 7.28 – 7.18 (m, 3H, Ar_a *p*-CH / N-Ar_b *m*-CH), 7.20 – 7.13 (m, 2H, Ar_a *m*-CH), 7.06 – 6.98 (m, 1H, N-Ar_b *p*-CH), 6.83 – 6.77 (m, 2H, N-Ar_b *o*-CH), 3.61 (t, J = 7.1 Hz, 2H, N_3-C*H*$_2$-CH_2), 3.01 (t, J = 7.1 Hz, 2H, N_3-CH_2-C*H*$_2$), 2.23 (s, 3H, CH_3).

^{13}C NMR (126 MHz, CD_2Cl_2): δ (ppm) = 172.50 (SN-*C*=N), 159.78 (Ar_aN-*C*=N), 152.83 (NN-*C*-CH_3), 147.34 (N-Ar_b C), 140.56 (N_3-CH_2-CH_2-Ar C), 135.85 (N-Ar C), 135.56 (Ar_a C), 130.87 (N-Ar *o*-CH), 129.99 (Ar_a *o*-CH), 129.73 (Ar_a *p*-CH), 129.31 (N-Ar_b *m*-CH), 128.52 (N-Ar *m*-CH), 128.28 (Ar_a *m*-CH), 123.61 (N-Ar_b *p*-CH), 122.88 (N-Ar_b *o*-CH), 52.68 (N_3-*C*H_2-CH_2), 35.58 (N_3-CH_2-*C*H_2), 17.61 (CH_3).

HR-ESI-MS: m/z calc. for $[C_{24}H_{22}N_7S]^+$ $[M+H]^+$: 440.16519, found: 440.16530.

FT-IR: $\tilde{\nu}$ (cm^{-1}) = 3392.91 (s), 2961.79 (w), 2920.12 (w), 2851.14 (w), 2359.66 (s), 2342.42 (s), 2164.22 (w), 1698.61 (s), 1652.63 (m), 1646.88 (m), 1635.38 (m), 1419.82 (w), 1363.78 (m), 1233.00 (m), 1093.61 (w), 719.97 (m), 668.24 (s), 533.15 (s).

Rf = 0.09 (100 % DCM).

4.2.3 RNF5 Biotinylated Recruiter

RNF5 recruiter – Biotin (94)

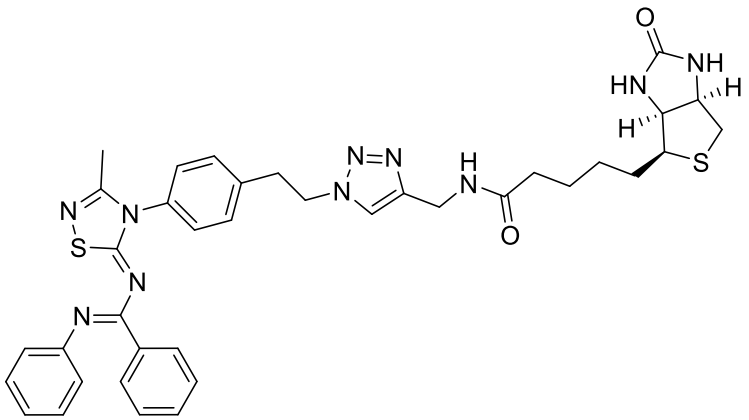

In a schlenk flask under Ar, the commercially available biotin alkyne **95** (10 mg, 36 µmol, 1.00 eq), *N*-(4-(4-(2-azidoethyl)phenyl)-3-methyl-1,2,4-thiadiazol-5-ylidene)-*N*'-phenylbenzimidamide (**92**) (20 mg, 46 µmol, 1.30 eq), TBTA (19 mg, 36 µmol, 1.00 eq) and CuBr (3 mg, 18 µmol, 0.50 eq) were dissolved in dry and degassed DMF (0.6 mL) and stirred at 50 °C for 2 hours. After this time, the solvent was removed under reduced vacuum and the residue treated with H_2O, extracted with MeOH and a large amount of DCM. The combined organic phase was dried over Na_2SO_4 and concentrated *in vacuo.* A first purification was performed via silica gel column chromatography (5 to 10 % MeOH/DCM) and after the product was purified again via preparative HPLC (50 to 80 % B in 45 minutes. Buffer A = H_2O, buffer B = MeCN) to obtain the desired product **94** (19 mg, 26 µmol, 74 %) as a white solid.

^{1}H NMR (500 MHz, MeOD): δ (ppm) = 7.71 (s, 1H, Triaz. NC-C=C*H*), 7.39 (d, J = 0.7 Hz, 4H, N-Ar *o/m*-CH), 7.30 (dd, J = 8.4, 1.4 Hz, 2H, Ar_a *o*-CH), 7.27 – 7.23 (m, 1H, Ar_a *p*-CH), 7.23 – 7.19 (m, 2H, N-Ar_b *m*-CH), 7.19 – 7.14 (m, 2H, Ar_a *m*-CH), 7.04 – 7.00 (m, 1H, N-Ar_b *p*-CH), 6.76 (dt, J = 7.7, 1.2 Hz, 2H, N-Ar_b *o*-CH), 4.70 (t, J = 7.1 Hz, 2H, Triaz.-CH_2-C*H*$_2$-Ar), 4.43 (ddd, J = 7.8, 5.0, 0.9 Hz, 1H, Biot. *CH), 4.32 (d, J = 2.2 Hz, 2H, Triaz.-C*H*$_2$-NHCO), 4.25 (dd, J = 7.9, 4.4 Hz, 1H, Biot. *CH), 3.35 – 3.31 (m, 2H, Triaz.-C*H*$_2$-CH_2-Ar), 3.15 (ddd, J = 8.9, 5.9, 4.5 Hz, 1H, Biot. CH), 2.87 (dd, J = 12.7, 4.9 Hz, 1H, Biot. CH_2), 2.66 (d, J = 12.7 Hz, 1H, Biot. CH_2), 2.22 (s, 3H, CH_3), 2.18 (t, J = 7.2 Hz, 2H, NCO-C*H*$_2$), 1.75 – 1.52 (m, 4H, NCO-C*H*$_2$-C*H*$_2$), 1.44 – 1.35 (m, 2H, NCO-CH_2-CH_2-C*H*$_2$).

^{13}C NMR (126 MHz, MeOD): δ (ppm) = 175.78 (C=O), 173.02 (SN-*C*=N), 166.07 (Biot. C=O), 160.38 (Ar_aN-*C*=N), 154.62 (NN-*C*-CH_3), 147.59 (N-Ar_b C), 146.16 (Triaz. NC-*C*=CH), 140.77 (Triaz.-CH_2-CH_2-Ar C), 136.55 (N-Ar C), 135.88 (Ar_a C), 131.46 (N-Ar *o*-CH), 130.65 (Ar_a *o*-CH), 130.58(Ar_a *p*-CH), 129.92 (N-Ar_b *m*-CH), 129.46 (N-Ar *m*-CH), 128.89 (Ar_a *m*-CH), 124.54 (N-Ar_b *p*-CH), 124.50 (Triaz. CH), 123.47 (N-Ar_b *o*-CH), 63.32 (Biot. *CH), 61.58 (Biot. *CH), 57.02 (Biot. CH), 52.23 (Triaz.-CH_2-

CH_2), 41.07 (Biot. CH_2), 37.13 (Triaz.-*C*H_2-CH_2), 36.53 (NCO-*C*H_2), 35.47 (Triaz.-*C*H_2-NHCO), 29.76 (*C*H_2-Biot.), 29.46 (NCO-CH_2-*C*H_2), 26.70 (NCO-CH_2-CH_2-*C*H_2), 17.17 (CH_3).

HR-ESI-MS: m/z calc. for $[C_{37}H_{41}N_{10}O_2S_2]^+$ $[M+H]^+$: 721.28499, found: 721.28986.

FT-IR: $\tilde{\nu}$ (cm^{-1}) = 2922.99 (m), 2851.14 (w), 2359.66 (m), 2343.86 (m), 1698.61 (m), 1654.06 (m), 1586.52 (m), 1573.59 (m), 1498.86 (s), 1484.49 (s), 1474.43 (s), 1381.02 (w), 1336.47 (s), 1267.49 (s), 1218.63 (w), 1158.28 (w), 1113.73 (w), 1050.50 (w), 1007.38 (m), 931.22 (m), 788.95 (m), 770.27 (m), 755.90 (m), 722.84 (m), 696.98 (s), 668.24 (m), 570.52 (m), 458.42 (m), 439.74 (m).

Rf = 0.10 (5 % MeOH/DCM).

4.2.4 STING PROTACs

4.2.4.1 cGAMP-CRBN STING PROTACs

cGAMP$_2$ – CRBN$_1$ recruiter (96)

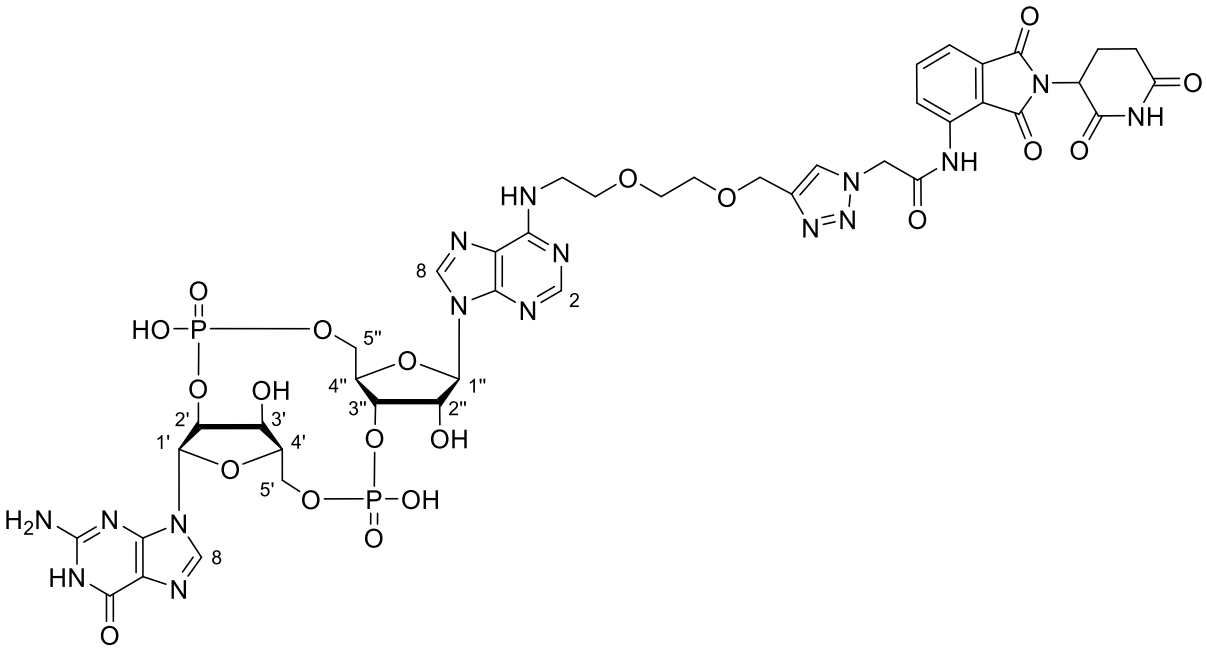

To a solution of cGAMP$_2$ alkyne **52** (15 mg, 19 µmol, 1.00 eq) and THPTA (24 mg, 56 µmol, 3.00 eq) in H_2O (400 µL), was added a 0.1 M water solution of $CuSO_4$ (187 µL, 187 µmol, 1.00 eq) and the corresponding CRBN recruiting azide **67** (13 mg, 38 µmol, 2.00 eq) previously dissolved in MeCN (1 mL) and few drops of DMSO. Then, a 1 M water solution of sodium ascorbate (187 µL, 187 µmol, 10.00 eq) was included, causing the colour to change from blue to pale yellow and the mixture was stirred at 50 °C for 2.5 hours under Ar. After this time, the mixture was diluted with H_2O and lyophilized. The crude was purified via semi-preparative HPLC (0 to 60 % B in 45 minutes. Buffer A = H_2O + 0.1 % TFA, buffer B = MeCN + 0.1 % TFA) to obtain the desired product **96** (19 mg, 16 µmol, 87 %) as a white solid.

^{1}H NMR (800 MHz, 9 D_2O : 1 MeCN): δ (ppm) = 9.05 (s, 1H, Triaz. CH), 8.59 (d, J = 87.1 Hz, 1H, H-8A), 8.48 (d, J = 48.1 Hz, 1H, H-8G), 8.40 (d, J = 8.5 Hz, 1H, H-2A), 8.20 (d, J = 6.6 Hz, 1H, Pom. NH-Ar *o*-CH), 7.92 (t, J = 8.9 Hz, 1H, Pom. NH-Ar *m*-CH), 7.79 (dd, J = 7.3, 2.6 Hz, 1H, Pom. NH-Ar *p*-CH), 6.32 – 6.21 (m, 1H, H-1'), 6.18 – 6.12 (m, 1H, H-1"), 5.76 (d, J = 63.0 Hz, 1H, H-2"), 5.67 – 5.56 (m, 2H, Pom. CO-C*H*$_2$-Triaz.), 5.24 (dd, J = 12.8, 5.6 Hz, 1H, Pom. N-C*H*), 5.10 – 5.00 (m, 1H, H-3'), 4.78 (d, J = 3.2 Hz, 2H, PEG O-C*H*$_2$-Triaz.), 4.65 (t, J = 4.6 Hz, 1H, H-3"), 4.53 (d, J = 18.9 Hz, 2H, H-4' / H-4''), 4.47 (d, J = 11.8 Hz, 1H, H-5'), 4.35 (s, 1H, H-5"), 4.25 (d, J = 12.0 Hz, 1H, H-5"), 4.11 (d, J = 11.9 Hz, 1H, H-5'), 3.99 (s, 1H, PEG CH_2), 3.96 – 3.90 (m, 2H, PEG CH_2), 3.91 – 3.79 (m, 5H, PEG CH_2), 2.99

(ddd, J = 18.4, 13.4, 5.3 Hz, 1H, Pom. $CH_{2b'}$), 2.96 – 2.91 (m, 1H, Pom. $CH_{2b'}$), 2.80 – 2.71 (m, 1H, Pom. $CH_{2a'}$), 2.30 (d, J = 12.3 Hz, 1H, Pom. $CH_{2a'}$).

^{13}C NMR (201 MHz, 9 D_2O : 1 MeCN): δ (ppm) = 175.45, 171.28, 168.24, 168.12, 166.35, 162.48, 162.30, 155.20, 154.68, 150.30, 149.38, 146.12, 144.75, 144.41, 141.17, 138.65, 136.80, 134.99, 131.65, 127.11, 126.65, 120.41, 118.32, 109.25, 89.98, 87.89, 84.48, 80.34, 74.58, 71.62, 70.73, 70.04, 69.08, 68.75, 65.69, 63.18, 62.07, 52.93, 49.32, 42.68, 30.87, 22.10.

^{31}P NMR (202 MHz, 9 D_2O : 1 MeCN): δ (ppm) = -1.21, -2.02.

HR-ESI-MS: m/z calc. for $[C_{42}H_{47}N_{16}O_{20}P_2]^+$ $[M+H]^+$: 1157.26223, found: 1157.26233.

FT-IR: $\tilde{\nu}$ (cm^{-1}) = 2361.10 (w), 2343.86 (w), 1771.90 (w), 1700.05 (s), 1645.44 (m), 1608.08 (m), 1539.10 (m), 1480.18 (w), 1396.83 (m), 1349.41 (w), 1251.68 (m), 1202.82 (m), 1072.05 (s), 994.45 (m), 883.80 (m), 860.80 (m), 820.56 (m), 778.89 (m), 747.27 (m), 668.24 (m), 642.37 (m), 602.13 (m), 528.84 (m), 517.34 (m), 505.85 (m), 490.04 (m), 461.30 (m), 448.36 (m), 422.50 (s), 408.13 (s).

Rf = 4.40 min (LC-MS: 5 to 40 % B in 7 min).

cGAMP$_3$ – CRBN$_1$ recruiter (**97**)

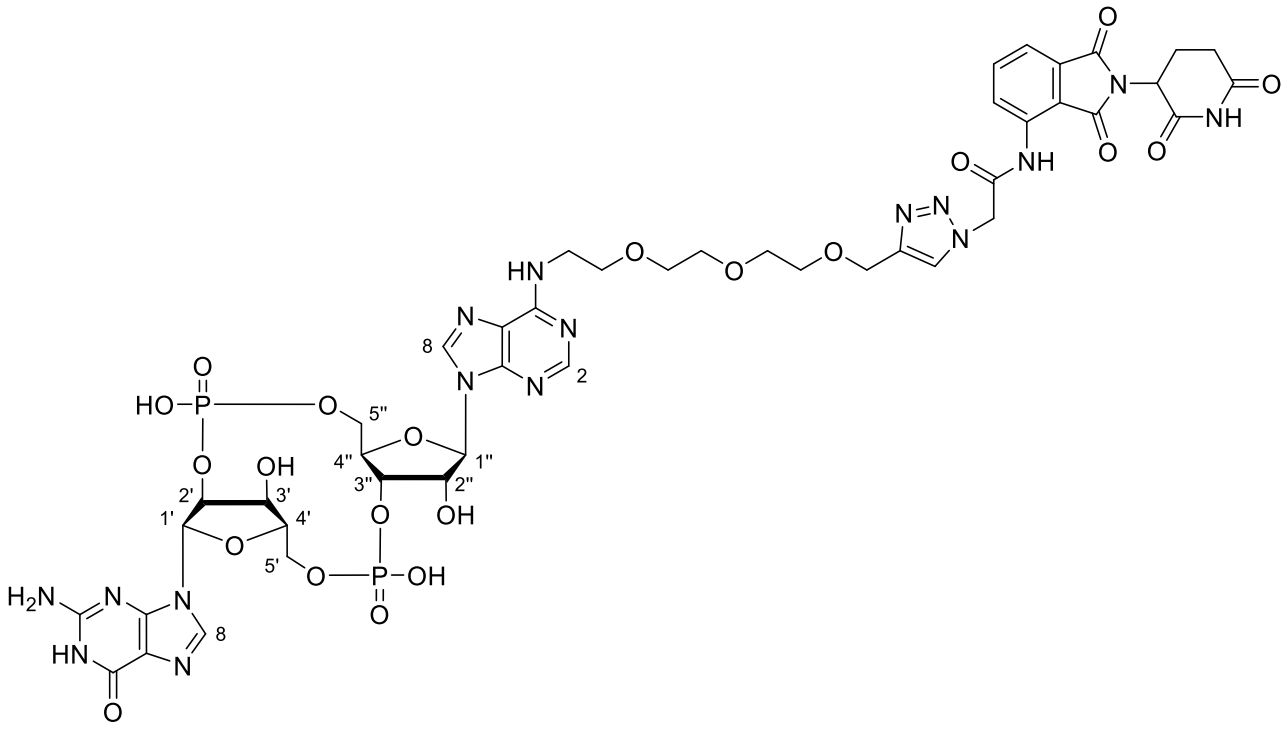

To a solution of cGAMP$_3$ alkyne **53** (10 mg, 12 µmol, 1.00 eq) and THPTA (26 mg, 59 µmol, 5.00 eq) in H_2O (500 µL), was added a 0.1 M water solution of $CuSO_4$ (118 µL, 12 µmol, 1.00 eq) and the corresponding CRBN recruiting azide **67** (8 mg, 24 µmol, 2.00 eq) previously dissolved in DMSO (500 µL). After vortexing the mixture and heating it up at 40 °C, DMSO (circa 600 µL) was added dropwise until complete dissolution of all the reagents. Then, a 1 M water solution of sodium ascorbate (142 µL, 142 µmol, 12.00 eq) was included, causing the colour to change from blue to pale yellow and the mixture was stirred at 55 °C for 2 hours under N_2. After this time, the mixture was diluted with H_2O and lyophilized. The crude was purified via semi-preparative HPLC (0 to 60 % B in 45 minutes. Buffer A = H_2O + 0.1 % TFA, buffer B = MeCN + 0.1 % TFA) to obtain the desired product **97** (9.5 mg, 8 µmol, 67 %) as a white solid.

^{1}H NMR (800 MHz, 9 D_2O : 1 MeCN): δ (ppm) = 9.08 (s, 1H, Triaz. CH), 8.62 (dd, J = 66.5, 4.5 Hz, 1H, H-8A), 8.53 (s, 1H, H-8G), 8.40 (dd, J = 8.4, 2.8 Hz, 1H, Pom. NH-Ar *o*-CH), 8.26 (t, J = 5.0 Hz, 1H, H-2A), 7.90 (td, J = 7.9, 3.6 Hz, 1H, Pom. NH-Ar *m*-CH), 7.78 (dd, J = 7.4, 2.3 Hz, 1H, Pom. NH-Ar *p*-CH), 6.29 (t, J = 5.9 Hz, 1H, H-1'), 6.20 (dd, J = 8.3, 3.4 Hz, 1H, H-1"), 5.79 (d, J = 63.6 Hz, 1H, H-2"), 5.65 (s, 2H, Pom. CO-C*H*$_2$-Triaz.), 5.27 (ddd, J = 13.1, 5.6, 2.8 Hz, 1H, Pom. N-C*H*), 5.08 (s, 1H, H-3'), 4.85 – 4.80 (m, 3H, H-2' / PEG O-C*H*$_2$-Triaz.), 4.70 (dd, J = 4.3, 2.2 Hz, 1H, H-3"), 4.58 (d, J = 9.6 Hz, 1H, H-4'), 4.56 (s, 1H, H-4''), 4.52 (d, J = 11.2 Hz, 1H, H-5'), 4.40 (ddd, J = 11.9, 5.8, 3.0 Hz, 1H, H-5"), 4.29 (d, J = 12.0 Hz, 1H, H-5"), 4.16 (d, J = 11.8 Hz, 1H, H-5'), 4.03 (q, J = 5.4 Hz, 1H, PEG CH_2), 3.98 (dd, J

= 10.8, 4.4 Hz, 1H, PEG CH_2), 3.96 – 3.89 (m, 2H, PEG CH_2), 3.89 – 3.76 (m, 8H, PEG CH_2), 3.02 (ddd, J = 18.5, 13.4, 5.4 Hz, 1H, Pom. $CH_{2b'}$), 2.96 (ddd, J = 17.9, 4.8, 2.6 Hz, 1H, Pom. $CH_{2b'}$), 2.77 (qdd, J = 12.9, 7.4, 4.8 Hz, 1H, Pom. $CH_{2a'}$), 2.36 – 2.31 (m, 1H, Pom. $CH_{2a'}$).

^{13}C NMR (201 MHz, 9 D_2O : 1 MeCN): δ (ppm) = 176.36, 172.16, 169.03, 168.94, 167.23, 163.48, 163.31, 156.09, 155.55, 151.15, 150.17, 146.93, 146.23, 145.70, 145.37, 142.02, 139.46, 137.55, 135.72, 132.40, 127.98, 127.48, 121.19, 119.69, 119.11, 110.17, 90.80, 88.66, 85.34, 81.22, 75.38, 74.83, 72.46, 71.64, 70.87, 70.59, 70.48, 69.91, 69.61, 66.55, 64.03, 62.96, 53.77, 50.14, 45.11, 43.53, 31.69, 22.93.

^{31}P NMR (202 MHz, 9 D_2O : 1 MeCN): δ (ppm) = -1.24, -2.03.

HR-ESI-MS: m/z calc. for $[C_{44}H_{49}N_{16}O_{21}P_2]^-$ $[M-H]^-$: 1199.27389, found: 1199.27330.

FT-IR: $\tilde{\nu}$ (cm^{-1}) = 2358.23 (m), 2343.86 (w), 1734.54 (m), 1717.29 (m), 1700.05 (s), 1684.24 (m), 1669.87 (m), 1654.06 (m), 1636.82 (m), 1616.70 (m), 1559.22 (m), 1533.35 (w), 1507.48 (w), 1472.99 (w), 1457.19 (w), 1395.39 (w), 1349.41 (w), 1199.95 (m), 1059.12 (s), 993.01 (m), 880.92 (m), 799.01 (m), 774.58 (m), 745.84 (m), 719.97 (m), 668.24 (m), 643.81 (m), 600.69 (m), 507.28 (m), 459.86 (s), 418.19 (s).

Rf = 4.73 min (LC-MS: 5 to 40 % B in 7 min).

cGAMP$_3$ – CRBN$_2$ recruiter (98)

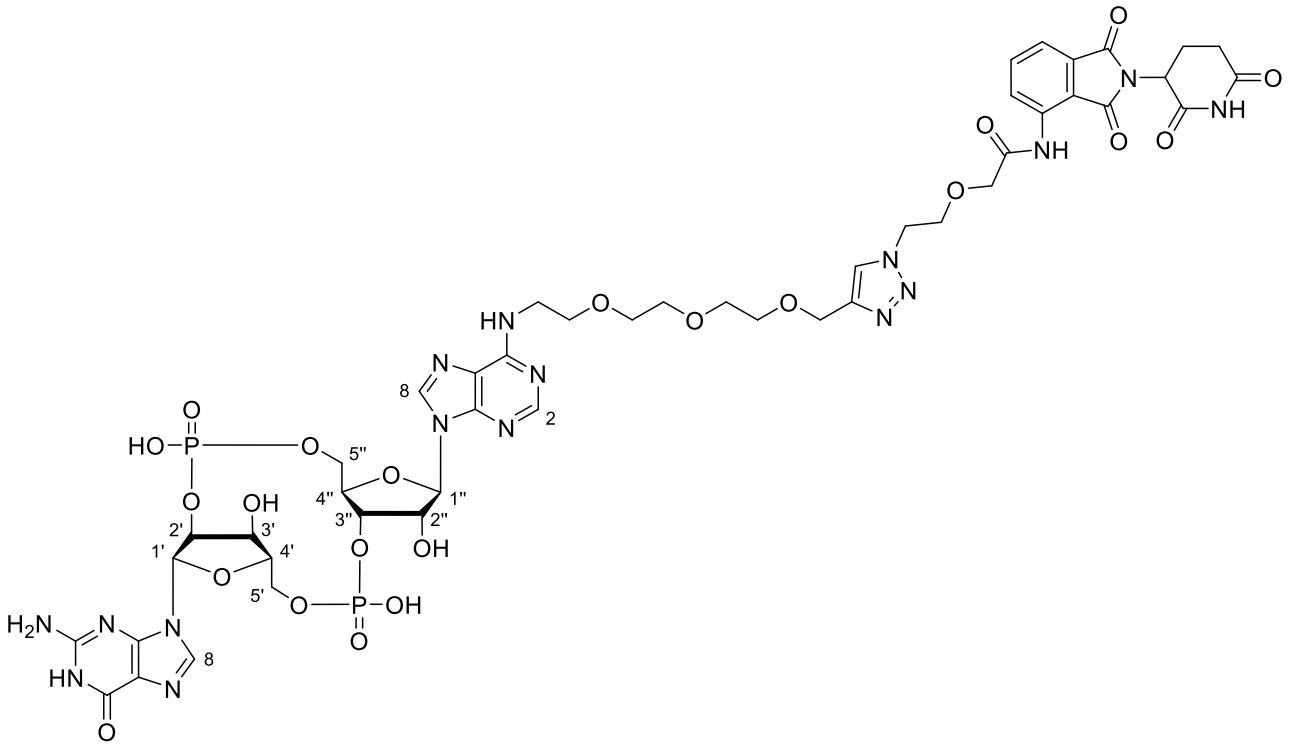

To a solution of cGAMP$_3$ alkyne **53** (20 mg, 24 µmol, 1.00 eq) and THPTA (31 mg, 71 µmol, 3.00 eq) in H_2O (250 µL), was added a 0.1 M water solution of $CuSO_4$ (237 µL, 24 µmol, 1.00 eq) and the corresponding CRBN recruiting azide **79** (19 mg, 47 µmol, 2.00 eq) previously dissolved in a mixture of MeCN (1 mL) and DMSO (200 µL). After vortexing the mixture and heating it up at 40 °C, a 1 M water solution of sodium ascorbate (237 µL, 237 µmol, 10.00 eq) was added, causing the colour to change from blue to pale yellow and the mixture was stirred at 45 °C for 2 hours under Ar. After this time, the mixture was diluted with H_2O and lyophilized. The crude was purified via semi-preparative HPLC (0 to 60 % B in 45 minutes. Buffer A = H_2O + 0.1 % TFA, buffer B = MeCN + 0.1 % TFA) to obtain the desired product **98** (26.4 mg, 21 µmol, 90 %) as a white solid.

^{1}H NMR (500 MHz, 9 D_2O : 1 MeCN): δ (ppm) = 9.00 (s, 1H, Triaz. CH), 8.61 – 8.44 (m, 1H, H-8A), 8.43 – 8.36 (m, 2H, H-8G / Pom. NH-Ar *o*-CH), 8.21 (d, J = 2.8 Hz, 1H, H-2A), 7.75 – 7.68 (m, 1H, Pom. NH-Ar *m*-CH), 7.56 (dd, J = 7.5, 4.4 Hz, 1H, Pom. NH-Ar *p*-CH), 6.20 (d, J = 15.1 Hz, 1H, H-1'), 6.10 (dd, J = 8.3, 2.2 Hz, 1H, H-1"), 5.78 – 5.61 (m, 1H, H-2"), 5.18 (dt, J = 13.0, 5.3 Hz, 1H, Pom. N-C*H*), 4.98 (t, J = 8.8 Hz, 1H, H-3'), 4.69 (d, J = 3.9 Hz, 1H, H-2'), 4.66 – 4.59 (m, 3H, H-3" / PEG O-C*H$_2$*-Triaz.), 4.54 – 4.45 (m, 2H, H-4' / H-4''), 4.43 (d, J = 11.9 Hz, 1H, H-5'), 4.31 (ddd, J = 11.8, 5.6, 2.9 Hz, 1H, H-5"), 4.21 (d, J = 3.6 Hz, 1H, H-5"), 4.18 (d, J = 3.5 Hz, 2H, Pom. CO-C*H$_2$*), 4.14 (q, J = 7.4, 4.5 Hz, 2H, Pom. C*H$_2$*-CH$_2$-Triaz), 4.07 (d, J = 12.0 Hz, 1H, H-5'), 3.93 – 3.75 (m, 3H, PEG CH$_2$), 3.75 – 3.67 (m, 2H, PEG

CH_2), 3.67 – 3.56 (m, 7H, PEG CH_2), 3.01 – 2.84 (m, 2H, Pom. $CH_{2b'}$), 2.69 (td, J = 12.4, 10.9, 6.7 Hz, 1H, Pom. $CH_{2a'}$), 2.26 (ddt, J = 10.4, 5.1, 2.7 Hz, 1H, Pom. $CH_{2a'}$).

^{13}C NMR (126 MHz, 9 D_2O : 1 MeCN): δ (ppm) = 174.94, 170.54, 169.84, 168.09, 167.35, 154.57, 154.05, 149.60, 148.60, 145.38, 144.20, 143.25, 140.49, 136.30, 134.53, 132.04, 128.28, 125.38, 124.61, 117.05, 115.90, 114.73, 108.60, 89.36, 87.25, 83.79, 79.72, 73.94, 70.97, 69.33, 69.19, 69.05, 68.95, 68.39, 65.12, 62.49, 61.48, 49.81, 48.69, 42.03, 30.23, 21.51.

^{31}P NMR (202 MHz, 9 D_2O : 1 MeCN): δ (ppm) = -1.38, -2.16.

HR-ESI-MS: m/z calc. for $[C_{46}H_{53}N_{16}O_{22}P_2]^-$ $[M-H]^-$: 1243.30010, found: 1243.30046.

FT-IR: $\tilde{\nu}$ (cm^{-1}) = 1171.90 (w), 1702.92 (s), 1602.33 (m), 1529.04 (m), 1478.74 (w), 1396.83 (m), 1350.84 (m), 1254.03 (m), 1199.95 (m), 1053.37 (s), 1023.19 (s), 993.01 (s), 911.10 (m), 856.49 (m), 820.56 (m), 747.27 (m), 719.97 (m), 640.93 (m), 592.07 (m), 531.71 (m), 474.23 (m), 465.61 (s), 448.36 (m), 431.12 (m), 413.88 (m), 403.82 (s).

Rf = 4.36 min (LC-MS: 5 to 80 % B in 7 min).

cGAMP$_3$ – CRBN$_4$ recruiter (**99**)

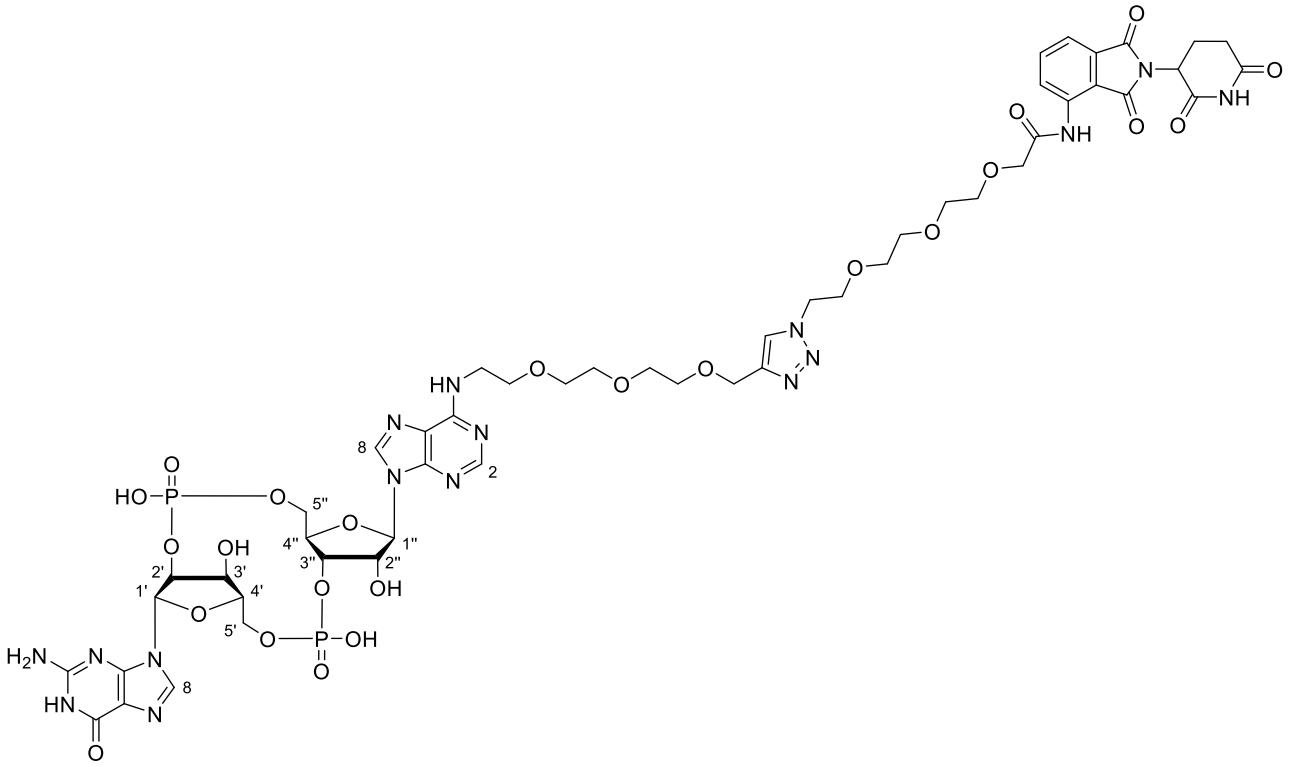

To a solution of cGAMP$_3$ alkyne **53** (20 mg, 24 µmol, 1.00 eq) and THPTA (31 mg, 71 µmol, 3.00 eq) in H_2O (250 µL), was added a 0.1 M water solution of $CuSO_4$ (237 µL, 24 µmol, 1.00 eq) and the corresponding CRBN recruiting azide **81** (23 mg, 47 µmol, 2.00 eq) previously dissolved in a mixture of MeCN (1 mL) and DMSO (200 µL). After vortexing the mixture and heating it up at 40 °C, a 1 M water solution of sodium ascorbate (237 µL, 237 µmol, 10.00 eq) was added, causing the colour to change from blue to pale yellow and the mixture was stirred at 45 °C for 3 hours under Ar. After this time, the mixture was diluted with H_2O and lyophilized. The crude was purified via semi-preparative HPLC (0 to 60 % B in 45 minutes. Buffer A = H_2O + 0.1 % TFA, buffer B = MeCN + 0.1 % TFA) to obtain the desired product **99** (20 mg, 15 µmol, 62 %) as a white solid.

^{1}H NMR (500 MHz, 9 D_2O : 1 MeCN): δ (ppm) = 9.05 (s, 1H, Triaz. CH), 8.63 – 8.50 (m, 2H, H-8A / Pom. NH-Ar *o*-CH), 8.47 (s, 1H, H-8G), 8.09 (d, J = 10.3 Hz, 1H, H-2A), 7.84 (t, J = 8.0 Hz, 1H, Pom. NH-Ar *m*-CH), 7.67 (d, J = 7.3 Hz, 1H, Pom. NH-Ar *p*-CH), 6.25 (d, J = 3.5 Hz, 1H, H-1'), 6.14 (dd, J = 8.3, 1.6 Hz, 1H, H-1"), 5.82 – 5.66 (m, 1H, H-2"), 5.21 (ddd, J = 13.0, 5.5, 1.6 Hz, 1H, Pom. N-C*H*), 5.08 – 4.99 (m, 1H, H-3'), 4.74 (d, J = 4.5 Hz, 1H, H-2'), 4.69 – 4.63 (m, 3H, H-3" / PEG O-C*H*$_2$-Triaz.), 4.63 – 4.59 (m, 2H, Pom. C*H*$_2$-Triaz.), 4.54 (d, J = 8.3 Hz, 1H, H-4'), 4.50 (dt, J = 3.4, 1.7 Hz, 1H, H-4''), 4.47 (d, J = 11.5 Hz, 1H, H-5'), 4.35 (ddd, J = 11.7, 5.6, 3.0 Hz, 1H, H-5"), 4.27 (s, 2H, Pom. CO-C*H*$_2$), 4.23 (d, J = 12.3 Hz, 1H, H-5"), 4.11 (dd, J = 11.8, 3.0 Hz, 1H, H-5'), 4.00 – 3.91 (m, 4H, Pom. C*H*$_2$-CH$_2$-Triaz.

/ PEG CH_2), 3.91 – 3.84 (m, 4H, PEG CH_2), 3.78 (dd, J = 5.8, 2.8 Hz, 4H, PEG CH_2), 3.71 (q, J = 7.6, 5.8 Hz, 10H, PEG CH_2), 2.97 (ddd, J = 18.3, 13.3, 5.3 Hz, 1H, Pom. $CH_{2b'}$), 2.90 (ddt, J = 17.9, 5.0, 2.5 Hz, 1H, Pom. $CH_{2b'}$), 2.70 (tdd, J = 14.0, 12.1, 6.8 Hz, 1H, Pom. $CH_{2a'}$), 2.33 – 2.25 (m, 1H, Pom. $CH_{2a'}$).

^{13}C NMR (126 MHz, 9 D_2O : 1 MeCN): δ (ppm) = 174.88, 170.73, 170.57, 168.07, 167.47, 162.16, 161.88, 154.55, 154.08, 149.62, 148.64, 145.41, 144.20, 143.19, 140.51, 136.31, 134.71, 130.64, 124.87, 121.51, 119.06, 117.06, 116.15, 114.74, 108.53, 89.37, 87.26, 83.79, 79.72, 73.92, 70.98, 70.55, 69.50, 69.38, 69.22, 69.08, 69.01, 68.45, 68.14, 68.07, 65.06, 62.47, 61.50, 49.65, 48.65, 42.04, 30.20, 21.51.

^{31}P NMR (202 MHz, 9 D_2O : 1 MeCN): δ (ppm) = -1.35, -2.13.

HR-ESI-MS: m/z calc. for $[C_{50}H_{61}N_{16}O_{24}P_2]^-$ $[M-H]^-$: 1331.35253, found: 1331.35246.

FT-IR: $\tilde{\nu}$ (cm^{-1}) = 2358.23 (m), 2343.86 (w), 1734.54 (m), 1715.86 (m), 1700.05 (m), 1684.24 (m), 1669.87 (s), 1654.06 (m), 1635.38 (m), 1616.70 (m), 1559.22 (m), 1540.54 (m), 1521.85 (m), 1507.48 (w), 1490.24 (w), 1472.99 (m), 1457.19 (w), 1437.07 (w), 1418.38 (m), 1398.27 (w), 1362.34 (m), 1202.82 (m), 1073.49 (s), 995.89 (w), 888.11 (m), 859.37 (m), 822.00 (m), 800.45 (m), 781.76 (m), 748.71 (m), 721.41 (m), 678.30 (m), 668.24 (m), 645.24 (m), 616.50 (m), 593.51 (m), 538.90 (m), 510.16 (m), 456.99 (m), 429.68 (s).

Rf = 5.90 min (LC-MS: 5 to 40 % B in 7 min).

4.2.4.2 cGAMP-VHL STING PROTACs

cGAMP$_2$ – VHL$_1$ (100)

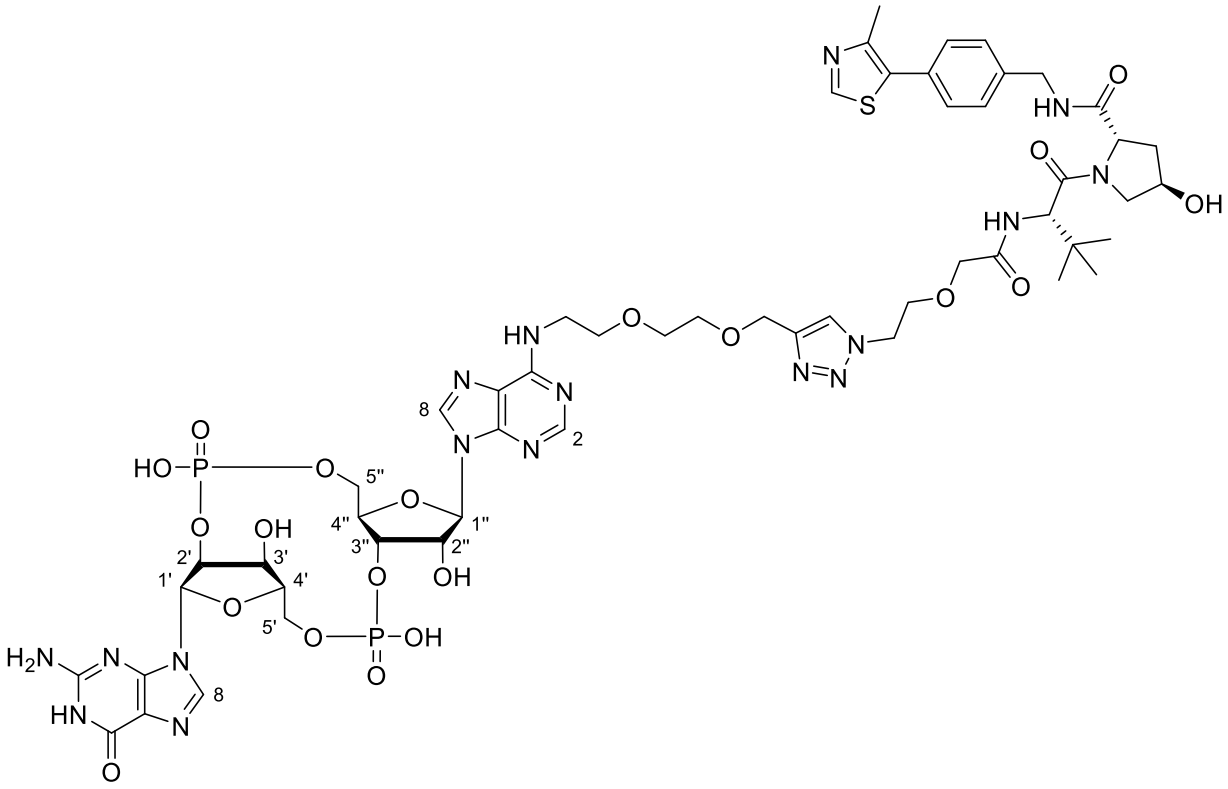

To a solution of cGAMP$_2$ alkyne **52** (10 mg, 13 µmol, 1.00 eq) and THPTA (16 mg, 38 µmol, 3.00 eq) in H_2O (300 µL), was added a 0.1 M water solution of $CuSO_4$ (125 µL, 15 µmol, 1.00 eq) and the corresponding VHL recruiter azide **VHL1** (9 mg, 16 µmol, 1.30 eq) previously dissolved in MeCN (300 µL) and the mixture was vortexed for a couple of minutes to ensure complete dissolution of the reagents. After this, a 1 M water solution of sodium ascorbate (125 µL, 125 µmol, 10.00 eq) was added and the mixture was stirred at 45 °C for 3.5 hours under Ar. After this time, the crude mixture was directly purified via preparative HPLC (0 to 60 % B in 45 minutes. Buffer A = H_2O + 0.1 % TFA, buffer B = MeCN + 0.1 % TFA) to obtain the desired product **100** (14 mg, 10 µmol, 83 %) as a white solid.

^{1}H NMR (500 MHz, 9 D_2O : 1 MeCN): δ (ppm) = 10.11 (s, 1H), 9.50 (s, 1H, H-8A), 9.11 (d, J = 39.1 Hz, 1H, H-8G), 8.94 (d, J = 39.1 Hz, 1H, H-2A), 8.64 (s, 1H), 8.10 – 8.00 (m, 4H), 6.76 (s, 1H, H-1'), 6.67 (d, J = 8.2 Hz, 1H, H-1''), 6.25 (d, J = 36.2 Hz, 1H, H-2''), 5.57 (s, 1H, H-3'), 5.30 – 5.22 (m, 3H, H-2'), 5.20 (d, J = 4.1 Hz, 2H), 5.18 – 5.11 (m, 4H, H-3''/ H-4''), 5.10 – 4.95 (m, 6H, H-5'), 4.86 (ddd, J = 11.7, 5.8, 2.9 Hz, 1H, H-5'), 4.75 – 4.72 (m, 1H), 4.67 – 4.60 (m, 3H), 4.58 (t, J = 5.0 Hz, 2H), 4.50 – 4.43 (m, 2H, H-5''), 4.43 – 4.35 (m, 3H, H-5''), 4.28 (dt, J = 14.7, 8.4 Hz, 4H), 3.14 (s, 3H), 2.93 – 2.85 (m, 1H), 2.71 – 2.65 (m, 1H), 1.53 (s, 9H).

^{13}C NMR (126 MHz, 9 D_2O : 1 MeCN): δ (ppm) = 173.96, 171.56, 171.46, 169.44, 169.39, 164.74, 163.62, 161.98, 155.42, 154.96, 146.96, 145.53, 144.81, 143.65, 141.97, 141.05, 135.57, 130.02, 128.72, 128.42, 126.11, 90.67, 88.51, 85.32, 85.24, 81.14, 75.36, 72.49, 72.43, 70.71, 70.64, 70.17, 69.80, 69.57, 66.47, 64.00, 62.93, 60.41, 57.88, 57.70, 50.94, 43.40, 43.17, 38.05, 36.40, 26.52, 14.02, 6.92.

^{31}P NMR (202 MHz, 9 D_2O : 1 MeCN): δ (ppm) = -1.38, -2.31.

HR-ESI-MS: m/z calc. for $[C_{53}H_{68}N_{17}O_{20}P_2S]^-$ $[M-H]^-$: 1356.40280, found: 1356.40308.

FT-IR: $\tilde{\nu}$ (cm^{-1}) = 2927.30 (w), 2874.13 (w), 2430.08 (w), 2375.47 (w), 1672.75 (s), 1638.26 (m), 1606.64 (m), 1534.79 (m), 1435.63 (m), 1419.82 (m), 1363.78 (m), 1352.28 (m), 1202.82 (m), 1133.85 (m), 1072.05 (s), 1040.44 (m), 997.32 (m), 968.58 (m), 888.11 (m), 853.62 (m), 800.45 (m), 781.76 (m), 721.41 (m), 686.92 (m), 642.37 (m), 605.00 (m), 583.45 (m), 543.21 (m), 501.54 (s), 477.11 (m), 456.99 (m), 400.94 (m).

Rf = 4.54 min (LC-MS: 5 to 80 % B in 7 min).

cGAMP$_3$ – VHL$_1$ (**101**)

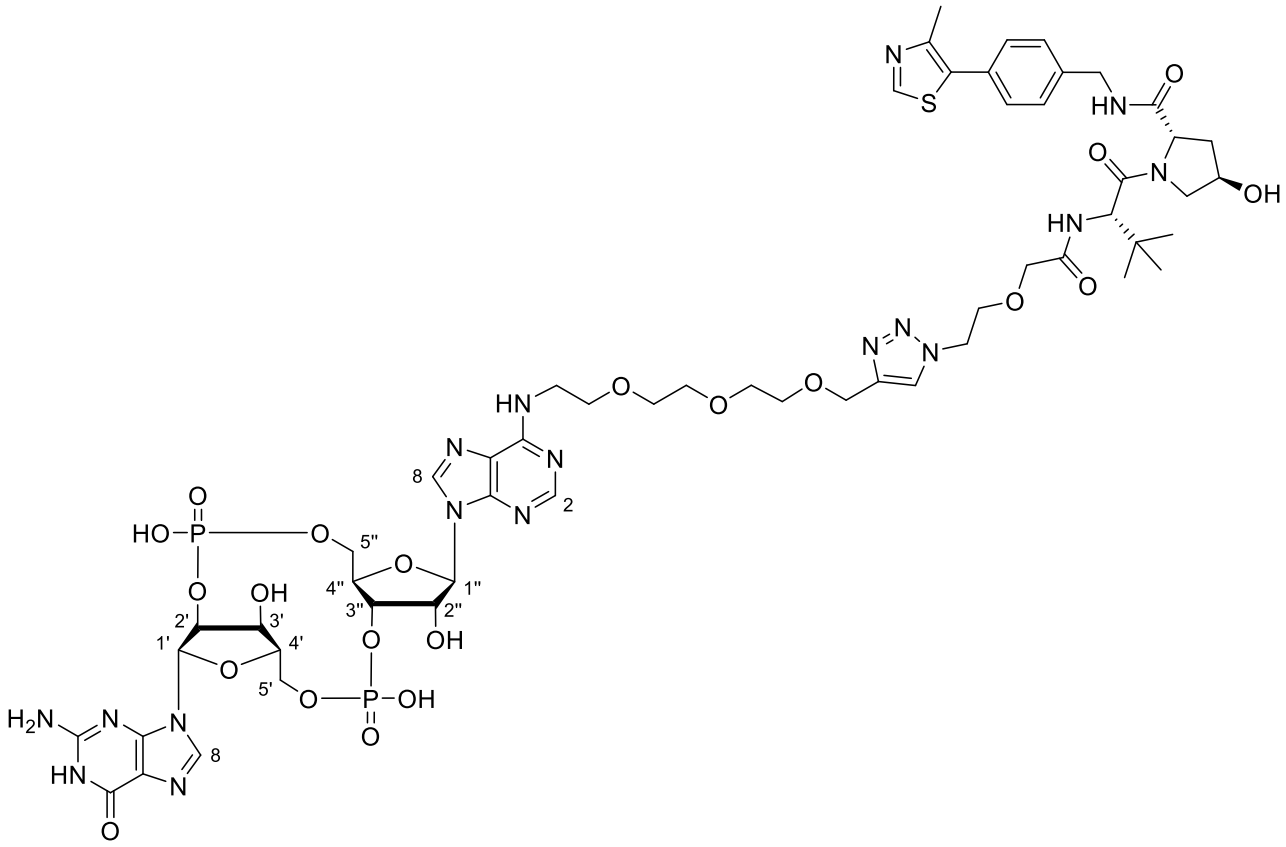

To a solution of cGAMP$_3$ alkyne **53** (10 mg, 12 µmol, 1.00 eq) and THPTA (15 mg, 36 µmol, 3.00 eq) in H_2O (300 µL), was added a 0.1 M water solution of $CuSO_4$ (118 µL, 12 µmol, 1.00 eq) and the corresponding VHL recruiter azide **VHL1** (9 mg, 15 µmol, 1.30 eq) previously dissolved in MeCN (300 µL) and the mixture was vortexed for a couple of minutes to ensure complete dissolution of the reagents. After this, a 1 M water solution of sodium ascorbate (118 µL, 118 µmol, 10.00 eq) was added and the mixture was stirred at 45 °C for 3.5 hours under Ar. After this time, the crude mixture was directly purified via preparative HPLC (0 to 60 % B in 45 minutes. Buffer A = H_2O + 0.1 % TFA, buffer B = MeCN + 0.1 % TFA) to obtain the desired product **101** (15 mg, 11 µmol, 90 %) as a white solid.

^{1}H NMR (500 MHz, 9 D_2O : 1 MeCN): δ (ppm) = 10.06 (s, 1H), 9.44 (s, 1H, H-8A), 9.06 (d, J = 39.1 Hz, 1H, H-8G), 8.92 (s, 1H, H-2A), 8.58 (d, J = 6.0 Hz, 1H), 8.06 – 7.95 (m, 4H), 6.72 (d, J = 6.8 Hz, 1H, H-1'), 6.60 (d, J = 8.2 Hz, 1H, H-1''), 6.27 – 6.11 (m, 1H, H-2''), 5.52 (d, J = 9.1 Hz, 1H, H-3'), 5.20 (dt, J = 9.7, 4.6 Hz, 3H, H-2'), 5.14 (d, J = 3.3 Hz, 2H), 5.12 – 5.05 (m, 4H, H-3'' / H-4''), 5.05 – 4.88 (m, 5H, H-4'), 4.68 (dt, J = 11.9, 2.1 Hz, 1H, H-5'), 4.60 – 4.53 (m, 3H), 4.50 (t, J = 5.0 Hz, 2H), 4.44 – 4.28 (m, 5H, H-5''), 4.27 – 4.19 (m, 2H), 4.16 (s, 6H, H-5'), 3.08 (s, 3H), 2.82 (ddt, J = 13.6, 7.7, 1.8 Hz, 1H), 2.60 (td, J = 9.5, 4.8 Hz, 1H), 1.47 (s, 9H).

^{13}C NMR (126 MHz, 9 D_2O : 1 MeCN): δ (ppm) = 173.96, 171.55, 171.48, 161.86, 155.58, 155.44, 155.02, 150.17, 149.45, 146.99, 145.62, 144.91, 143.55, 142.00, 141.10, 139.26, 139.18, 135.65, 130.08, 128.77, 128.37, 126.03, 118.51, 116.19, 110.31, 90.66, 85.30, 85.23, 83.82, 81.18, 75.35,

72.47, 70.63, 70.55, 70.19, 70.15, 69.82, 69.57, 66.45, 64.03, 62.92, 60.39, 57.89, 57.68, 50.94, 43.18, 38.02, 36.37, 26.51, 13.95.

^{31}P NMR (202 MHz, 9 D_2O : 1 MeCN): δ (ppm) = -1.39, -2.26.

HR-ESI-MS: m/z calc. for $[C_{55}H_{72}N_{17}O_{21}P_2S]^-$ $[M-H]^-$: 1400.42901, found: 1400.43079.

FT-IR: $\tilde{\nu}$ (cm^{-1}) = 2925.87 (w), 2856.89 (w), 2368.29 (w), 2317.99 (w), 1675.62 (s), 1636.82 (m), 1608.08 (m), 1559.22 (m), 1540.54 (m), 1457.19 (m), 1437.07 (m), 1418.38 (m), 1353.72 (m), 1202.82 (s), 1133.85 (m), 1073.49 (m), 995.89 (m), 967.15 (m), 890.98 (m), 856.49 (m), 800.45 (m), 781.76 (m), 721.41 (m), 689.79 (m), 643.81 (m), 605.00 (m), 541.77 (m), 510.16 (m), 446.93 (m), 405.25 (m).

Rf = 4.74 min (LC-MS: 5 to 80 % B in 7 min).

cGAMP$_3$ – VHL$_2$ (**102**)

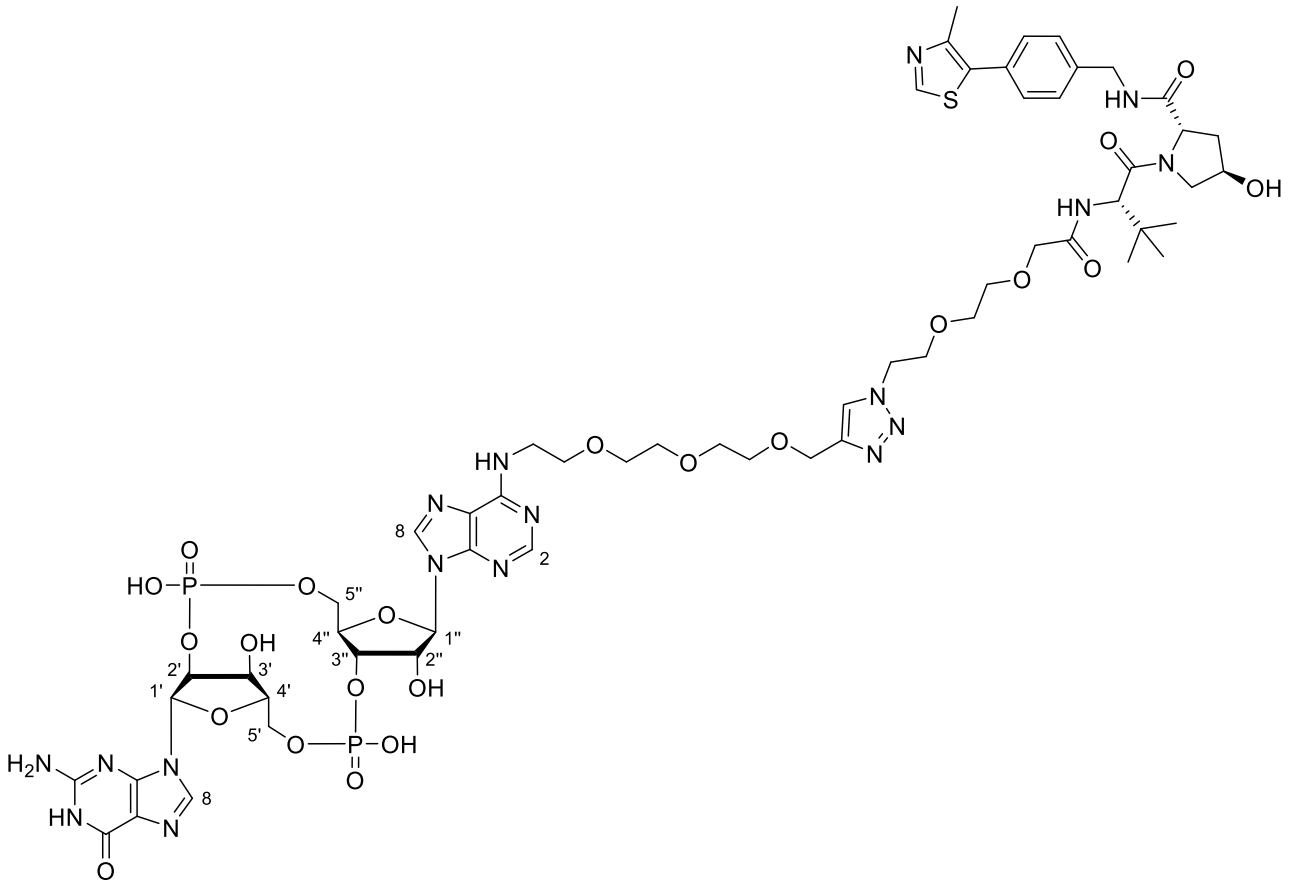

To a solution of cGAMP$_3$ alkyne **53** (10 mg, 12 µmol, 1.00 eq) and THPTA (15 mg, 36 µmol, 3.00 eq) in H_2O (300 µL), was added a 0.1 M water solution of $CuSO_4$ (118 µL, 12 µmol, 1.00 eq) and the corresponding VHL recruiter azide **VHL2** (10 mg, 15 µmol, 1.30 eq) previously dissolved in MeCN (300 µL) and the mixture was vortexed for a couple of minutes to ensure complete dissolution of the reagents. After this, a 1 M water solution of sodium ascorbate (118 µL, 118 µmol, 10.00 eq) was added and the mixture was stirred at 45 °C for 3.5 hours under Ar. After this time, the crude mixture was directly purified via preparative HPLC (0 to 40 % B in 45 minutes. Buffer A = H_2O + 0.1 % TFA, buffer B = MeCN + 0.1 % TFA) to obtain the desired product **102** (15 mg, 10 µmol, 88 %) as a white solid.

^{1}H NMR (500 MHz, 9 D_2O : 1 MeCN): δ (ppm) = 10.03 (s, 1H), 9.49 (s, 1H, H-8A), 9.15 (d, J = 41.7 Hz, 1H, H-8G), 8.99 (d, J = 5.3 Hz, 1H, H-2A), 8.61 (d, J = 5.8 Hz, 1H), 8.05 (s, 4H), 6.79 (d, J = 6.5 Hz, 1H, H-1'), 6.67 (d, J = 8.2 Hz, 1H, H-1''), 6.25 (d, J = 39.2 Hz, 1H, H-2''), 5.58 (s, 1H, H-3'), 5.29 (d, J = 4.2 Hz, 1H, H-2'), 5.22 (s, 1H), 5.21 – 5.16 (m, 4H), 5.16 – 5.10 (m, 3H, H-3'' / H-4''), 5.10 – 5.03 (m, 2H), 5.03 – 4.94 (m, 3H), 4.86 (ddd, J = 11.9, 5.9, 3.0 Hz, 1H, H-5'), 4.77 – 4.72 (m, 1H, H-5'), 4.64 (dd, J =

8.9, 3.2 Hz, 3H), 4.57 – 4.45 (m, 4H, H-5''), 4.46 – 4.35 (m, 4H, H-5''), 4.35 – 4.17 (m, 13H), 3.13 (s, 3H), 2.93 – 2.86 (m, 1H), 2.68 (ddd, J = 13.9, 9.6, 4.6 Hz, 1H), 1.58 (s, 9H).

^{13}C NMR (126 MHz, 9 D_2O : 1 MeCN): δ (ppm) = 173.93, 172.11, 171.54, 155.41, 154.72, 153.41, 151.22, 150.25, 145.70, 144.77, 144.27, 140.95, 139.19, 137.56, 137.28, 135.21, 130.02, 128.78, 128.72, 126.09, 126.07, 90.69, 88.43, 85.30, 84.19, 81.22, 75.35, 72.44, 71.61, 70.79, 70.65, 70.57, 70.54, 70.45, 70.36, 69.88, 69.82, 66.47, 64.02, 62.95, 62.90, 60.42, 57.89, 57.71, 50.90, 43.38, 43.17, 38.04, 36.47, 26.58, 14.25.

^{31}P NMR (202 MHz, 9 D_2O : 1 MeCN): δ (ppm) = -1.37, -2.26.

HR-ESI-MS: m/z calc. for $[C_{57}H_{78}N_{17}O_{22}P_2S]^+$ $[M+H]^+$: 1446.4698, found: 1446.4698.

FT-IR: $\tilde{\nu}$ (cm^{-1}) = 2918.68 (w), 2874.13 (w), 2374.03 (w), 2323.74 (w), 1675.62 (s), 1654.06 (m), 1636.82 (m), 1606.64 (m), 1559.22 (m), 1540.54 (m), 1521.85 (m), 1507.48 (m), 1457.19 (m), 1437.07 (m), 1419.82 (m), 1353.72 (m), 1201.39 (s), 1135.28 (s), 1061.99 (m), 994.45 (m), 967.15 (m), 888.11 (m), 855.05 (m), 803.32 (m), 721.41 (m), 669.67 (m), 640.93 (m), 605.00 (m), 546.09 (m), 502.97 (m), 469.92 (m), 438.31 (m), 413.88 (m).

Rf = 4.73 min (LC-MS: 5 to 80 % B in 7 min).

cGAMP$_3$ – VHL$_3$ (**103**)

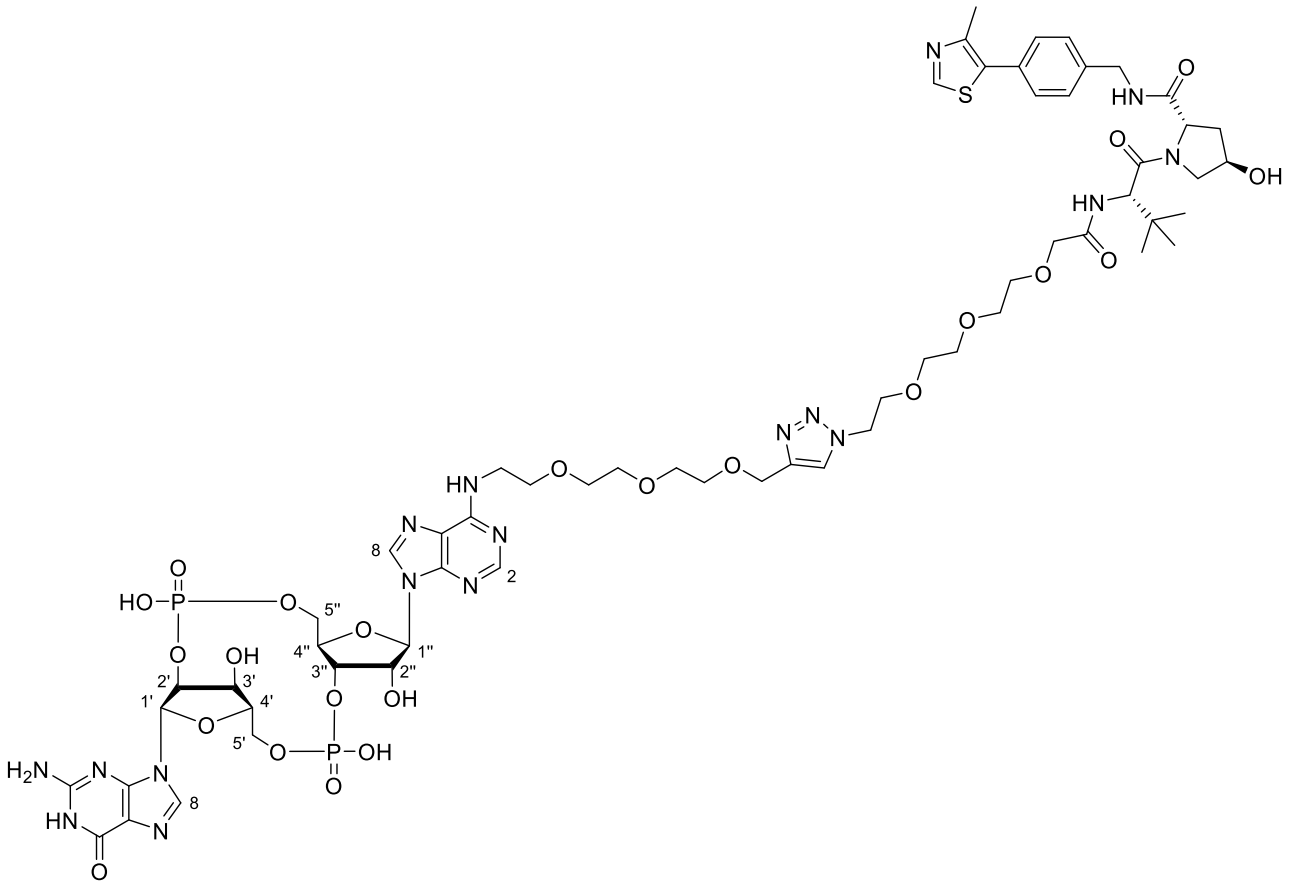

To a solution of cGAMP$_3$ alkyne **53** (10 mg, 12 µmol, 1.00 eq) and THPTA (15 mg, 36 µmol, 3.00 eq) in H_2O (300 µL), was added a 0.1 M water solution of $CuSO_4$ (118 µL, 12 µmol, 1.00 eq) and the corresponding VHL recruiter azide **VHL3** (10 mg, 15 µmol, 1.30 eq) previously dissolved in MeCN (300 µL) and the mixture was vortexed for a couple of minutes to ensure complete dissolution of the reagents. After this, a 1 M water solution of sodium ascorbate (118 µL, 118 µmol, 10.00 eq) was added and the mixture was stirred at 45 °C for 3.5 hours under Ar. After this time, the crude mixture was directly purified via preparative HPLC (0 to 40 % B in 45 minutes. Buffer A = H_2O + 0.1 % TFA, buffer B = MeCN + 0.1 % TFA) to obtain the desired product **103** (16 mg, 11 µmol, 91 %) as a white solid.

^{1}H NMR (500 MHz, 9 D_2O : 1 MeCN): δ (ppm) = 10.17 (s, 1H), 9.62 (s, 1H, H-8A), 9.26 (d, J = 36.7 Hz, 1H, H-8G), 9.12 (d, J = 5.4 Hz, 1H, H-2A), 8.71 (s, 1H), 8.19 (s, 4H), 6.91 (d, J = 7.1 Hz, 1H, H-1'), 6.79 (d, J = 8.2 Hz, 1H, H-1''), 6.37 (d, J = 38.3 Hz, 1H, H-2''), 5.70 (d, J = 12.1 Hz, 1H, H-3'), 5.41 (d, J = 4.2 Hz, 1H, H-2'), 5.33 (d, J = 11.2 Hz, 3H), 5.30 – 5.22 (m, 5H, H-3'' / H-4''), 5.19 (dd, J = 9.7, 5.6 Hz, 2H, H-4'), 5.15 – 5.08 (m, 3H), 4.99 (ddd, J = 12.3, 5.9, 2.9 Hz, 1H, H-5'), 4.94 – 4.84 (m, 2H, H-5'), 4.65 – 4.46 (m, 8H, H-5''), 4.45 – 4.28 (m, 17H), 3.26 (s, 3H), 3.01 (dd, J = 13.5, 7.6 Hz, 1H), 2.80 (ddd, J = 13.7, 9.4, 4.4 Hz, 1H), 1.72 (s, 9H).

^{13}C NMR (126 MHz, 9 D_2O : 1 MeCN): δ (ppm) = 173.90, 172.10, 171.58, 161.69, 161.41, 155.47, 154.78, 151.23, 150.21, 149.53, 145.67, 144.78, 144.20, 142.05, 141.84, 141.09, 139.18, 135.33, 130.07, 128.79, 128.69, 126.02, 118.43, 116.11, 110.42, 90.72, 88.44, 85.36, 85.28, 81.21, 75.37, 72.47, 71.64, 70.82, 70.72, 70.70, 70.66, 70.62, 70.57, 70.49, 70.40, 69.90, 69.69, 69.64, 66.51, 64.06, 62.98, 60.41, 57.94, 57.73, 51.02, 45.07, 43.44, 43.15, 38.09, 36.41, 26.62, 14.23.

^{31}P NMR (202 MHz, 9 D_2O : 1 MeCN): δ (ppm) = -1.38, -2.30.

HR-ESI-MS: m/z calc. for $[C_{59}H_{82}N_{17}O_{23}P_2S]^+$ $[M+H]^+$: 1490.4960, found: 1490.4954.

FT-IR: $\tilde{\nu}$ (cm^{-1}) = 2944.55 (w), 2877.01 (w), 2361.10 (w), 2323.74 (w), 1684.24 (s), 1636.82 (s), 1608.08 (m), 1559.22 (m), 1540.54 (m), 1521.85 (m), 1507.48 (m), 1457.19 (m), 1437.07 (m), 1418.38 (m), 1362.34 (m), 1201.39 (s), 1063.43 (s), 997.32 (m), 967.15 (m), 885.23 (m), 849.31 (m), 801.88 (m), 781.76 (m), 719.97 (m), 669.67 (m), 642.37 (m), 600.69 (m), 540.34 (m), 495.79 (m), 439.74 (m), 403.82 (m).

Rf = 4.89 min (LC-MS: 5 to 80 % B in 7 min).

4.2.4.3 cGAMP-RNF5 STING PROTACs

cGAMP$_2$ – RNF5 recruiter (**104**)

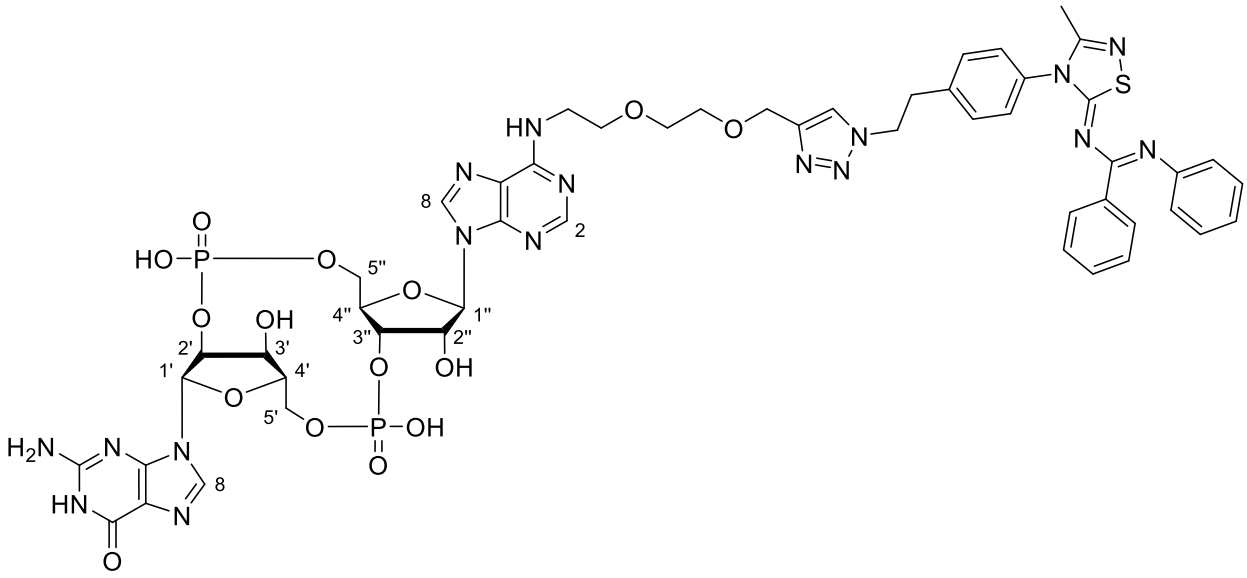

To a solution of cGAMP$_2$ alkyne **52** (15 mg, 19 µmol, 1.00 eq) and THPTA (41 mg, 94 µmol, 5.00 eq) in H_2O (400 µL), was added a 0.1 M water solution of $CuSO_4$ (187 µL, 19 µmol, 1.00 eq) and RNF5 recruiting azide **92** (12 mg, 28 µmol, 1.50 eq) previously dissolved in DMF (400 µL). After vortexing the mixture and heating it up at 40 °C, DMF (circa 1 mL) was added dropwise until complete dissolution of all the reagents. Then, a 1 M water solution of sodium ascorbate (187 µL, 187 µmol, 10.00 eq) was included causing the colour to change from blue to pale yellow and the mixture was stirred at 45 °C for 2 hours under Ar. After this time, the mixture was taken to dryness under N_2 flow and the crude was directly purified via preparative HPLC (10 to 30 % B in 45 minutes. Buffer A = H_2O + 0.1 % TFA, buffer B = MeCN + 0.1 % TFA) to obtain the desired product **104** (11.2 mg, 9 µmol, 48 %) as a pale yellow solid.

^{1}H NMR (800 MHz, 9 MeCN : 1 D_2O): δ (ppm) = 8.71 (s, 1H, H8A), 8.42 (d, J = 24.9 Hz, 1H, H8G), 8.26 (d, J = 19.8 Hz, 1H, H2A), 7.75 (s, 1H), 7.68 – 7.50 (m, 5H), 7.47 – 7.27 (m, 6H), 7.26 – 7.17 (m, 3H), 6.04 (s, 1H, H1’), 5.97 (d, J = 8.1 Hz, 1H, H1’’), 5.53 (d, J = 53.0 Hz, 1H, H2’’), 4.92 (s, 1H, H3’), 4.67 – 4.57 (m, 3H, H2’), 4.46 (d, J = 3.9 Hz, 1H, H3’’), 4.44 – 4.38 (m, 2H), 4.36 (d, J = 8.3 Hz, 1H, H4’), 4.30 (s, 2H, H4’’ + H5’), 4.18 (d, J = 9.0 Hz, 1H, H5’’), 4.15 – 4.08 (m, 1H, H5’’), 3.96 (d, J = 11.3 Hz, 1H, H5’), 3.78 – 3.65 (m, 4H), 3.56 – 3.45 (m, 4H), 3.26 (t, J = 7.3 Hz, 2H), 2.15 (s, 3H).

^{13}C NMR (201 MHz, 9 MeCN : 1 D_2O): δ (ppm) = 183.73, 167.69, 160.56, 160.38, 160.20, 160.01, 158.51, 155.56, 154.74, 150.73, 149.67, 148.87, 146.43, 145.24, 144.07, 141.37, 141.17, 138.37, 136.51, 134.09, 133.63, 130.89, 130.57, 129.26, 129.03, 128.08, 124.73, 123.51, 117.19, 115.74,

90.16, 84.73, 80.70, 74.70, 71.94, 70.13, 69.11, 68.98, 66.01, 63.35, 62.48, 51.20, 42.69, 35.74, 17.06.

^{31}P NMR (162 MHz, 9 MeCN : 1 D_2O): δ (ppm) = -1.40, -2.46.

HR-ESI-MS: m/z calc. for $[C_{51}H_{54}N_{17}O_{15}P_2S]^-$ $[M-H]^-$: 1238.31867, found: 1238.31897.

FT-IR: $\tilde{\nu}$ (cm^{-1}) = 2362.54 (m), 2343.86 (w), 1734.54 (w), 1717.29 (m), 1682.80 (m), 1602.33 (m), 1516.11 (m), 1506.05 (m), 1488.80 (m), 1472.99 (m), 1450.00 (m), 1356.59 (m), 1217.20 (m), 1070.61 (s), 1008.82 (m), 889.54 (m), 855.05 (m), 781.76 (m), 694.10 (m), 643.81 (m), 590.63 (m), 528.84 (m), 504.41 (m), 461.30 (m), 438.31 (m), 411.00 (s).

Rf = 5.60 min (LC-MS: 5 to 80 % B in 7 min).

cGAMP$_3$ – RNF5 recruiter (**105**)

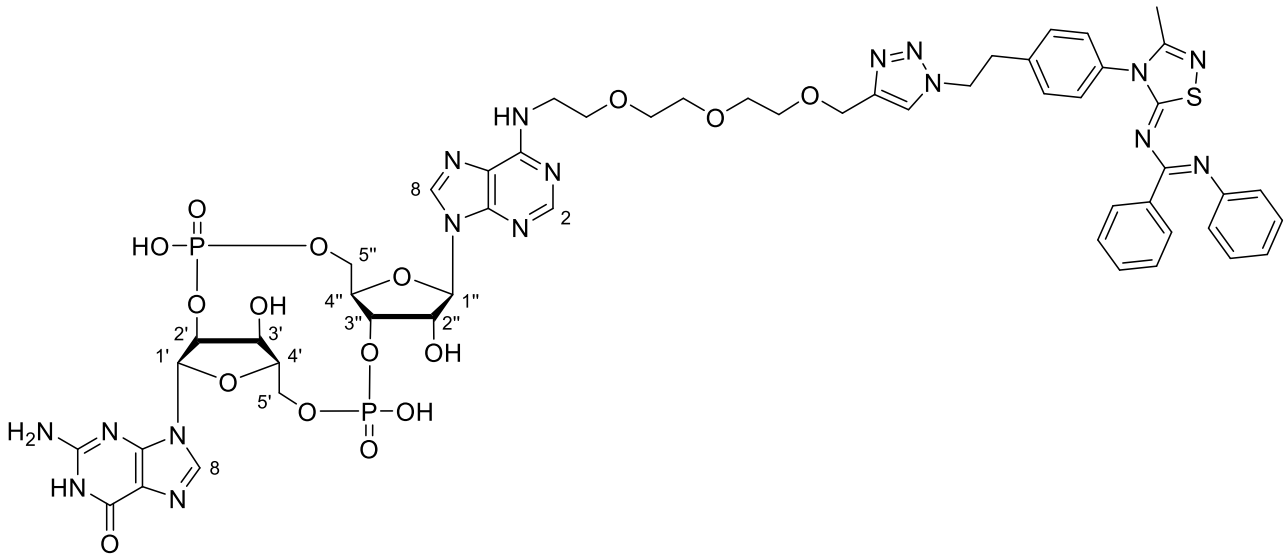

To a solution of cGAMP$_3$ alkyne **53** (15 mg, 18 µmol, 1.00 eq) and THPTA (39 mg, 89 µmol, 5.00 eq) in H_2O (300 µL), was added a 0.1 M water solution of $CuSO_4$ (178 µL, 18 µmol, 1.00 eq) and RNF5 recruiting azide **92** (12 mg, 27 µmol, 1.50 eq) previously dissolved in a mixture of MeCN (600 µL) and DMF (600 µL). After vortexing the mixture and heating it up at 40 °C, DMF (circa 300 µL) was added dropwise until complete dissolution of all the reagents. Then, a 1 M water solution of sodium ascorbate (178 µL, 178 µmol, 10.00 eq) was included causing the colour to change from blue to pale yellow and the mixture was stirred at 45 °C for 2 hours under Ar. After this time, the mixture was lyophilized and the crude was directly purified via preparative HPLC (10 to 30 % B in 45 minutes. Buffer A = H_2O + 0.1 % TFA, buffer B = MeCN + 0.1 % TFA) to obtain the desired product **105** (10.5 mg, 8 µmol, 46 %) as a pale yellow solid.

^{1}H NMR (800 MHz, 9 D_2O : 1 MeCN): δ (ppm) = 8.52 (d, J = 66.7 Hz, 1H, H-8A), 8.42 (s, 1H, H-8G), 8.22 (s, 1H, H-2A), 7.95 (s, 1H), 7.82 (s, 2H), 7.71 (d, J = 7.3 Hz, 2H), 7.50 – 7.40 (m, 7H), 7.35 (d, J = 6.8 Hz, 3H), 6.20 (s, 1H, H-1'), 6.07 (d, J = 8.3 Hz, 1H, H-1"), 5.71 (s, 1H, H-2"), 5.12 (s, 1H, H-3'), 4.84 (d, J = 4.1 Hz, 1H, H-2'), 4.82 – 4.81 (m, 2H), 4.68 (d, J = 4.1 Hz, 1H, H-3"), 4.56 (d, J = 9.4 Hz, 1H, H-4'), 4.53 (s, 2H), 4.51 (d, J = 12.0 Hz, 1H, H-5'), 4.48 (q, J = 2.7 Hz, 1H, H-4"), 4.36 – 4.30 (m, 1H, H-5"), 4.26 (d, J = 12.0 Hz, 1H, H-5"), 4.22 – 4.18 (m, 1H, H-5'), 4.00 – 3.89 (m, 3H), 3.81 (s, 2H), 3.77 – 3.71 (m, 2H), 3.69 (d, J = 4.9 Hz, 2H), 3.65 (ddd, J = 11.7, 6.5, 0.6 Hz, 1H), 3.63 – 3.57 (m, 2H), 3.43 (t, J = 6.6 Hz, 2H), 2.33 (s, 3H).

^{13}C NMR (201 MHz, 9 D2O : 1 MeCN): δ (ppm) = 183.82, 180.12, 178.91, 177.69, 168.08, 163.25, 163.07, 159.11, 158.38, 153.98, 152.04, 144.15, 141.31, 137.83, 136.46, 134.55, 133.68, 133.05, 132.13, 131.15, 130.75, 129.84, 129.50, 128.93, 128.28, 128.04, 126.28, 125.54, 123.65, 123.37, 122.85, 117.77, 116.32, 90.31, 86.96, 84.22, 80.81, 74.69, 72.66, 72.11, 71.25, 70.35, 70.20, 70.15, 69.26, 66.26, 63.44, 63.11, 62.72, 51.76, 47.23, 35.88, 17.20, 16.85, 8.83.

^{31}P NMR (202 MHz, 9 D_2O : 1 MeCN): δ (ppm) = -1.33, -2.33.

HR-ESI-MS: m/z calc. for $[C_{53}H_{58}N_{17}O_{16}P_2S]^-$ $[M-H]^-$: 1282.34489, found: 1282.34467.

FT-IR: $\tilde{\nu}$ (cm^{-1}) = 2359.66 (m), 2340.98 (w), 1679.93 (m), 1600.89 (m), 1559.22 (m), 1516.11 (w), 1506.05 (m), 1472.99 (m), 1450.00 (m), 1359.46 (m), 1202.82 (m), 1073.49 (s), 888.11 (m), 856.49 (m), 799.01 (m), 719.97 (m), 691.23 (m), 668.24 (m), 643.81 (m), 540.34 (m), 502.97 (m), 445.49 (m), 438.31 (m), 428.25 (m), 408.13 (m).

Rf = 5.60 min (LC-MS: 5 to 80 % B in 7 min).

4.2.4.4 Inh-CRBN STING PROTACs

STING Inhibitor – $CRBN_1$ (106)

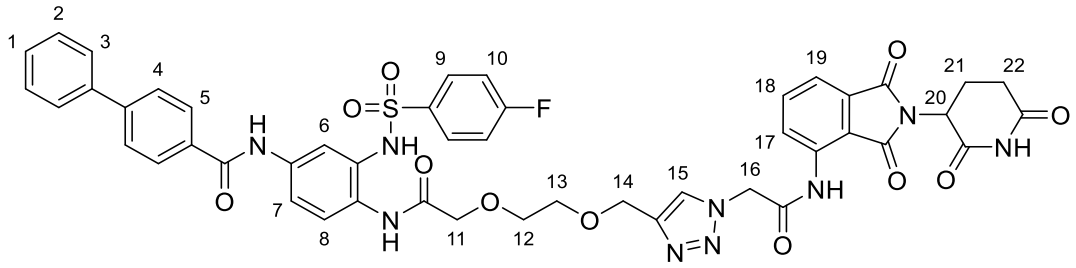

In a schlenk flask under Ar, STING inhibitor alkyne **64** (20 mg, 33 µmol, 1.00 eq), 2-azido-*N*-pomalidomide acetamide **67** (24 mg, 67 µmol, 2.00 eq), TBTA (18 mg, 33 µmol, 1.00 eq) and CuBr (2 mg, 17 µmol, 0.50 eq) were dissolved in dry and degassed DMF (0.6 mL) and stirred at 50 °C for 2 hours. After this time, the solvent was removed under reduced vacuum and the residue treated with pH 3.5 HCl solution (10 mL), extracted with EtOAc (3 x 20 mL) and the combined organic phase was dried over Na_2SO_4 and concentrated *in vacuo.* A first purification was performed via silica gel column chromatography (2 to 3 % MeOH/DCM) and after the product was purified again via preparative HPLC (60 to 70 % B in 45 minutes. Buffer A = H_2O + 0.1 % TFA, buffer B = MeCN + 0.1 % TFA) to obtain the desired product **106** (15 mg, 16 µmol, 47 %) as a pale yellow solid.

^{1}H NMR (500 MHz, Acetone): δ (ppm) = 10.03 (s, 1H, NH), 9.68 (s, 1H, NH), 9.66 (s, 1H, NH), 9.10 (s, 1H, NH), 8.87 (s, 1H, NH), 8.68 (dd, J = 8.6, 3.2 Hz, 1H, H-17), 8.17 (s, 1H, H-15), 8.04 – 7.99 (m, 2H, H-5), 7.85 – 7.74 (m, 7H, H-18 / H-9 / H-4 / H-3), 7.74 – 7.70 (m, 2H, H-6 / H-8), 7.58 – 7.53 (m, 1H, H-19), 7.50 (td, J = 8.4, 7.8, 1.8 Hz, 2H, H-2), 7.45 – 7.38 (m, 2H, H-1 / H-7), 7.33 – 7.26 (m, 2H, H-10), 5.66 (s, 2H, H-16), 5.11 (dd, J = 12.7, 5.4 Hz, 1H, H-20), 4.76 (s, 2H, H-14), 4.02 (s, 2H, H-11), 3.79 (dt, J = 5.3, 1.9 Hz, 2H, H-12), 3.75 (dt, J = 6.7, 2.2 Hz, 2H, H-13), 2.91 (m, 5H, H-22' / H_2O), 2.76 – 2.63 (m, 2H, H-21' / H-22'), 2.19 – 2.10 (m, 1H, H-21').

^{13}C NMR (126 MHz, Acetone): δ (ppm) = 172.59, 170.01, 169.28, 167.39, 167.06, 166.20, 165.76, 165.05, 145.36, 144.84, 140.59, 138.03, 137.38, 137.18, 134.43, 132.52, 130.81, 129.87, 128.97, 127.91, 127.61, 126.39, 125.96, 124.49, 120.56, 119.98, 119.29, 117.25, 117.07, 72.02, 70.69, 70.09, 64.95, 53.66, 50.23, 31.89, 23.17.

FT-IR: $\tilde{\nu}$ (cm^{-1}) = 2957.48 (w), 2921.56 (m), 2851.14 (w), 2359.66 (s), 2342.42 (s), 1700.05 (m), 1684.24 (m), 1669.87 (m), 1654.06 (m), 1646.88 (m), 1635.38 (m), 1559.22 (w), 1540.54 (w), 1521.85 (w), 1507.48 (w), 1457.19 (w), 1418.38 (w), 1396.83 (w), 1373.84 (w), 1362.34 (w), 1260.31 (w), 1235.88 (w), 1092.17 (w), 719.97 (m), 678.30 (s), 668.24 (s), 649.55 (s), 617.94 (m), 537.46 (m), 472.79 (m).

HR-ESI-MS: m/z calc. for $[C_{47}H_{39}FN_9O_{11}S]^-$ $[M-H]^-$: 956.24793, found: 956.24689.

Rf = 0.39 (5 % MeOH/DCM).

STING Inhibitor – $CRBN_2$ (**107**)

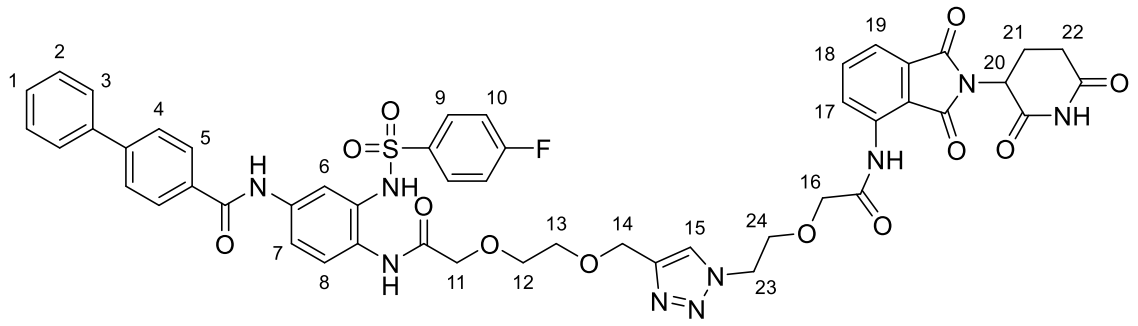

In a schlenk flask under Ar, STING inhibitor alkyne **64** (20 mg, 33 µmol, 1.00 eq), $CRBN_2$ recruiter azide **79** (27 mg, 67 µmol, 2.00 eq), TBTA (18 mg, 33 µmol, 1.00 eq) and CuBr (2 mg, 17 µmol, 0.50 eq) were dissolved in dry and degassed DMF (0.6 mL) and stirred at 50 °C for 2 hours. After this time, the solvent was removed under reduced vacuum and the residue treated with pH 3.5 HCl solution (10 mL), extracted with EtOAc (3 x 20 mL) and the combined organic phase was dried over Na_2SO_4 and concentrated *in vacuo.* A first purification was performed via silica gel column chromatography (2 to 3 % MeOH/DCM) and after the product was purified again via preparative HPLC (iso 60 % B in 15 minutes. Buffer A = H_2O + 0.1 % TFA, buffer B = MeCN + 0.1 % TFA) to obtain the desired product **107** (27 mg, 27 µmol, 81 %) as a pale yellow solid.

^{1}H NMR (500 MHz, Acetone): δ (ppm) = 10.43 (s, 1H, NH), 10.03 (s, 1H, NH), 9.72 (s, 1H, NH), 9.16 (s, 1H, NH), 8.97 (s, 1H, NH), 8.79 (d, J = 8.4 Hz, 1H, H-17), 8.20 (s, 1H, H-15), 8.08 (d, J = 8.3 Hz, 2H, H-5), 7.83 – 7.72 (m, 9H, H-18 / H-9 / H-4 / H-3 / H-6 / H-8), 7.58 (d, J = 7.3 Hz, 1H, H-19), 7.56 – 7.48 (m, 3H, H-7 / H-2), 7.45 – 7.39 (m, 1H, H-1), 7.29 (t, J = 8.6 Hz, 2H, H-10), 5.23 (dd, J = 12.6, 5.4 Hz, 1H, H-20), 4.79 (t, J = 5.0 Hz, 2H, H-23), 4.70 (q, J = 12.1 Hz, 2H, H-14), 4.21 (s, 2H, H-16), 4.12 (td, J = 5.4, 2.5 Hz, 2H, H-24), 3.99 (s, 2H,H-11), 3.73 (p, J = 5.2, 4.3 Hz, 4H, H-12 / H-13), 3.06 – 2.94 (m, 1H, H-22'), 2.84 – 2.76 (m, 2H, H-21' / H-22'), 2.30 (tdd, J = 10.1, 6.5, 3.5 Hz, 1H, H-21').

^{13}C NMR (126 MHz, Acetone): δ (ppm) = 172.71, 170.12, 169.92, 169.77, 169.20, 167.55, 165.86, 144.90, 140.67, 137.92, 137.60, 137.19, 134.64, 132.57, 130.83, 130.76, 129.87, 128.93, 127.92, 127.69, 125.84, 125.23, 124.34, 120.26, 119.84, 118.97, 117.21, 117.15, 117.03, 71.99, 70.99, 70.81, 69.69, 64.65, 55.45, 50.69, 50.35, 31.96, 23.29.

FT-IR: $\tilde{\nu}$ (cm^{-1}) = 3359.86 (m),2960.36 (w), 2920.12 (m), 2851.14 (w), 2361.10 (s), 2342.42 (m), 1705.80 (w), 1654.06 (m), 1632.51 (m), 1260.31 (m), 1095.04 (m), 1023.19 (m), 799.01 (s), 668.24 (s), 472.79 (s).

HR-ESI-MS: m/z calc. for $[C_{49}H_{43}FN_9O_{12}S]^-$ $[M-H]^-$: 1000.27414, found: 1000.27361.

Rf = 0.44 (5 % MeOH/DCM).

STING Inhibitor – $CRBN_3$ (**108**)

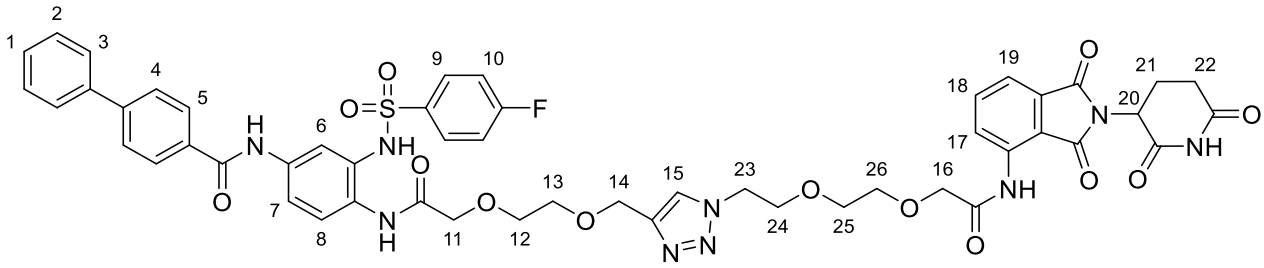

In a schlenk flask under Ar, STING inhibitor alkyne **64** (22 mg, 37 µmol, 1.00 eq), $CRBN_3$ recruiter azide **80** (16 mg, 37 µmol, 1.00 eq), TBTA (20 mg, 37 µmol, 1.00 eq) and CuBr (3 mg, 18 µmol, 0.50 eq) were dissolved in dry and degassed DMF (0.6 mL) and stirred at 50 °C for 2 hours. After this time, the solvent was removed under reduced vacuum and the residue treated with pH 3.5 HCl solution (10 mL), extracted with EtOAc (3 x 20 mL) and the combined organic phase was dried over Na_2SO_4 and concentrated *in vacuo.* A first purification was performed via silica gel column chromatography (50 % Acetone/DCM) and after the product was purified again via preparative HPLC (iso 60 % B in 15 minutes. Buffer A = H_2O + 0.1 % TFA, buffer B = MeCN + 0.1 % TFA) to obtain the desired product **108** (35 mg, 34 µmol, 92 %) as a pale pink solid.

^{1}H NMR (500 MHz, $CDCl_3$): δ (ppm) = 10.34 (s, 1H, NH), 9.17 (s, 1H, NH), 9.07 (s, 1H, NH), 8.78 (dd, J = 8.5, 0.8 Hz, 1H, H-17), 8.34 (s, 2H, 2NH), 7.91 (d, J = 8.1 Hz, 2H, H-5), 7.80 (s, 1H, H-15), 7.76 (dd, J = 8.7, 4.9 Hz, 2H, H-9), 7.66 – 7.57 (m, 5H, H-18 / H-4 / H-6 / H-8), 7.55 – 7.44 (m, 5H, H19 / H-1 / H-3 / H-7), 7.43 – 7.36 (m, 2H, H-2), 7.11 (t, J = 8.4 Hz, 2H, H-10), 5.00 (dd, J = 12.4, 5.4 Hz, 1H, H-20), 4.72 (s, 2H, H-14), 4.57 – 4.41 (m, 2H, H-23), 4.13 (d, J = 1.7 Hz, 2H, H-16), 4.05 (s, 2H, H-11), 3.91 (t, J = 6.3 Hz, 2H, H-24), 3.80 (q, J = 3.5 Hz, 2H, H-25), 3.77 – 3.67 (m, 6H, H-26 / H-12 / H-13), 2.93 – 2.66 (m, 3H, H-22 / H-21'), 2.14 (dt, J = 12.5, 4.3 Hz, 1H, H-21').

^{13}C NMR (126 MHz, $CDCl_3$): δ (ppm) = 171.75, 169.94, 169.42, 168.93, 168.72, 167.62, 166.78, 166.43, 165.85, 164.40, 159.61, 159.28, 145.01, 143.51, 139.75, 136.59, 136.53, 136.30, 135.49, 132.76, 131.38, 130.20, 130.12, 129.13, 128.84, 128.39, 128.28, 127.88, 127.45, 127.35, 125.42, 125.15, 124.50, 119.43, 119.16, 118.83, 116.57, 116.39, 116.20, 71.74, 71.57, 70.91, 70.42, 70.03, 69.52, 63.79, 50.98, 49.40, 31.42, 22.85.

FT-IR: $\tilde{\nu}$ (cm^{-1}) = 2958.92 (m), 2921.56 (m), 2852.58 (w), 2359.66 (s), 2343.86 (s), 2158.47 (w), 1981.71 (w), 1701.49 (m), 1652.63 (s), 1633.94 (s), 1559.22 (w), 1539.10 (m), 1457.19 (w), 1398.27

(w), 1294.80 (w), 1260.31 (m), 1198.51 (w), 1092.17 (m), 1021.75 (m), 837.81 (m), 797.57 (m), 719.97 (m), 668.24 (s).

HR-ESI-MS: m/z calc. for $[C_{49}H_{43}FN_9O_{12}S]^-$ $[M-H]^-$: 1044.30036, found: 1044.29823.

Rf = 0.39 (5 % MeOH/DCM).

STING Inhibitor – $CRBN_4$ (**109**)

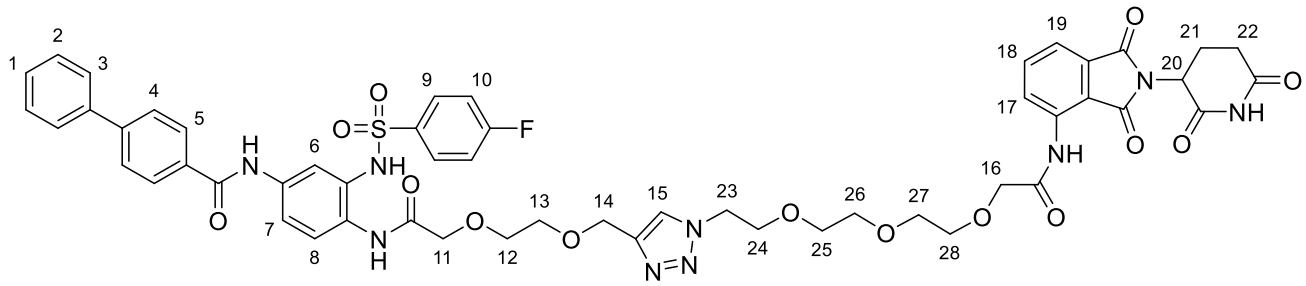

In a schlenk flask under Ar, STING inhibitor alkyne **64** (20 mg, 33 µmol, 1.00 eq), $CRBN_4$ recruiter azide **81** (21 mg, 43 µmol, 1.30 eq), TBTA (18 mg, 33 µmol, 1.00 eq) and CuBr (2 mg, 17 µmol, 0.50 eq) were dissolved in dry and degassed DMF (0.6 mL) and stirred at 50 °C for 2.5 hours. After this time, the solvent was removed under reduced vacuum and the residue treated with pH 3.5 HCl solution (10 mL), extracted with EtOAc (3 x 20 mL) and the combined organic phase was dried over Na_2SO_4 and concentrated *in vacuo.* The residue was dissolved in MeOH and filtered finely through an HPLC filter. After having evaporated the solvent *in vacuo*, the crude was purified via preparative HPLC (iso 60 % B in 25 minutes. Buffer A = H_2O + 0.1 % TFA, buffer B = MeCN + 0.1 % TFA) to obtain the desired product **109** (35 mg, 32 µmol, 97 %) as a white solid.

^{1}H NMR (500 MHz, $CDCl_3$): δ (ppm) = 10.39 (s, 1H, NH), 9.19 (s, 1H, NH), 8.96 (s, 1H, NH), 8.76 (dd, J = 8.5, 0.7 Hz, 1H, H-17), 8.48 (s, 1H, NH), 8.21 (s, 1H, NH), 7.93 – 7.89 (m, 2H, H-5), 7.86 (s, 1H, H-15), 7.76 – 7.69 (m, 2H, H-9), 7.68 – 7.63 (m, 3H, H-18 / H-4), 7.62 – 7.58 (m, 2H, H-3), 7.51 (dd, J = 7.3, 0.8 Hz, 1H, H-19), 7.50 – 7.47 (m, 1H, H-6), 7.46 (d, J = 1.3 Hz, 2H, H-7 / H-8), 7.46 – 7.43 (m, 2H, H-2), 7.43 – 7.37 (m, 1H, H-1), 7.13 – 7.06 (m, 2H, H-10), 5.00 – 4.94 (m, 1H, H-20), 4.77 (s, 2H, H-14), 4.47 (t, J = 5.0 Hz, 2H, H-23), 4.16 (s, 2H, H-16), 4.06 (s, 2H, H-11), 3.85 – 3.78 (m, 4H, H-24 / PEG CH_2), 3.78 – 3.73 (m, 4H, PEG CH_2), 3.71 (dd, J = 6.0, 3.4 Hz, 2H, PEG CH_2), 3.62 (dd, J = 5.9, 3.5 Hz, 2H, PEG CH_2), 3.58 (dd, J = 6.4, 3.7 Hz, 2H, H-12 / H-13), 2.90 – 2.81 (m, 1H, H-22'), 2.81 – 2.69 (m, 2H, H-22' / H-21'), 2.12 (tt, J = 11.9, 4.1 Hz, 1H, H-21').

^{13}C NMR (126 MHz, $CDCl_3$): δ (ppm) = 171.85, 170.09, 169.88, 168.76, 168.59, 166.82, 166.46, 166.25, 164.43, 159.56, 159.23, 145.12, 143.45, 139.73, 136.55, 136.52, 136.28, 135.32, 135.30, 132.70, 131.40, 130.20, 130.12, 129.14, 128.68, 128.54, 128.41, 127.97, 127.46, 127.33, 125.44,

125.29, 124.53, 119.74, 119.22, 119.18, 116.58, 116.40, 116.32, 116.23, 113.96, 71.56, 71.54, 70.91, 70.61, 70.54, 70.48, 70.37, 70.02, 68.93, 63.61, 51.09, 49.36, 31.42, 22.73.

FT-IR: $\tilde{\nu}$ (cm^{-1}) = 2925.87 (m), 2855.45 (w), 2359.66 (s), 2343.86 (w), 1744.60 (m), 1700.05 (m), 1652.63 (m), 1636.82 (m), 1457.19 (w), 1437.07 (w), 1372.40 (w), 1258.87 (m), 1240.19 (m), 1222.94 (m), 1093.61 (w), 1050.50 (w), 1020.32 (w), 793.26 (m), 668.24 (s).

HR-ESI-MS: m/z calc. for $[C_{53}H_{51}FN_9O_{14}S]^-$ $[M-H]^-$: 1088.32657, found: 1088.32793.

Rf = 0.65 (5 % MeOH/DCM).

4.2.4.5 Inh-VHL STING PROTACs

STING Inhibitor – VHL_1 (110)

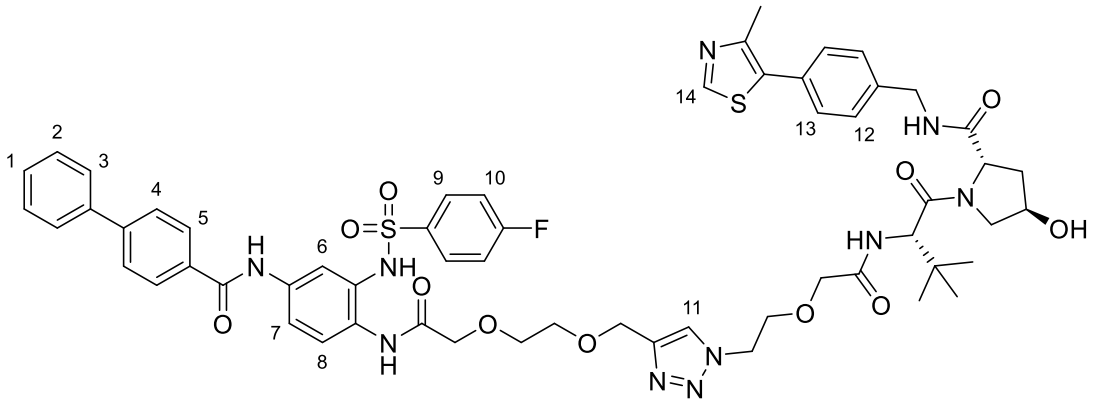

In a schlenk flask under Ar, STING inhibitor alkyne **64** (12 mg, 20 µmol, 1.00 eq), **VHL1** recruiter azide (14 mg, 24 µmol, 1.20 eq), TBTA (11 mg, 20 µmol, 1.00 eq) and CuBr (1 mg, 10 µmol, 0.50 eq) were dissolved in dry and degassed DMF (0.6 mL) and stirred at 50 °C for 2 hours during which the solution turned dark brown. After this time, the solvent was removed under reduced vacuum and the residue treated with a saturated solution of NH_4Cl (10 mL), extracted with EtOAc (3 x 20 mL). The combined organic phase was dried over Na_2SO_4, washed with brine and concentrated *in vacuo.* The crude was purified via preparative HPLC (30 to 40 % B in 10 minutes + isocratic 40 % B for 10 minutes. Buffer A = H_2O + 0.1 % TFA, buffer B = MeCN + 0.1 % TFA) to obtain the desired product **110** (21 mg, 18 µmol, 91 %) as a pale yellow solid.

^{1}H NMR (500 MHz, MeCN): δ (ppm) = 9.23 (s, 1H, NH), 9.05 (s, 1H, NH), 9.01 (s, 1H, NH), 8.67 (s, 1H, NH), 7.98 – 7.94 (m, 2H, H-5), 7.88 (s, 1H, H-11), 7.75 (d, J = 8.4 Hz, 2H, H-4), 7.72 – 7.67 (m, 4H, H-3 / H-9), 7.63 (d, J = 2.4 Hz, 1H, H-6), 7.56 (dd, J = 8.8, 2.4 Hz, 1H, H-8), 7.52 – 7.47 (m, 3H, H-2 / H-1), 7.44 – 7.40 (m, 1H, H-7), 7.39 – 7.35 (m, 4H, H-12 / H-13), 7.32 (t, J = 6.2 Hz, 1H, H-14), 7.21 (t, J = 8.8 Hz, 2H, H-10), 7.04 (d, J = 9.3 Hz, 1H, -OH), 4.65 (d, J = 2.9 Hz, 2H), 4.58 (d, J = 9.4 Hz, 1H), 4.54 (dt, J = 5.6, 4.0 Hz, 2H), 4.47 (dd, J = 9.0, 7.6 Hz, 1H), 4.45 – 4.39 (m, 2H), 4.29 (dd, J = 15.8, 5.8 Hz, 1H), 4.00 – 3.95 (m, 2H), 3.94 (s, 1H), 3.91 (s, 1H), 3.89 – 3.84 (m, 2H), 3.78 (dt, J = 11.3, 1.8 Hz, 1H), 3.70 (d, J = 3.9 Hz, 1H), 3.67 (s, 4H), 2.46 (s, 3H), 2.15 (ddt, J = 13.2, 7.6, 2.0 Hz, 1H), 2.05 (ddd, J = 13.2, 9.0, 4.4 Hz, 1H), 0.92 (s, 9H).

^{13}C NMR (126 MHz, MeCN): δ (ppm) = 173.03, 171.46, 170.31, 169.69, 167.26, 166.52, 165.25, 159.67, 159.36, 154.47, 145.13, 145.00, 144.68, 141.53, 140.62, 137.63, 136.47, 136.45, 135.41, 134.39, 131.04, 130.96, 130.09, 130.03, 129.90, 129.19, 129.14, 129.02, 128.85, 128.78, 128.09, 127.94, 125.58, 124.72, 120.40, 120.20, 117.53, 117.43, 117.24, 115.25, 72.13, 70.94, 70.73, 70.67, 70.20, 70.01, 64.66, 60.42, 57.77, 57.46, 50.91, 43.13, 38.54, 36.51, 26.68, 14.41.

HR-ESI-MS: m/z calc. for $[C_{58}H_{62}FN_{10}O_{11}S_2]^-$ $[M-H]^-$: 1157.40305, found: 1157.40357.

FT-IR: $\tilde{\nu}$ (cm^{-1}) = 2951.73 (w), 2871.26 (w), 2359.66 (w), 2330.92 (m), 1771.90 (w), 1734.54 (w), 1669.87 (m), 1654.06 (m), 1609.51 (m), 1559.22 (m), 1540.54 (m), 1521.85 (m), 1507.48 (m), 1490.24 (m), 1457.19 (m), 1437.07 (m), 1418.38 (m), 1339.35 (m), 1294.80 (m), 1198.51 (m), 1153.96 (m), 1090.73 (s), 1057.68 (m), 1007.38 (m), 888.11 (w), 836.37 (m), 816.25 (m), 797.57 (m), 781.76 (m), 747.27 (m), 718.53 (m), 699.85 (m), 668.24 (m), 567.64 (m), 544.65 (s), 518.78 (m), 456.99 (m).

Rf = 4.60 min (LC-MS: 5 to 80 % B in 7 min).

STING Inhibitor – VHL_2 (**111**)

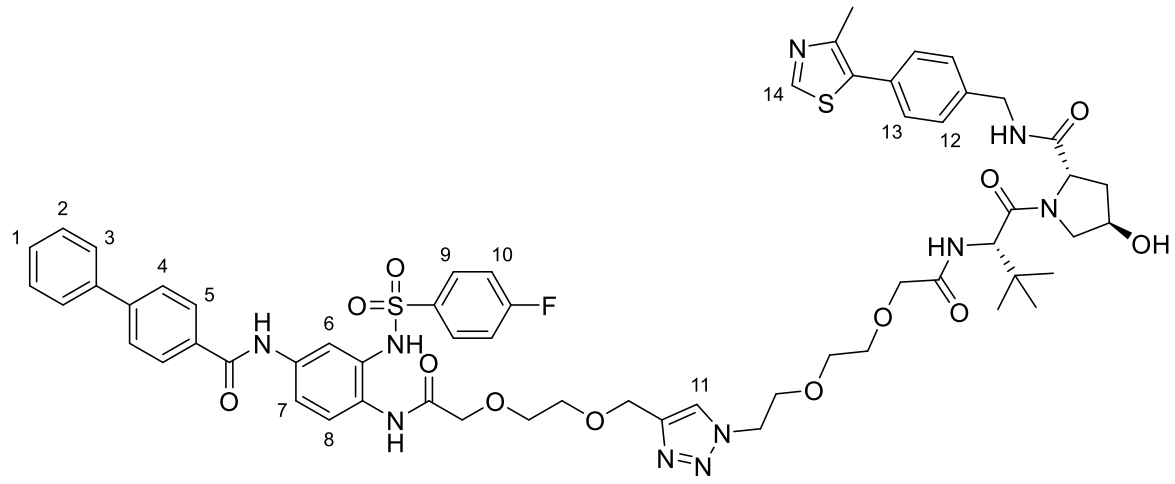

In a schlenk flask under Ar, STING inhibitor alkyne **64** (12 mg, 20 µmol, 1.00 eq), **VHL2** recruiter azide (12 mg, 20 µmol, 1.20 eq), TBTA (11 mg, 20 µmol, 1.00 eq) and CuBr (1 mg, 10 µmol, 0.50 eq) were dissolved in dry and degassed DMF (0.5 mL) and stirred at 50 °C for 2 hours during which the solution turned dark brown. After this time, the solvent was removed under reduced vacuum and the residue treated with a saturated solution of NH_4Cl (10 mL), extracted with EtOAc (3 x 20 mL). The combined organic phase was dried over Na_2SO_4, washed with brine and concentrated *in vacuo.* The crude was purified via preparative HPLC (40 to 50 % B in 10 minutes + isocratic 50 % B for 10 minutes. Buffer A = H_2O + 0.1 % TFA, buffer B = MeCN + 0.1 % TFA) to obtain the desired product **111** (23.5 mg, 20 µmol, 98 %) as a pale yellow solid.

^{1}H NMR (500 MHz, MeCN): δ (ppm) = 9.22 (s, 1H, NH), 9.04 (s, 1H, NH), 9.00 (s, 1H, NH), 8.74 (s, 1H, NH), 7.97 – 7.93 (m, 2H, H-5), 7.92 (s, 1H, H-11), 7.77 – 7.73 (m, 2H, H-4), 7.73 – 7.68 (m, 4H, H-9 / H-3), 7.66 (d, J = 2.4 Hz, 1H, H-6), 7.56 (dd, J = 8.8, 2.4 Hz, 1H, H-8), 7.52 – 7.47 (m, 3H, H-1 / H-2), 7.44 – 7.39 (m, 1H, H-7), 7.38 – 7.31 (m, 5H, H-12 / H-13 / H-14), 7.29 (d, J = 9.4 Hz, 1H, -OH), 7.24 – 7.18 (m, 2H, H-10), 4.64 (s, 2H), 4.62 (d, J = 9.5 Hz, 1H), 4.55 – 4.40 (m, 5H), 4.27 (dd, J = 15.8, 5.7 Hz, 1H), 3.98 (s, 2H), 3.93 (d, J = 15.7 Hz, 1H), 3.86 (d, J = 15.8 Hz, 1H), 3.82 (dt, J = 6.7, 4.7 Hz, 2H),

3.76 (dt, J = 11.2, 1.7 Hz, 1H), 3.72 – 3.66 (m, 5H), 3.63 – 3.49 (m, 4H), 2.46 (s, 3H), 2.14 (ddt, J = 13.2, 7.6, 1.9 Hz, 1H), 2.05 (ddd, J = 13.2, 9.0, 4.4 Hz, 1H), 0.94 (s, 9H).

^{13}C NMR (126 MHz, MeCN): δ (ppm) = 173.01, 171.37, 170.59, 170.33, 167.24, 166.53, 165.23, 159.92, 159.61, 154.36, 145.12, 144.88, 144.72, 141.49, 140.62, 137.69, 136.63, 135.25, 134.44, 131.00, 130.92, 130.06, 130.02, 129.82, 129.19, 129.14, 129.10, 128.95, 128.80, 128.09, 127.94, 125.85, 124.84, 120.37, 120.25, 117.65, 117.42, 117.24, 115.36, 72.08, 71.84, 70.92, 70.79, 70.75, 70.10, 70.06, 64.52, 60.39, 57.81, 57.39, 51.08, 43.16, 38.53, 36.71, 26.71, 14.47.

HR-ESI-MS: m/z calc. for $[C_{60}H_{66}FN_{10}O_{12}S_2]^-$ $[M-H]^-$: 1201.42926, found: 1201.43025.

FT-IR: $\tilde{\nu}$ (cm^{-1}) = 2933.05 (w), 2871.26 (w), 2359.66 (w), 2322.30 (w), 1800.64 (w), 1771.90 (w), 1734.54 (w), 1669.87 (m), 1654.06 (s), 1636.82 (m), 1540.54 (s), 1520.42 (s), 1507.48 (s), 1490.24 (m), 1457.19 (m), 1437.07 (m), 1418.38 (m), 1398.27 (m), 1339.35 (m), 1293.36 (m), 1230.13 (m), 1166.90 (m), 1153.96 (m), 1090.73 (m), 1057.68 (m), 1007.38 (m), 908.23 (w), 837.81 (m), 817.69 (m), 780.33 (m), 745.84 (m), 718.53 (m), 698.41 (m), 668.24 (m), 635.18 (m), 567.64 (m), 544.65 (s), 497.22 (m), 456.99 (m).

Rf = 4.75 min (LC-MS: 5 to 80 % B in 7 min).

STING Inhibitor – VHL$_3$ (**112**)

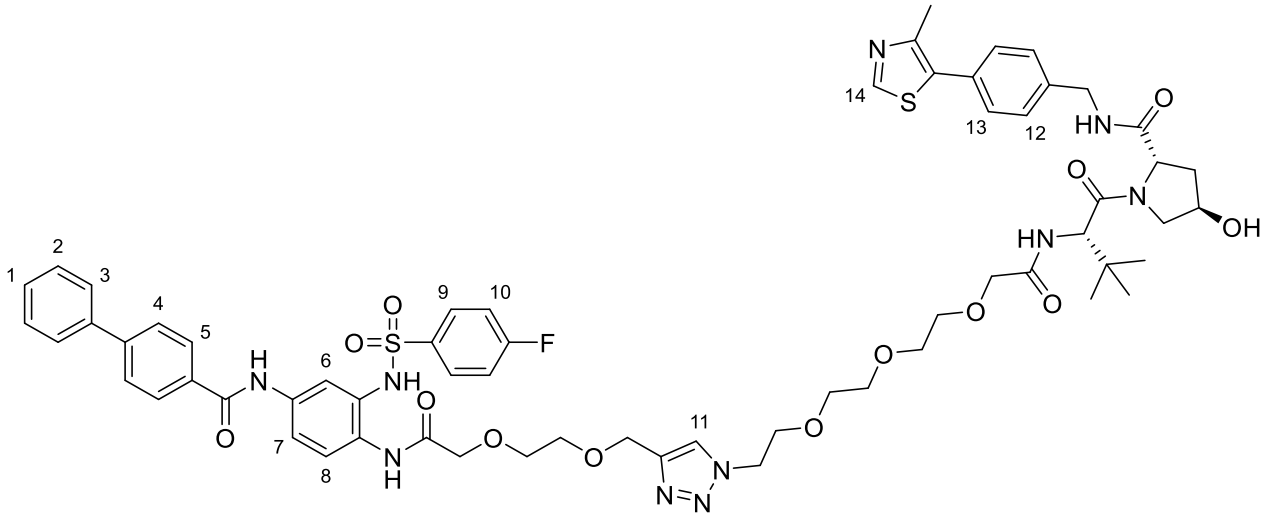

In a schlenk flask under Ar, STING inhibitor alkyne **64** (12 mg, 20 µmol, 1.00 eq), **VHL3** recruiter azide (13 mg, 20 µmol, 1.00 eq), TBTA (11 mg, 20 µmol, 1.00 eq) and CuBr (1 mg, 10 µmol, 0.50 eq) were dissolved in dry and degassed DMF (0.5 mL) and stirred at 50 °C for 2 hours during which the solution turned dark brown. After this time, the solvent was removed under reduced vacuum and the residue treated with a saturated solution of NH_4Cl (10 mL), extracted with EtOAc (3 x 20 mL). The combined organic phase was dried over Na_2SO_4, washed with brine and concentrated *in vacuo.* The crude was

purified via preparative HPLC (isocratic 40 % B for 10 minutes + 40 to 50 % B in 10 minutes. Buffer A = H_2O + 0.1 % TFA, buffer B = MeCN + 0.1 % TFA) to obtain the desired product **112** (22 mg, 18 µmol, 88 %) as a pale yellow solid.

^{1}H NMR (500 MHz, MeCN): δ (ppm) = 9.23 (s, 1H, NH), 9.03 (s, 1H, HN), 8.99 (s, 1H, NH), 8.69 (s, 1H, NH), 7.98 – 7.93 (m, 2H, H-5), 7.87 (s, 1H, H-11), 7.78 – 7.73 (m, 2H, H-4), 7.73 – 7.67 (m, 4H, H-3 / H-9), 7.65 (d, J = 2.5 Hz, 1H, H-6), 7.57 (dd, J = 8.8, 2.4 Hz, 1H, H-8), 7.52 – 7.46 (m, 3H, H-1 / H-2), 7.44 – 7.32 (m, 6H, H-7 / H-12 / H-13 / H-14), 7.28 (d, J = 9.3 Hz, 1H, -OH), 7.25 – 7.17 (m, 2H, H-10), 4.65 (s, 2H), 4.61 (d, J = 9.4 Hz, 1H), 4.54 – 4.39 (m, 5H), 4.29 (dd, J = 15.8, 5.7 Hz, 1H), 3.99 (s, 2H), 3.94 (d, J = 1.8 Hz, 2H), 3.82 – 3.74 (m, 3H), 3.73 – 3.65 (m, 5H), 3.61 – 3.56 (m, 2H), 3.56 – 3.49 (m, 6H), 2.47 (s, 3H), 2.13 (ddt, J = 13.3, 7.7, 2.0 Hz, 1H), 2.04 (ddd, J = 13.2, 8.9, 4.4 Hz, 1H), 0.95 (s, 9H).

^{13}C NMR (126 MHz, MeCN): δ (ppm) = 173.05, 171.33, 170.70, 170.34, 167.25, 166.52, 165.24, 159.87, 159.56, 154.43, 145.12, 144.84, 144.73, 141.57, 140.61, 137.70, 136.62, 135.31, 134.45, 131.00, 130.92, 130.10, 130.03, 129.82, 129.19, 129.14, 129.10, 128.94, 128.82, 128.09, 127.94, 125.67, 124.84, 120.37, 120.24, 117.63, 117.43, 117.25, 115.34, 72.07, 71.90, 71.07, 70.93, 70.82, 70.76, 70.75, 70.17, 69.76, 64.50, 60.31, 57.76, 57.44, 51.21, 43.14, 38.51, 36.57, 26.70, 14.45.

HR-ESI-MS: m/z calc. for $[C_{62}H_{70}FN_{10}O_{13}S_2]^-$ $[M-H]^-$: 1245.45548, found: 1245.45572.

FT-IR: $\tilde{\nu}$ (cm^{-1}) = 2922.99 (w), 2872.70 (w), 2374.03 (w), 2313.68 (m), 1792.02 (w), 1771.90 (w), 1750.35 (w), 1734.54 (w), 1717.29 (m), 1684.24 (m), 1669.87 (s), 1654.06 (m), 1646.88 (m), 1636.82 (s), 1559.22 (s), 1540.54 (s), 1521.85 (m), 1507.48 (m), 1490.24 (m), 1457.19 (m), 1437.07 (m), 1418.38 (m), 1398.27 (m), 1339.35 (m), 1293.36 (m), 1228.69 (m), 1153.96 (m), 1090.73 (m), 1057.68 (m), 1007.38 (m), 911.10 (w), 837.81 (m), 819.13 (m), 745.84 (m), 698.41 (m), 668.24 (m), 566.20 (m), 544.65 (s), 458.42 (m), 402.38 (m).

Rf = 4.88 min (LC-MS: 5 to 80 % B in 7 min).

4.2.4.6 Inh-RNF5 STING PROTAC

STING Inhibitor – RNF5 recruiter (113)

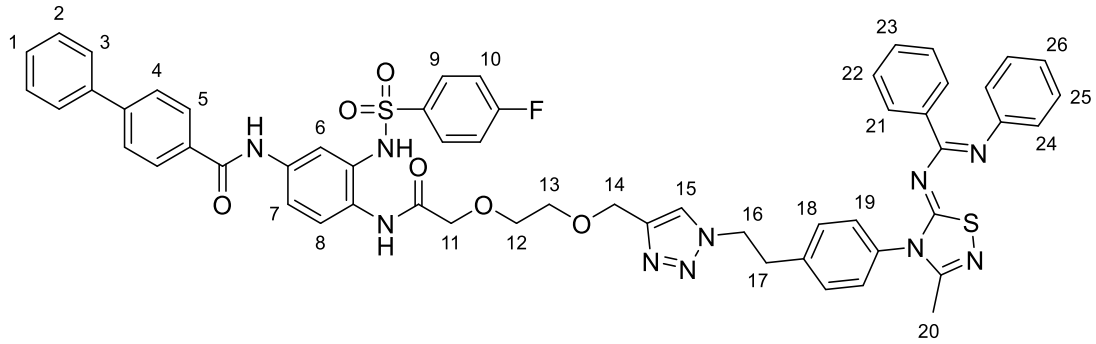

In a schlenk flask under Ar, STING inhibitor alkyne **64** (25 mg, 42 µmol, 1.00 eq), RNF5 recruiting azide **92** (24 mg, 54 µmol, 1.30 eq), TBTA (23 mg, 42 µmol, 1.00 eq) and CuBr (3 mg, 21 µmol, 0.50 eq) were dissolved in dry and degassed DMF (0.7 mL) and stirred at 50 °C for 2 hours. After this time, the solvent was removed under reduced vacuum and the residue treated with a saturated solution of NH_4Cl (10 mL), extracted with EtOAc (3 x 20 mL). The combined organic phase was dried over Na_2SO_4 and concentrated *in vacuo.* The crude was purified via silica gel column chromatography (0 to 5 % MeOH/DCM) to obtain the desired product **113** (42 mg, 40 µmol, 97 %) as a white solid.

^{1}H NMR (500 MHz, Acetone): δ (ppm) = 9.74 (s, 1H, NH), 9.20 (s, 1H, NH), 9.02 (s, 1H, NH), 8.09 – 8.06 (m, 2H, H-5), 7.85 (s, 1H, H-15), 7.82 (dd, J = 8.8, 2.5 Hz, 1H, H-6), 7.80 – 7.75 (m, 5H, H-3 / H-4 / H-8), 7.73 – 7.70 (m, 2H, H-9), 7.56 – 7.39 (m, 8H, H-7 / H-18 / H-19 / H-10 / H-1), 7.34 – 7.29 (m, 4H, H-2 / H-21), 7.27 – 7.20 (m, 3H, H-22 / H-23), 7.20 – 7.15 (m, 2H, H-25), 7.01 (tt, J = 7.4, 1.2 Hz, 1H, H-26), 6.80 – 6.75 (m, 2H, H-24), 4.75 (dd, J = 8.1, 6.8 Hz, 2H, H-16), 4.63 (s, 2H, H-14), 4.02 (s, 2H, H-11), 3.73 (dd, J = 6.2, 2.7 Hz, 2H, H-12), 3.71 – 3.67 (m, 2H, H-13), 3.34 (t, J = 7.4 Hz, 2H, H-17), 2.18 (s, 3H, H-20).

^{13}C NMR (126 MHz, Acetone): δ (ppm) = 172.68, 169.83, 169.75, 167.04, 165.90, 165.04, 159.84, 153.28, 148.02, 144.95, 144.83, 140.67, 140.21, 137.96, 137.19, 136.47, 135.93, 134.65, 130.96, 130.88, 130.80, 130.39, 130.13, 129.87, 129.83, 129.68, 129.16, 129.04, 128.93, 128.57, 127.92, 127.72, 124.62, 124.33, 123.83, 123.03, 120.30, 119.86, 117.24, 117.06, 72.02, 70.85, 69.82, 64.77, 51.52, 36.77, 17.24.

FT-IR: $\tilde{\nu}$ (cm^{-1}) = 2922.99 (m), 2852.58 (m), 2359.66 (s), 2343.86 (s), 1700.05 (w), 1684.24 (m), 1669.87 (m), 1654.06 (m), 1589.40 (m), 1576.46 (m), 1559.22 (m), 1540.54 (m), 1533.35 (s), 1516.11 (s), 1507.48 (s), 1497.42 (s), 1488.80 (m), 1472.99 (m), 1465.81 (m), 1457.19 (m), 1447.13 (w), 1418.38 (w), 1337.91 (m), 1293.36 (w), 1267.49 (m), 1166.90 (m), 1155.40 (m), 1090.73 (m), 1007.38 (w), 931.22 (w), 837.81 (w), 819.13 (w), 747.27 (m), 696.98 (m), 668.24 (s), 569.08 (m), 544.65 (m).

HR-ESI-MS: m/z calc. for $[C_{56}H_{48}FN_{10}O_6S_2]^-$ $[M-H]^-$: 1039.31892, found: 1039.31918.

Rf = 0.51 (4 % MeOH/DCM).

6 List of Abbreviations

AcOH	acetic acid
ADCC	antibody-dependent cell-mediated cytotoxicity
AGS	Aicardi-Goutières Syndrome
AIM2	absent in melanoma 2
ALS	amyotrophic lateral sclerosis
ALR	AIM2-like receptor
APC	antigen-presenting cell
AR	androgen receptor
Ar	aromatic
ATP	adenosine triphosphate
ATR	attenuated total reflection
Boc	tert-butyloxycarbonyl
BTT	benzylthio tetrazole
Bz	benzoyl
CD8	cluster of differentiation 8
CDN	cyclic dinucleotide

c-di-AMP	cyclic di-adenosine monophosphate
c-di-GMP	cyclic di-guanosine monophosphate
CES	carboxylesterase
cGAMP	cyclic guanosine monophosphate-adenosine monophosphate
cGAS	cyclic guanosine monophosphate-adenosine monophosphate synthase
CLR	C-type lectin receptor
cIAP	inhibitor of apoptosis protein
CIN	chromosomal instability
COP	coat protein complex
COSY	correlated spectroscopy
CRBN	cereblon
CTT	C-terminus tail
CuAAC	Cu(I)-catalysed azide-alkyne cycloaddition
CUL4	cullin-4
Cy3	Cyanine3®
DAMP	damage-associated molecular pattern
DDB1	damage specific DNA binding protein 1
DC	dendritic cell
DC_{50}	half maximal degrading concentration

DCA	dichloroacetic acid
DCC	*N*,*N*'-dicyclohexylcarbodiimide
DCM	dichloromethane
DCS	differential scanning calorimetry
DDR	DNA damage response
DEAD	diethyl azodicarboxylate
diABZI	diamidobenzimidazole
DMAP	4-dimethylaminopyridine
DMF	dimethylformamide
DMSO	dimethylsulfoxide
DMTr	4,4'-dimethoxytrityl
DMXAA	5,6-dimethylxanthenone-4-acetic acid
DNA	2'-deoxyribonucleic acid
DNase	deoxyribonuclease
DSC	differential scanning calorimetry
dsDNA	double stranded DNA
DSF	differential scanning fluorimetry
dsRNA	double stranded RNA
EC_{50}	half maximal effective concentration

EDC	1-ethyl-3-(3-dimethylaminopropyl)carbodiimide
EDTA	ethylenediaminetetraacetic acid
EI	electron ionization
ENPP1	ectonucleotide pyrophosphatase/phosphodiesterase 1
eq	equivalents
ER	endoplasmic reticulum / estrogen receptor
ERGIC	endoplasmic-reticulum-Golgi intermediate compartment
ESI	electrospray ionization
Et	ethyl
EtOAc	ethyl acetate
EtOH	ethanol
FA	fatty acids
FLS	fibroblast-like synoviocytes
FT-IR	fourier transform infrared
GTP	guanosine triphosphate
HDAcs	histone deacetylases
HIF	hypoxia-inducible factor
HIV	human immunodeficiency virus
HMBC	heteronuclear multiple bond correlation

HOBt	hydroxybenzotriazole
HPLC	high pressure liquid chromatography
HR-MS	high resolution mass spectroscopy
HSQC	heteronuclear single quantum coherence
hSTING	human STING
HSV	herpes simplex virus
HTS	high throughput screening
IAP	inhibitor of apoptosis protein
iBu	iso-butyryl
IC_{50}	half maximal inhibitory concentration
IDO	immune checkpoint indoleamine 2,3-dioxygenase
IFN	interferon
iHex	iso-hexane
IKK	I kappa B kinase
IL-6	interleukin 6
ILC	innate lymphoid cell
IMiDs	immunomodulatory drugs
Inh	inhibitor
IRAK	immune response interleukin-1 receptor-associated kinase

IRF	interferon regulatory factor
ISG	interferon-stimulated gene
ITC	isothermal titration calorimetry
K_D	dissociation constant
LBD	ligand binding domain
LC	liquid chromatography
LRRC8	leucine-rich repeat containing 8 family member A
MAPK	mitogen-activated protein kinase
MDA5	melanoma differentiation-associated protein 5
MDM2	mouse double minute 2
Me	methyl
MeCN	acetonitrile
MeOH	methanol
MetAP-2	methionine aminopeptidase 2
MHC	major histocompatibility complex
min	minutes
MOMP	mitochondrial outer membrane permeabilization
MS	mass spectrometry
MSNT	1-(mesitylene-2-sulfonyl)-3-nitro-1H-1,2,4-triazole

MSQ	mass single quadrupole
mSTING	mouse STING
mtDNA	mitochondrial DNA
NEt_3	triethylamine
NF-κB	nuclear factor kappa-light-chain-enhancer of activated B-cells
NK cell	natural killer cell
NLR	NOD-like receptor
NMR	nuclear magnetic resonance
NOD	nucleotide-binding oligomerization domain
NTase	nucleotidyltransferase
P2XR7	purinergic receptor P2X 7
PAMP	pathogen-associated molecular pattern
PEG	polyethylene glycol
PD-I	programmed cell death protein 1
Ph	phenyl
PIDA	phenyliodine(III) diacetate
PINK1	parkin and ubiquitin kinase
POI	protein of interest
Pom	pomalidomide

PPI	protein-protein interaction
PROTAC	proteolysis targeting chimera
PRR	pattern recognition receptor
Py	pyridine
RA	rheumatoid arthritis
RBX1	ring-box protein 1
RCC	renal cell carcinoma
Rf	retention factor
RIG-I	retinoic acid-inducible gene I
RIPk2	receptor interacting serine/threonine kinase 2
RLR	RIG-I-like receptor
RNA	ribonucleic acid
RNF5	RING finger protein 5
ROS	reactive oxygen species
RP	reversed phase
r.t.	room temperature
SAMHD1	SAM domain and HD domain-containing protein 1
SASP	senescence-associated secretory phenotype
SAR	structure-activity relationship

SAVI	STING-associated vasculopathy with onset of infancy
ssDNA	single stranded DNA
ssRNA	single stranded RNA
SLC19A1	solute carrier family 19 member 1
SLC46A2	solute carrier family 46 member 2
STAT1	signal transducer and activator of transcription 1
STING	stimulator of interferon genes
TAM	tumor associated macrophages
TBK1	TANK-binding kinase 1
TBDMS	*t*-butyldimethylsilyl
TBS	*t*-butyldimethylsilyl
TBTA	tris((1-benzyl-4-triazolyl)methyl)amine
***t*Bu**	*t*-butyl
***t*BuOOH**	*t*-butylhydroperoxide
TDP43	transactive response DNA-binding protein 43
TEAA	triethylammonium acetate
Tf	triflate
TFA	trifluoroacetic acid
TFAM	transcription factor A mitochondrial

THF	tetrahydrofuran
THP-1	human leukaemia monocytic cell line
THPTA	tris-hydroxypropyltriazolylmethylamine
TLC	thin-layer chromatography
TLR	Toll-like receptor
TME	tumour microenvironment
TMS	trimethylsilyl
Tos	tosyl
TPD	targeted protein degradation
Treg	regulatory T cells
TREX	transcription and export complex
Ub	ubiquitin
UHPLC	ultra-high performance liquid chromatography
UPS	ubiquitin-proteasome system
UV-vis	ultra violet – visible
VBC	VHL-elongin B-elongin C
VHL	Von-Hippel Lindau

7 Literature

1. Danilova, N. The Evolution of Adaptive Immunity. In *Self and Nonself*, López-Larrea, C., (ed.) Springer US, New York, NY, (2012), pp 218-235.

2. Boehm, T. & Swann, J. B. Origin and evolution of adaptive immunity. *Annu. Rev. Anim. Biosci.* **2**, 259-283 (2014).

3. Netea, M. G. *et al.* Innate and Adaptive Immune Memory: an Evolutionary Continuum in the Host's Response to Pathogens. *Cell Host Microbe* **25**, 13-26 (2019).

4. Chaplin, D. D. Overview of the immune response. *J. Allergy Clin. Immunol.* **125**, S3-23 (2010).

5. Paludan, S. R. *et al.* Constitutive immune mechanisms: mediators of host defence and immune regulation. *Nat. Rev. Immunol.* **21**, 137-150 (2021).

6. Medzhitov, R. Origin and physiological roles of inflammation. *Nature* **454**, 428-435 (2008).

7. Schroder, K. & Tschopp, J. The inflammasomes. *Cell* **140**, 821-832 (2010).

8. Vesely, M. D. *et al.* Natural innate and adaptive immunity to cancer. *Annu. Rev. Immunol.* **29**, 235-271 (2011).

9. Netea, M. G. *et al.* Innate and Adaptive Immune Memory: an Evolutionary Continuum in the Host's Response to Pathogens. *Cell Host Microbe* **25**, 13-26 (2019).

10. McNab, F. *et al.* Type I interferons in infectious disease. *Nat. Rev. Immunol.* **15**, 87-103 (2015).

11. Negishi, H., Taniguchi, T. & Yanai, H. The Interferon (IFN) Class of Cytokines and the IFN Regulatory Factor (IRF) Transcription Factor Family. *Cold Spring Harb. Perspect. Biol.* **10**, (2018).

12. Dunn, G. P. *et al.* A critical function for type I interferons in cancer immunoediting. *Nat. Immunol.* **6**, 722-729 (2005).

13. Janeway, C. A., Jr. Approaching the asymptote? Evolution and revolution in immunology. *Cold Spring Harb. Symp. Quant. Biol.* **54 Pt 1**, 1-13 (1989).

14. Silva-Gomes, S., Decout, A. & Nigou, J. Pathogen-Associated Molecular Patterns (PAMPs). In *Encyclopedia of Inflammatory Diseases*, Parnham, M., (ed.) Springer Basel, Basel, (2015), pp 1-16.

15. Roh, J. S. & Sohn, D. H. Damage-Associated Molecular Patterns in Inflammatory Diseases. *Immune Netw.* **18**, (2018).

16. Tang, D. *et al.* PAMPs and DAMPs: signal 0s that spur autophagy and immunity. *Immunol. Rev.* **249**, 158-175 (2012).

17. Johnson, G. L. & Lapadat, R. Mitogen-activated protein kinase pathways mediated by ERK, JNK, and p38 protein kinases. *Science* **298**, 1911-1912 (2002).

18. Lawrence, T. The nuclear factor NF-kappaB pathway in inflammation. *Cold Spring Harb. Perspect. Biol.* **1**, a001651 (2009).

19. Ysebrant de Lendonck, L., Martinet, V. & Goriely, S. Interferon regulatory factor 3 in adaptive immune responses. *Cell Mol. Life Sci.* **71**, 3873-3883 (2014).

20. Okude, H., Ori, D. & Kawai, T. Signaling Through Nucleic Acid Sensors and Their Roles in Inflammatory Diseases. *Front. Immunol.* **11**, (2021).

21. Roers, A., Hiller, B. & Hornung, V. Recognition of Endogenous Nucleic Acids by the Innate Immune System. *Immunity* **44**, 739-754 (2016).

22. Barnett, K. C. *et al.* Phosphoinositide Interactions Position cGAS at the Plasma Membrane to Ensure Efficient Distinction between Self- and Viral DNA. *Cell* **176**, 1432-1446.e1411 (2019).

23. Civril, F. *et al.* Structural mechanism of cytosolic DNA sensing by cGAS. *Nature* **498**, 332-337 (2013).

24. Kranzusch, P. J. *et al.* Structure of human cGAS reveals a conserved family of second-messenger enzymes in innate immunity. *Cell Rep.* **3**, 1362-1368 (2013).

25. Li, X. *et al.* Cyclic GMP-AMP synthase is activated by double-stranded DNA-induced oligomerization. *Immunity* **39**, 1019-1031 (2013).

26. Zhang, X. *et al.* The cytosolic DNA sensor cGAS forms an oligomeric complex with DNA and undergoes switch-like conformational changes in the activation loop. *Cell Rep.* **6**, 421-430 (2014).

27. Gao, P. *et al.* Cyclic [G(2',5')pA(3',5')p] Is the Metazoan Second Messenger Produced by DNA-Activated Cyclic GMP-AMP Synthase. *Cell* **153**, 1094-1107 (2013).

28. Andreeva, L. *et al.* cGAS senses long and HMGB/TFAM-bound U-turn DNA by forming protein–DNA ladders. *Nature* **549**, 394-398 (2017).

29. Du, M. & Chen, Z. J. DNA-induced liquid phase condensation of cGAS activates innate immune signaling. *Science* **361**, 704-709 (2018).

30. Zhang, X. *et al.* Cyclic GMP-AMP containing mixed phosphodiester linkages is an endogenous high-affinity ligand for STING. *Mol. Cell* **51**, 226-235 (2013).

31. Diner, E. J. *et al.* The innate immune DNA sensor cGAS produces a noncanonical cyclic dinucleotide that activates human STING. *Cell Rep.* **3**, 1355-1361 (2013).

32. Ishikawa, H., Ma, Z. & Barber, G. N. STING regulates intracellular DNA-mediated, type I interferon-dependent innate immunity. *Nature* **461**, 788-792 (2009).

33. Ishikawa, H. & Barber, G. N. STING is an endoplasmic reticulum adaptor that facilitates innate immune signalling. *Nature* **455**, 674-678 (2008).

34. Yin, Q. *et al.* Cyclic di-GMP Sensing via the Innate Immune Signaling Protein STING. *Mol. Cell* **46**, 735-745 (2012).

35. Shang, G. *et al.* Crystal structures of STING protein reveal basis for recognition of cyclic di-GMP. *Nat. Struct. Mol. Biol.* **19**, 725-727 (2012).

36. Ouyang, S. *et al.* Structural analysis of the STING adaptor protein reveals a hydrophobic dimer interface and mode of cyclic di-GMP binding. *Immunity* **36**, 1073-1086 (2012).

37. Shang, G. *et al.* Cryo-EM structures of STING reveal its mechanism of activation by cyclic GMP–AMP. *Nature* **567**, 389-393 (2019).

38. Zhang, X. *et al.* Cyclic GMP-AMP Containing Mixed Phosphodiester Linkages Is An Endogenous High-Affinity Ligand for STING. *Mol. Cell* **51**, 226-235 (2013).

39. Ergun, S. L. *et al.* STING Polymer Structure Reveals Mechanisms for Activation, Hyperactivation, and Inhibition. *Cell* **178**, 290-301.e210 (2019).

40. Dobbs, N. *et al.* STING Activation by Translocation from the ER Is Associated with Infection and Autoinflammatory Disease. *Cell Host Microbe* **18**, 157-168 (2015).

41. Mukai, K. *et al.* Activation of STING requires palmitoylation at the Golgi. *Nat. Commun.* **7**, 11932 (2016).

42. Zhao, B. *et al.* A conserved PLPLRT/SD motif of STING mediates the recruitment and activation of TBK1. *Nature* **569**, 718-722 (2019).

43. Zhang, C. *et al.* Structural basis of STING binding with and phosphorylation by TBK1. *Nature* **567**, 394-398 (2019).

44. Mukai, K. *et al.* Homeostatic regulation of STING by retrograde membrane traffic to the ER. *Nat. Commun.* **12**, 61 (2021).

45. Gonugunta, V. K. *et al.* Trafficking-Mediated STING Degradation Requires Sorting to Acidified Endolysosomes and Can Be Targeted to Enhance Anti-tumor Response. *Cell Rep.* **21**, 3234-3242 (2017).

46. Zhong, B. *et al.* The ubiquitin ligase RNF5 regulates antiviral responses by mediating degradation of the adaptor protein MITA. *Immunity* **30**, 397-407 (2009).

47. Abe, T. & Barber, G. N. Cytosolic-DNA-mediated, STING-dependent proinflammatory gene induction necessitates canonical NF-κB activation through TBK1. *J. Virol.* **88**, 5328-5341 (2014).

48. Dunphy, G. *et al.* Non-canonical Activation of the DNA Sensing Adaptor STING by ATM and IFI16 Mediates NF-κB Signaling after Nuclear DNA Damage. *Mol. Cell* **71**, 745-760.e745 (2018).

49. Gui, X. *et al.* Autophagy induction via STING trafficking is a primordial function of the cGAS pathway. *Nature* **567**, 262-266 (2019).

50. Glück, S. *et al.* Innate immune sensing of cytosolic chromatin fragments through cGAS promotes senescence. *Nat. Cell. Biol.* **19**, 1061-1070 (2017).

51. Gulen, M. F. *et al.* Signalling strength determines proapoptotic functions of STING. *Nat. Commun.* **8**, 427 (2017).

52. Petrasek, J. *et al.* STING-IRF3 pathway links endoplasmic reticulum stress with hepatocyte apoptosis in early alcoholic liver disease. *PNAS* **110**, 16544-16549 (2013).

53. Zierhut, C. *et al.* The Cytoplasmic DNA Sensor cGAS Promotes Mitotic Cell Death. *Cell* **178**, 302-315.e323 (2019).

54. Ablasser, A. *et al.* Cell intrinsic immunity spreads to bystander cells via the intercellular transfer of cGAMP. *Nature* **503**, 530-534 (2013).

55. Bridgeman, A. *et al.* Viruses transfer the antiviral second messenger cGAMP between cells. *Science* **349**, 1228-1232 (2015).

56. Gentili, M. *et al.* Transmission of innate immune signaling by packaging of cGAMP in viral particles. *Science* **349**, 1232-1236 (2015).

57. Ahn, J. *et al.* Extrinsic Phagocyte-Dependent STING Signaling Dictates the Immunogenicity of Dying Cells. *Cancer Cell* **33**, 862-873.e865 (2018).

58. Luteijn, R. D. *et al.* SLC19A1 transports immunoreactive cyclic dinucleotides. *Nature* **573**, 434-438 (2019).

59. Cordova, A. F. *et al.* Human SLC46A2 Is the Dominant cGAMP Importer in Extracellular cGAMP-Sensing Macrophages and Monocytes. *ACS Cent Sci* **7**, 1073-1088 (2021).

60. Zhou, Y. *et al.* Blockade of the Phagocytic Receptor MerTK on Tumor-Associated Macrophages Enhances P2X7R-Dependent STING Activation by Tumor-Derived cGAMP. *Immunity* **52**, 357-373.e359 (2020).

61. Lahey, L. J. *et al.* The LRRC8A:C Heteromeric Channel Is a cGAMP Transporter and the Dominant cGAMP Importer in Human Vasculature Cells. *bioRxiv*, 2020.2002.2013.948273 (2020).

62. Zhou, C. *et al.* Transfer of cGAMP into Bystander Cells via LRRC8 Volume-Regulated Anion Channels Augments STING-Mediated Interferon Responses and Anti-viral Immunity. *Immunity* **52**, 767-781.e766 (2020).

63. Maltbaek, J. H., Snyder, J. M. & Stetson, D. B. ABCC1/MRP1 exports cGAMP and modulates cGAS-dependent immunity. *bioRxiv*, 2021.2012.2003.470980 (2021).

64. Li, L. *et al.* Hydrolysis of 2'3'-cGAMP by ENPP1 and design of nonhydrolyzable analogs. *Nat. Chem. Biol.* **10**, 1043-1048 (2014).

65. Eaglesham, J. B. *et al.* Viral and metazoan poxins are cGAMP-specific nucleases that restrict cGAS–STING signalling. *Nature* **566**, 259-263 (2019).

66. Collins, A. C. *et al.* Cyclic GMP-AMP Synthase Is an Innate Immune DNA Sensor for Mycobacterium tuberculosis. *Cell Host Microbe* **17**, 820-828 (2015).

67. Watson, R. O. *et al.* The Cytosolic Sensor cGAS Detects Mycobacterium tuberculosis DNA to Induce Type I Interferons and Activate Autophagy. *Cell Host Microbe* **17**, 811-819 (2015).

68. Hansen, K. *et al.* Listeria monocytogenes induces IFNβ expression through an IFI16-, cGAS- and STING-dependent pathway. *Embo J.* **33**, 1654-1666 (2014).

69. Woodward, J. J., Iavarone, A. T. & Portnoy, D. A. c-di-AMP secreted by intracellular Listeria monocytogenes activates a host type I interferon response. *Science* **328**, 1703-1705 (2010).

70. Gao, D. *et al.* Cyclic GMP-AMP Synthase Is an Innate Immune Sensor of HIV and Other Retroviruses. *Science* **341**, 903-906 (2013).

71. Lio, C. W. *et al.* cGAS-STING Signaling Regulates Initial Innate Control of Cytomegalovirus Infection. *J. Virol.* **90**, 7789-7797 (2016).

72. Paijo, J. *et al.* cGAS Senses Human Cytomegalovirus and Induces Type I Interferon Responses in Human Monocyte-Derived Cells. *PLoS Pathog.* **12**, e1005546 (2016).

73. Li, X. D. *et al.* Pivotal roles of cGAS-cGAMP signaling in antiviral defense and immune adjuvant effects. *Science* **341**, 1390-1394 (2013).

74. West, A. P. *et al.* Mitochondrial DNA stress primes the antiviral innate immune response. *Nature* **520**, 553-557 (2015).

75. Wiens, K. E. & Ernst, J. D. The Mechanism for Type I Interferon Induction by Mycobacterium tuberculosis is Bacterial Strain-Dependent. *PLoS Pathog.* **12**, e1005809 (2016).

76. Aguirre, S. *et al.* Dengue virus NS2B protein targets cGAS for degradation and prevents mitochondrial DNA sensing during infection. *Nat. Microbiol.* **2**, 17037 (2017).

77. Zeng, L. *et al.* ALK is a therapeutic target for lethal sepsis. *Sci. Transl. Med.* **9**, eaan5689 (2017).

78. Dou, Z. *et al.* Cytoplasmic chromatin triggers inflammation in senescence and cancer. *Nature* **550**, 402-406 (2017).

79. Ivanov, A. *et al.* Lysosome-mediated processing of chromatin in senescence. *J. Cell. Biol.* **202**, 129-143 (2013).

80. Harding, S. M. *et al.* Mitotic progression following DNA damage enables pattern recognition within micronuclei. *Nature* **548**, 466-470 (2017).

81. Mackenzie, K. J. *et al.* cGAS surveillance of micronuclei links genome instability to innate immunity. *Nature* **548**, 461-465 (2017).

82. Kwon, J. & Bakhoum, S. F. The Cytosolic DNA-Sensing cGAS-STING Pathway in Cancer. *Cancer Discov.* **10**, 26-39 (2020).

83. Bernsmeier, C., van der Merwe, S. & Périanin, A. Innate immune cells in cirrhosis. *J. Hepatol.* **73**, 186-201 (2020).

84. Bruns, H. *et al.* Vitamin D-dependent induction of cathelicidin in human macrophages results in cytotoxicity against high-grade B cell lymphoma. *Sci. Transl. Med.* **7**, 282ra247 (2015).

85. Cunha, L. D. *et al.* LC3-Associated Phagocytosis in Myeloid Cells Promotes Tumor Immune Tolerance. *Cell* **175**, 429-441.e416 (2018).

86. Noy, R. & Pollard, Jeffrey W. Tumor-Associated Macrophages: From Mechanisms to Therapy. *Immunity* **41**, 49-61 (2014).

87. Zhang, Y. *et al.* Identification of α-Mangostin as an Agonist of Human STING. *ChemMedChem* **13**, 2057-2064 (2018).

88. Farhood, B., Najafi, M. & Mortezaee, K. CD8(+) cytotoxic T lymphocytes in cancer immunotherapy: A review. *J. Cell. Physiol.* **234**, 8509-8521 (2019).

89. Kurachi, M. CD8+ T cell exhaustion. *Semin. Immunopathol.* **41**, 327-337 (2019).

90. Dimeloe, S. *et al.* T-cell metabolism governing activation, proliferation and differentiation; a modular view. *Immunology* **150**, 35-44 (2017).

91. Woo, S. R. *et al.* STING-dependent cytosolic DNA sensing mediates innate immune recognition of immunogenic tumors. *Immunity* **41**, 830-842 (2014).

92. Fuertes, M. B. *et al.* Host type I IFN signals are required for antitumor CD8+ T cell responses through CD8{alpha}+ dendritic cells. *J. Exp. Med.* **208**, 2005-2016 (2011).

93. An, X. *et al.* An Analysis of the Expression and Association with Immune Cell Infiltration of the cGAS/STING Pathway in Pan-Cancer. *Mol. Ther. Nucleic Acids* **14**, 80-89 (2019).

94. Padovan, E. *et al.* IFN-alpha2a induces IP-10/CXCL10 and MIG/CXCL9 production in monocyte-derived dendritic cells and enhances their capacity to attract and stimulate CD8+ effector T cells. *J. Leukoc. Biol.* **71**, 669-676 (2002).

95. Marcus, A. *et al.* Tumor-Derived cGAMP Triggers a STING-Mediated Interferon Response in Non-tumor Cells to Activate the NK Cell Response. *Immunity* **49**, 754-763.e754 (2018).

96. Zheng, J. *et al.* Comprehensive elaboration of the cGAS-STING signaling axis in cancer development and immunotherapy. *Mol. Cancer* **19**, 133 (2020).

97. Bakhoum, S. F. *et al.* Chromosomal instability drives metastasis through a cytosolic DNA response. *Nature* **553**, 467-472 (2018).

98. Cheng, A. N. *et al.* Mitochondrial Lon-induced mtDNA leakage contributes to PD-L1–mediated immunoescape via STING-IFN signaling and extracellular vesicles. *J. Immunother. Cancer.* **8**, e001372 (2020).

99. Harlin, H. *et al.* Chemokine Expression in Melanoma Metastases Associated with CD8+ T-Cell Recruitment. *Cancer Res.* **69**, 3077-3085 (2009).

100. Tas, S. W. *et al.* Noncanonical NF-κB signaling in dendritic cells is required for indoleamine 2,3-dioxygenase (IDO) induction and immune regulation. *Blood* **110**, 1540-1549 (2007).

101. Lemos, H. *et al.* STING Promotes the Growth of Tumors Characterized by Low Antigenicity via IDO Activation. *Cancer Res.* **76**, 2076-2081 (2016).

102. Li, J. *et al.* Metastasis and Immune Evasion from Extracellular cGAMP Hydrolysis. *Cancer Discov.* **11**, 1212-1227 (2021).

103. Vijayan, D. *et al.* Targeting immunosuppressive adenosine in cancer. *Nat. Rev. Cancer* **17**, 709-724 (2017).

104. Gulen, M. F. *et al.* Signalling strength determines proapoptotic functions of STING. *Nat. Commun.* **8**, 427 (2017).

105. Wu, J. *et al.* Interferon-Independent Activities of Mammalian STING Mediate Antiviral Response and Tumor Immune Evasion. *Immunity* **53**, 115-126.e115 (2020).

106. Concepcion, A. R. *et al.* The volume-regulated anion channel LRRC8C suppresses T cell function by regulating cyclic dinucleotide transport and STING–p53 signaling. *Nat. Immunol.* **23**, 287-302 (2022).

107. Jneid, B. *et al.* Cellular selectivity of STING stimulation determines priming of anti-tumor T cell responses. *bioRxiv*, 2021.2012.2001.469893 (2021).

108. Samson, N. & Ablasser, A. The cGAS–STING pathway and cancer. *Nat. Cancer* **3**, 1452-1463 (2022).

109. te Poele, R. H. *et al.* DNA damage is able to induce senescence in tumor cells in vitro and in vivo. *Cancer Res.* **62**, 1876-1883 (2002).

110. Childs, B. G. *et al.* Cellular senescence in aging and age-related disease: from mechanisms to therapy. *Nat. Med.* **21**, 1424-1435 (2015).

111. Kuilman, T. & Peeper, D. S. Senescence-messaging secretome: SMS-ing cellular stress. *Nat. Rev. Cancer* **9**, 81-94 (2009).

112. Sagiv, A. & Krizhanovsky, V. Immunosurveillance of senescent cells: the bright side of the senescence program. *Biogerontology* **14**, 617-628 (2013).

113. Song, P., An, J. & Zou, M.-H. Immune Clearance of Senescent Cells to Combat Ageing and Chronic Diseases. *Cells* **9**, 671 (2020).

114. Baker, D. J. *et al.* Naturally occurring p16Ink4a-positive cells shorten healthy lifespan. *Nature* **530**, 184-189 (2016).

115. Freund, A. *et al.* Lamin B1 loss is a senescence-associated biomarker. *Mol. Biol. Cell* **23**, 2066-2075 (2012).

116. Liu, Y. *et al.* Activated STING in a vascular and pulmonary syndrome. *N. Engl. J. Med.* **371**, 507-518 (2014).

117. Lin, B. *et al.* Case Report: Novel SAVI-Causing Variants in STING1 Expand the Clinical Disease Spectrum and Suggest a Refined Model of STING Activation. *Front. Immunol.* **12**, (2021).

118. Wang, Y., Wang, F. & Zhang, X. STING-associated vasculopathy with onset in infancy: a familial case series report and literature review. *Ann. Transl. Med.* **9**, 176 (2021).

119. David, C. & Frémond, M. L. Lung Inflammation in STING-Associated Vasculopathy with Onset in Infancy (SAVI). *Cells* **11**, (2022).

120. Hansen, A. L. *et al.* Nitro-fatty acids are formed in response to virus infection and are potent inhibitors of STING palmitoylation and signaling. *PNAS* **115**, E7768-e7775 (2018).

121. Hong, Z. *et al.* STING inhibitors target the cyclic dinucleotide binding pocket. *PNAS* **118**, e2105465118 (2021).

122. Stetson, D. B. *et al.* Trex1 Prevents Cell-Intrinsic Initiation of Autoimmunity. *Cell* **134**, 587-598 (2008).

123. Park, K. *et al.* Aicardi-Goutières syndrome-associated gene SAMHD1 preserves genome integrity by preventing R-loop formation at transcription-replication conflict regions. *PLoS Genet.* **17**, e1009523 (2021).

124. Mackenzie, K. J. *et al.* Ribonuclease H2 mutations induce a cGAS/STING-dependent innate immune response. *Embo J.* **35**, 831-844 (2016).

125. Rodero, M. P. *et al.* Type I interferon-mediated autoinflammation due to DNase II deficiency. *Nat. Commun.* **8**, 2176 (2017).

126. Gall, A. *et al.* Autoimmunity initiates in nonhematopoietic cells and progresses via lymphocytes in an interferon-dependent autoimmune disease. *Immunity* **36**, 120-131 (2012).

127. Gao, D. *et al.* Activation of cyclic GMP-AMP synthase by self-DNA causes autoimmune diseases. *PNAS* **112**, E5699-E5705 (2015).

128. Gray, E. E. *et al.* Cutting Edge: cGAS Is Required for Lethal Autoimmune Disease in the Trex1-Deficient Mouse Model of Aicardi-Goutières Syndrome. *J. Immunol.* **195**, 1939-1943 (2015).

129. Deng, Z. *et al.* A defect in COPI-mediated transport of STING causes immune dysregulation in COPA syndrome. *J. Exp. Med.* **217**, (2020).

130. Lepelley, A. *et al.* Mutations in COPA lead to abnormal trafficking of STING to the Golgi and interferon signaling. *J. Exp. Med.* **217**, (2020).

131. Steiner, A. *et al.* Activation of STING due to COPI-deficiency. *bioRxiv*, 2020.2007.2009.194399 (2020).

132. Namjou, B. *et al.* Evaluation of the TREX1 gene in a large multi-ancestral lupus cohort. *Genes Immun.* **12**, 270-279 (2011).

133. Günther, C. *et al.* Defective removal of ribonucleotides from DNA promotes systemic autoimmunity. *J. Clin. Investig.* **125**, 413-424 (2015).

134. You, S. *et al.* Review: The Tumor-Like Phenotype of Rheumatoid Synovium: Molecular Profiling and Prospects for Precision Medicine. *Arthritis Rheumatol.* **70**, 637-652 (2018).

135. Li, R. *et al.* cGAS/STING signaling in the regulation of rheumatoid synovial aggression. *Ann. Transl. Med.* **10**, 431 (2022).

136. Glass, C. K. *et al.* Mechanisms underlying inflammation in neurodegeneration. *Cell* **140**, 918-934 (2010).

137. Yu, C. H. *et al.* TDP-43 Triggers Mitochondrial DNA Release via mPTP to Activate cGAS/STING in ALS. *Cell* **183**, 636-649.e618 (2020).

138. Sliter, D. A. *et al.* Parkin and PINK1 mitigate STING-induced inflammation. *Nature* **561**, 258-262 (2018).

139. Bozner, P. *et al.* The amyloid beta protein induces oxidative damage of mitochondrial DNA. *J. Neuropathol. Exp. Neurol.* **56**, 1356-1362 (1997).

140. Moya, G. E., Rivera, P. D. & Dittenhafer-Reed, K. E. Evidence for the Role of Mitochondrial DNA Release in the Inflammatory Response in Neurological Disorders. *Int. J. Mol. Sci.* **22**, 7030 (2021).

141. Xie, X. *et al.* Activation of innate immune cGAS-STING pathway contributes to Alzheimer's pathogenesis in 5×FAD mice. *Nat. Aging* **3**, 202-212 (2023).

142. Baguley, B. C. & Ching, L. M. DMXAA: an antivascular agent with multiple host responses. *Int. J. Radiat. Oncol. Biol. Phys.* **54**, 1503-1511 (2002).

143. Lara, P. N., Jr. *et al.* Randomized phase III placebo-controlled trial of carboplatin and paclitaxel with or without the vascular disrupting agent vadimezan (ASA404) in advanced non-small-cell lung cancer. *J. Clin. Oncol.* **29**, 2965-2971 (2011).

144. Conlon, J. *et al.* Mouse, but not human STING, binds and signals in response to the vascular disrupting agent 5,6-dimethylxanthenone-4-acetic acid. *J. Immunol.* **190**, 5216-5225 (2013).

145. Kim, S. *et al.* Anticancer flavonoids are mouse-selective STING agonists. *ACS Chem Biol* **8**, 1396-1401 (2013).

146. Cavlar, T. *et al.* Species-specific detection of the antiviral small-molecule compound CMA by STING. *Embo J.* **32**, 1440-1450 (2013).

147. Xu, N. *et al.* STING agonist promotes CAR T cell trafficking and persistence in breast cancer. *J. Exp. Med.* **218**, (2020).

148. Ramanjulu, J. M. *et al.* Design of amidobenzimidazole STING receptor agonists with systemic activity. *Nature* **564**, 439-443 (2018).

149. Xi, Q. *et al.* Design, Synthesis, and Biological Evaluation of Amidobenzimidazole Derivatives as Stimulator of Interferon Genes (STING) Receptor Agonists. *J. Med. Chem.* **63**, 260-282 (2020).

150. Kong, X. *et al.* STING as an emerging therapeutic target for drug discovery: Perspectives from the global patent landscape. *J. Adv. Res.* **44**, 119-133 (2023).

151. Iannitti, T., Morales-Medina, J. C. & Palmieri, B. Phosphorothioate oligonucleotides: effectiveness and toxicity. *Curr. Drug Targets* **15**, 663-673 (2014).

152. Johannes, L. & Lucchino, M. Current Challenges in Delivery and Cytosolic Translocation of Therapeutic RNAs. *Nucleic Acid Ther.* **28**, 178-193 (2018).

153. Fu, J. *et al.* STING agonist formulated cancer vaccines can cure established tumors resistant to PD-1 blockade. *Sci. Transl. Med.* **7**, 283ra252 (2015).

154. Dubensky, T. W., Jr. *et al.* Compositions and methods for activating "stimulator of interferon gene"-dependent signalling. WO2014189805A1, (2014).

155. Katibah, G. E. Compositions and Methods for Activating “Stimulator of Interferon Gene” - Dependent Signalling. WO2017075477A1, (2017).

156. Wiemer, A. J. & Wiemer, D. F. Prodrugs of phosphonates and phosphates: crossing the membrane barrier. *Top. Curr. Chem.* **360**, 115-160 (2015).

157. Pimková Polidarová, M. *et al.* Synthesis and Biological Evaluation of Phosphoester and Phosphorothioate Prodrugs of STING Agonist 3’,3’-c-Di(2’F,2’dAMP). *J. Med. Chem.* **64**, 7596-7616 (2021).

158. Smola, M. *et al.* Ligand Strain and Its Conformational Complexity Is a Major Factor in the Binding of Cyclic Dinucleotides to STING Protein. *Angew. Chem. Int. Ed.* **60**, 10172-10178 (2021).

159. Stazzoni, S. *et al.* Novel Poxin Stable cGAMP-Derivatives Are Remarkable STING Agonists. *Angew. Chem. Int. Ed.* **61**, e202207175 (2022).

160. Sivick, K. E. *et al.* Magnitude of Therapeutic STING Activation Determines CD8(+) T Cell-Mediated Anti-tumor Immunity. *Cell Rep.* **25**, 3074-3085.e3075 (2018).

161. Corrales, L. *et al.* Direct Activation of STING in the Tumor Microenvironment Leads to Potent and Systemic Tumor Regression and Immunity. *Cell Rep.* **11**, 1018-1030 (2015).

162. Kim, D. S. *et al.* E7766, a Macrocycle-Bridged Stimulator of Interferon Genes (STING) Agonist with Potent Pan-Genotypic Activity. *ChemMedChem* **16**, 1740-1743 (2021).

163. Lioux, T. *et al.* Design, Synthesis, and Biological Evaluation of Novel Cyclic Adenosine-Inosine Monophosphate (cAIMP) Analogs That Activate Stimulator of Interferon Genes (STING). *J. Med. Chem.* **59**, 10253-10267 (2016).

164. Zhang, Y. *et al.* Function of Protein S-Palmitoylation in Immunity and Immune-Related Diseases. *Front. Immunol.* **12**, 661202 (2021).

165. Haag, S. M. *et al.* Targeting STING with covalent small-molecule inhibitors. *Nature* **559**, 269-273 (2018).

166. Hansen, A. L. *et al.* Nitro-fatty acids are formed in response to virus infection and are potent inhibitors of STING palmitoylation and signaling. *PNAS* **115**, E7768-E7775 (2018).

167. Vinogradova, E. V. *et al.* An Activity-Guided Map of Electrophile-Cysteine Interactions in Primary Human T Cells. *Cell* **182**, 1009-1026.e1029 (2020).

168. Humphries, F. *et al.* Targeting STING oligomerization with small-molecule inhibitors. *PNAS* **120**, e2305420120 (2023).

169. Guo, J. *et al.* Distinct Dynamic and Conformational Features of Human STING in Response to 2'3'-cGAMP and c-di-GMP. *ChemBioChem* **20**, 1838-1847 (2019).

170. Li, S. *et al.* The Cyclopeptide Astin C Specifically Inhibits the Innate Immune CDN Sensor STING. *Cell Rep.* **25**, 3405-3421.e3407 (2018).

171. Siu, T. *et al.* Discovery of a Novel cGAMP Competitive Ligand of the Inactive Form of STING. *ACS Med. Chem. Lett.* **10**, 92-97 (2019).

172. Gao, J. *et al.* CDK inhibitor Palbociclib targets STING to alleviate autoinflammation. *EMBO Rep.* **23**, e53932 (2022).

173. Long, J. *et al.* Discovery of fusidic acid derivatives as novel STING inhibitors for treatment of sepsis. *Eur. J. Med. Chem.* **244**, 114814 (2022).

174. Ong, W. W. S. *et al.* STING antagonists, synthesized via Povarov–Doebner type multicomponent reaction. *RSC Med. Chem.* **14**, 1101-1113 (2023).

175. Chang, J. *et al.* Discovery of Novel STING Inhibitors Based on the Structure of the Mouse STING Agonist DMXAA. *Molecules* **28**, 2906 (2023).

176. Chen, Y. *et al.* Gelsevirine is a novel STING-specific inhibitor and mitigates STING-related inflammation in sepsis. *Front. Immunol.* **14**, 1190707 (2023).

177. Yao, T. *et al.* Recent Advances in PROTACs for Drug Targeted Protein Research. *Int. J. Mol. Sci.* **23**, (2022).

178. Kelm, J. M. *et al.* PROTAC'ing oncoproteins: targeted protein degradation for cancer therapy. *Mol. Cancer* **22**, 62 (2023).

179. Jackson, M. P. & Hewitt, E. W. Cellular proteostasis: degradation of misfolded proteins by lysosomes. *Essays Biochem.* **60**, 173-180 (2016).

180. Nandi, D. *et al.* The ubiquitin-proteasome system. *J. Biosci.* **31**, 137-155 (2006).

181. Vijay-Kumar, S., Bugg, C. E. & Cook, W. J. Structure of ubiquitin refined at 1.8 A resolution. *J. Mol. Biol.* **194**, 531-544 (1987).

182. Livneh, I. *et al.* The life cycle of the 26S proteasome: from birth, through regulation and function, and onto its death. *Cell Res.* **26**, 869-885 (2016).

183. Willems, A. R., Schwab, M. & Tyers, M. A hitchhiker's guide to the cullin ubiquitin ligases: SCF and its kin. *Biochim. Biophys. Acta* **1695**, 133-170 (2004).

184. Swatek, K. N. & Komander, D. Ubiquitin modifications. *Cell Res.* **26**, 399-422 (2016).

185. Buckley, D. L. & Crews, C. M. Small-Molecule Control of Intracellular Protein Levels through Modulation of the Ubiquitin Proteasome System. *Angew. Chem. Int. Ed.* **53**, 2312-2330 (2014).

186. Douglass, E. F., Jr. *et al.* A comprehensive mathematical model for three-body binding equilibria. *J. Am. Chem. Soc.* **135**, 6092-6099 (2013).

187. Roy, R. D., Rosenmund, C. & Stefan, M. I. Cooperative binding mitigates the high-dose hook effect. *BMC Syst. Biol.* **11**, 74 (2017).

188. Pettersson, M. & Crews, C. M. PROteolysis TArgeting Chimeras (PROTACs) - Past, present and future. *Drug Discov. Today Technol.* **31**, 15-27 (2019).

189. Adjei, A. A. What is the right dose? The elusive optimal biologic dose in phase I clinical trials. *J. Clin. Oncol.* **24**, 4054-4055 (2006).

190. Tanaka, N. *et al.* Clinical Acquired Resistance to KRAS(G12C) Inhibition through a Novel KRAS Switch-II Pocket Mutation and Polyclonal Alterations Converging on RAS-MAPK Reactivation. *Cancer Discov.* **11**, 1913-1922 (2021).

191. Dang, C. V. *et al.* Drugging the 'undruggable' cancer targets. *Nat. Rev. Cancer* **17**, 502-508 (2017).

192. Oprea, T. I. *et al.* Unexplored therapeutic opportunities in the human genome. *Nat. Rev. Drug Discov.* **17**, 317-332 (2018).

193. Pathmanathan, S. *et al.* Drugging the undruggable proteins in cancer: A systems biology approach. *Curr. Opin. Chem. Biol.* **66**, 102079 (2022).

194. Burslem, G. M. *et al.* The Advantages of Targeted Protein Degradation Over Inhibition: An RTK Case Study. *Cell Chem. Biol.* **25**, 67-77.e63 (2018).

195. Smith, B. E. *et al.* Differential PROTAC substrate specificity dictated by orientation of recruited E3 ligase. *Nat. Commun.* **10**, 131 (2019).

196. Burke, M. R., Smith, A. R. & Zheng, G. Overcoming Cancer Drug Resistance Utilizing PROTAC Technology. *Front. Cell Dev. Biol.* **10**, (2022).

197. Bondeson, D. P. *et al.* Catalytic in vivo protein knockdown by small-molecule PROTACs. *Nat. Chem. Biol.* **11**, 611-617 (2015).

198. Salami, J. *et al.* Androgen receptor degradation by the proteolysis-targeting chimera ARCC-4 outperforms enzalutamide in cellular models of prostate cancer drug resistance. *Commun. Biol.* **1**, 100 (2018).

199. Montgomery, R. B. *et al.* Maintenance of intratumoral androgens in metastatic prostate cancer: a mechanism for castration-resistant tumor growth. *Cancer Res.* **68**, 4447-4454 (2008).

200. Pei, H. *et al.* Small molecule PROTACs: an emerging technology for targeted therapy in drug discovery. *RSC Adv.* **9**, 16967-16976 (2019).

201. Sun, X. *et al.* PROTACs: great opportunities for academia and industry. *Signal Transduct. Target. Ther.* **4**, 64 (2019).

202. Cecchini, C. *et al.* From Conception to Development: Investigating PROTACs Features for Improved Cell Permeability and Successful Protein Degradation. *Front. Chem.* **9**, 672267 (2021).

203. Kiely-Collins, H., Winter, G. E. & Bernardes, G. J. L. The role of reversible and irreversible covalent chemistry in targeted protein degradation. *Cell Chem. Biol.* **28**, 952-968 (2021).

204. Mares, A. *et al.* Extended pharmacodynamic responses observed upon PROTAC-mediated degradation of RIPK2. *Commun. Biol.* **3**, 140 (2020).

205. Bassi, Z. I. *et al.* Modulating PCAF/GCN5 Immune Cell Function through a PROTAC Approach. *ACS Chem Biol* **13**, 2862-2867 (2018).

206. Oh, E., Akopian, D. & Rape, M. Principles of Ubiquitin-Dependent Signaling. *Annu. Rev. Cell. Dev. Biol.* **34**, 137-162 (2018).

207. Schapira, M. *et al.* Targeted protein degradation: expanding the toolbox. *Nat. Rev. Drug Discov.* **18**, 949-963 (2019).

208. Cao, C. *et al.* Chemistries of bifunctional PROTAC degraders. *Chem. Soc. Rev.* **51**, 7066-7114 (2022).

209. Stebbins, C. E., Kaelin, W. G., Jr. & Pavletich, N. P. Structure of the VHL-ElonginC-ElonginB complex: implications for VHL tumor suppressor function. *Science* **284**, 455-461 (1999).

210. Kamura, T. *et al.* Rbx1, a component of the VHL tumor suppressor complex and SCF ubiquitin ligase. *Science* **284**, 657-661 (1999).

211. Cardote, T. A. F., Gadd, M. S. & Ciulli, A. Crystal Structure of the Cul2-Rbx1-EloBC-VHL Ubiquitin Ligase Complex. *Structure* **25**, 901-911.e903 (2017).

212. Schneekloth, J. S., Jr. *et al.* Chemical genetic control of protein levels: selective in vivo targeted degradation. *J. Am. Chem. Soc.* **126**, 3748-3754 (2004).

213. Buckley, D. L. *et al.* Targeting the von Hippel–Lindau E3 Ubiquitin Ligase Using Small Molecules To Disrupt the VHL/HIF-1α Interaction. *J. Am. Chem. Soc.* **134**, 4465-4468 (2012).

214. Buckley, D. L. *et al.* Small-molecule inhibitors of the interaction between the E3 ligase VHL and HIF1α. *Angew. Chem. Int. Ed. Engl.* **51**, 11463-11467 (2012).

215. Van Molle, I. *et al.* Dissecting fragment-based lead discovery at the von Hippel-Lindau protein:hypoxia inducible factor 1α protein-protein interface. *Chem. Biol.* **19**, 1300-1312 (2012).

216. Galdeano, C. *et al.* Structure-Guided Design and Optimization of Small Molecules Targeting the Protein–Protein Interaction between the von Hippel–Lindau (VHL) E3 Ubiquitin Ligase and the Hypoxia Inducible Factor (HIF) Alpha Subunit with in Vitro Nanomolar Affinities. *J. Med. Chem.* **57**, 8657-8663 (2014).

217. Frost, J. *et al.* Potent and selective chemical probe of hypoxic signalling downstream of HIF-α hydroxylation via VHL inhibition. *Nat. Commun.* **7**, 13312 (2016).

218. Soares, P. *et al.* Group-Based Optimization of Potent and Cell-Active Inhibitors of the von Hippel-Lindau (VHL) E3 Ubiquitin Ligase: Structure-Activity Relationships Leading to the Chemical Probe (2S,4R)-1-((S)-2-(1-Cyanocyclopropanecarboxamido)-3,3-dimethylbutanoyl)-4-hydroxy-N-(4-(4-methylthiazol-5-yl)benzyl)pyrrolidine-2-carboxamide (VH298). *J. Med. Chem.* **61**, 599-618 (2018).

219. Fischer, E. S. *et al.* Structure of the DDB1–CRBN E3 ubiquitin ligase in complex with thalidomide. *Nature* **512**, 49-53 (2014).

220. Kim, H. K. *et al.* Cereblon in health and disease. *Pflug. Arch. Eur. J.* **468**, 1299-1309 (2016).

221. Ito, T. *et al.* Identification of a primary target of thalidomide teratogenicity. *Science* **327**, 1345-1350 (2010).

222. Pacini, C. *et al.* Integrated cross-study datasets of genetic dependencies in cancer. *Nat. Commun.* **12**, 1661 (2021).

223. Shirasaki, R. *et al.* Functional Genomics Identify Distinct and Overlapping Genes Mediating Resistance to Different Classes of Heterobifunctional Degraders of Oncoproteins. *Cell Rep.* **34**, 108532 (2021).

224. Zhang, L. *et al.* Acquired Resistance to BET-PROTACs (Proteolysis-Targeting Chimeras) Caused by Genomic Alterations in Core Components of E3 Ligase Complexes. *Mol. Cancer Ther.* **18**, 1302-1311 (2019).

225. Ottis, P. *et al.* Cellular Resistance Mechanisms to Targeted Protein Degradation Converge Toward Impairment of the Engaged Ubiquitin Transfer Pathway. *ACS Chem.l Biol.* **14**, 2215-2223 (2019).

226. Gooding, S. *et al.* Multiple cereblon genetic changes are associated with acquired resistance to lenalidomide or pomalidomide in multiple myeloma. *Blood* **137**, 232-237 (2021).

227. Barrio, S. *et al.* IKZF1/3 and CRL4(CRBN) E3 ubiquitin ligase mutations and resistance to immunomodulatory drugs in multiple myeloma. *Haematologica* **105**, e237-e241 (2020).

228. Hu, Z. & Crews, C. M. Recent Developments in PROTAC-Mediated Protein Degradation: From Bench to Clinic. *Chembiochem* **23**, e202100270 (2022).

229. Cyrus, K. *et al.* Impact of linker length on the activity of PROTACs. *Mol. Biosyst.* **7**, 359-364 (2011).

230. Bemis, T. A., La Clair, J. J. & Burkart, M. D. Unraveling the Role of Linker Design in Proteolysis Targeting Chimeras. *J. Med. Chem.* **64**, 8042-8052 (2021).

231. Han, X. *et al.* Discovery of ARD-69 as a Highly Potent Proteolysis Targeting Chimera (PROTAC) Degrader of Androgen Receptor (AR) for the Treatment of Prostate Cancer. *J. Med. Chem.* **62**, 941-964 (2019).

232. Han, X. *et al.* Discovery of Highly Potent and Efficient PROTAC Degraders of Androgen Receptor (AR) by Employing Weak Binding Affinity VHL E3 Ligase Ligands. *J. Med. Chem.* **62**, 11218-11231 (2019).

233. Troup, R. I., Fallan, C. & Baud, M. G. J. Current strategies for the design of PROTAC linkers: a critical review. *Explor. Target. Antitumor Ther.* **1**, 273-312 (2020).

234. Kargbo, R. B. PROTAC-Mediated Degradation of Bruton's Tyrosine Kinase as a Therapeutic Strategy for Cancer. *ACS Med. Chem. Lett.* **12**, 688-689 (2021).

235. Zeng, M. *et al.* Exploring Targeted Degradation Strategy for Oncogenic KRAS(G12C). *Cell Chem. Biol.* **27**, 19-31.e16 (2020).

236. He, S. *et al.* Strategies for designing proteolysis targeting chimaeras (PROTACs). *Med. Res. Rev.* **42**, 1280-1342 (2022).

237. Sakamoto, K. M. *et al.* Protacs: Chimeric molecules that target proteins to the Skp1–Cullin–F box complex for ubiquitination and degradation. *PNAS* **98**, 8554-8559 (2001).

238. Zhang, D. *et al.* Degradation of target protein in living cells by small-molecule proteolysis inducer. *Bioorg. Med. Chem. Lett.* **14**, 645-648 (2004).

239. Lee, H. *et al.* Targeted degradation of the aryl hydrocarbon receptor by the PROTAC approach: a useful chemical genetic tool. *Chembiochem* **8**, 2058-2062 (2007).

240. Schneekloth, A. R. *et al.* Targeted intracellular protein degradation induced by a small molecule: En route to chemical proteomics. *Bioorg. Med. Chem. Lett.* **18**, 5904-5908 (2008).

241. Itoh, Y. *et al.* Protein knockdown using methyl bestatin-ligand hybrid molecules: design and synthesis of inducers of ubiquitination-mediated degradation of cellular retinoic acid-binding proteins. *J. Am. Chem. Soc.* **132**, 5820-5826 (2010).

242. Lu, J. *et al.* Hijacking the E3 Ubiquitin Ligase Cereblon to Efficiently Target BRD4. *Chem. Biol.* **22**, 755-763 (2015).

243. Buckley, D. L. *et al.* Targeting the von Hippel-Lindau E3 ubiquitin ligase using small molecules to disrupt the VHL/HIF-1α interaction. *J. Am. Chem. Soc.* **134**, 4465-4468 (2012).

244. Galdeano, C. *et al.* Structure-guided design and optimization of small molecules targeting the protein-protein interaction between the von Hippel-Lindau (VHL) E3 ubiquitin ligase and the hypoxia inducible factor (HIF) alpha subunit with in vitro nanomolar affinities. *J. Med. Chem.* **57**, 8657-8663 (2014).

245. Li, D. *et al.* A bibliometric analysis of PROTAC from 2001 to 2021. *Eur. J. Med. Chem.* **244**, 114838 (2022).

246. Chirnomas, D., Hornberger, K. R. & Crews, C. M. Protein degraders enter the clinic — a new approach to cancer therapy. *Nat. Rev. Clin. Oncol.* **20**, 265-278 (2023).

247. Degorce, S. L. *et al.* Discovery of Proteolysis-Targeting Chimera Molecules that Selectively Degrade the IRAK3 Pseudokinase. *J. Med. Chem.* **63**, 10460-10473 (2020).

248. Nunes, J. *et al.* Targeting IRAK4 for Degradation with PROTACs. *ACS Med. Chem. Lett.* **10**, 1081-1085 (2019).

249. Zhang, J. *et al.* Assessing IRAK4 Functions in ABC DLBCL by IRAK4 Kinase Inhibition and Protein Degradation. *Cell Chem. Biol.* **27**, 1500-1509.e1513 (2020).

250. Chen, Y. *et al.* Design, Synthesis, and Biological Evaluation of IRAK4-Targeting PROTACs. *ACS Med. Chem. Lett.* **12**, 82-87 (2021).

251. Cao, F. *et al.* Induced protein degradation of histone deacetylases 3 (HDAC3) by proteolysis targeting chimera (PROTAC). *Eur. J. Med. Chem.* **208**, 112800 (2020).

252. Xiao, Y. *et al.* Discovery of histone deacetylase 3 (HDAC3)-specific PROTACs. *Chem. Commun.* **56**, 9866-9869 (2020).

253. Hu, M. *et al.* Discovery of the first potent proteolysis targeting chimera (PROTAC) degrader of indoleamine 2,3-dioxygenase 1. *Acta Pharm. Sin. B* **10**, 1943-1953 (2020).

254. Schiedel, M. *et al.* Chemically Induced Degradation of Sirtuin 2 (Sirt2) by a Proteolysis Targeting Chimera (PROTAC) Based on Sirtuin Rearranging Ligands (SirReals). *J. Med. Chem.* **61**, 482-491 (2018).

255. Schiedel, M. *et al.* HaloTag-Targeted Sirtuin-Rearranging Ligand (SirReal) for the Development of Proteolysis-Targeting Chimeras (PROTACs) against the Lysine Deacetylase Sirtuin 2 (Sirt2)*. *Chembiochem* **21**, 3371-3376 (2020).

256. Cantrill, C. *et al.* Fundamental aspects of DMPK optimization of targeted protein degraders. *Drug Discov. Today* **25**, 969-982 (2020).

257. Bai, N. *et al.* Rationalizing PROTAC-Mediated Ternary Complex Formation Using Rosetta. *J. Chem. Inf. Model.* **61**, 1368-1382 (2021).

258. Zaidman, D., Prilusky, J. & London, N. PRosettaC: Rosetta Based Modeling of PROTAC Mediated Ternary Complexes. *J. Chem. Inf. Model.* **60**, 4894-4903 (2020).

259. Weng, G. *et al.* Integrative Modeling of PROTAC-Mediated Ternary Complexes. *J. Med. Chem.* **64**, 16271-16281 (2021).

260. Imrie, F. *et al.* Deep Generative Models for 3D Linker Design. *J. Chem. Inf. Model.* **60**, 1983-1995 (2020).

261. Liu, J. *et al.* Novel CRBN-Recruiting Proteolysis-Targeting Chimeras as Degraders of Stimulator of Interferon Genes with In Vivo Anti-Inflammatory Efficacy. *J. Med. Chem.* **65**, 6593-6611 (2022).

262. Zhu, Z. *et al.* Development of VHL-recruiting STING PROTACs that suppress innate immunity. *Cell Mol. Life Sci.* **80**, 149 (2023).

263. Stazzoni, S. Design and synthesis of clickable nucleic acid analogues for cancer therapy and diagnosis. LMU Munich2020.

264. Lebraud, H. & Heightman, T. D. Protein degradation: a validated therapeutic strategy with exciting prospects. *Essays Biochem.* **61**, 517-527 (2017).

265. Klein, V. G. *et al.* Understanding and Improving the Membrane Permeability of VH032-Based PROTACs. *ACS Med. Chem. Lett.* **11**, 1732-1738 (2020).

266. Zagidullin, A. *et al.* Novel approaches for the rational design of PROTAC linkers. *Explor. Target. Antitumor Ther.* **1**, 381-390 (2020).

267. Gao, P. *et al.* Cyclic [G(2',5')pA(3',5')p] is the metazoan second messenger produced by DNA-activated cyclic GMP-AMP synthase. *Cell* **153**, 1094-1107 (2013).

268. Schwede, F., Genieser, H.-G. & Rentsch, A. The Chemistry of the Noncanonical Cyclic Dinucleotide 2’3’-cGAMP and Its Analogs. In *Non-canonical Cyclic Nucleotides*, Seifert, R., (ed.) Springer International Publishing, Cham, (2017), pp 359-384.

269. Dialer, C. R. *et al.* A Click-Chemistry Linked 2'3'-cGAMP Analogue. *Chemistry* **25 8**, 2089-2095 (2019).

270. Kusachi, S. *et al.* Dog coronary artery adenosine receptor. Structure of the N6-aryl subregion. *J. Med. Chem.* **29**, 989-996 (1986).

271. Hao, Y. *et al.* Synthesis and antiviral evaluation of novel N-6 substituted adenosine analogues. *Tetrahedron Lett.* **58**, 190-193 (2017).

272. Tao, Z. *et al.* Design, synthesis and in vitro anti-Zika virus evaluation of novel Sinefungin derivatives. *Eur. J. Med. Chem.* **157**, 994-1004 (2018).

273. Gao, J. *et al.* CDK inhibitor Palbociclib targets STING to alleviate autoinflammation. *EMBO Rep.* **23**, e53932 (2022).

274. Long, J. *et al.* Discovery of fusidic acid derivatives as novel STING inhibitors for treatment of sepsis. *Eur. J. Med. Chem.* **244**, 114814 (2022).

275. Hayashi, K. *et al.* Observation of Circularly Polarized Luminescence of the Excimer from Two Perylene Cores in the Form of [4]Rotaxane. *Chem. Eur. J.* **24**, 14613-14616 (2018).

276. Sharma, A. *et al.* Overcoming Drug Resistance by Targeting Cancer Bioenergetics with an Activatable Prodrug. *Chem* **4**, 2370-2383 (2018).

277. Veth, S. *et al.* Chemical Synthesis of the Fluorescent, Cyclic Dinucleotides c(th) GAMP. *Chembiochem* **23**, e202200005 (2022).

278. Sondo, E. *et al.* Pharmacological Inhibition of the Ubiquitin Ligase RNF5 Rescues F508del-CFTR in Cystic Fibrosis Airway Epithelia. *Cell Chem. Biol.* **25**, 891-905.e898 (2018).

279. Principi, E. *et al.* Targeting of Ubiquitin E3 Ligase RNF5 as a Novel Therapeutic Strategy in Neuroectodermal Tumors. *Cancers* **14**, 1802 (2022).

280. Tumula, N. *et al.* Hypervalent Iodine(III)-Mediated Solvent-Free, Regioselective Synthesis of 3,4-Disubstituted 5-Imino-1,2,4-thiadiazoles and 2-Aminobenzo[d]thiazoles. *Adv. Synth. Catal.* **360**, 2806-2812 (2018).

281. Bromberg, K. D. *et al.* Increased expression of the E3 ubiquitin ligase RNF5 is associated with decreased survival in breast cancer. *Cancer Res.* **67**, 8172-8179 (2007).

282. Zhang, Y. *et al.* Six genes as potential diagnosis and prognosis biomarkers for hepatocellular carcinoma through data mining. *J. Cell. Physiol.* **234**, 9787-9792 (2019).

283. Khateb, A. *et al.* The ubiquitin ligase RNF5 determines acute myeloid leukemia growth and susceptibility to histone deacetylase inhibitors. *Nat. Commun.* **12**, 5397 (2021).

284. Jeon, Y. J. *et al.* Regulation of glutamine carrier proteins by RNF5 determines breast cancer response to ER stress-inducing chemotherapies. *Cancer Cell* **27**, 354-369 (2015).

285. Reist, M. *et al.* Chiral Inversion and Hydrolysis of Thalidomide: Mechanisms and Catalysis by Bases and Serum Albumin, and Chiral Stability of Teratogenic Metabolites. *Chemical Research in Toxicology* **11**, 1521-1528 (1998).

286. Krečmerová, M. *et al.* Phosphonates and Phosphonate Prodrugs in Medicinal Chemistry: Past Successes and Future Prospects. *Front. Chem.* **10**, (2022).

287. Heller, K. *et al.* Covalent Protein Labeling by Enzymatic Phosphocholination. *Angew. Chem. Int. Ed.* **54**, 10327-10330 (2015).